5-2021

Investigation of Interactions between 1,3 Dialkyl Imidazolium Ionic Liquids and Lignocellulosic Polymers

Aparna Annamraju
University of Tennessee, aannamr1@vols.utk.edu

To the Graduate Council:

I am submitting herewith a dissertation written by Aparna Annamraju entitled "Investigation of Interactions between 1,3 Dialkyl Imidazolium Ionic Liquids and Lignocellulosic Polymers." I have examined the final electronic copy of this dissertation for form and content and recommend that it be accepted in partial fulfillment of the requirements for the degree of Doctor of Philosophy, with a major in Natural Resources.

Nicole Labbé, Major Professor

We have read this dissertation and recommend its acceptance:

Hugh O Neill, Loukas Petridis, David P Harper, Timothy G Rials

Accepted for the Council:

Dixie L. Thompson

Vice Provost and Dean of the Graduate School

(Original signatures are on file with official student records.)

Investigation of Interactions between 1,3 Dialkyl Imidazolium Ionic Liquids and Lignocellulosic Polymers

A Dissertation Presented for the

Doctor of Philosophy

Degree

The University of Tennessee, Knoxville

Aparna Annamraju

May 2021

DEDICATION

To my parents, my husband and my kids

For listening to me, guiding me, and helping me during this journey.

ACKNOWLEDGMENTS

I sincerely thank my mentor, Dr. Nicole (Niki) Labbé for giving me the opportunity to work with her. Niki, I am forever indebted to you for the guidance you have provided me over these last four years. Under your mentorship I have developed the ability to design and develop research projects. You have given me freedom to direct my research project and your feedback on my writing skills served me well while I prepare this document. I thank Drs. Hugh O'Neill, Loukas Petridis, David Harper and Timothy Rials, for serving as my committee members and providing valuable feedback and perspective based on your expertise.

I am also grateful to, Dr. Kalavathy Rajan for serving the role of mentor in Niki's absence. Kala, I thank you helping me with your long buck up talks, manuscript edits and most of all for addressing all my questions. I also thank Dr. Priya Voothuluru, Dr. Nihal Kanbargi, Ms. Anna Kim and Ms. Choo Hamilton and Conner Pope for their valuable feedback during the weekly group meeting sessions. My sincere thanks to the staff of the Center for Renewable Carbon, Ms. Lyssa McKenry, Ms. Marina Lavendar and Mr. Chris Helton. I also would like to thank Ms. Jennie Swanson and Ms. Heather Inman of Forestry, Wildlife and Fisheries department. I also extend my sincere thanks to Dr. Lisa Muller for coordinating with the Graduate school on timely submission of the necessary paperwork.

Finally, I thank my family and friends for supporting me through this PhD. Journey. I reserve my sincere thankyous to my husband and kids who took my absence from their many daily activities in stride and encouraged me to finish the process I started four years ago.

ABSTRACT

Lignocellulosic biomass is a potential energy source for fuels, chemicals and materials production in a sustainable manner. A network of covalent and non-covalent bonds between the three main polymers of biomass, i.e., cellulose, hemicellulose and lignin, results in a compact structure which is resistant to chemical and biological attacks and therefore challenging for the efficient utilization of lignocellulosic biomass. Ionic liquids (ILs) have been reported to disrupt the bonds between these polymers and dissolve biomass at temperature below 100 ˚C. Research through the years has shown that biomass pretreatment with IL brings out selective dissolution of biomass polymers and reduces cellulose crystallinity with enhanced saccharification rates. However, the specific nature of interactions between the biomass polymers and ILs and the role of IL ion pairs remain largely unknown. In this work, we report on the progress achieved in understanding interactions between ILs and biomass polymers. Herein using four different imidazolium ILs, we developed a unique experimental approach using spectroscopic, scattering and rheological techniques to investigate interactions between individual biomass polymers and ILs. The spectroscopic approach provided evidence for IL cation and anion roles. Scattering studies not only offered conformational details on polymers but also provided a quantitative estimation of the qualitative data acquired using spectroscopy. Rheology studies helped identify dispersive interactions not accounted for by the other two techniques. Finally, our multilength scale approach helped us identify the two ILs with differential interactions towards cellulose and lignin. These two ILs were selected to perform *in-situ* biomass dissolution study using small angle neutron scattering (SANS), which showed that cellulose microfibril architecture altered in size and shape as a function of time in acetate anion IL as opposed to the formate anion IL. In summary,

the molecular level information on IL biomass polymers presented in this work will aid in making a rationale choice of IL ideal for the field of biomass processing.

TABLE OF CONTENTS

LIST OF TABLES

LIST OF FIGURES

Chapter 1. Introduction

1.1. Energy sources in the US

The energy sources utilized across the world are broadly classified as renewable and non-renewable. The non-renewables such as crude oil, coal and natural gas were formed in the earth's core from the remains of plants and animals over hundreds of years and hence, they are often referred to as "*fossil fuels*". Layers of sand, silt, and rock cover these remains and heat and pressure from these layers turn the remains into crude oil. Currently, the non-renewable energy sources provide fuel to the transportation sector and electricity to households, industrial operations and commercial buildings. Gasoline, diesel fuel, heating oil, jet fuel, petrochemical feedstocks, waxes, lubricating oils, plastics and asphalt are few of products made from crude oil. In 2019, 37 % of all the energy consumed in the US were generated from crude oil (Figure 1.1).[1] In the same year, of the over 20,504,000 barrels per day of petroleum consumed in the US, 70 % were used as fuel for the transportation sector.[2] Although the consumption of fossil fuels peaked in the US in 1966, petroleum and petroleum derived products continue to dominate the US energy production and consumption landscape.[3] This continuous and constant utilization of fossil fuels has led to the gradual increase of certain greenhouse gases (GHG) in the earth's atmosphere.[3]

1.2. Greenhouse gas effect

Greenhouse gases (GHG's) such as carbon dioxide, nitrous oxide and methane are present in earth's atmosphere and help regulate the temperature by trapping the sun's heat.[4] However, due to human activity, the amount of the GHG has increased disproportionately over time. From 1990 to 2018, CO_2 emissions from the transportation sector increased by 21 % in part due to the increased demand for travel.[5]

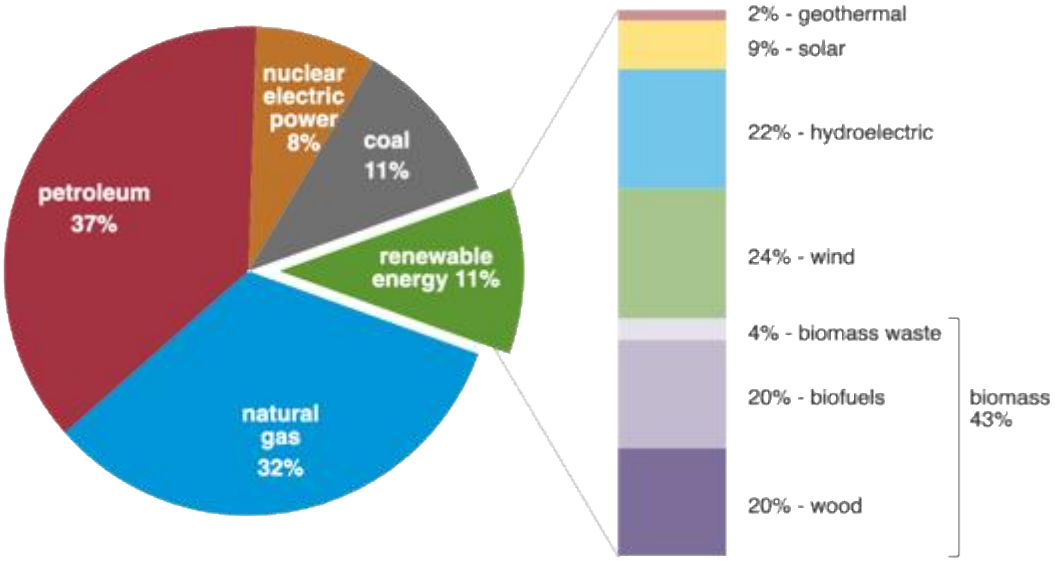

Figure 1. 1. US energy consumption by source for the year 2019. Figure source: Energy Information Administration (EIA) website. (1)

In fact, in 2018, the transportation sector accounted for 28 % of total CO_2 emissions in the US. Light duty vehicles such as passenger cars and light-duty trucks accounted for almost 58 % of total CO_2 emissions in the US.[6]

The effect of these increased emissions is reflected in the heightened CO_2 concentration in the atmosphere. As of August 2020, the CO_2 concentration is at 414 parts per million (Mauna Loa Observatory, Hawaii), a number not seen in the past 650,000 years (Figure 2).[7] This rise of CO_2 concentration has already resulted in the increase of earth's surface temperature by as much as 0.9 $^{\circ}C$.[8]

1.3. Overview of energy policies implemented under Environmental Protection Agency

In order to mitigate the negative impact of fossil fuels and develop a cohesive federal response, the Environmental Protection Agency (EPA) was established in 1970, which then initiated several policies with the Clean Air Act (CAA) as the foremost policy.[9] Under the CAA, EPA has set standards for the size of particulate matter in air, created Air Quality Index (AQI), developed visibility protection regulations, proposed for the limit of lead (tetraethyl lead) addition in gasoline, limited volatile organic compounds (VOC) in commercial products and established preliminary clean fuel standards for diesel trucks and buses. Starting in 1979, methyl tertiary butyl ether (MTBE) replaced lead in gasoline to fulfill the oxygenate standards set under the CAA. However, MTBE is easily soluble in water and within few years was detected in most of the drinking supplies throughout the US.[10] Increased levels of MTBE (>40 ppb) in drinking water can cause offensive taste and odor. Therefore, under the CAA amendment of 1990, ethanol was proposed as an alternative to MTBE. Further, in 2005 when CAA was expanded as Energy Policy Act to include the Renewable Fuel Standard (RFS) Program, MTBE was removed as oxygenate requirement in favor of ethanol.[11]

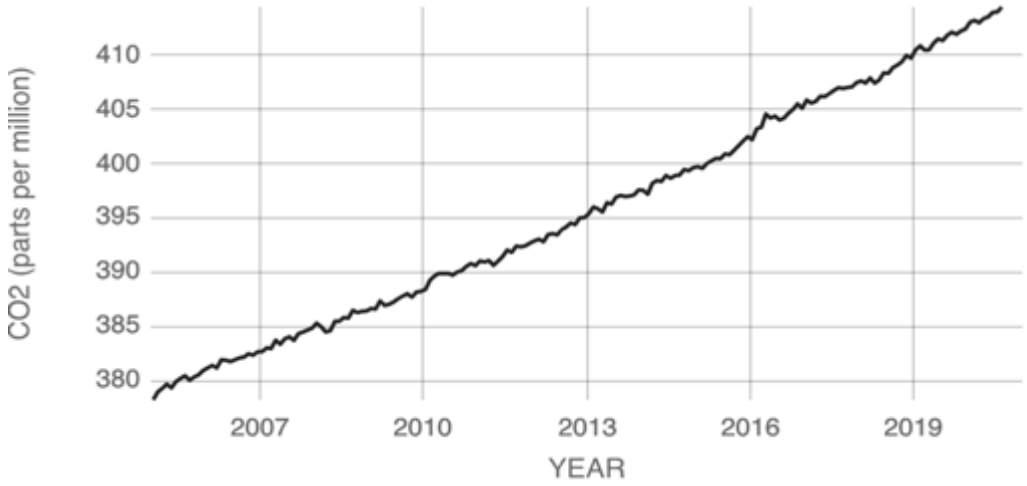

Figure 1. 2. Graph of year versus CO_2 levels measured at Mauna Loa Observatory, Hawaii over the last fourteen years. (7)

1.4. Corn starch ethanol (First generation biofuel) [12]

Ethanol, a renewable fuel, can be made from various plant materials. Regardless of the source, ethanol has the same chemical formula (C_2H_5OH) whether it is produced from starch- or sugar-based feedstocks, such as corn grain (the United States), sugar cane (Brazil), or from cellulosic feedstocks (such as wood chips or crop residues). Ethanol has higher octane number than gasoline, thus increasing vehicle performance and power. The most common way in which ethanol is consumed by transportation sector is in the form of E10 fuel (10 % ethanol and 90 % gasoline). This inclusion of ethanol in gasoline started in 1990 that helped kick off the US ethanol industry. In 1996 when the recognition of MTBE at higher levels (>90 ppb) in water resources coincided with development of Flex Fuel Vehicles (FFV), ethanol production and consumption increased further. FFV's include internal combustion engine that is equipped to run on E85 blend (51 to 83 % ethanol with gasoline) gasoline. In addition to contributing towards reduced emissions, US ethanol industry also created close to 68,000 jobs in rural communities.

Since 1990's corn starch has been and continues to remain as the major source for ethanol in the US (Figure 1.3). However, corn is a food source. Moreover, corn fields consume high amounts of water and ethanol produced from corn relies on coal as energy source. Therefore, when the Energy Independence and Security Act (EISA) of 2007 further mandated the inclusion of ethanol, cellulosic ethanol was proposed as an additional option.[14] Under the act, ethanol production was set to rise steadily to a level of 36 billion gallons by 2022, with 16 billion gallons of cellulosic ethanol contribution.

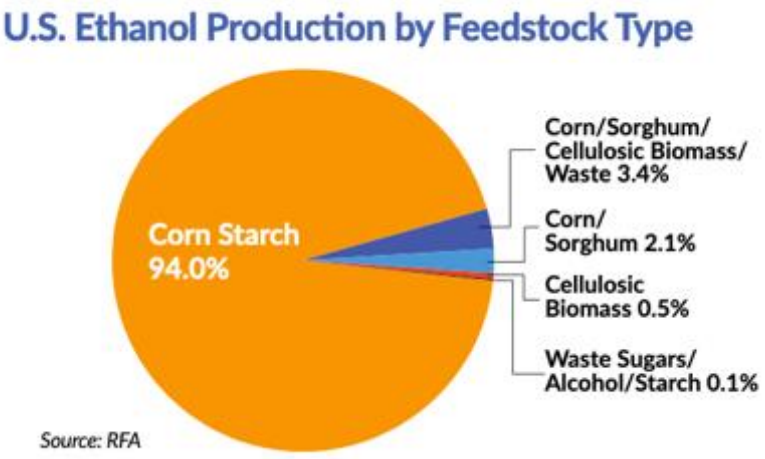

Figure 1. 3. US ethanol production by feedstock for the year 2019. (13)

1.5. Cellulosic ethanol (Advanced biofuel)

Cellulosic ethanol is produced from non-food sources that include dedicated energy crops (miscanthus, switchgrass, hybrid poplar), industrial wastes, agricultural residues, wood residues and municipal waste. These feedstocks contain three main polymers, i.e., cellulose, hemicellulose and lignin. Cellulosic ethanol offers a better energy balance when compared with corn starch ethanol, as the feedstocks are not food sources and the fertilizer/water requirements are significantly lower. In terms of the emission reduction, life cycle analysis revealed that while corn ethanol can reduce GHG's by 34%, cellulosic ethanol can bring about a reduction in the range of 88% to 108% (based on the feedstock used).[12]

In addition to serving as fuel source, biomass has the potential to produce bio-based products to replace petroleum derived chemicals and plastics. The bio-preferred program first established in the Farm Security and Rural Investment Act of 2002 and strengthened by the Food, Conservation, and Energy Act of 2008, reports on the progress made in the field of bio-based products. As of 2015, over 20,000 bio-based products are reported in the US.[17]

Despite the mentioned advantages, production of cellulosic ethanol lagged behind other sources in the past decade (Figure 1.4). In 2019, greater than 90% of ethanol consumed in the transportation sector were produced from corn starch. In fact, in 2019, of the 14.5 billion gallons of ethanol consumed, cellulosic ethanol contribution was 418 million barrels (Figure 1.3). The reduced contribution of cellulosic ethanol is in line with the trend noted since Congress passed EISA, more than a decade ago. There are several reasons for the slower increase of cellulosic bio-fuel production. In the US, the consumption of gasoline slowed down in the past decade, which lead to the decreased amount of gasoline available for ethanol blend.[18] Further, only E10 blend was/is predominantly used across US, reducing the necessity for higher ethanol production.[1]

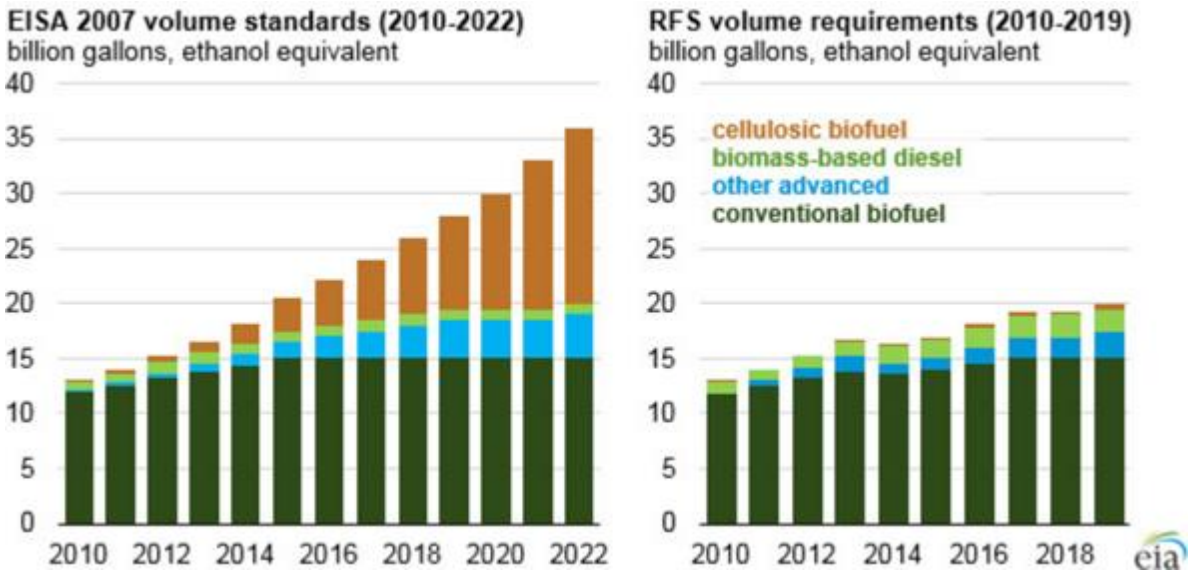

Figure 1. 4. A) Target for cellulosic ethanol as per the EISA volume standards. B) Cellulosic ethanol contribution over the last 10 years (16).

However, the major reason for the continued lag is the under-developed technology used in the isolation of individual polymers of biomass and their efficient conversion into value-added products.

1.6. Traditional pretreatment technology

The four main steps of cellulosic ethanol production are biomass procurement and preprocessing, pretreatment of biomass, cellulose/hemicellulose hydrolysis into sugars, and finally their fermentation into alcohol (Figure 1.5). The first two steps are estimated to contribute towards 70% of expenses.[20] Specifically, the step of pretreatment is energy intensive. The three polymers of biomass are interconnected by network of covalent and non-covalent interactions. In order to disrupt this intricate network of bonds, several mechanical, physical and chemical systems were developed overtime.

Mechanical pretreatments, such as size reduction by chipping, milling and grinding, reduce biomass particle size, decrease cellulose crystallinity and cellulose degree of polymerization.[21] Chemical pretreatments, such as using hot water extraction,[22] dilute acid[23] and ammonia fiber expansion [24], bring about a partial deconstruction of the biomass cell wall, thereby improving cellulose accessibility by increasing biomass porosity, reducing cellulose crystallinity, and partial removal of lignin. However, most of these traditional approaches suffer from deficiencies such as high energy needs (high temperature and pressure), high enzyme loading and low sugar yields.[25]

To overcome the challenges posed by the traditional pretreatment methodologies, research in the past decade has shifted focus on 1) understanding the fundamental interactions that govern the process of biomass dissociation and conversion and 2) utilization of biomass not only for cellulosic ethanol production but also for production of products and chemicals (mimicking the petroleum industry) .[26, 27]

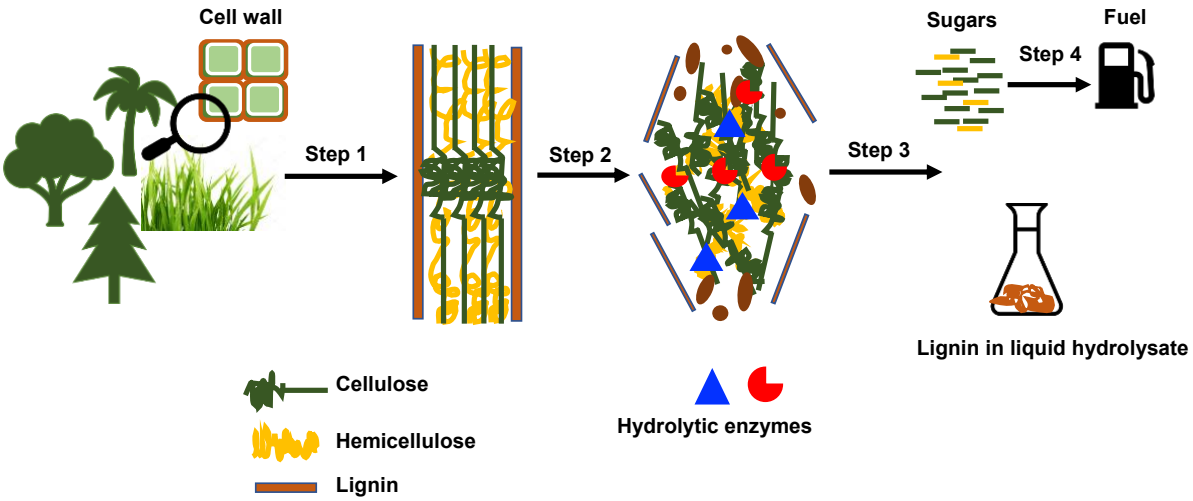

Figure 1. 5. Schematic of traditional pretreatment technology. Step 1: procurement and preprocessing of biomass, step 2: pretreatment of biomass, step 3: enzymatic hydrolysis, step 4: fermentation of sugars to ethanol for fuel.

1.7. Modern pretreatment technology

Solvent systems such as water/gamma valerolactone (GVL),[28] water/tetrahydrofuran (THF),[29] and ionic liquids (ILs)[30] are few examples of modern pretreatment options. These three solvent systems are shown to function as "good solvents" for biomass, i.e., the interactions between biomass polymers and solvent outweigh the interactions between solvent-solvent and polymer-polymer. While the three systems are known to be effective, ILs offer distinct advantages. ILs are liquid salts with unique physical properties such as low volatility and high thermal stability.[31] In addition to pretreatment technology, ILs are exceptional solvents for whole biomass dissolution under mild conditions for direct product production.[32] Previous research has shown that ILs can be recycled making the process cost-effective.[31] Despite these advantages there is a huge gap in translating laboratory IL set up to industrial scale.

The most common reason cited for the slow transition of ILs to industrial scale is their cost prohibitive nature.[33] However, with the advent of carbonate-based IL synthesis (CBILS®) technology in 2017, the production cost of several ILs has reduced considerably.[34] For example, the CBILS® technology brought down the average cost of 1-ethyl-3-methylimidazolium acetate ([EMIM]acetate), the most frequently used IL for biomass processing from $870 to $200 per kg.[35] Additionally, to meet the growing demand of IL research work, Iolitec, a company based in Germany, started work on 1t reactor in May 2020, which will bring down the costs of ILs even further.[36]

The other reason for the IL lag is the sheer number of ILs available for research purposes. Over the past decade, more than 1000 research papers have showcased the efficiency of one IL over the other.[37] The differences between the ILs are often discerned on the basis of either macroscopic

solubility measurement, pre- and post-biomass structural analysis or on the basis of physicochemical properties of IL such as viscosity and H-bond basicity.[38] As a result of this experimental approach even though we gained a good knowledge of the changes induced by IL treatment, the reason for how those changes are initiated at atomic/molecular level of biomass remains largely unknown. In addition to the lack of clear picture of the fundamental interactions, the numerous IL options make the identification of an ideal candidate for commercialization challenging.

As the IL industry continues to make progress to improve the cost of IL manufacturing, the task of identifying ideal candidate biomass processing can be done by focusing on the aspects of specific interactions between biomass polymers and ILs in addition to application orientated research. Therefore, we hypothesize that individual interactions at micro, meso and molecular levels between particular ILs and biomass polymers such as cellulose, hemicellulose and lignin will predict the capabilities of ILs to dissolve whole biomass. The following goal and objectives will help us towards substantiating this claim.

1.8. Project goal and objectives

The primary goal of this thesis project is to investigate the interactions between four different imidazolium ILs and biomass polymers (i.e., cellulose, hemicellulose and lignin) to aid in the rational design, selection and implementation of ILs in biomass processing. To achieve this goal, we have identified the following three objectives:

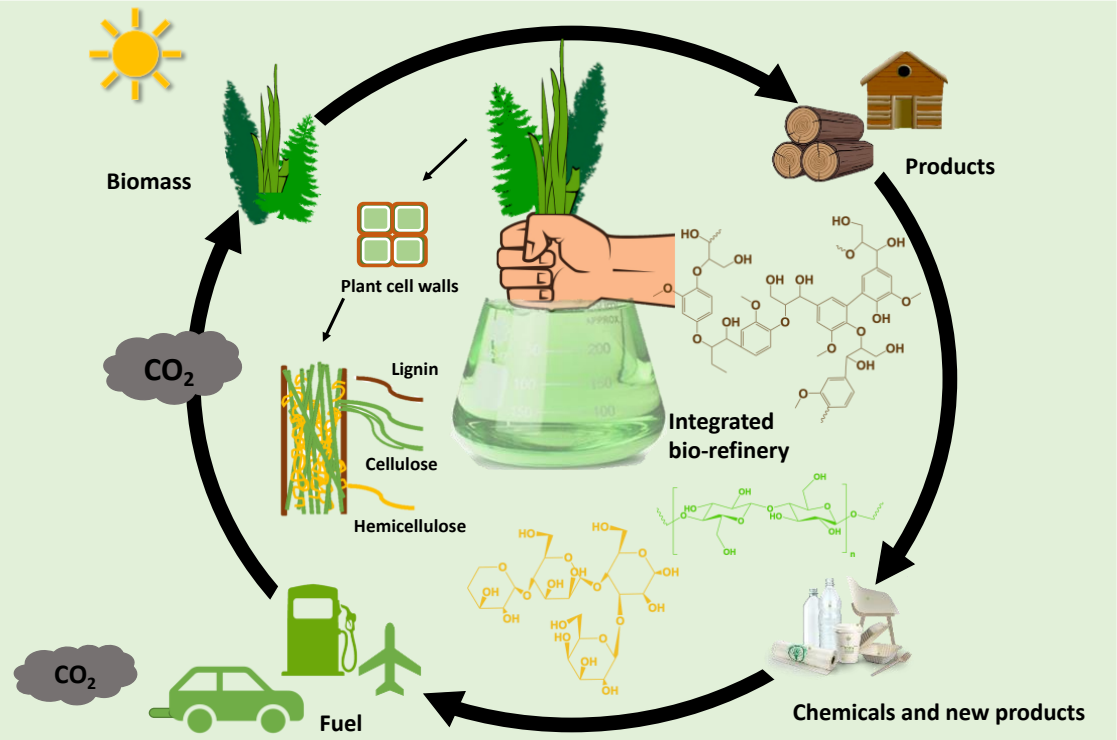

Figure 1. 6. A schematic of self-sustainable bio-refinery based on the modern pretreatment technologies such as ILs.

1) Developing a comprehensive characterization strategy which will measure the molecular, meso-scale and microscopic level conformation of biopolymers in ILs by utilizing spectroscopic, scattering and rheological techniques.
2) Employing the comprehensive characterization strategy to measure the interactions and conformation of purified cellulose, hemicellulose and lignin fractions in select 1, 3-dialkyl imidazolium ILs.
3) Characterizing the *in-situ* state of biomass polymers during dissolution with select 1, 3-dialkyl imidazolium ILs, using advanced scattering and spectroscopic techniques.

The thesis is presented in multipart paper format and it has a total of six chapters including introduction. Ionic liquids are unique natured solvents due to their ionic composition a trait similar to solids. In simple terms ILs are "flowing solids". When considering the interactions of ILs with biomass, which in itself is complex due to the compact and multilength scale nature, the dissolution process is influenced by several factors. So, in chapter 2 an overview of structural details of plant cell wall assembly, biomass polymers and a brief summary of lignin carbohydrate complex (LCC) interactions are provided. The chapter also provides a brief summary of the various solvent systems used for separation of biomass polymers. In the next section of the chapter, an overview of the various factors along with the main physicochemical properties of ILs influencing biomass dissolution in ILs is presented. Finally, an introduction to the characterization techniques used to investigate the interactions between biomass and ILs is presented. For the current research work, nuclear magnetic resonance spectroscopy (NMR), attenuated total reflectance Fourier transform infra-red spectroscopy (ATR FTIR), small angle X-ray scattering (SAXS), small angle neutron scattering (SANS) and rheology were used to understand the interactions between ILs and biomass polymers. Therefore, a brief overview of each these techniques is discussed.

In chapter 3, we report the results of our first study in which we compare the interactions between cellulose and four selected imidazolium ILs. Cellulose is the major biopolymer of biomass and many different ILs have demonstrated exceptional solubility of cellulose. However, the specific nature of interactions between ILs and cellulose is not known. To explore the interactions between cellulose and 1-alkyl-3-methylimidazolium ionic liquids, we selected two cations (1-ethyl-3-methylimidazolium [EMIM] and 1-allyl-3-methylimidazolium [AMIM]) and two anions (formate and acetate) in four combinations. Molecular interactions were investigated by measuring chemical shift differences using ^{13}C NMR spectroscopy. The results showed that at the molecular level, both cation and anion interact with cellulose. NMR study also identified [EMIM]acetate and [AMIM]formate as the ILs with the most and least interactions, respectively. The conformational details of cellulose from the SAXS study implied that cellulose attained the same molecular level dispersion in the two ILs. However, twice the number of acetate anions were found to cellulose fibril than formate anions. Microscale interactions measured by rheology confirmed the higher number of interactions between acetate IL than formate IL. This multilength scale study facilitated not only to understand the differences in the way ILs interact with cellulose but also provided a new approach to better understand the fundamental interactions between cellulose and 1-alkyl-3-methylimidazolium ILs.

In chapter 4, the work on interactions between xylan (major hemicellulose of hardwoods) and lignin in the four imidazolium ILs is presented. Understanding these interactions is beneficial as it can identify the most efficient IL either for fractionating or extracting individual biomass polymers. NMR results in terms of ^{13} C NMR chemical shift differences showed that both cation and anion of IL interact with xylan and lignin. The structural details obtained by SAXS study revealed that xylan conformation is similar in the tested ILs and the number of anions bound to a

single xylan strand was also the same. When acetate anion was the counter anion, lignin dispersed as a monomer, while in the formate containing ILs, lignin assumed an oligomeric form. Macroscopic solubility aside the two chapters summarizes how acetate and formate ILs have similar interactions towards xylan but differ towards cellulose and lignin.

In chapter 5, we present our work on *in-situ* biomass dissolution on two ILs that have been identified in the earlier chapters to have different interactions towards cellulose and lignin. Utilizing small angle neutron scattering (SANS), the real time changes in cellulose fibrils within native biomass system were tracked over a period of ~ 2 days. In [EMIM]acetate treated biomass system the cellulose microfibril feature altered in size and shape with no interference or structure factor. This result implied that [EMIM]acetate permeates through the biomass to bring about the changes in cellulose microfibril architecture. In [AMIM]formate biomass system, although IL diffuses into the biomass, the cellulose architecture remained unaltered with progress of time. The scattering profile in the low Q region for [AMIM]formate biomass system instead provided with next neighbor distance value of ~27 Å. The complementary IR analysis performed on recovered biomass samples after scattering showed that biomass sample treated with [EMIM]acetate underwent ~ 4.5% mass loss corresponding to acetyl groups loss. Biomass recovered from [AMIM]formate had no mass loss but IR data showed that the IL-recovered sample was different from the control sample. The nano level changes showcased in this *in-situ* study along with our earlier chapter results provide an integrated scientific reasoning that cellulose microfibril separation is key step in the biomass treatment of ILs.

Chapter 6 summarizes the main conclusions of this thesis work. In the first half of the thesis by adopting a unique experimental approach spanning multiple length scales we have shown the

fundamental interactions at play between individual biomass polymers and ILs. In the second half of the study, using neutron scattering, nano level changes of cellulose microfibrils in native biomass system were showcased. The combined results help advance our knowledge of interactions between ILs and biomass and therefore will aid in making a rationale choice of IL for biomass processing.

References

1) U.S energy sources: https://www.eia.gov/energyexplained/us-energy-facts/
2) Transportation sector energy consumption: https://www.eia.gov/totalenergy/data/monthly/pdf/sec2.pdf
3) U.S fossil fuels share: https://www.eia.gov/todayinenergy/detail.php?id=4509
4) Ehhalt, D, Prather, M, Dentener, F, Derwent, R, Dlugokencky, Edward J, Holland, E, Isaksen, I, Katima, J, Kirchhoff, V, Matson, P, Midgley, P, Wang, M, Berntsen, T, Bey, I, Brasseur, G, Buja, L, Collins, W J, Daniel, J S, DeMore, W B, Derek, N, Dickerson, R, Etheridge, D, Feichter, J, Fraser, P, Friedl, R, Fuglestvedt, J, Gauss, M, Grenfell, L, Grubler, Arnulf, Harris, N, Hauglustaine, D, Horowitz, L, Jackman, C, Jacob, D, Jaegle, L, Jain, Atul K, Kanakidou, M, Karlsdottir, S, Ko, M, Kurylo, M, Lawrence, M, Logan, J A, Manning, M, Mauzerall, D, McConnell, J, Mickley, L J, Montzka, S, Muller, J F, Olivier, J, Pickering, K, Pitari, G, Roelofs, G -J, Rogers, H, Rognerud, B, Smith, Steven J, Solomon, S, Staehelin, J, Steele, P, Stevenson, D S, Sundet, J, Thompson, A, van Weele, M, von Kuhlmann, R, Wang, Y, Weisenstein, D K, Wigley, T M, Wild, O, Wuebbles, D J, Yantosca, R, Joos, Fortunat, & McFarland, M. *Atmospheric chemistry and greenhouse gases* (No. PNNL-SA-39647). Pacific Northwest National Lab. (PNNL), Richland, WA (United States).
5) Fast Facts on Transportation Greenhouse Gas Emissions. https://www.epa.gov/greenvehicles/fast-facts-transportation-greenhouse-gas-emissions.
6) Greenhouse gas emission: https://www.epa.gov/ghgemissions/overview-greenhouse-gases
7) CO2 levels over the last 100 years: https://climate.nasa.gov/
8) *Turn Down the Heat: Confronting the New Climate Normal*. The World Bank.: Washington D.C., 2014.
9) https://www.epa.gov/sites/production/files/2015-08/documents/peg.pdf
10) Hartley, W. R.; Englande, A. J.; Harrington, D. J., Health risk assessment of groundwater contaminated with methyl tertiary butyl ether (MTBE). *Water Science and Technology* **1999,** *39* (10), 305-310.
11) Renewable Fuel Standard Program: https://www.epa.gov/renewable-fuel-standard-program/overview-renewable-fuel-standard#structure
12) Ethanol energy basics: https://afdc.energy.gov/fuels/ethanol_fuel_basics.html
13) US Ethanol production 2019: https://ethanolrfa.org/wp-content/uploads/2019/02/RFA2019Outlook.pdf
14) EISA act: https://www.epa.gov/laws-regulations/summary-energy-independence-and-security-act
15) https://www.eia.gov/todayinenergy/detail.php?id=37712
16) Bio-preferred program: https://www.biopreferred.gov/BioPreferred/faces/pages/BiobasedProducts.xhtml
17) https://www.eia.gov/energyexplained/us-energy-facts/imports-and-exports.php
18) Ethanol blends: https://afdc.energy.gov/fuels/ethanol_blends.html
19) Seidl, P. R.; Goulart, A. K., Pretreatment processes for lignocellulosic biomass conversion to biofuels and bioproducts. *Current Opinion in Green and Sustainable Chemistry* **2016**, *2*, 48-53.

20) Cheng, M.; H., Huang, H.; Dien, B. S.; Singh, V., The costs of sugar production from different feedstocks and processing technologies. *Biofuels, Bioproducts and Biorefining* **2019**, *13*(3), 723-739.
21) Jiang, J.; Wang, J.; Zhang, X.; Wolcott, M., Microstructure change in wood cell wall fracture from mechanical pretreatment and its influence on enzymatic hydrolysis. *Industrial Crops and Products* **2017**, *97*, 498-508.
22) Castro-Puyana, M.; Marina, M. L.; Plaza, M., Water as green extraction solvent: principles and reasons for its use. *Current Opinion in Green and Sustainable Chemistry* **2017**, *5*, 31-36.
23) Lee, Y. Y.; Iyer, P.; Torget, R. W., Dilute-acid hydrolysis of lignocellulosic biomass. In *Recent progress in bioconversion of lignocellulosics* (pp. 93-115). 1999 Springer, Berlin, Heidelberg.
24) Chundawat, S.P.; Vismeh, R.; Sharma, L.N.; Humpula, J.F.; da Costa Sousa, L.; Chambliss, C.K.; Jones, A.D.; Balan, V.; Dale, B.E., Multifaceted characterization of cell wall decomposition products formed during ammonia fiber expansion (AFEX) and dilute acid -based pretreatments. *Bioresource Technology* **2010**, *101*(21), 8429-8438.
25) Larsson, S.; Palmqvist, E.; Hahn-Hägerdal, B.; Tengborg, C.; Stenberg, K.; Zacchi, G.; Nilvebrant, N. O., The generation of fermentation inhibitors during dilute acid hydrolysis of softwood. *Enzyme and microbial technology* **1999**, *24*(3-4), 151-159.
26) Langan, P.; Petridis, L.; O'Neill, H.M.; Pingali, S.V.; Foston, M.; Nishiyama, Y.; Schulz, R.; Lindner, B.; Hanson, B.L.; Harton, S.; Heller, W.T., Common processes drive the thermochemical pretreatment of lignocellulosic biomass. *Green Chemistry* **2014**, *16*(1), 63-68.
27) Ragauskas, A.J.; Beckham, G.T.; Biddy, M.J.; Chandra, R.; Chen, F.; Davis, M.F.; Davison, B.H.; Dixon, R.A.; Gilna, P.; Keller, M and Langan, P., Lignin valorization: improving lignin processing in the biorefinery. *Science* **2014**, *344*(6185).
28) Luterbacher, J.S.; Rand, J.M.; Alonso, D.M.; Han, J.; Youngquist, J.T.; Maravelias, C.T.; Pfleger, B.F.; Dumesic, J.A., Nonenzymatic sugar production from biomass using biomass-derived γ-valerolactone. *Science* **2014**, *343*(6168), 277-280.
29) Nguyen, T. Y.; Cai, C. M.; Kumar, R.; Wyman, C. E., Co-solvent pretreatment reduces costly enzyme requirements for high sugar and ethanol yields from lignocellulosic biomass. *ChemSusChem* **2015**, *8*(10), 1716-1725.
30) Rogers, R. D.; Seddon, K. R., Ionic liquids--solvents of the future? *Science* **2003**, *302*(5646), 792-793.
31) Brandt, A.; Gräsvik, J.; Hallett, J. P.; & Welton, T., Deconstruction of lignocellulosic biomass with ionic liquids. *Green chemistry* **2013**, *15*(3), 550-583.
32) Nguyen, N. A.; Kim, K.; Bowland, C. C.; Keum, J. K.; Kearney, L. T.; André, N.; Labbé, N.; Naskar, A. K., A fundamental understanding of whole biomass dissolution in ionic liquid for regeneration of fiber by solution-spinning. *Green Chemistry* **2019**, *21*(16), 4354-4367.
33) Weerachanchai, P.; Lee, J. M., (2014). Recyclability of an ionic liquid for biomass pretreatment. *Bioresource technology* **2014**, *169*, 336-343.
34) Kalb, R. S.; Stepurko, E. N.; Emel'yanenko, V. N.; Verevkin, S. P., Carbonate based ionic liquid synthesis (CBILS®): thermodynamic analysis. *Physical Chemistry Chemical Physics* **2016**, *18*(46), 31904-31913.
35) Cost reduction of [EMIM]acetate: https://proionic.com/bestseller/EMIM-OAc.php

36) Iolitec reactor news: https://cen.acs.org/materials/ionic-liquids/time-ionic-liquids/98/i5?utm_source=NonMember&utm_medium=Newsletter&utm_campaign=CEN
37) Cao, Y.; Zhang, R.; Cheng, T.; Guo, J.; Xian, M.; Liu, H., Imidazolium-based ionic liquids for cellulose pretreatment: recent progresses and future perspectives. *Applied microbiology and biotechnology* **2017**, *101*(2), 521-532.
38) Moyer, P.; Smith, M. D.; Abdoulmoumine, N.; Chmely, S. C.; Smith, J. C.; Petridis, L.; Labbé, N., Relationship between lignocellulosic biomass dissolution and physicochemical properties of ionic liquids composed of 3-methylimidazolium cations and carboxylate anions. *Physical Chemistry Chemical Physics* **2018**, *20*(4), 2508-2516.

Chapter 2. Lignocellulosic biomass – plant cell wall structure

Lignocellulosic biomass has been proposed as a potential source for production of renewable bioenergy and polymer products. Unlike petroleum-based products, lignocellulosic biomass from bioenergy crops, agricultural and forest residues, and municipal waste, produced from atmospheric CO_2, is a renewable source. Hence, chemicals and products generated from biomass are potentially carbon neutral. Polymers are made up of identical molecules connected through strong chemical bonds and have a wide variety of textures, permeability and strength and hence their broad application in chemical, physical and biological fields. However, most of the currently utilized polymers are produced from fossil fuel. Due to the long-term environmental impact caused by non-sustainable production of polymer products from fossil fuels alternate sources of polymers are pursued as viable option.

2.1.Biomass polymers

The three polymers of lignocellulosic biomass are cellulose, hemicellulose and lignin. The proportion of each of these components varies in different kinds of plants species. The table below lays out the general ranges of these components which are adapted from references.[1-7]

2.1.1. Cellulose

Cellulose constitutes to about 35-50% of plant cell wall and it is the most abundant biopolymer on earth. It is a linear homopolymer with individual anhydroglucose units linked via 1,4-β glycosidic link (Figure 2.1). The extensive inter and intra molecular hydrogen bonds (H) present in cellulose impart cellulose many unique and physical properties.[8] However, this same H-bond network makes cellulose insoluble in common solvents such as water.[9] The length of cellulose chains is obtained in terms of degree of polymerization (DP).

Table 2. 1. Composition of hardwoods, softwoods, switchgrass and corn stover

Chemical composition of lignocellulosic biomass (% dry basis) *			
	Cellulose	**Hemicellulose**	**Lignin**
Hardwoods	40-55	24-40	18-25
Softwoods	45-50	25-35	25-35
Switchgrass	32-37	21-27	18-21
Corn Stover	36-41	26-35	17-21

*% do not add up to 100% due to the presence of other constituents like ash and extractives

The DP is then used to calculate molecular weight either as number average molecular weight (Mn) or weight average molecular weight (Mw) of cellulose. In order to analyze DP of cellulose, it must be isolated from native source. Gel permeation chromatography (GPC) and viscometry are the two common methods to calculate DP of cellulose. However, due to derivatization process used in both the techniques cellulose undergoes certain amount of degradation. Viscometric measurements of cellulose DP were found to align closer to the native wood cellulose DP. The DP values of agricultural residues, hardwoods and softwoods were found to range from ~ 925 to 5000.[10]

Cellulose has a hierarchical structure in plant cell wall. Individual glucan strands are laterally arranged in parallel configuration to form microfibrils. The cross-sectional area of cellulose fiber is estimated to be between 2 to 10 nm.[11] Cellulose microfibrils have distinct crystalline and amorphous regions, which interact with hemicellulose and pectin. The common representation for cellulose microfibril has been a hexagonal arrangement of 36 chains in a "rosette" shape, based on transmission electron microscopy (TEM).[12] But more recently, studies using solid state nuclear magnetic resonance (ss NMR), small angle neutron scattering (SANS), wide-angle X-ray scattering (WAXS) and polarized infra-red (IR) spectroscopy have revised the number of chains to 18-24 chains.[13, 14, 15] The 18-chain microfibril model fits best with genetic results indicating concurrent expression of three cellulose synthase (CESA) genes. However, certain structural details of cellulose remain unclear. At the glucan chain level, the orientation of hydroxymethyl group (CH_2OH) at the C6 position remains unresolved. Based on the models generated using X-ray diffraction studies of cellulose, the hydroxymethyl group can have three possible orientations, which are gauche-gauche (gg), gauche-tauche (gt) and tauche-gauche (tg). While past studies

implied a single orientation (tg) for the hydroxymethyl group, more recently it was suggested that the group adopts different orientations on cellulose surface (gg) versus cellulose core (tg).[16, 17, 18]

Cellulose is semi-crystalline in nature and based on the variations in the unit cell structure, is classified as cellulose I (Iα and Iβ), cellulose II, cellulose III (III_1 and III_{11}) and cellulose IV (IV_1 and IV_{11}). The most common and the oldest use of cellulose has been in the paper and pulp industry. As cellulose is made up of glucose, hydrolysis of cellulose has been extensively studied to obtain monosugars to make products such as hydroxy methyl furfural (HMF). The crystalline nature and lack of solubility of cellulose in water are the two major impediments in the total utilization of cellulose.

2.1.2. Hemicellulose

Hemicellulose is another carbohydrate-based polymer in plant cell wall. However, unlike cellulose, it is not chemically homogeneous. Hemicellulose backbone is made up of either homopolymers or heteropolymers linked by 1,4 glycosidic bonds or 1,3 glycosidic bonds. The sugars that make up hemicellulose include pentoses (such as xylose, rhamnose and arabinose), hexoses (glucose, mannose and galactose), and uronic acids (4-o-methyl glucuronic, D-glucoronic and D-galactouronic). Hemicellulose has short branches in its structure, and some have a certain degree of acetylation. Hemicellulose differs in the composition across different species of plants.[21, 22] Softwoods predominantly contain glucogalactomannan, while xylan is the major hemicellulose in hardwoods (Figure 2.3).[23, 24] The molecular weight of hemicellulose is lower when compared to cellulose and the short branches can be easily hydrolyzed. Hemicellulose is widely used as film coatings of food, additive to plastics and in food industry as emulsifiers.[25-27]

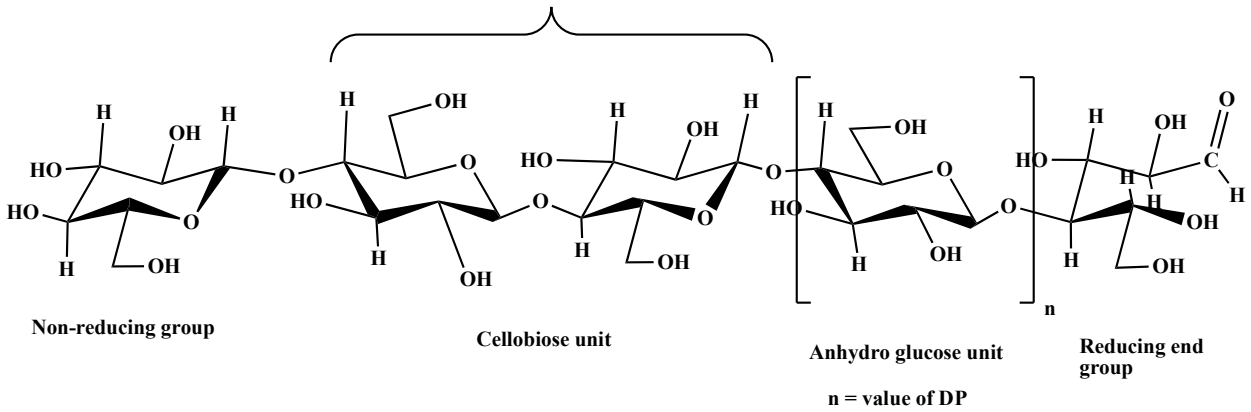

Figure 2. 1. Repeat unit in cellulose.

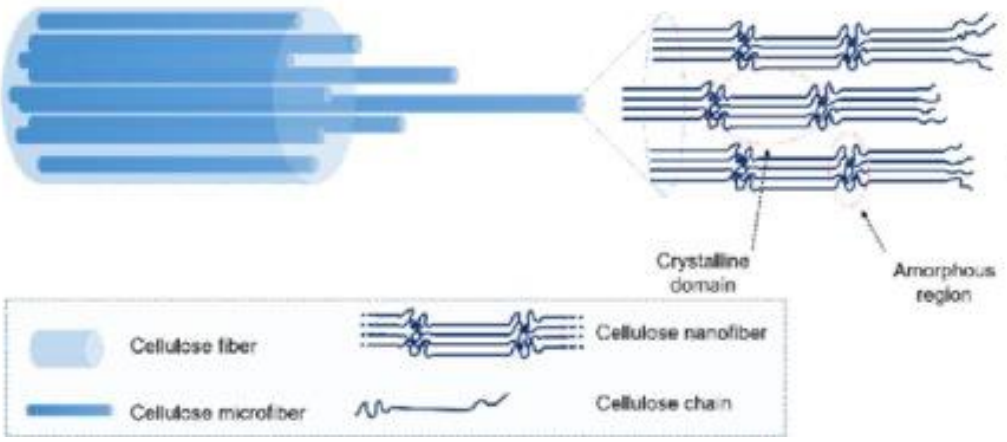

Figure 2. 2. Hierarchical structure of cellulose (19).

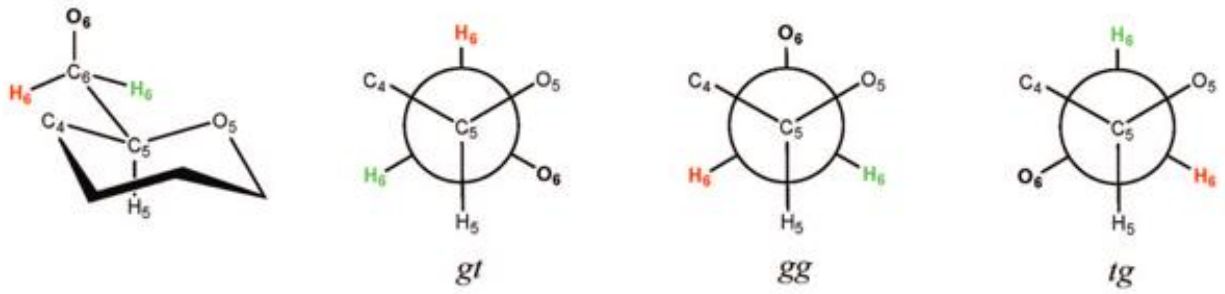

Figure 2. 3. The three most probable positions of the hydroxymethyl group of cellulose (20).

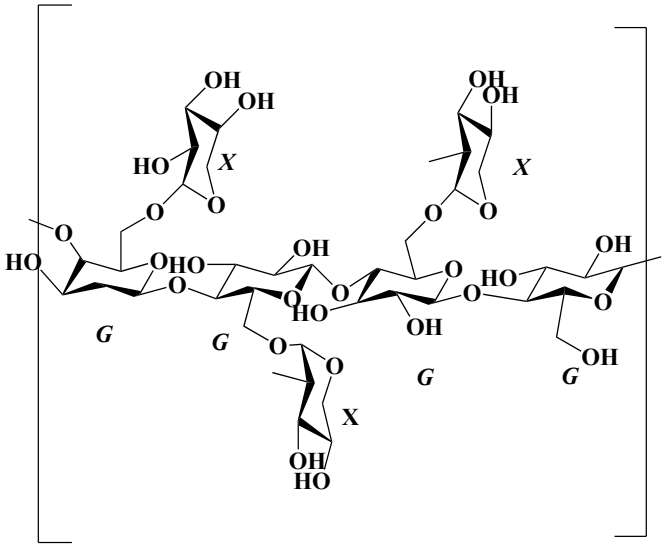

X = xylose G= glucose

Xyloglucan

Figure 2. 4. Repeat units in xyloglucan, galactoglucomannan and arabinoglucuronoxylan.

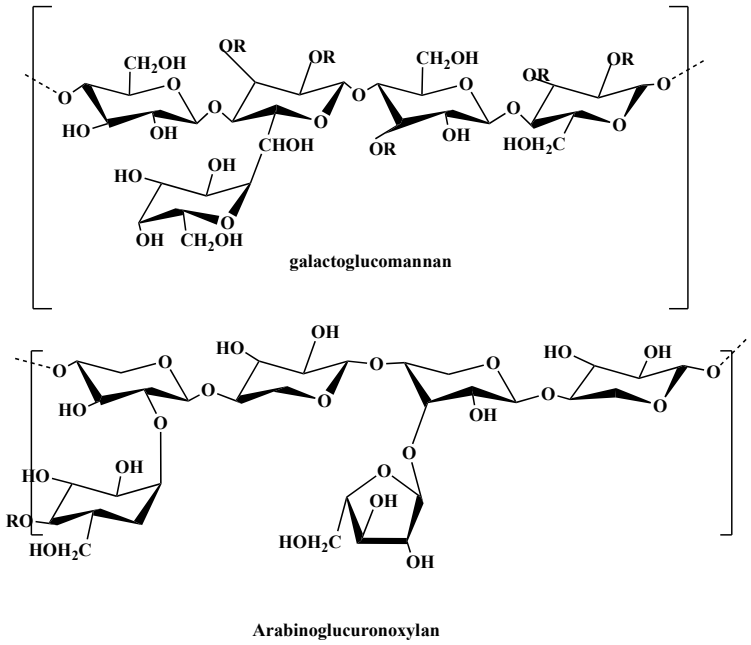

Figure 2. 4. Continued

2.1.3. Lignin

Lignin is compositionally different from cellulose and hemicellulose; it is an aromatic polyphenolic compound. The presence of lignin is critical to the plant cell wall as it imparts structural support, impermeability and resistance against microbial attacks.[28] The three major precursors involved in lignin synthesis are coniferyl alcohol (guaiacyl propanol), coumaryl alcohol (p-hydroxyphenyl propanol), and sinapyl alcohol (syringyl alcohol). Alkyl-aryl, alkyl-alkyl, and aryl-aryl ether bonds link these phenolic compounds together (Figure 2.4). The alcohols have different functional groups attached to them and alter the lignin structure significantly during the isolation process.[27] At present the utilization of lignin for producing value-added products is a crucial element for realizing a budget friendly biorefinery.[29] Lignin fibers and its use as an expander in lead storage batteries are potential applications of isolated lignin.[30, 31]

2.2.Structure of plant cell walls

Plant cell walls are hierarchically organized, starting from polysaccharide components of biopolymers.[32] The two main forces that guide the arrangement of polymers are molecular level interactions and spatial organization. Despite the recent progress on cell wall composition, our knowledge on the microstructure of plant cell walls remains limited. In the next section the main aspects pertaining to the plant cell walls are discussed.

Cell walls are an important characteristic feature of plants capable of performing a variety of functions, such as provide mechanical strength, serve as exoskeleton to provide shape and withstand high turgor pressure, and function as diffusion barrier.[33] To perform such varied functions, over the years plant cell walls have evolved into a complex and dynamic system. Fundamentally plant cell walls are classified into two major types: primary and secondary cell walls.

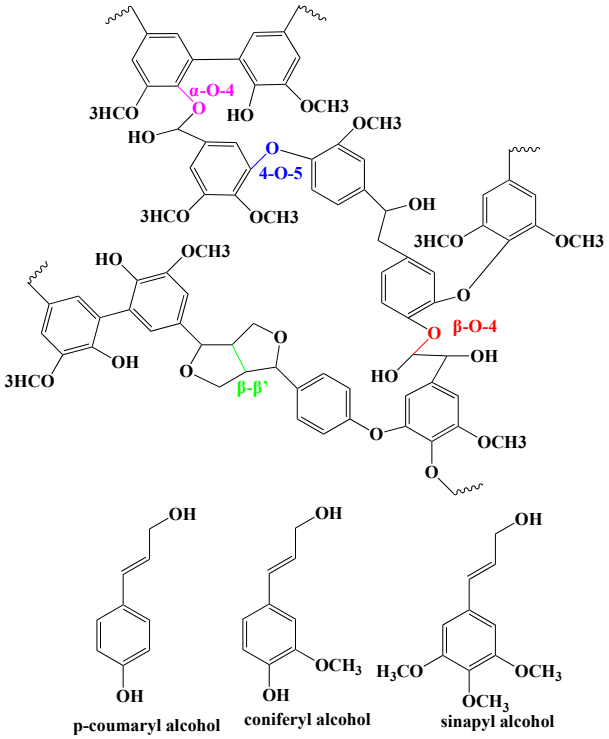

Figure 2. 5. Structural units of lignin and lignin structure with main linkages.

2.2.1 Primary cell wall

Primary cell walls are present in young growing plants (young leaves, root tips or shoots). It is composed of cellulose (25%), hemicellulose (25%), pectin (35%) and 1-8% structural proteins on a dry weight basis.[34, 35] Primary cell walls also contain significant amount of water.[36] Cell adhesion, signal transduction, and cell wall structural integrity are some the main functionalities of primary cell wall.[34] Cellulose embedded in matrix polysaccharides and glycoproteins are the main components of primary cell wall.[35]

Primary cell wall assembly

One of the earliest interpretations of primary cell wall was of that of macromolecular composite of covalently linked domains.[37] The idea of covalent or non-covalent interactions between polymers is central to any model, as many of the matrix molecules of wall polymers are soluble in aqueous medium but the cell wall itself is not. Thus, later models focused on understanding the extent of covalent interactions between the polymeric components.

To account for the mechanical extensibility and flexibility, the early matrix model was replaced with the much widely accepted "tethered model".[38-41] As per the tethered model, hemicellulose (xyloglucan or arabinoxylan) binds strongly to cellulose microfibrils (coating them) and functions as a cross linker between two cellulose microfibrils. The evidence for such tight network was realized from a sequential extraction process. The residual wall material was found to contain glycosyl residues that are representative of both cellulose and hemicellulose, suggesting a strong association between these macromolecules.

The tethered model was called into question when multidimensional solid-state NMR studies (ss NMR) indicated that only a small proportion of xyloglucan was in contact with cellulose.[42] Additionally, an Arabidopsis double mutant that lacked xyloglucan in cell wall exhibited only

slight alteration in growth. When biomechanical studies were performed on the mutant cell walls, the creep essays did not show significant alteration. The cell walls of the mutants were more sensitive to treatments that removed pectin and xylan, implying a prominent role for polymers other than xyloglucans.[43] A more recent opinion is that cell wall pectin is linked more extensively to cellulose than xyloglucan. Few NMR studies have confirmed close proximity of pectin and cellulose. When up to 40% of pectin were removed, NMR data implied a close contact between cellulose and pectin suggesting the interaction between pectin and cellulose to have a more functional role. Further evidence from *in vitro* experiments confirmed association of pectins (with arabinan and galactan) with cellulose sidechains.[44] Another study confirmed the covalent interactions between pectin and cellulose utilizing bacterial cellulose.[45] The reason for the association was hypothesized due to non-covalent and physical entrapment between bacterial cellulose and pectin. More recently, pectin and xyloglucan interactions were confirmed by ss NMR.[46] The tethered model versus the new model of primary cell wall are shown in figure 2.6.

In the past five years, by focusing on the concepts of cell wall softening and extension as two distinct phenomena, great progress has been made to understand the structure of primary cell wall.[47] When cell wall degrading enzymes that remove cellulose were utilized, cell wall softening but no extension was observed.[48] On the other hand, when cell walls were treated with xyloglucanase and cellulase, there was increase in cell wall extension, but no softening was observed.[49] Atomic force microscopy (AFM) was utilized to show the viscoelasticity of the matrix as the basis of cell wall enlargement.[50] More studies on cell wall creep assays continue to provide evidence for plant cell wall models.[51] The current version of the primary cell wall structure is shown in Figure 2.7.

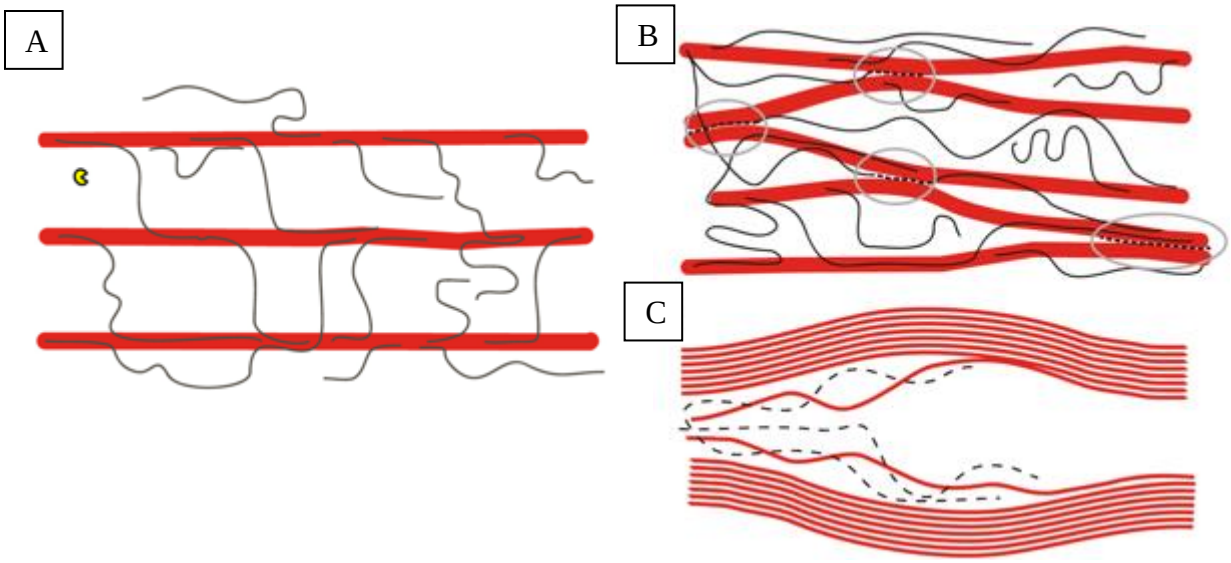

Figure 2. 6. Cartoon of tethered model (A) of primary cell wall. Xylogulcans (thin black strands) bind to surface of cellulose (thick red rods). (B) Revised cartoon of primary cell wall (right). The thick lines are cellulose fibrils and thin black lines are xyloglucan. The black dashed line (highlighted with gray circles) shows the load bearing xyloglucan acting as the molecular binders between two cellulose strands. (C) A closeup of the hypothetical load bearing junctions. (47)

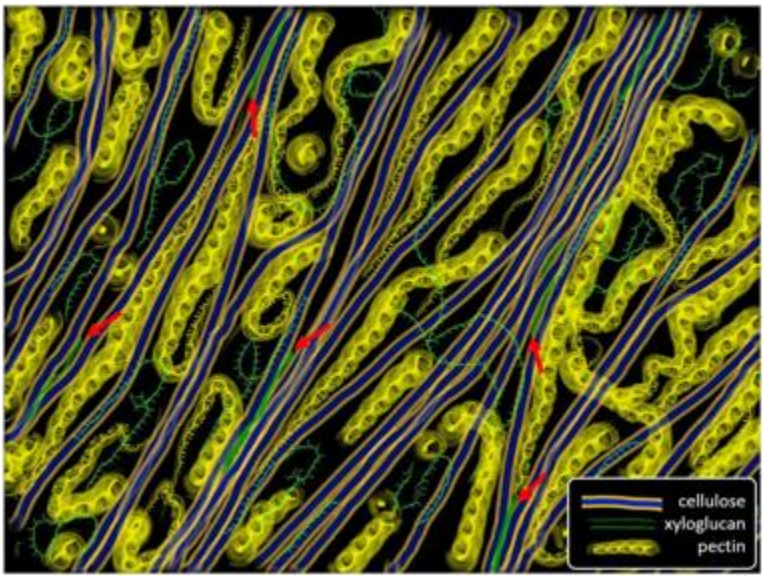

Figure 2. 7. The current version of primary plant cell wall developed based on the AFM, mechanical studies of cell walls, solid state NMR and field emission scanning electron microscopy. Cellulose microfibrils are represented as thick rods with hydrophobic (blue) and hydrophilic (orange). Pectins (yellow) with coiled structures fill the space between cellulose microfibrils and bind to hydrophilic surface of cellulose. Xyloglucan is found in two different conformations: extended form at hydrophobic surfaces of cellulose and solvated coiled conformations. (48)

2.2.2. Secondary cell wall

Secondary cell walls provide strength and rigidity to plant tissue and are formed inside of the primary cell wall.[52] They are made of higher amounts of cellulose and large amount of lignin, accounting for almost 60 % of the secondary cell walls. A variety of cross links is present between lignin and other cell wall polysaccharides, referred to as lignin carbohydrate complexes (LCC's).[53] Based on the woody species secondary cell walls hemicelluloses include xylans glucuronoxylans and glucomannans. In addition to these polymers, secondary cell walls also contain glycosylated proteins and small amounts of minerals.

Secondary cell wall assembly

Similar to primary cell walls, secondary cell walls have a composite structure with cellulose surrounded by the matrix polymers, i.e., hemicellulose and lignin, which is absent in the primary cell walls.[54] Secondary cell walls are critical for plant growth and development. These type of cell walls are present in conducting tissues of plants playing a main role in the transport of water and nutrients. Lignin mainly provides mechanical strength and cell wall rigidity for the secondary cell walls. Arabinoxylan, xylan, glucoronoxylan and glucomannans make up the hemicelluloses of secondary cell wall. In contrast to the primary cell wall, secondary cell walls have lower water content and cellulose fibers are oriented with directionality. Secondary cell walls are further divided into S1, S2 and S3 layers. Based on the viscoelastic and viscoplastic behavior of wood it is estimated that, similar to biomechanical spots in primary cell walls, loosely aggregated cellulose microfibrils are coated with disordered regions of hemicellulose and lignin in secondary cell walls.[55] NMR studies have confirmed the interactions between lignin and cell wall polysaccharides.[56]

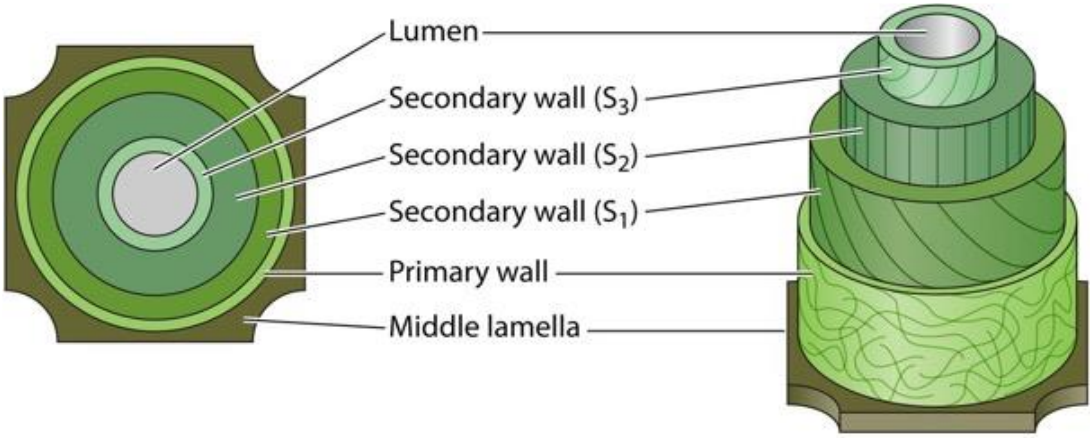

Figure 2. 8. A pictorial representation of different layers (S1, S2 and S3) of secondary plant cell wall (57)

2.3. Lignin carbohydrate complexes (LCC's)

In the context of plant cell wall structures a discussion on lignin carbohydrate complexes (LCC) is warranted. The proposed structures of plant cell wall imply that the biomass polymers do not exist in their own domain. The physical and chemical interlocking of polymers results in the formation of different kinds of lignin-carbohydrate bonds, a specific subset of these bonds is speculated as the basis for the existence of lignin carbohydrate complexes (LCC).[58] Five different kinds of bonds are suggested between lignin and carbohydrates of plant cell wall namely, phenyl glycosides (PG),[59-63] benzyl ethers (BE),[64-68] γ-esters (GE),[65,69-72] ferulate/coumarate esters (FE/CE) [73-81] and hemiacetal and acetal linkages [82] (Figure 2.9). Low yield of milled wood lignin, the presence of residual lignin in sulfite pulps and delignified softwood kraft lignin suggest that lignin might be covalently bound to sugars of biomass. [83, 84] In addition to milled wood extraction, acid and alkali hydrolysis methods have been beneficial in understanding LCC's. [85, 86] Although hydrolysis methods are useful, the native structure of LCC is lost during the process having been modified either to a sequential or selective extraction methods.[87] Liquid state 2D NMR has been one of the most effective tools by far to gain insights into LCC structure. [88-90] More recently, biomimetic synthetic approach of lignin has been beneficial in understanding LCC's structure as well.[91] When a lignin analogue commonly known as dehydrogenation polymer (DHP) was synthesized in presence of glucuronoxylan, an NMR signal indicative of the presence of γ-ester was observed. However, a similar ester signal was not noted in presence of glucuronic acid.[92] Despite several indications, the existence of LCC's cannot be confirmed due to the multi-length scale and complex nature of plant cell walls that pose as a major barrier for isolation protocol. Additionally, low resolution of current techniques is the another limiting factor to gain insights into native LCC structure.

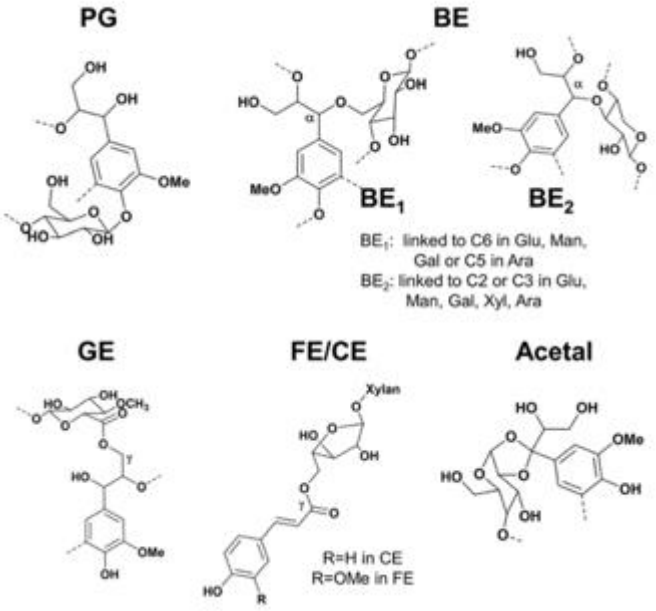

Figure 2. 9. The five different types of LCC's proposed in the woody biomass and grasses. PG = phenyl glycosides, BE = benzyl ethers, GE = γ-esters, FE = ferulate esters and CE = coumarate esters.

2.4. Lignocellulosic biomass pretreatment

The amorphous matrix polymers, hemicellulose and lignin surround cellulose microfibrils and impart plant its natural recalcitrance. Thus, to gain access to cellulose several thermochemical pretreatment methods have been developed. For efficient breakdown of the extensive network present in lignocellulosic biomass, a wide range of solvents can be employed. The physio-chemical change brought about by the use of either a chemical or mechanical process is known as pretreatment. The key objectives of pretreatment are to 1) gain accessibility to cellulose which can be further converted into sugars by enzymatic hydrolysis along with its crystallinity reduction, 2) remove lignin for further processing, and 3) hydrolyze hemicellulose for further fermentation.

Kraft pulping, a form of chemical pulping, is the oldest known form of chemical treatment of lignocellulosic biomass. In this process, wood chips are treated with aqueous sodium hydroxide and sodium sulfide at 170 ˚C for 2 h. Lignin is chemically modified by the hydroxides and hydrogen sulfide ions into the water-soluble fraction.[93] The residual liquor obtained during the process is known as "black liquor", a solution containing lignin, sulfated compounds, sodium salts and hemicellulose-derived molecules. Production of high value products from this black liquor is difficult due to two main reasons. The exact composition of the black liquor is difficult to determine and a multistep separation process is necessary to remove waste leading to low yields of lignin. Therefore, the primary use of the liquor has been for combustion purposes and the recovery of the process chemicals. High energy consumption, low cellulose pulp yields and lack of hemicellulose recovery are the major drawbacks of the kraft pulping process. Many other pretreatment approaches have since been developed and have been classified into four broad categories of physical, chemical, physiochemical and biological pretreatments. A few examples of each kind are listed in Figure 2.10.

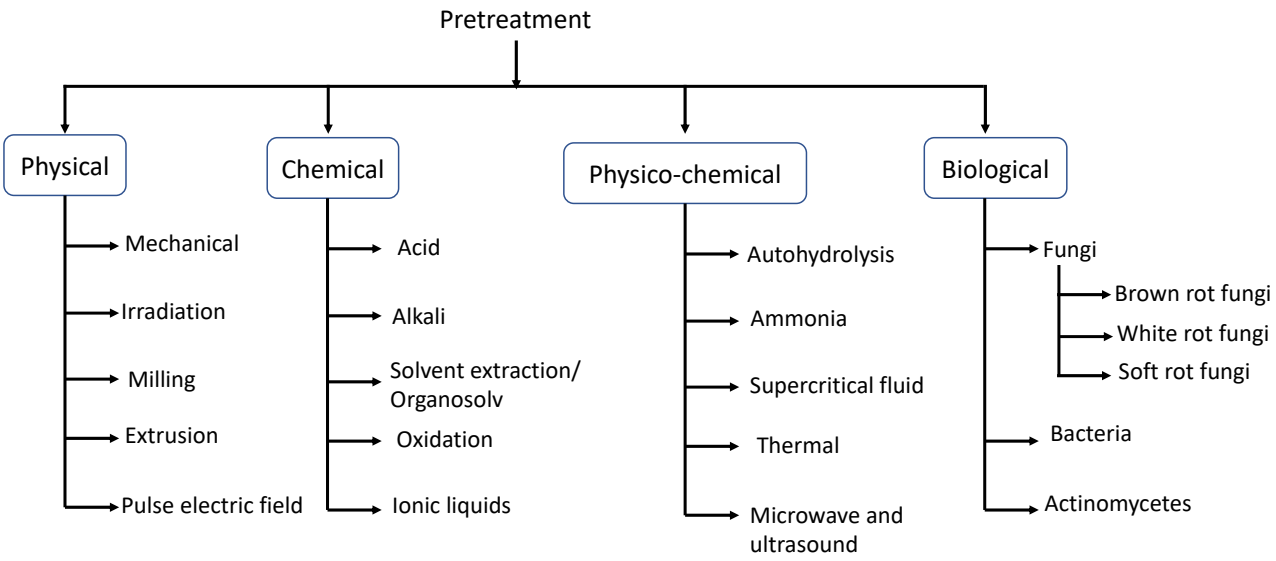

Figure 2. 10. Different kinds of pretreatment for biomass.

2.5. Lignocellulosic biomass fractionation

Most of the pretreatment methods are designed around cellulose accessibility for biofuel production. However, lignocellulosic biomass polymers have potential to be utilized as value added products and chemicals, similar to the utilization of crude oil. Therefore, existing pretreatment techniques were modified to obtain all the three major polymers of biomass either in their native form or as fractions by the process known as fractionation. Aliphatic/aromatic alcohols (organosolv), γ-valerolactone, tertahydrofuran and ionic liquids are examples of solvents commonly used for fractionation. In addition to being designated to as biomass fractionation these processes are referred to as solvent liquefaction or modern pretreatment technology. In the following section important details and specific differences between these solvents are presented.

2.5.1. Organosolv

Organosolv fractionation process uses aqueous organic solvents along with catalytic amounts of acid to separate lignocellulosic biomass components into two main streams: cellulose and lignin. Organosolv process is versatile where aliphatic (ethanol and methanol), aromatic (phenol), and polyols (glycerol) are used. During the process, a cellulose-rich fraction, a lignin fraction, and a water-soluble fraction containing sugars (mainly hemicellulose-based sugars), acid soluble lignin, carbohydrate degradation products, organic acids, and other components are obtained. Lignin isolated during the process can be transformed into high value chemicals. However, hemicellulose is not recovered through the process as it is associated with other degradation products in the water-soluble phase. Ethanol and methanol are most commonly used alcohols for organosolv process.[94] More recently n-butanol and acetone are also used for organosolv process to extract high purity fraction lignin.[95, 96]

To address the shortcoming of hemicellulose recovery in traditional organosolv method, Black and co- workers at National Renewable Energy Laboratory (NREL) used methyl isobutyl ketone (MIBK) along with aqueous alcohol to isolate all three polymers of biomass under "Clean Fractionation" (CF) technology.[97] During the CF process biomass is treated with a ternary solvent mixture (MIBK, ethyl alcohol and water) in the presence of an acid catalyst. Lignin and hemicellulose are extracted into ternary solvent layer, leaving cellulose as undissolved solid. In the subsequent step, when the organic phase is treated with water, hemicellulose is precipitated out leaving organic lignin portion.[98] The acquired hemicellulose fraction can be utilized for synthesis of chemicals such as furfural. Although, the organic solvents utilized in this organosolv process are either available as bulk commodity chemicals or can be procured as products from renewable sources, prohibitive costs, low energy efficiency and corrosion issues continue to be the major roadblocks that limit large-scale adoption of organosolv process.

2.5.2. γ-valerolactone

γ-valerolactone (GVL) is a cyclic ether with 5 carbons (valero).[99] Similar to alcohols used in the organosolv process, GVL is stable at room temperature and can be synthesized from levulinic acid, a product of cellulose. Horvath has performed preliminary studies on GVL, wherein its utility as green processing solvent was showcased.[100] In 2014, Luterbacher and colleagues have developed a lab scale set up using GVL to isolate sugars from biomass.[101, 102] With 80/20 GVL/water in presence of catalytic amounts of mineral acid (0.05% sulfuric acid) 90-95% of biomass polysaccharides were recovered as furfural, 5-hydroxymethyl furfural and levulinic acid. Further, for all the three types of biomass utilized in the study, the 80/20 GVL/water system achieved >80% C5 and C6 sugar isolation without any need for additional separation processes.[101]

2.5.3. Tetrahydrofuran

THF is a polar ether that can be sustainably produced from furfural, a product of hemicellulose. In earlier research THF was used as a solvent to dissolve kraft lignin and methylated lignin. Similar to GVL water system, THF water system was developed to fractionate biomass efficiently at lower temperature. Briefly, in a cosolvent enhanced lignocellulosic fractionation (CELF), THF water mixture with minor amount of acid (<0.05%) fractionates biomass to recover about 80-90% lignin and >95% hemicellulose sugars in solution.[103, 104] The remaining solids are converted into sugars in high yields. The fractionation process is likely the result of varied chemical and physical interactions similar to the ones noted for GVL-water system. Studies using molecular dynamic simulations revealed that THF functions as a good solvent towards lignin unlike water.[105] Further, it was also hypothesized that THF-water system facilitates cellulose separation by increased contact with the cellulose hydrophobic surface.

2.5.4. Ionic liquids

Ionic liquids (ILs) are the other set of fractionation solvents utilized in the field of biomass processing. ILs are liquid salts and they have unique properties such as low vapor pressure, high boiling point and high thermal stability. Several different combinations of ILs have been utilized for dissolution of either biomass or individual polymers (cellulose and lignin). It is believed that ILs bring about dissolution by disrupting the network of H-bonds.[106, 107, 108, 109] Similar to GVL, IL solvents reduce the activation energy barrier for hydrolysis of crystalline cellulose.

In summary, the complex and reinforce structure of lignocellulosic biomass necessitates a "pretreatment" method. The classic pretreatment methods are centered around lignin separation and carbohydrate extraction. This initial approach is replaced with the concept of isolating and valorizing all three main polymers simultaneously. Modern pretreatment methods using THF,

GVL and ILs offer an innovative route for biomass polymer separation and utilization. However, both THF and GVL suffer from the drawbacks associated with safety and sustainability issues. ILs on the other hand offer an environmental benign option for biomass processing under milder processing conditions. Owing to these advantages, going forward the reminder of the thesis will only focus on IL biomass processing technologies.

2.6. Lignocellulosic biomass and ionic liquids

ILs are liquid salts with organic natured cation and either organic/inorganic based anion. Due their unique composition, ILs have properties of solids such as low vapor pressure and high thermal stability but with ability to flow like a liquid.[110] The physical properties of ILs are manipulated by altering constituent anions and cations. ILs have a variety of applications in the fields of pharmaceuticals, energy storage (batteries) and membrane filtration, to cite a few.[111, 112, 113] So far in the literature over 300 unique ILs have been reported.[114] By altering physiochemical parameters such as time and temperature, ILs can be utilized in the field of biomass processing for pretreatment, fractionation, activation, and complete dissolution for product production (Figure 2.11).

2.6.1. Pretreatment of biomass in ionic liquids

ILs have been utilized for chemical pretreatment of biomass at temperatures above 100 °C. Similar to other pretreatment options such as dilute acid, IL pretreatment is used to separate lignin and hemicellulose from cellulose.[115] The major changes brought about by IL pretreatment are reduction in cellulose crystallinity, increase cellulose accessible surface area, increased cellulose porosity and digestibility. These changes significantly increase the hydrolytic activity (50-fold) of cellulose.[116]

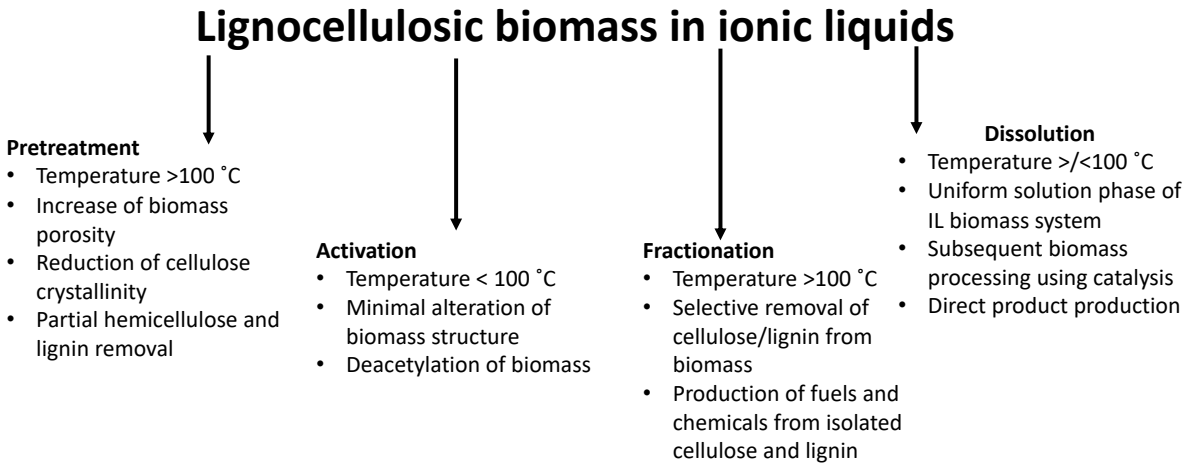

Figure 2. 11. Four different ways in which ILs are used in the field of biomass processing.

When IL pretreatment was compared with the most commonly used dilute acid pretreatment (DAP) it was observed that IL-pretreated biomass was far less crystalline than dilute acid pretreated biomass. The authors speculated that IL was more effective than dilute acid due to specific cation-anion interactions with biomass.[115, 117] More recently, using small angle scattering techniques finer structural details such as alteration of surface roughness after pretreatment was estimated.[118] ILs such as 1-ethyl-3-methylimidazolium acetate ([EMIM]acetate), 1-allyl-3-methylimidazolium acetate ([AMIM]acetate) and 1-butyl-3-methylimidazolium chloride ([BMIM]Cl) are frequently used for biomass pretreatment.[119, 120] Acetate set of ILs are found to be most efficient in dissociating cellulose from biomass, although the true nature of these favorable interactions remains unresolved.[119] Similar to other chemical and biochemical pretreatment methods, IL pretreatment of biomass mainly targets isolation and conversion of cellulose fraction. Additionally, due to high temperatures (>150 °C) residual hemicellulose and lignin fractions are severely depolymerized, thus hampering their utilization. In recent times a milder version of IL pretreatment known as IL activation has gained momentum.

2.6.2. Activation of biomass in ILs

IL activation is similar to pretreatment with one major distinction in the processing conditions.[121] IL activation is generally performed at temperatures below 100 °C. During the activation process, biomass (5-10 wt.%) is dissolved and stirred in IL for a specific amount of time (3-6 h). The activated biomass is regenerated almost in its entirety upon addition of anti-solvent such as water, thus preserving the carbon content during the process. Acetyl groups of hemicellulose are cleaved during the process, with minimal changes to lignin structure.[122] The regenerated biomass is then subjected to enzymatic saccharification for isolation of sugars and lignin with minimal loss of either hemicellulose or lignin. Although the mono sugar yields are high

after the saccharification step, the amount of water needed to regenerate the biomass drives the cost of IL- activation process significantly higher.

2.6.3. Fractionation of biomass in ionic liquids

Biomass fractionation through ILs is targeted to achieve the isolation of all three components of biomass in high purity by employing a multistep approach.[123, 124] Utilizing autohydrolysis, IL activation and enzymatic saccharification, Wang et al. isolated high purity (>90%) lignin.[125] De costa Lopes et al. performed pretreatment and fractionation of wheat straw (5 wt%) using [EMIM]acetate.[126] Complete dissolution of wheat straw was achieved at 110 °C/120 °C in 6 h. To the dissolved mixture, sodium hydroxide was added to separate out the carbohydrate solid fraction from lignin. To isolate hemicellulose and cellulose from the solid fraction two additional extraction steps were needed. The isolated biomass polymers could be used either for ethanol production or for the synthesis of value-added products and chemicals.[127, 128] Currently, IL fractionation coupled with either acid hydrolysis or dehydration is used to isolate and utilize all the three main biopolymers of biomass.[129, 130] Although, IL fractionation technique ensures the recovery of all three biopolymers, the multistep approach hinders the product yields also contributing to additional costs. [131]

2.6.4. Dissolution of lignocellulosic biomass in ionic liquids

The fourth way in which ILs are used for biomass processing is for complete dissolution, i.e., uniform one phase system of biomass-IL solution, which allows for direct product processing such as films and fibers to be utilized in textile and packaging industry.[132] ILs are known to efficiently disrupt the hydrogen bonds in ILs, thus aiding in completer dissolution of biomass. The primary advantage of complete dissolution is the aspect of preserving the carbon content of biomass. Although, the low mass loadings of the process continue to limit the efficiency of the process.

In 2002, dissolution of cellulose and cellulose derivatives was observed in a series of 1-butyl-3-methylimidazolium ILs with various anions at 100 °C.[110] Scanning electron micrographs of regenerated cellulose revealed a significant morphological change with increased roughness of surface and conglomeration of fibers. Thin fibers and rods were prepared from the cellulose/IL solution in aqueous medium. The authors hypothesized that chloride anion ILs were most effective in dissolving cellulose due to disruption of existing H-bonds in cellulose with new chloride hydroxyl H-bonds. In a following study performed by Zhang et al. a new IL 1-allyl-3-methylimidazolium chloride [AMIM]Cl was shown to dissolve up to 14.5% cellulose at 80 °C.[133] X-ray diffraction characterization of cellulose films revealed a significant reduction in crystallinity of cellulose and conversion of cellulose I to cellulose II, suggesting disruption of intra and intermolecular H-bonding in cellulose during dissolution process.

As the bulk of cellulose on earth is trapped in biomass, dissolution of biomass in IL would be beneficial as was demonstrated in the study performed by Fort et al.[106] Partial dissolution of 5 wt.% woody biomass in 1-butyl-3-methylimidazolium chloride [BMIM]Cl was observed at 100 °C for varying time lengths (2-24 h). ^{13}C NMR spectroscopic data of biomass revealed the dissolution of cellulose, lignin and hemicellulose. The cellulosic fraction of the biomass was regenerated upon the addition of an acetone-water mixture. The morphology of the cast cellulose films was similar to films cast from cellulose IL solutions. Complete dissolution (up to 8% w/w) of fine saw dust particles (0.1-2mm) was observed in [BMIM]Cl and [AMIM]Cl.[112] In addition to these two ILs, a new IL, 1-benzyl-3-methylimidazolium chloride [BZMIM]Cl, was shown to exhibit superior solubility which was reasoned to π-π interaction between the aromatic benzyl ring of the IL and the aromatic rings of lignin. A subsequent step of acetylation of biomass confirmed the dispersion of wood/biomass in IL. IL-regenerated biomass exhibited enhanced enzymatic

saccharification rate. Although the chloride anion ILs exhibit superior solubility capacity, these ILs are highly viscous and corrosive thus prompting the researchers to synthesize new class ILs.

Dissolution of different sized (0.125-1 mm) biomass (hardwood and softwood) was observed at 110 °C for 16 h in a new IL, 1-ethyl-3-methylimidazolium acetate ([EMIM]acetate).[134] Further when chloride IL [BMIM]chloride was compared with [EMIM]acetate, [EMIM]acetate was found to dissolve more biomass at identical processing conditions (98.5% vs 52.6%). Similar to previous studies cellulose rich fractions were regenerated from the IL-biomass system upon anti-solvent (acetone/water) addition. X-ray diffraction and scanning electron micrographs indicated a reduction in cellulose crystallinity. The superior solubility of [EMIM]acetate was surmised to the high basicity/ H-bond acceptor ability of the acetate anion when compared with chloride anion. Ease of synthesis, lower viscosity (compared with chloride ILs) and high solvating ability (cellulose and biomass) of [EMIM]acetate resulted in its extensive utilization in the field of IL processing.

The above studies illustrate that dissolution of biomass in ILs is a complex phenomenon with consequences such as dissolution/loosening of rigid network between the three main polymers, reduction in cellulose crystallinity and increase of surface roughness or porosity. The dissolution process is influenced by several physicochemical properties of ILs (viscosity, thermal stability) and various process criteria (biomass particle size, temperature/time effect), few of which are listed below.

2.7. Process criteria influencing biomass dissolution

2.7.1. Biomass type

Lignocellulosic biomass is broadly classified into three varieties: hardwoods, softwoods and grasses. The distinction between hardwoods and softwoods is not only based on botanical

differences, but also anatomical. Hardwoods have lesser amount of lignin compared to softwoods hence the lignocellulosic matrix of softwoods is more difficult to deconstruct than hardwoods with common organic solvents. Grasses like wheat straw, barley straw and cane bagasse have an extra layer of cell wall, strengthening the cell wall structure further. Initial cellulose dissolution studies were followed by dissolution of other polymers such as xylan, dextrose, and chitin. [135, 136] Rice straw,[137] switchgrass,[138] rice husk,[139] sugarcane bagasse,[140] Japanese beech[141] and corn stover [142] to name a few, exhibit solubility in variety of ILs suggesting the scope of these unique solvents.

2.7.2. Biomass particle size

Prior to dissolution of biomass in IL, size reduction of biomass is necessary as large pieces of wood take several weeks to dissolve.[106, 112] Theoretically the dispersion of IL would be much faster when the biomass particle size is smallest where surface area for IL dispersion is maximum. However, a study performed on dissolution of different particle sizes of rice straw suggested that there is an optimum size for maximum dissolution.[137] In a comparative study between ILs, [EMIM]acetate and [EMIM]chloride on different sizes of cotton stalks, it was observed that cotton stalk of small sizes were soluble in chloride IL while larger ones dissolved in acetate ionic liquid, suggesting varied action of the ionic liquids.[143] These studies thus, indicate that every IL may have an ideal biomass particle size at which interaction between the biomass and the IL is at an optimum level resulting in dissolution.

2.7.3. Water content in biomass and ionic liquids

One of the main drawbacks of ILs is that the majority of them are hygroscopic in nature. Vitz et al. monitored the effect of water content in ionic liquid towards dissolution and suggested aggressive drying of IL as a crucial first step for biomass dissolution.[144] Water content greater than

1% was found to strongly alter biomass dissolution. Along with ILs, biomass naturally contains a certain amount of water. Therefore, proper drying of biomass is recommended.

Chloride ILs are highly hygroscopic and thorough drying ensures a free anion available co-ordination with OH of cellulose thus, resulting in dissolution. On the other hand, if carboxylate ILs have high water content they would not have the H-bond acceptor capable of dissolution. However, recent studies suggested that ILs with 10-20% water content during pretreatment of cellulose are acceptable.[145] A more recent study exploring the nature of interactions between IL/ water system during the pretreatment process indicated that the action of 100% IL is similar to IL/aqueous system containing 50% or 80% of IL. It was observed that the proportion of IL to water determines the cellulose solubility, lignin/hemicellulose removal, cellulose accessibility, and enzyme digestibility.[146] Utilizing MD simulations, it was speculated that at higher water concentration the interaction energy of IL-water dominates over the IL-cellulose interactions thus, negatively affecting dissolution process.[147] More studies are underway to explore the true nature of interactions between IL and biomass in presence of water.

2.7.4. Solid to liquid ratio

The two main factors of biomass that determine the amount of biomass that can be dissolved in ILs are the chemical composition and the recalcitrant nature of biomass. Furthermore, amount of water in the biomass also determines the amount that can be accommodated in IL at specific conditions. When Sun et al. studied different concentrations of biomass in [EMIM]acetate, 5 wt. % solution was found to be optimal amount of biomass capable of diffusing in IL without any overcrowding problem.[134] In addition, agitation of biomass becomes difficult as the mass percentage increases. High temperatures and sonication treatments are recommended for highly viscous high mass load solutions. For corn stover, maple wood flour, poplar and switchgrass the

ideal solid liquid ratio of 33% (w/w) in IL [EMIM]acetate was proposed.[148] The authors hypothesized that at this ratio there are enough number of anions to co-ordinate with the hydroxyls of cellulose to bring about dissolution. More studies are underway to determine the optimum solid-liquid ratio for different natured biomass in various ILs.

2.7.5. Temperature and time influence

Temperature versus time used for dissolution is a delicate balance for achieving efficient dissolution of biomass in ILs. High temperatures for less time or mild temperatures for longer times theoretically should result in similar results. But past work done in this regard yielded mixed results which in part could be explained on the basis of possible degradation of cellulose and hemicellulose at high temperature.[149] Nguyen et al. reported increased solubility of rice straw in [EMIM]acetate for the first 24h at 130 °C, but after 48h the amount of regenerated cellulose decreased.[150] Along with cellulose degradation, IL stability and potential side reactions must also be considered when processing conditions extend into days. A linear increase in glucose recovery along with increased lignin solubility and higher diffusion rates of IL ([BMIM]chloride) were reported when temperature was increased from 60°C to 100°C for oil palm frond.[151] When wood powder was pretreated with [EMIM]acetate with varying times, the amount of extracted lignin increased from 40% (5h) to 85% (70h).[152] However, the amount of lignin extracted to cellulose degradation to diffusion rates of IL are implicitly related to the nature of biomass under study. Consequently, a systemic study showing the effects of variation in time and temperature for various ILs would help us answer some outstanding questions about biomass dissolution in ILs.

In conclusion, owing to the structural complexity of biomass, a significant number of factors influence the dissolution/dispersion of biomass in ILs. As the IL biomass processing field continues to evolve, the variability among these parameters will be better understood. In addition

to these process criteria, IL physical characteristics also influence the process of IL biomass dissolution. Three such factors are highlighted in the section below.

2.8. Physicochemical characteristics of IL influencing biomass dissolution

2.8.1. Viscosity

Understanding the physical properties of IL is critical as it can help us understand the nature of intermediate species present during the dissolution process. Viscosity, density and refractive index are few of the properties that can help us understand the ability of IL to facilitate mixing and phase separation. Viscosity of IL is a complex property dependent on a variety of factors.[153] Due to H-bond interactions between IL ion pairs, nano-sized domains are formed in ILs, effectively altering their fluid behavior.[154] Therefore, the fluid behavior of ILs is not only the result of the dispersive coulombic interactions but also due to the interactions between the nano-domains. Additionally, Van der Waals interactions between alkyl side chains give rise to viscous aggregates, further altering the fluid behavior of ILs.[155] In addition to the complex structure of ILs, owing to under reporting of the water and halide content and other contaminations during synthesis process in general, the reported viscosity values of the same set of ILs are not consistent across the literature. [133, 156]

Viscosity of ILs is sensitive to variation in molecular weight of solute, water content, halide content and solute concentration. As solute (cellulose/biomass) comes in contact with IL, swelling of solute molecules alters the viscosity of the IL. Temperature is another parameter that greatly alters the viscosity of ILs. For example, when processing temperature is increased by 10 °C, the viscosity of most ILs reduces by 50%.[157] Viscosity is also altered by anion/cation combination and nucleophilicity of anion. Chloride ILs are highly viscous when compared with acetate, formate and phosphonate ILs. The higher viscosity of chloride ILs is attributed to the substantial network

of H-bonds between the ion pairs. Despite this fact, most chloride ILs have high dissolving capacity towards cellulose and biomass; (cellulose solubilities: [BMIM]chloride >24 wt.%, [AMIM]chloride >20 wt.%, [EMIM]acetate>27 wt.% and [AMIM]formate> 20 wt.%) .[135] ILs are highly hygroscopic in nature. As with any viscous system, when water content increases, viscosity of IL decreases. However, using theoretical calculations it was shown that the reduction in viscosity is not linear, but three distinct regimes of varying viscosity exist for most ILs. Allyl side chain containing ILs such as [AMIM]formate and [AMIM]acetate have low viscosity compared with ethyl side chain containing ILs.[156] It is speculated that the free rotation of allyl side group is the probable reason for low viscosity.

Viscosity is one of the most frequent physicochemical characteristics used to discern the macroscopic solubility trends of ILs. Generally, based on the principle of mass transfer, it can be assumed that low viscous ILs will exhibit high solubility rates. Overall, the trend holds good with one exception of chloride anion ILs, such as [AMIM]chloride and [BMIM]chloride which exhibit exceptional solubility towards cellulose and biomass.[110, 133] This observation implies that, when solubility behavior is correlated to viscosity of IL, the water content of IL and a detailed chemical profile are necessary to ascertain the validity of result. Further, the exception also implies that solubility of biomass or its constituent polymers is brought about by a conglomerate of microscale interactions in conjunction with physical parameters such as viscosity.

More recently, research efforts are directed towards understanding the rheological behavior of cellulose-IL and biomass-IL solutions in order to identify suitable IL for direct product processing. Despite the complicated set of variables influencing viscosity of individual ILs, the behavior of cellulose/biomass IL solutions follows the basics of polymer physics i.e., with gradual increase of biomass/cellulose, shear thinning behavior and steady increase of viscosity are observed.[158, 159]

The viscosity of biomass-IL solutions is significantly higher than simple cellulose-IL solutions. The complex architecture of biomass is cited as the reason for the increased viscosity and limited flow behavior. In recent times, ternary setup with polar aprotic solvents such as dimethyl sulfoxide (DMSO) along with ILs is adopted for spinning of fibers from cellulose-IL solutions.[160]

2.8.2. Cation and anion combination

Perhaps the most unique feature of ILs is their composition, which is made of ions in entirety. Tetraalkyl ammonium, 1,3 di-alkyl imidazolium, pyrrolidium and tetraalkyl phosphonium cations, and halides, phosphonates, carboxylate/carbonate (acetate and formate) anions are the most commonly used combinations of ILs in the field of biomass processing. The traditional method of preparation for halide ILs is by combining alkyl halide and N-methyl imidazole, while carboxylate/carbonate ILs are synthesized via a metathesis reaction following ion exchange from halide ILs.[133] However, more recently, alkyl carbonate based synthetic route known as CBILS ® is gaining ground for synthesis of carboxylate ILs. [161]

Since the early report of cellulose dissolution in chloride ILs, understanding the roles of IL anion and cation has been the subject of many studies. As most of the IL anions are conjugate bases, their preferred mode of interaction is via a H-bond. In fact, it is due to the H-bond forming ability of ILs that the existing network of inter and intra chain H-bonds of cellulose/biomass is disrupted.[110] A linear relationship between anions of high H-bond basicity and high cellulose/biomass solubility further confirmed the role of H-bond interaction as the primary reason for dissolution. [162]

The role of cation remains an actively contested topic in the field of IL biomass processing. As primary and secondary plant cell walls have both hydrophobic and hydrophilic functional domains, the claim that only polar H-bonds as the only reason for dissolution cannot be valid. In addition to

the structural details, the variable action of the same anion with two different cations also implies that IL dissolution process could be influenced by both the cation and anion of ILs.[112] A quick literature review reveals that IL cation is assigned either a direct or a supporting role during IL dissolution. For example, using cellulose model compounds, formation of carbene intermediate species via cation was proposed.[163] However, in the case of cellulose IL systems carbene intermediates were not observed. Zavrel et al. speculated that the cations perform a supporting role of stabilizing H-bond (between anion and hydroxyl groups of cellulose) without offering significant experimental evidence.[164] Additionally, an "odd-even" effect of side chain on cation was reported, where cations with even numbered side chain have a participatory role in dissolution process when compared with odd numbered side chains.[165] Allyl side chain with odd number of carbons (3) proved to be an exception to this rule.[133] Therefore, understanding the specific role of IL cation continues to be actively a researched topic in the field of IL-biomass processing.

2.8.3. Solvation properties (Kamlet-Taft parameters)

Macroscopic solvent properties such as density and refractive index, microscopic intermolecular forces such as dipole-dipole interactions or electron pair acceptor – electron pair donor interactions and solvation ability are commonly referred to as polarity of solvents. By measuring the polarity of solvent, one will be able to understand the strength of interactions (solubility) between solvent and solute. Reichardt's E_T (30), Kamlet-Taft and Hildebrand are commonly used polarity scales for solvents.[166] In case of ILs, Kamlet-Taft parameters are the most commonly used and are made of three terms:

- π^*-Dipolarity/ polarizability effects
- α-Hydrogen bond donor
- β-Hydrogen bond acceptor

Kamlet-Taft parameters are obtained by measuring the absorbance values of ILs by adding dyes such as 4-nitroaniline and N, N-diethyl-4-nitroaniline.[167] α value is the measure of H-bond donating capacity of cation and β value represents the H-bond accepting ability of anion. The higher the values of α and β the greater the polarity of IL, and therefore the interaction/solvation ability of IL. Overall, a linear correlation is obtained between ILs with high cellulose solubility and higher H-bond basicity of anion (β value).[160] However, similar to viscosity and cation role there are exceptions to the correlation with chloride anion ILs as the most prominent examples.[168] No study thus far has been able to offer a rationale for the exception. The non-significant variation in α values of most commonly used cations also fail to explain the differences in interaction/solubility of ILs.[162]

The role of π^* is more complex, as the value is influenced by both the cation and anion. The pairing strength of IL is interpreted in terms of π^* value. Once again, a non-significant variation between the values makes it difficult to interpret and understand the differences between the ILs. In addition to IL ion pairs, alkyl side chain length on the cation is also shown to influence the β, α and π^* values. [169, 170] The solvation parameters are therefore useful to understand the differences in the solubility capacity of only few ILs (example halide vs acetate/formate). Other experimental techniques are needed to understand more subtle differences between the ILs. Solvation parameters of some of the most commonly used ILs are listed in Table 2.3 adapted from references. [156, 162]

2.9. Characterization of interactions between ILs and biomass polymers

The common step among the various biomass IL technologies is dissolution. While in this solution state, IL ion pairs interact with various functional groups (hydroxyl, acetyl, methoxy) of biomass polymers. These atomic-level interactions are often reflected as measurable macroscale changes such as increase of cellulose pore size, swelling of cell wall, peeling of individual cellulose

fibers from microfibril, reduction of cellulose crystallinity, enhanced saccharification rates and deacetylation of hemicellulose.[110, 111, 112, 116, 118, 140, 156, 171, 172, 173] In addition to the morphological changes, previous research has established that hydrogen bond (H-bond), Vander Waals, π-π stacking and electron donor acceptor complexes as some of the common type of interactions between biomass polymers and ILs.[110, 156, 174, 175]

The dissolution of biomass in IL is believed to induce changes locally and dynamically at a multiscale level. This process becomes more complicated, when changes in cellulose microfibril integrity and its interactions with hemicellulose and lignin must be accounted for at the same time. Hence, a suite of techniques spanning length scale from angstroms to microns are useful to gather the information on physical and chemical structural aspects of biomass. Our work has combined spectroscopic, scattering and rheological measurements to understand the interactions between ILs and biomass polymers. In the sections below fundamentals of each technique and their application in recent research are presented.

2.9.1. Spectroscopic techniques

Spectroscopic techniques such as solution state nuclear magnetic resonance (NMR) and attenuated total reflectance (ATR) infrared spectroscopy (IR) are easily accessible powerful techniques useful in understanding interactions between biomass polymers and ILs. The main advantages of spectroscopic techniques are minimum sample preparation, easy data acquisition, interpretation and analysis. Using solution NMR, information on dynamics (relaxation time), diffusion rate and change in chemical environment (chemical resonance) of IL ion pairs can be obtained. On the other hand, ATR-FTIR is a useful technique to assess the changes in biomass by measuring the functional group vibration stretching frequencies.

Table 2. 2. Kamlet-Taft parameters of some common ILs [156, 162]

IL	β (H-bonding donor ability)	α (H-bonding donating capacity)	π* (Polarizability effect)
[EMIM]acetate	1.07	0.50	1.03
[AMIM]chloride	0.83	0.46	1.17
[BMIM]chloride	0.87	0.47	1.10
[AMIM]formate	1.01	0.46	1.09
[BMIM]acetate	1.09	0.55	1.03
[AMIM]acetate	1.11	0.43	1.13
[EMIM](MeO)HPO_2	1.00	0.52	1.06

- ***Fundamentals of NMR***

NMR is a physical technique and in simple terms it can be described as follows. When an atomic nucleus with odd proton number, placed in an external magnetic field, is subjected to radio wave perturbation (at appropriate frequency), then it absorbs the radiation. Due to this absorption, the atomic nuclei align themselves against the external magnetic field. Whenever such nuclei transition back to its state original state, the excess energy is dissipated as thermal relaxation. It is this transition that is noted as the NMR signal of the atomic nuclei. In order to be utilized for NMR experiments the radiofrequency needs to have the following characteristics: 1) A unique frequency for each nucleus (e.g., ^{1}H, ^{13}C, ^{15}N), 2) dependency on the chemical environment of the nucleus and 3) susceptibility to the spatial location of the external magnetic field especially if the external field is not uniform.[176]

The NMR parameter chemical shift or chemical resonance is the direct consequence of the unique radiofrequency (gyromagnetic ratio) of each atomic nucleus. However, it also turns out that within the same nuclei the resonance condition (the energy needed to flip the spin) is at different frequencies. The primary reason for the difference is due to the different local magnetic field experienced by each nucleus in the molecule.

The reason for the local magnetic field can be understood on the basis of the simple electromagnetic theory. If a molecule with nucleus of interest ($^{1}H/^{13}C/^{15}N$) is put in the presence of an external magnetic field, electron currents perpendicular to the external magnetic field are created in the molecule (Figure 2.12). These currents create a small induced magnetic field that cancel out the effect of the external magnetic field and effectively shielding the nucleus. In general, this induced magnetic field is many magnitudes lower than the external field. In addition to the electronic currents directly around the nucleus, the molecule also has additional currents that

further increase the induced magnetic field. Despite these additional contributions the difference between the induced magnetic fields of nuclei of same atom are very small. Therefore, a reference signal is chosen, and the difference between the reference and position of nuclei of interest is measured as chemical shift or chemical resonance.[177]

The proton (^{1}H) or carbon (^{13}C) chemical shifts of IL ion pairs are a useful analytical tool to understand the change in chemical environment. Early on, in the field of IL research, it was realized that the chemical shifts of IL hydrogen/carbon atoms changed due to the IL anion composition, concentration of solute, alkyl group of IL cation and the solvent used to dilute IL.[178] By using regular and variable temperature (VT) ^{1}H NMR, a significant variation in chemical shift values of ring hydrogens was observed. These changes were inferred as due to H-bond formation between cellobiose hydroxyl groups and imidazolium cation.[179] Beside the NMR chemical shift variation, spin-lattice relaxation time measurements[180] and diffusion rate measurements (DOSY)[181] can also be used to understand the interactions between ILs and biomass polymers.

- ***Fundamentals of FT-IR***

Fourier transform infrared spectroscopy (FT-IR) is a versatile tool for measuring chemical compositional changes of solids and liquids. Similar to NMR, IR spectra are obtained quickly with little or no sample preparation. While NMR provides us with information on the chemical environment of atoms, IR examines the molecular-level vibrations of compounds and provides information about the surface chemistry and architecture of different samples.

For FT-IR measurement, a sample is placed on the internal reflection element, where ATR (attenuated total reflectance) crystal is mounted on the instrument setup (Figure 2.13).

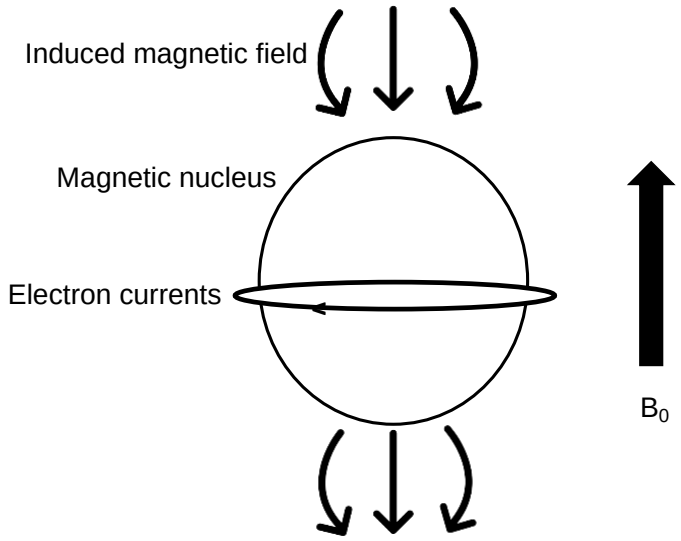

Figure 2. 12. Schematic of electronic currents around an atomic nucleus in external magnetic field (176).

IR beam is directed onto element at an angle $\boldsymbol{\theta}$, greater than the critical angle ($\boldsymbol{\theta}$c) so that the infrared light undergoes internal reflection. An evanescent wave is produced at each point of total internal reflection. The evanescent wave has limited penetration depth. This smaller depth along with short pathlengths of waves allow for IR measurements. The basic setup of IR instrument is shown in Figure 2.13.

Each functional group has a characteristic IR absorption band. Any non-linear molecule with N atoms has 3N - 6 vibrational motions and 3N - 6 normal modes. Molecules with permanent dipole movements (polarity difference between atoms is high example: C-O bond) are also IR active. The stretching vibrations can be modeled to a harmonic oscillator, the frequency of which is given by the equation below.

$$\nu = (1/2\pi c)\sqrt{k(m1+m2)/m1m2} \qquad \text{Eqn. 2.1}$$

Where ν = bond strength, c = spring constant, m1=mass of atom 1, m2= mass of atom 2.

FT-IR stretching mode frequencies are sensitive to functional group environment, electronegativity of atoms in functional groups, H-bond interactions. To understand the interactions between biomass and ILs, FT-IR measurement of functional groups such as C-O, C=O, C-O-C, C-C, C=C and C-H have been used.[183] For example, in case of lignin dissolution in phosphate ILs, aromatic signal of lignin carbons at 1510 cm^{-1} was monitored.[184] On the other hand, during biomass dissolution in imidazolium ILs, vibrational modes at C-O and C=O of hemicellulose acetyl groups were monitored.[185] For cellulose dissolution, crystallinity changes were measured using the ratio of C-H bending (1375 cm^{-1}) to crystalline O-H stretching at 2900 cm^{-1}.[186]

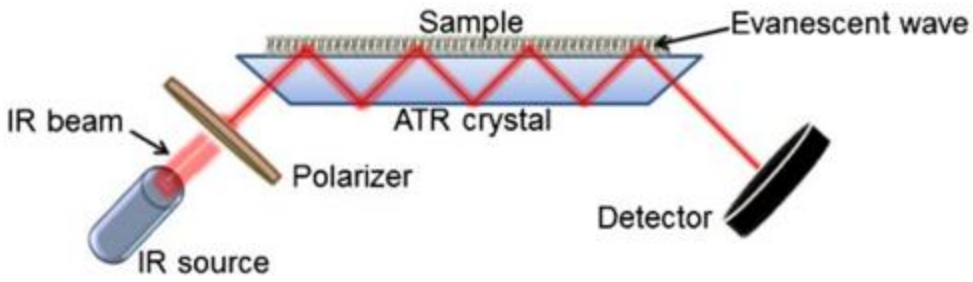

Figure 2. 13. ATR FTIR instrument setup. Adapted from reference (182)

2.9.2. Scattering techniques

Small angle scattering techniques using X-rays and neutrons are useful to probe chemical structures at multiple length scales, from a few angstroms to a few thousand angstroms. It allows microscale and nanoscale characterization of biomass in terms of size, shape, distribution of biomass components and interactions between different biomass components. The main advantages of SAS are minimum sample preparation and versatile sample environment. If neutrons are used as source, then the sample can be recovered due to minimum radiation damage. However, scattering techniques remain underutilized in the field of biomass characterization as data analysis is difficult and time consuming. In the section below an overview of the scattering fundamentals is provided along with the differences between X-ray and neutron scattering.

- ***Basic concepts of scattering***

When an electromagnetic radiation passes through matter (solid/liquid/gas) most of the incident beam comes out unaltered. However, the radiation undergoes two small but significant alterations. A small portion of radiation is absorbed and transformed into other forms of energy such as heat or radiation and another small part of the incident beam undergoes "scattering". The scattering process in which the scattered beam has the same energy as the incident beam while undergoing a change in direction and momentum is called Thompson scattering or elastic scattering. [187, 188, 189] On the other hand, in Compton or inelastic scattering, the scattered beam has lower energy than the incident beam. As X-rays have higher energy compared to neutrons, small angle X-ray scattering (SAXS) is almost always elastic scattering, but neutrons can undergo inelastic scattering as well. For the purpose of this dissertation only the details pertaining to elastic scattering will be discussed.

The change in the momentum of incident beam is described by the momentum transfer vector or the scattering vector, Q. This vector is calculated from the angle difference between transmitted and scattered beam referred to as scattering angle (θ), and the wavelength of the incident beam, as shown in the equation below:

$$Q = \frac{4\pi \, Sin \, \boldsymbol{\theta}}{\boldsymbol{\lambda}} \qquad \text{Eqn. 2.2}$$

Q has the unit of inverse length, therefore, scattering image shows the scattering object in the reciprocal space. For lignocellulosic biomass the commonly employed Q range is $0.001 Å^{-1} < Q < 0.6 Å^{-1}$, which corresponds to the dimension of 600 nm to 1nm.

As the scattering medium (sample) is composed of several different scattering centers, i.e., individual atoms, many different scattering events occur in the sample. Each of the scattering wave from an atom travels as a spherical wave. In case of elastic scattering, the waves from adjacent scattering centers create an interference pattern. Depending on the magnitude of constructive interference the intensity of scattered beam will be observed as a bright spot on the detector. The pattern of the dots on the detector can offer a perspective on the atom arrangement in the sample. For example, if the sample is made up of densely packed material, we can gather information on the structural factor of sample. But if the sample is a dilute solution, then scattering pattern on the detector can provide information about the shape and size of the particles in the sample. Each scattering wave from a scattering center has an amplitude and direction and energy of the wave is given by Equation 2.3.

$$E = A \, sin \, (2\pi\nu t - \Phi) \qquad \text{Eqn. 2.3}$$

Where E = electric field intensity of the incoming electromagnetic radiation (X-ray/neutron), ν = frequency of wave and Φ = phase of the wave.

As the scattered wave is spherical, the wave function is dependent on scattering length (b) of the individual atoms in sample. Each atom in the sample has a characteristic scattering length. In case of X-rays scattering, the length is determined by the number of electrons in the sample or in other words scattering length is dependent on the atomic number of the scattering medium. On the other hand, the neutron scattering length of atoms is determined by quantum mechanics, isotope composition and neutron-nucleus interactions. The fundamental quantity measured in any scattering experiment is the differential scattering cross section ($d\sigma_s/d\Omega$), which in turn is the probability of the scattering event occurring at the incident angle $d\Omega$. In a sample with N scattering centers, each with scattering length b, the differential scattering cross section expressed in terms of scattering vector Q is given by the equation below:

$$\frac{d\sigma}{d\Omega}(Q) = \frac{1}{N}\left|\sum_i^N b_i e^{i\vec{Q}\vec{r}}\right|^2 \qquad \text{Eqn. 2.4}$$

Where r is the distance between scattering center and detector. As the distribution of scattering centers in the sample is inhomogeneous, the scattering length term is replaced by scattering length distribution, ρ(r), which is the summation of b over volume V and r is the scattering distance. Integrating over the entire sample volume we get:

$$I(Q) = \frac{d\Sigma}{d\Omega}(Q) = \frac{N}{V}\frac{d\sigma}{d\Omega}(Q) = \frac{1}{V}\left|\int_v^0 \boldsymbol{\rho}(r)\, e^{iQr} dr\right|^2 \qquad \text{Eqn. 2.5}$$

Where, $\frac{d\Sigma}{d\Omega}$ is macroscopic scattering cross section, often denoted as I(Q). Scattering length distribution has important implication while analyzing a complex system such as biomass. All the three polymers of biomass are composed of same scattering centers: carbon, hydrogen and oxygen. In X-ray scattering where the scattering length is influenced by number of electrons, it would be

tough to distinguish cellulose from hemicellulose due to the above-mentioned reason. However, for neutrons, the scattering length is dependent on isotope composition. Hence, biomass systems with the hydrogen atoms replaced by deuterium are highly suitable for neutron scattering, where one polymer can be selectively investigated over another.

- ***Form and structure factors***

As stated in the earlier section small angle scattering techniques can provide information about the scattering object's size and shape, often referred to as form factor P(Q).[190,191] Form factor distribution functions for cylindrical, spherical and ellipsoidal structures are easily accessible from the free resource site for IRENA statistical package.[192] However, unlike microscopy, where the exact location of atoms is used to generate real space images, scattering experiments obtain information in the reciprocal space. Therefore, small angle scattering techniques are complementary to first-hand information collected using imaging or other such studies.

In addition to the form factor information, scattering patterns can also provide information on the distance between a regularly ordered system, often referred to as structure factor S(Q). When scattering objects have regular arrangement a peak characteristic of this periodic arrangement is often observed. By combining the discussed aspects of form and structure factors, the most common form of I(Q) used in the scattering experiments is:

$$I(Q) = \frac{N}{V}\rho^2 \, {V_p}^2 \, P(Q) \, S(Q) \qquad \text{Eqn. 2.6}$$

Where N is number of particles, V is the volume of sample irradiated and V_p is the volume of scattering object.

- ***Experimental setup***

The experimental setup of a neutron scattering instrument is shown in Figure 2.14. Electromagnetic radiation, either X-rays or neutrons, are the sources for scattering experiments.

X-rays can be produced from lab source such as copper, but neutrons are produced from isotope fission process. The source beam is then sent through the monochromator where only one wave of a particular wavelength can pass through. The monochromatic beam is then passed through a collimator with either a pin hole or slit geometry to make the incident beam of radiation narrow enough to form a defined shape. The collimated beam is then incident on the sample. The incident beam either undergoes transmission or scattering. The scattered beam is collected at the detector. The distance between the sample and detector defines the Q range of the experiment.

Data analysis for small angle scattering experiments

The small angle scattering curves are often complex and require multiple stages of data analysis. The scattering profile of sample is obtained as 2-D intensity profile. If the scattering medium has no orientation, then the scattering profile is referred to as isotropic scattering. On the other hand, scattering profiles of oriented sample is known as anisotropic scattering. In case of isotopic scattering the 2-D data is converted into 1-D format by radial averaging in azimuthal direction. Any object with atomic composition has the ability to scatter. Therefore, to obtain the sample scattering, the scattering profiles of solvent and sample cell need to be subtracted. Once the sample profile is obtained, the choice of an appropriate model will allow for accurate interpretation of the observed features.

- ***Unified fit for hierarchical structure***

Unified fit approach was developed by Beaucage *et al*. to analyze complex multicomponent systems such as lignocellulosic biomass.[194] Biomass has multi length scale features such as nanometer cellulose fibrils to micron range pores (1 μm to 10 Å).

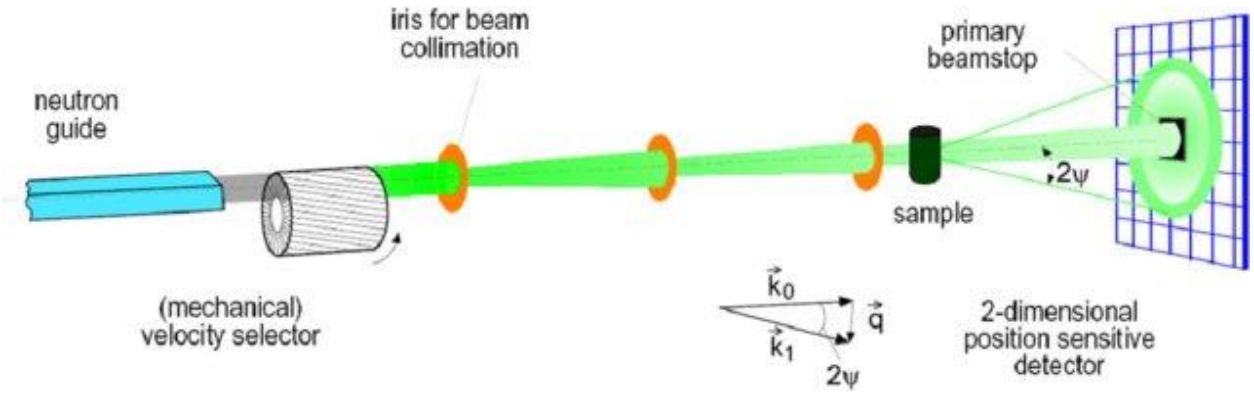

Figure 2. 14. Schematic of small angle neutron scattering experimental setup (193)

The scattering profile of such complex system encompasses over five-decade Q range with information on various scattering structures. In Q range of 0.001$Å^{-1}$ to 0.01 $Å^{-1}$ cell wall morphology information is obtained. For Q-range of 0.01$Å^{-1}$ to 0.08 $Å^{-1}$ mass fractal scattering of cell wall polymers is obtained. In the Q-range of 0.08$Å^{-1}$ to 0.2 $Å^{-1}$, scattering from cross-section of cellulose microfibrils and distance between the microfibrils is obtained. And finally, in the Q-range of 0.2$Å^{-1}$ to 0.5 $Å^{-1}$, scattering from the nanosized particles with a sharp interface is obtained. Unified fit approach offers flexibility to cover wide Q-range which is often beneficial when studying multilength and multi component systems. However, the results from the Unified fit approach need to be confirmed by the information from other techniques.

- ***Modeling tool***

Modeling tools in the IRENA package is another option to fit scattering profiles,[195] where multiple data sets can be analyzed at the same time. There are options available to model the population of scattering objects while simultaneously performing the form fit factor analysis. Additionally, IRENA modeling tools offer a way to fit for any structure factors in the sample. It also has the option of performing simplified unified level analysis in conjunction with either form factor fit, mass fractal or structure factor of a sample. However, one of the main disadvantages of this tool is its complicated nature where the user needs to have enough background of mathematical functions to understand and discern the fit results. Therefore, similar to the results of unified fit analysis, a complementary technique is necessary to validate the results.

2.9.3. Rheological techniques

Rheological measurements of biomass/cellulose IL solutions are useful in understanding the underlying set of interactions between ILs and cellulose/biomass. Similar to spectroscopic techniques rheological measurements can be performed easily as it involves minimum sample

preparation and equipment is easily accessible. However, as ILs with biomass or biomass polymers tend to have higher viscosity handling of samples is not straight forward. Further, viscosity measurement is sensitive to chemical profiles and water content of ILs therefore are not easy to perform.

- ***Fundamentals of rheology***

Rheology is defined as science of deformation and flow of materials. [196, 197, 198, 199, 200] During rheological studies, the parameters defining how the materials deform as a function of time, force and orientation are measured. The two common terms we come across during rheological measurement are shear rate and shear stress. Shear rate is defined as the force applied per unit area on a sample, while shear stress is the motion caused by the application of force. So, when a material is subjected to any force the tendency to displace is natural. However, the extent to which this displacement occurs is primarily governed by the interactions within the material and the resistance to these set of interactions is defined as shear viscosity. Or in other words, viscosity is the resistance to flow. Lower viscosity fluids flow fast, and higher viscosity fluids flow slow.

Polymer rheology is dependent on several factors such as intermolecular forces, degree of branching, molecular weight, polymer concentration and temperature. Under low shear rates polymer solutions have high viscosity due to high degree of entanglement. With increased shear rates, the polymers align in the direction of flow and the viscosity is reduced. A Newtonian polymer solution is one where the shear viscosity is independent of shear rate. On the other hand, the viscosity of Newtonian fluid is altered by temperature and pressure. At higher pressure, viscosity is higher. At lower temperature viscosity is high and as the temperature increases viscosity is reduced drastically. A non-Newtonian polymer solution is one where the viscosity is

altered by the shear rates. Non-Newtonian solutions are further classified as shear thinning where viscosity decreases with increased shear rates and shear thickening where viscosity increases with increased shear rate.

IL solutions with biomass polymers tend to exhibit Newtonian behavior.[201] As with typical polymer solutions, viscosity of IL-polymer solution increases with increase of polymer concentration. Intrinsic viscosity of IL-polymer solution is a vital tool to understand the interactions between ILs and biopolymers. As the measurement of intrinsic viscosity is performed for dilute IL-polymer solutions, where polymer-polymer interactions are non-existent, the viscosity of the solution represents the nature of IL-polymer interactions. Interestingly, between [EMIM]acetate and [BMIM]chloride, the intrinsic viscosity of cellulose is almost identical.[202, 203] This observation implies that, at a molecular level (rheology is a molecular length scale measurement), the interactions between acetate IL and chloride IL are similar and therefore, to understand the differences in their mode of action atomic or mesoscale studies are necessary.

2.10. Summary

The dissolution of biomass is a complex process owing to the inherent variability associated with biomass along with the multicomponent structure. The process is not only influenced by process criteria such as temperature and solid ratio, but also by the various physicochemical characteristics of ILs. However, owing to the multiscale nature of biomass it is obvious that a single technique cannot give us the whole picture. A few of the outstanding questions remaining during dissolution process include 1) what are the changes induced in biomass *during* dissolution process? and 2) the role of the IL cation and anion. Addressing these questions is critical, as it can shine light on some of the fundamental interactions between ionic liquids and biomass

References

1) Xu, F.; Shi, Y. C.; Wang, D. H., X-ray scattering studies of lignocellulosic biomass: A review. *Carbohydrate Polymers* **2013**, *94* (2), 904-917.
2) Alizadeh, H.; Teymouri, F.; Gilbert, T. I.; Dale, B. E., Pretreatment of switchgrass by ammonia fiber explosion (AFEX). *Applied Biochemistry and Biotechnology* **2005**, *124* (1), 1133-1141.
3) Lloyd, T. A.; Wyman, C. E., Combined sugar yields for dilute sulfuric acid pretreatment of corn stover followed by enzymatic hydrolysis of the remaining solids. *Bioresource Technology* **2005**, *96* (18), 1967-1977.
4) Saha, B. C.; Iten, L. B.; Cotta, M. A.; Wu, Y. V., Dilute acid pretreatment, enzymatic saccharification, and fermentation of rice hulls to ethanol. *Biotechnol Progress* **2005**, *21* (3), 816-22.
5) Sun, F.; Chen, H., Enhanced enzymatic hydrolysis of wheat straw by aqueous glycerol pretreatment. *Bioresource Technology* **2008**, *99* (14), 6156-6161.
6) Sun, Y.; Cheng, J., Hydrolysis of lignocellulosic materials for ethanol production: a review. *Bioresource Technology* **2002**, *83* (1), 1-11.
7) Suryawati, L.; Wilkins, M. R.; Bellmer, D. D.; Huhnke, R. L.; Maness, N. O.; Banat, I. M., Simultaneous saccharification and fermentation of Kanlow switchgrass pretreated by hydrothermolysis using Kluyveromyces marxianus IMB4. *Biotechnology and Bioengineering* **2008**, *101* (5), 894-902.
8) Delmer, D. P., Cellulose biosynthesis. *Annual Review of Plant Physiology* **1987**, *38*, 259-290.
9) Medronho, B.; Romano, A.; Miguel, M. G.; Stigsson, L.; Lindman, B., Rationalizing cellulose (in)solubility: reviewing basic physicochemical aspects and role of hydrophobic interactions. *Cellulose* **2012**, *19* (3), 581-587.
10) Hallac, B. B.; Ragauskas, A. J., Analyzing cellulose degree of polymerization and its relevancy to cellulosic ethanol. *Biofuels, Bioproducts and Biorefining* **2011**, *5*(2), 215-225.
11) Fernandes, A. N.; Thomas, L. H.; Altaner, C. M.; Callow, P.; Forsyth, V. T.; Apperley, D. C.;Kennedy, J.C.; Jarvis, M. C., Nanostructure of cellulose microfibrils in spruce wood. *Proceedings of the National Academy of Sciences* **2011**, *108*(47), E1195-E1203.
12) Ding, S. Y.; Zhao, S.; Zeng, Y., Size, shape and arrangement of native cellulose fibrils in maize cell walls. *Cellulose* **2014**, *21*, 863-871.
13) Newman, R. H.; Hill, S. J.; Harris, P. J., Wide-Angle X-Ray Scattering and Solid-State Nuclear Magnetic Resonance Data Combined to Test Models for Cellulose Microfibrils in Mung Bean Cell Walls. *Plant Physiology* **2013**, *163* (4), 1558-1567.
14) Thomas, L. H.; Forsyth, V. T.; Šturcová, A.; Kennedy, C. J.; May, R. P.; Altaner, C. M.; Apperley, D. C.; Wess, T. J.; Jarvis, M. C., Structure of Cellulose Microfibrils in Primary Cell Walls from Collenchyma. *Plant Physiology* **2013**, *161* (1), 465-476.
15) Vandavasi, V. G.; Putnam, D. K.; Zhang, Q.; Petridis, L.; Heller, W. T.; Nixon, B. T.; Haigler, C. H.; Kalluri, U.; Coates, L.; Langan, P.; Smith, J. C.; Meiler, J.; O'Neill, H., A Structural Study of CESA1 Catalytic Domain of Arabidopsis Cellulose Synthesis Complex: Evidence for CESA Trimers. *Plant Physiology* **2016**, *170* (1), 123-135.

16) Nishiyama, Y.; Langan, P.; Chanzy, H., Crystal Structure and Hydrogen-Bonding System in Cellulose Iβ from Synchrotron X-ray and Neutron Fiber Diffraction. *Journal of the American Chemical Society* **2002**, *124* (31), 9074-9082.
17) Nishiyama, Y.; Sugiyama, J.; Chanzy, H.; Langan, P., Crystal Structure and Hydrogen Bonding System in Cellulose Iα from Synchrotron X-ray and Neutron Fiber Diffraction. *Journal of the American Chemical Society* **2003**, *125* (47), 14300-14306.
18) Funahashi, R.; Okita, Y.; Hondo, H.; Zhao, M.; Saito, T.; Isogai, A., Different Conformations of Surface Cellulose Molecules in Native Cellulose Microfibrils Revealed by Layer-by-Layer Peeling. *Biomacromolecules* **2017**, *18* (11), 3687-3694.
19) Fiorati, A.; Bellingeri, A.; Punta, C.; Corsi, I.; Venditti, I., Silver Nanoparticles for Water Pollution Monitoring and Treatments: Ecosafety Challenge and Cellulose-Based Hybrids Solution. *Polymers* **2020**, *12*(8), 1635.
20) Habibi, Y.; Lucia, L. A.; Rojas, O. J., Cellulose nanocrystals: chemistry, self-assembly, and applications. *Chemical reviews* **2010**, *110*(6), 3479-3500.
21) Scheller, H. V.; Ulvskov, P., Hemicelluloses. *Annual Review of Plant Biology* **2010,** *61* (1), 263-289.
22) Sella Kapu, N.; Trajano, H. L., (2014). Review of hemicellulose hydrolysis in softwoods and bamboo. *Biofuels, Bioproducts and Biorefining* **2014**, *8*(6), 857-870.
23) Moreira, L. R. S.; Filho, E. X. F., An overview of mannan structure and mannan-degrading enzyme systems. *Applied Microbiology and Biotechnology* **2008,** *79* (2), 165.
24) Capek, P.; Kubačková, M.; Alföldi, J.; Bilisics, L.; Lišková, D.; Kákoniová, D., Galactoglucomannan from the secondary cell wall of Picea abies L. Karst. *Carbohydrate Research* **2000,** *329* (3), 635-645.
25) Hansen, N. M.; Plackett, D., Sustainable films and coatings from hemicelluloses: a review. *Biomacromolecules* **2008**, *9*(6), 1493-1505.
26) Farhat, W.; Venditti, R.; Quick, A.; Taha, M.; Mignard, N.; Becquart, F.; Ayoub, A., Hemicellulose extraction and characterization for applications in paper coatings and adhesives. *Industrial Crops and Products* **2017**, *107*, 370-377.
27) Mikkonen, K.S.; Kirjoranta, S.; Xu, C.; Hemming, J.; Pranovich, A.; Bhattarai, M.; Peltonen, L.; Kilpeläinen, P.; Maina, N.; Tenkanen, M.; Lehtonen, M., Environmentally compatible alkyd paints stabilized by wood hemicelluloses. *Industrial Crops and Products* **2019**, *133*, pp.212-220.
28) Liu, Q.; Luo, L.; Zheng, L., Lignins: biosynthesis and biological functions in plants. *International journal of molecular sciences* **2018**, *19*(2), 335.
29) Xu, Z., Lei, P.; Zhai, R.; Wen, Z.; Jin, M., Recent advances in lignin valorization with bacterial cultures: microorganisms, metabolic pathways, and bio-products. *Biotechnology for biofuels* **2019**, *12*(1), 32.
30) Yang, J.; Ching, Y. C.; Chuah, C. H., Applications of lignocellulosic fibers and lignin in bioplastics: A review. *Polymers* **2019**, *11*(5), 751.
31) Espinoza-Acosta, J. L.; Torres-Chávez, P. I.; Olmedo-Martínez, J. L.; Vega-Rios, A.; Flores-Gallardo, S.; Zaragoza-Contreras, E. A., Lignin in storage and renewable energy applications: A review. *Journal of energy chemistry* **2018**, *27*(5), 1422-1438.
32) Chanliaud, E.; Gidley, M. J., In vitro synthesis and properties of pectin/Acetobacter xylinus cellulose composites. *Plant J* **1999**, *20* (1), 25-35.
33) Cosgrove, D. J., Growth of the plant cell wall. *Nature Reviews Molecular Cell Biology* **2005**, *6* (11), 850-61.

34) Cosgrove, D. J., Assembly and enlargement of the primary cell wall in plants. *Annu Review of Cell and Developmental Biology* **1997**, *13*, 171-201.
35) Schopfer, P., Biomechanics of plant growth. *American Journal of Botany* **2006**, *93* (10), 1415-25.
36) McNeil, M., Darvill, A.G., Fry, S.C., and Albershaeim, P., Structure and function of the primary cell walls of higher plants. *Annual Review of Biochemistry* **1984**, *53*, 625-663.
37) Keegstra, K.; Talmadge, K. W.; Bauer, W. D.; Albersheim, P., The Structure of Plant Cell Walls: III. A Model of the Walls of Suspension-cultured Sycamore Cells Based on the Interconnections of the Macromolecular Components. *Plant Physiology* **1973**, *51* (1), 188-97.
38) Carpita, N. C.; Gibeaut, D. M., Structural models of primary cell walls in flowering plants: consistency of molecular structure with the physical properties of the walls during growth. *Plant Journal* **1993**, *3* (1), 1-30.
39) Hayashi, T., Xyloglucans in the Primary Cell Wall. *Annual Review of Plant Physiology and Plant Molecular Biology* **1989**, *40* (1), 139-168.
40) Cosgrove, D. J., Wall Structure and Wall Loosening. A Look Backwards and Forwards. *Plant Physiology* **2001**, *125* (1), 131-134.
41) Hayashi, T.; Maclachlan, G., Pea xyloglucan and cellulose : I. Macromolecular organization. *Plant Physiology* **1984**, *75* (3), 596-604.
42) Cosgrove, D. J., Wall Structure and Wall Loosening. A Look Backwards and Forwards. *Plant Physiology* **2001**, *125* (1), 131-134.
43) Hayashi, T.; Maclachlan, G., Pea xyloglucan and cellulose : I. Macromolecular organization. *Plant Physiology* **1984**, *75* (3), 596-604.
44) Talbott, L. D.; Ray, P. M., Molecular size and separability features of pea cell wall polysaccharides : implications for models of primary wall structure. *Plant Physiology* **1992**, *98* (1), 357-68.
45) Zykwinska, A.; Thibault, J. F.; Ralet, M. C., Organization of pectic arabinan and galactan side chains in association with cellulose microfibrils in primary cell walls and related models envisaged. *Journal of Experimental Botany* **2007**, *58* (7), 1795-802.
46) Park, Y. B.; Cosgrove, D. J., A Revised Architecture of Primary Cell Walls Based on Biomechanical Changes Induced by Substrate-Specific Endoglucanases. *Plant Physiology* **2012,** *158* (4), 1933-1943.
47) Cosgrove, D.J., Diffuse growth of plant cell walls. *Plant Physiology* **2018**, *176*(1), 16-27.
48) Cosgrove, D. J., Nanoscale structure, mechanics and growth of epidermal cell walls. *Current Opinion in Plant Biology* **2018**, *46*, 77-86.
49) Zhang, T.; Vavylonis, D.; Durachko, D. M.; Cosgrove, D. J., Nanoscale movements of cellulose microfibrils in primary cell walls. *Nature Plants* **2017**, *3*(5), 1-6.
50) Zheng, Y.; Wang, X.; Chen, Y.; Wagner, E.; Cosgrove, D. J., Xyloglucan in the primary cell wall: assessment by FESEM, selective enzyme digestions and nanogold affinity tags. *The Plant Journal* **2018**, *93*(2), 211-226.
51) Maron, L., Rethinking our models of the plant cell wall. *The Plant Journal* **2019**, *100*(6), 1099-1100.
52) Chanliaud, E.; Gidley, M. J., In vitro synthesis and properties of pectin/Acetobacter xylinus cellulose composites. *Plant J* **1999**, *20* (1), 25-35.

53) Balakshin, M. Y.; Capanema, E. A.; Chang, H.-m., MWL fraction with a high concentration of lignin-carbohydrate linkages: Isolation and 2D NMR spectroscopic analysis. *Holzforschung* **2007**, *61* (1), 1-7.
54) Carpita, N. C., The Chemical Structure of the Cell Walls of Higher Plants. In *Dietary Fiber: Chemistry, Physiology, and Health Effects*, Kritchevsky, D.; Bonfield, C.; Anderson, J. W., Eds. Springer US: Boston, MA, 1990; pp 15-30.
55) Dyson, R. J.; Band, L. R.; Jensen, O. E., A model of crosslink kinetics in the expanding plant cell wall: yield stress and enzyme action. *Journal of theoretical biology* **2012**, *307* (9-10), 125-136.
56) Zykwinska, A.; Thibault, J. F.; Ralet, M. C., Organization of pectic arabinan and galactan side chains in association with cellulose microfibrils in primary cell walls and related models envisaged. *Journal of Experimental Botany* **2007**, *58* (7), 1795-802.
57) Rytioja, J.; Hildén, K.; Yuzon, J.; Hatakka, A.; de Vries, R. P.; Mäkelä, M. R., Plant-polysaccharide-degrading enzymes from basidiomycetes. *Microbiology and Molecular Biology Reviews* **2014**, *78*(4), 614-649.
58) T. Koshijima and T. Watanabe, Association Between Lignin and Carbohydrates in Wood and Other Plant Tissues, Springer Series in Wood Science, Springer, Berlin, Heidelberg, 2003.
59) Smelstorius, J. A., Chemical composition of wood of Australian-grown Pinus radiata. III. Lignin-polysaccharide complexes. *Holzforschung* **1974**, 28(3), 99–101.
60) Kondo, R.; Sako, T.; Iimori, T.; Imamura, H., Formation of glycosidic lignin-carbohydrate complex in the dehydro- genative polymerization of coniferyl alcohol. *Mokuzai Gakkaishi* **1990**, 36, 332–338.
61) Joseleau, J. P.; Kesaraoui, R.; Glycosidic bonds between lignin and carbohydrates, *Holzforschung* **1986**, 40, 163–168.
62) Kosikova, B.; Joniak, D.; Skamla, J., Lignin-carbohydrate bonds in beech wood, *Journal of Cellulose Chemistry and Technology* **1972**, 6, 579–588.
63) Yaku, F.; Yamada, Y.; Koshijima, T., Lignin-carbohydrate complex. Part II. Enzymatic degradation of acidic polysaccharide in Björkman LCC. *Holzforschung* **1976**, 30, 148–156.
64) Freudenberg, K.; Grion, G., Contribution to the mecha- nism of formation of lignin and of the lignin-carbohydrate bond *Chemische Berichte* **1959**, 92, 1355–1363.
65) Eriksson, Ö.; Lindgren, B. O., About the linkage between lignin and hemicelluloses in wood, Sven. *Papperstidn* **1977**, 59–63.
66) Kosikova, B.; Joniak, D.; Kosikova, L., On the properties of benzyl ether bonds in lignin-saccharidic complex iso- lated from spruce *Holzforschung* **1979**, 33, 11–14.
67) Yaku, F.; Tanaka, R.; Koshijima, T., Lignin carbohydrate complex. Part IV. Lignin as side chain of the carbohydrate in Björkman LCC. *Holzforschung* **1981**, 35(4), 177–181.
68) Koshijima, T.; Watanabe, T.; Azuma, J., Existence of benzylated carbohydrate moiety in lignin-carbohydrate complex from pine wood *Chemistry Letters* **1984**, 13(10), 1737– 1740.
69) Freudenberg, K.; Harkin, J. M., Models for the linkage of lignin to carbohydrates *Chemische Berichte* **1960**, 93, 2814– 2819.
70) Watanabe, T.; Koshijima, T., Evidence for an ester linkage between lignin and glucuronic acid in lignin- carbohydrate complexes by DDQ-oxidation *Agricultural and Biological Chemistry* **1988** 52(11), 2953–2955.
71) Lundquist, K.; Simonson, R.; Tingsvik, K., Studies on lignin carbohydrates linkages in milled wood lignin preparations, Sven. *Papperstidn* **1983**, 86(6), R44–R47.

72) Obst, J. R.; Frequency and alkali resistance of lignin-carbohydrate bonds in wood, *Tappi* **1982**, 65(4), 109–112.
73) Kato, A.; Azuma, J.; Koshijima, T., A new feruloylated tri- saccharide from bagasse, *Chemistry Letters* **1983**, 1, 137–140.
74) Kato, Y.; Nevins, D. J.,Isolation and identification of O- (5-O-feruloyl-α-L-arabinofuranosyl)-1 (→ 3)-O-β-D-xylopyranosyl-(1→ 4)-D-xylopyranose as a component of Zea shoot cell-walls, *Carbohydrate. Research* **1985**, 137, 139–150.
75) Kato, A.; Azuma, J.; Koshijima, T., Isolation and identification of a new feruloylated tetra saccharide from bagasse lignin-carbohydrate complex containing phenolic acid, *Agricultural and Biological Chemistry* **1987**, 51(6), 1691–1693.
76) Ishii, T.; Hiroi, T., Isolation and characterization of feruloylated arabinoxylan oligosaccharides from bamboo shoot cell walls *Carbohydrate Research* **1990**, 196, 175–183.
77) Smith, M. M.; Hartley, R. D.; Occurrence and nature of ferulic acid substitution of cell-wall polysaccharides in graminaceous plants *Carbohydrate Research* **1983**, 118, 65–80.
78) Mueller-Harvey, I.; Hartley, R. D.; Harris, P. J.; Curzon, E. H., Linkage of p-coumaroyl and feruloyl groups to cell-wall polysaccharides of barley straw *Carbohydrate Research* **1986**, 148(1), 71–85.
79) Yamamoto, E.; Bokelman, G. H. Lewis, N. G., Phenylpropanoid metabolism in cell walls: an overview, in ACS Symposium series, American Chemical Society, USA, 1989.
80) Ralph, J.; Lundquist, K.; Brunow, G.; Lu, F.; Kim, H.; Schatz, P. F.; Marita, J. M.; Hatfield, R.; Ralph, S. A.; Christensen, J. H.; Boerjan, W., Lignins: natural polymers from oxidative coupling of 4-hydroxyphenyl-propanoids *Phytochemistry. Reviews* **2004**, 3, 29–60.
81) Bolker, H. I., A lignin carbohydrate bond as revealed by infra-red spectroscopy *Nature* **1963**, 197(4866), 489.
82) Xie, Y.; Yasuda, S.; Wu, H.; Liu, H., Analysis of the structure of lignin-carbohydrate complexes by specific 13C tracer method. *Journal of Wood Science* **2000**, 46, 130–136.
83) A. Björkman, Studies on finely divided wood. Part 1. Extraction of lignin with neutral solvents, Sven. Papperstidn., **1956**, 59, 477–485.
84) M. Lawoko, G. Henriksson and G. Gellerstedt, Characterization of lignin-carbohydrate complexes from spruce sulphite pulp, *Holzforchung* **2006**, 60, 162–165.
85) J. Li, G. Henriksson and G. Gellerstedt, Lignin depolymerization/repolymerization and its critical role for delignifcation of aspen wood by steam explosion *Bioresource Technology* **2007**, 98, 3061–3068.
86) T. J. McDonough, The chemistry of organosolv lignin, *Tappi Journal* **1993**, 76, 186–193.
87) M. Lawoko, Unveiling the structure and ultrastructure of lignin carbohydrate complexes in softwoods *International Journal of Biological Macromolecules* **2013**, 62, 705–713.
88) D. V. Evtuguin, B. J. Goodfellow, C. Pascoal Neto and N. Terashima, Characterization of lignin-carbohydrate lin- kages in Eucalyptus globulus by 2D/3D NMR spectroscopy using specific carbon-13 labeling technique, Proceedings of the 13th ISWFPC, Auckland, New Zealand, 2005, vol. 2, 439–444.
89) Miyagawa, Y.; Mizukami, T.; Kamitakahara, H.; Takano, T., Synthesis and fundamental HSQC NMR data of monolignol β-glycosides, dihydromonolignol β-glycosides and p-hydroxybenzaldehyde derivative β-glycosides for the analysis of phenyl glycoside type lignin-carbohydrate complexes (LCCs) *Holzforschung* **2014**, 68(7), 747–760.

90) Nylander, F.; Sunner, H.; Olsson, L.; Christakopoulos, P.; Westman, G., Synthesis and enzymatic hydrolysis of a diaryl benzyl ester model of a lignin-carbohydrate complex (LCC) *Holzforschung*, **2016**, 70(5), 385–391.
91) Li, K.; Helm, R. F., Synthesis and Rearrangement Reactions of Ester-Linked Lignin-Carbohydrate Model Compounds, *Journal of Agricultural and Food Chemistry*, **1995**, 43, 2098–2103.
92) Giummarella, N., Pu, Y., Ragauskas, A. J., Lawoko, M., A critical review on the analysis of lignin carbohydrate bonds. *Green Chemistry*, **2019** *21*(7), 1573-1595.
93) Chakar, F. S.; Ragauskas, A. J., Review of current and future softwood kraft lignin process chemistry. *Industrial Crops and Products* **2004,** *20* (2), 131-141.
94) Zhang, K.; Pei, Z. J.; Wang, D. H., Organic solvent pretreatment of lignocellulosic biomass for biofuels and biochemicals: A review. *Bioresource Technology* **2016,** *199*, 21-33.
95) Black SK, Hames BR, Myers MD. U.S. patent 5,730,837 to Midwest Research Institute, 1998.
96) Teramura, H.; Sasaki, K.; Oshima, T.; Matsuda, F.; Okamoto, M.; Shirai, T.; Kawaguchi, H.; Ogino, C.; Hirano, K.; Sazuka, T.; Kitano, H., Organosolv pretreatment of sorghum bagasse using a low concentration of hydrophobic solvents such as 1-butanol or 1-pentanol. *Biotechnology for biofuels* **2016**, *9*(1), 1-11.
97) Wu, M.; Pang, J.; Zhang, X.; Sun, R., Enhancement of lignin biopolymer isolation from hybrid poplar by organosolv pretreatments. *International Journal of Polymer Science* **2014**,
98) Bozell, J. J.; Black, S. K.; Myers, M.; Cahill, D.; Miller, W. P.; Park, S., Solvent fractionation of renewable woody feedstocks: Organosolv generation of biorefinery process streams for the production of biobased chemicals. *Biomass and bioenergy* **2011**, *35*(10), 4197-4208.
99) Alonso, D. M.; Wettstein, S. G.; Dumesic, J. A., Gamma-valerolactone, a sustainable platform molecule derived from lignocellulosic biomass. *Green Chemistry* **2013,** *15* (3), 584-595
100) Horváth, I. T.; Mehdi, H.; Fábos, V.; Boda, L.; Mika, L. T., γ-Valerolactone—a sustainable liquid for energy and carbon-based chemicals. *Green Chemistry*, **2008** *10*(2), 238-242.
101) Luterbacher, J. S.; Rand, J. M.; Alonso, D. M.; Han, J.; Youngquist, J. T.; Maravelias, C. T.; Pfleger, B. F.; Dumesic, J. A., Nonenzymatic sugar production from biomass using biomass-derived γ-valerolactone. *Science* **2014,** *343* (6168), 277-280.
102) Luterbacher, J. S.; Azarpira, A.; Motagamwala, A. H.; Lu, F.; Ralph, J.; Dumesic, J. A., Lignin monomer production integrated into the γ-valerolactone sugar platform. *Energy & Environmental Science* **2015,** *8* (9), 2657-2663.
103) Nguyen, T. Y.; Cai, C. M.; Kumar, R.; Wyman, C. E., Co-solvent pretreatment reduces costly enzyme requirements for high sugar and ethanol yields from lignocellulosic biomass. *ChemSusChem* **2015,** *8* (10), 1716-25.
104) Smith, M. D.; Cheng, X.; Petridis, L.; Mostofian, B.; Smith, J. C., Organosolv-Water Cosolvent Phase Separation on Cellulose and its Influence on the Physical Deconstruction of Cellulose: A Molecular Dynamics Analysis. *Scientific Reports* **2017,** *7* (1), 14494.
105) Meng, X.; Parikh, A.; Nagane, N.; Seemala,B.; Kumar,R.; Cai, C. M.; Pu,Y.; Wyman, C. E.; Ragauskas, A.J., Chemical transformations of poplar lignin during co-solvent enhanced lignocellulosic fractionation process. *ACS Sustainable Chemistry and Engineering* **2018**,6(7), 8711–8718.

106) Fort, D. A.; Remsing, R. C.; Swatloski, R. P.; Moyna, P.; Moyna, G.; Rogers, R. D., Can ionic liquids dissolve wood? Processing and analysis of lignocellulosic materials with 1-n-butyl-3-methylimidazolium chloride. *Green Chemistry* **2007,** *9* (1), 63-69.
107) Endo, T.; Hosomi, S.; Fujii, S.; Ninomiya, K.; Takahashi, K., Anion Bridging-Induced Structural Transformation of Cellulose Dissolved in Ionic Liquid. *Journal of Physical Chemistry Letters* **2016,** *7* (24), 5156-5161.
108) Mostofian, B.; Smith, J. C.; Cheng, X., Simulation of a cellulose fiber in ionic liquid suggests a synergistic approach to dissolution. *Cellulose* **2013,** *21* (2), 983-997.
109) Hirosawa, K.; Fujii, K.; Hashimoto, K.; Shibayama, M., Solvated Structure of Cellulose in a Phosphonate-Based Ionic Liquid. *Macromolecules* **2017,** *50* (17), 6509-6517.
110) Swatloski, R. P.; Spear, S. K.; Holbrey, J. D.; Rogers, R. D., Dissolution of Cellose with Ionic Liquids. *Journal of the American Chemical Society* **2002,** *124* (18), 4974-4975.
111) Fort, D. A.; Remsing, R. C.; Swatloski, R. P.; Moyna, P.; Moyna, G.; Rogers, R. D., Can ionic liquids dissolve wood? Processing and analysis of lignocellulosic materials with 1-n-butyl-3-methylimidazolium chloride. *Green Chemistry* **2007,** *9* (1), 63-69.
112) Kilpeläinen, I.; Xie, H.; King, A.; Granstrom, M.; Heikkinen, S.; Argyropoulos, D. S., Dissolution of Wood in Ionic Liquids. *Journal of Agricultural and Food Chemistry* **2007,** *55* (22), 9142-9148.
113) Badgujar, K. C.; Bhanage, B. M., Factors governing dissolution process of lignocellulosic biomass in ionic liquid: current status, overview and challenges. *Bioresource Technology* **2015,** *178*, 2-18.
114) Brandt-Talbot, A.; Gschwend, F. J.; Fennell, P. S.; Lammens, T. M.; Tan, B.; Weale, J.; Hallett, J. P., An economically viable ionic liquid for the fractionation of lignocellulosic biomass. *Green Chemistry* **2017**, *19*(13), 3078-3102.
115) Singh, S.; Simmons, B. A.; Vogel, K. P., Visualization of biomass solubilization and cellulose regeneration during ionic liquid pretreatment of switchgrass. *Biotechnology and Bioengineering* **2009,** *104*,
116) Dadi, A. P.; Varanasi, S.; Schall, C. A., Enhancement of cellulose saccharification kinetics using an ionic liquid pretreatment step. *Biotechnology and Bioenergy* **2006,** *95* (5), 904-910.
117) Li, C.; Knierim, B.; Manisseri, C.; Arora, R.; Scheller, H. V.; Auer, M.; Vogel, K. P.; Simmons, B. A.; Singh, S., Comparison of dilute acid and ionic liquid pretreatment of switchgrass: Biomass recalcitrance, delignification and enzymatic saccharification. *Bioresource Technology* **2010,** *101* (13), 4900-4906.
118) Cheng, G.; Varanasi, P.; Li, C. L.; Liu, H. B.; Menichenko, Y. B.; Simmons, B. A.; Kent, M. S.; Singh, S., Transition of Cellulose Crystalline Structure and Surface Morphology of Biomass as a Function of Ionic Liquid Pretreatment and Its Relation to Enzymatic Hydrolysis. *Biomacromolecules* **2011,** *12* (4), 933-941.
119) Grasvik, J.; Winestrand, S.; Normark, M.; Jonsson, L. J.; Mikkola, J. P., Evaluation of four ionic liquids for pretreatment of lignocellulosic biomass. *BMC Biotechnology* **2014,** *14*, 34.
120) Shi, J.; Gladden, J. M.; Sathitsuksanoh, N.; Kambam, P.; Sandoval, L.; Mitra, D.; Zhang, S.; George, A.; Singer, S. W.; Simmons, B. A., One-pot ionic liquid pretreatment and saccharification of switchgrass. *Green Chemistry* **2013,** *15* (9), 2579-2589.
121) Parthasarathi, R.; Sun, J.; Dutta, T.; Sun, N.; Pattathil, S.; Konda, N.M.; Peralta, A.G.; Simmons, B.A.; Singh, S., Activation of lignocellulosic biomass for higher sugar yields

using aqueous ionic liquid at low severity process conditions. *Biotechnology for biofuels* 2016, *9*(1), 160-173.

122) Labbe, N.; Kline, L. M.; Moens, L.; Kim, K.; Kim, P. C.; Hayes, D. G., Activation of lignocellulosic biomass by ionic liquid for biorefinery fractionation. *Bioresource Technology* **2012,** *104*, 701-707.

123) Li, B.; Filpponen, I.; Argyropoulos, D. S., Acidolysis of wood in ionic liquids. *Industrial & engineering chemistry research* **2010**, *49*(7), 3126-3136.

124) Gschwend, F. J.; Malaret, F.; Shinde, S.; Brandt-Talbot, A.; Hallett, J. P., Rapid pretreatment of Miscanthus using the low-cost ionic liquid triethylammonium hydrogen sulfate at elevated temperatures. *Green Chemistry* **2018**, *20*(15), 3486-3498.

125) Wang, J.; Boy, R.; Nguyen, N. A.; Keum, J. K.; Cullen, D. A.; Chen, J.; Soliman, M.; Littrell, K. C.; Harper, D.; Tetard, L.; Rials, T. G.; Naskar, A. K.; Labbé, N., Controlled Assembly of Lignocellulosic Biomass Components and Properties of Reformed Materials. *ACS Sustainable Chemistry & Engineering* **2017,** *5* (9), 8044-8052.

126) da Costa Lopes, A. M.; João, K. G.; Morais, A. R. C.; Bogel-Łukasik, E.; Bogel-Łukasik, R., Ionic liquids as a tool for lignocellulosic biomass fractionation. *Sustainable Chemical Processes* **2013**, *1*(1), 1-31.

127) Cheng, F.; Zhao, X.; Hu, Y., Lignocellulosic biomass delignification using aqueous alcohol solutions with the catalysis of acidic ionic liquids: A comparison study of solvents. *Bioresource technology* **2018**, *249*, 969-975.

128) Matsagar, B.M.; Hossain, S.A.; Islam, T.; Alamri, H.R.; Alothman, Z.A.; Yamauchi, Y.; Dhepe, P.L.; Wu, K.C.W., Direct production of furfural in one-pot fashion from raw biomass using Brønsted acidic ionic liquids. *Scientific reports* **2017**, *7*(1), 1-7.

129) Liu, F.; Liu, Q.; Wang, A.; Zhang, T., Direct catalytic hydrogenolysis of kraft lignin to phenols in choline-derived ionic liquids. *ACS Sustainable Chemistry & Engineering* **2016**, *4*(7), 3850-3856.

130) Das, L.; Xu, S.; Shi, J., Catalytic oxidation and depolymerization of lignin in aqueous ionic liquid. *Frontiers in Energy Research* **2017**, *5*, 21.

131) da Costa Lopes, A. M.; João, K. G.; Bogel-Łukasik, E.; Roseiro, L. B.; Bogel-Łukasik, R., Pretreatment and fractionation of wheat straw using various ionic liquids. *Journal of agricultural and food chemistry* **2013**, *61*(33), 7874-7882.

132) Mahmood, H.; Moniruzzaman, M.; Iqbal, T.; Yusup, S., Effect of ionic liquids pretreatment on thermal degradation kinetics of agro-industrial waste reinforced thermoplastic starch composites. *Journal of Molecular Liquids* **2017**, *247*, 164-170.

133) Zhang, H.; Wu, J.; Zhang, J.; He, J., 1-Allyl-3-methylimidazolium Chloride Room Temperature Ionic Liquid: A New and Powerful Nonderivatizing Solvent for Cellulose. *Macromolecules* **2005,** *38* (20), 8272-8277.

134) Sun, N.; Rahman, M.; Qin, Y.; Maxim, M. L.; Rodríguez, H.; Rogers, R. D., Complete dissolution and partial delignification of wood in the ionic liquid 1-ethyl-3-methylimidazolium acetate. *Green Chemistry* **2009,** *11* (5), 646-655.

135) Fukaya, Y.; Sugimoto, A.; Ohno, H., Superior Solubility of Polysaccharides in Low Viscosity, Polar, and Halogen-Free 1,3-Dialkylimidazolium Formates. *Biomacromolecules* **2006,** *7* (12), 3295-3297.

136) Nguyen, T. A.; Kim, K. R.; Han, S. J.; Cho, H. Y.; Kim, J. W.; Park, S. M.; Park, J. C.; Sim, S. J., Pretreatment of rice straw with ammonia and ionic liquid for lignocellulose conversion to fermentable sugars. *Bioresource Technology* **2010,** *101* (19), 7432-8.

137) Zhao, H.; Baker, G. A.; Cowins, J. V., Fast enzymatic saccharification of switchgrass after pretreatment with ionic liquids. *Biotechnology Progress* **2010,** *26* (1), 127-133.
138) Ang, T. N.; Ngoh, G. C.; Chua, A. S. M.; Lee, M. G., Elucidation of the effect of ionic liquid pretreatment on rice husk via structural analyses. *Biotechnology for Biofuels* **2012,** *5*, 1-10.
139) Sant'Ana Da Silva, A.; Lee, S. H.; Endo, T.; Bon, E., Major improvement in the rate and yield of enzymatic saccharification of sugarcane bagasse via pretreatment with the ionic liquid 1-ethyl-3-methylimidazolium acetate ([Emim][Ac]). *Bioresource Technology* **2011,** *102*, 10505-10509.
140) Kanbayashi, T.; Miyafuji, H., Raman Microscopic Study of Japanese Beech (Fagus crenata) As Treated with the Ionic Liquid, 1-Ethyl-3-Methylimidazolium Chloride. *Journal of Wood Chemistry and Technology* **2015,** *36* (3), 224-234.
141) Geng, X.; Henderson, W. A., Pretreatment of corn stover by combining ionic liquid dissolution with alkali extraction. *Biotechnology Bioenergy* **2011,** *109*, 84-91.
142) Bahcegul, E.; Apaydin, S.; Haykir, N. I.; Tatli, E.; Bakir, U., Different ionic liquids favor different lignocellulosic biomass particle sizes during pretreatment to function efficiently. *Green Chemistry* **2012,** *14*, 1896-1903.
143) Vitz, J.; Erdmenger, T.; Haensch, C.; Schubert, U. S., Extended dissolution studies of cellulose in imidazolium based ionic liquids. *Green Chemistry* **2009,** *11* (3), 417-424.
144) Shi, J.; Gladden, J. M.; Sathitsuksanoh, N.; Kambam, P.; Sandoval, L.; Mitra, D.; Zhang, S.; George, A.; Singer, S. W.; Simmons, B. A.; Singh, S., One-pot ionic liquid pretreatment and saccharification of switchgrass. *Green Chemistry* **2013,** *15* (9), 2579-2589.
145) Shi, J.; Balamurugan, K.; Parthasarathi, R.; Sathitsuksanoh, N.; Zhang, S.; Stavila, V.; Subramanian, V.; Simmons, B. A.; Singh, S., Understanding the role of water during ionic liquid pretreatment of lignocellulose: co-solvent or anti-solvent? *Green Chem.* **2014,** *16* (8), 3830-3840.
146) Fatemi, S. M.; Foroutan, M., Recent findings about ionic liquids mixtures obtained by molecular dynamics simulation. *Journal of Nanostructure in Chemistry* **2015**, *5*(3), 243-253.
147) Wu, H.; Mora-Pale, M.; Miao, J.; Doherty, T. V.; Linhardt, R. J.; Dordick, J. S., Facile pretreatment of lignocellulosic biomass at high loadings in room temperature ionic liquids. *Biotechnology and Bioengineering* **2011,** *108*, 2865-2875.
148) Yoon, L. W.; Ang, T. N.; Ngoh, G. C.; Chua, A. S. M., Regression analysis on ionic liquid pretreatment of sugarcane bagasse and assessment of structural changes. *Biomass Bioenergy* **2012,** *36*.
149) Nguyen, T. A. D.; Kim, K. R.; Han, S. J.; Cho, H. Y.; Kim, J. W.; Park, S. M.; Park, J. C.; Sim, S. J., Pretreatment of rice straw with ammonia and ionic liquid for lignocellulose conversion to fermentable sugars. *Bioresour Technol* **2010,** *101*.
150) Tan, H. T.; Lee, K. T., Understanding the impact of ionic liquid pretreatment on biomass and enzymatic hydrolysis. *Chem Eng J* **2012,** *183*.
151) Lee, S. H.; Doherty, T. V.; Linhardt, R. J.; Dordick, J. S., Ionic liquid-mediated selective extraction of lignin from wood leading to enhanced enzymatic cellulose hydrolysis. *Biotechnology and Bioengineering* **2009,** *102* (5), 1368-1376.

152) Seddon, K. R.; Stark, A.; Torres, M. J., Influence of chloride, water, and organic solvents on the physical properties of ionic liquids. *Pure and Applied Chemistry* **2000**, *72*(12), 2275-2287.
153) Triolo, A.; Russina, O.; Bleif, H. J.; Di Cola, E., Nanoscale segregation in room temperature ionic liquids. *The Journal of Physical Chemistry B* **2007**, *111*(18), 4641-4644.
154) Green, S. M.; Ries, M. E.; Moffat, J.; Budtova, T., NMR and rheological study of anion size influence on the properties of two imidazolium-based ionic liquids. *Scientific reports* **2017**, *7*(1), 1-12.
155) Moyer, P.; Smith, M. D.; Abdoulmoumine, N.; Chmely, S. C.; Smith, J. C.; Petridis, L.; Labbé, N., Relationship between lignocellulosic biomass dissolution and physicochemical properties of ionic liquids composed of 3-methylimidazolium cations and carboxylate anions. *Physical Chemistry Chemical Physics* **2018**, *20*(4), 2508-2516.
156) Fendt, S.; Padmanabhan, S.; Blanch, H. W.; Prausnitz, J. M., Viscosities of Acetate or Chloride-Based Ionic Liquids and Some of Their Mixtures with Water or Other Common Solvents. *Journal of Chemical & Engineering Data* **2011,** *56* (1), 31-34.
157) Sescousse, R.; Le, K. A.; Ries, M. E.; Budtova, T., Viscosity of Cellulose−Imidazolium-Based Ionic Liquid Solutions. *The Journal of Physical Chemistry B* **2010,** *114* (21), 7222-7228.
158) Liu, W.; Budtova, T., Ionic liquid: A powerful solvent for homogeneous starch–cellulose mixing and making films with tuned morphology. *Polymer* **2012,** *53* (25), 5779-5787.
159) Lei, L.; Lindbråthen, A.; Sandru, M.; Gutierrez, M. T. G.; Zhang, X.; Hillestad, M.; He, X., Spinning cellulose hollow fibers using 1-ethyl-3-methylimidazolium acetate–dimethylsulfoxide co-solvent. *Polymers* **2018**, *10*(9), 972.
160) Kalb, R. S.; Stepurko, E. N.; Emel'yanenko, V. N.; Verevkin, S. P., Carbonate based ionic liquid synthesis (CBILS®): thermodynamic analysis. *Physical Chemistry Chemical Physics* **2016**, *18*(46), 31904-31913.
161) Lu, B.; Xu, A.; Wang, J., Cation does matter: how cationic structure affects the dissolution of cellulose in ionic liquids. *Green Chemistry* **2014,** *16* (3), 1326-1335.
162) Hollóczki, O.; Gerhard, D.; Massone, K.; Szarvas, L.; Németh,B.; Veszprémi, T.; Nyulászi, L. Carbenes in Ionic Liquids. *New Journal of Chemistry* **2010**,34, 3004−3009.
163) Zavrel, M.; Bross, D.; Funke, M.; Büchs, J.; Spiess, A. C., High-throughput screening for ionic liquids dissolving (ligno-) cellulose. *Bioresource technology*, **2009**, *100*(9), 2580-2587.
164) Erdmenger, T.; Haensch, C.; Hoogenboom, R.; Schubert, U. S., Homogeneous tritylation of cellulose in 1-butyl-3-methylimidazolium chloride. *Macromolecular bioscience* **2007**, *7*(4), 440-445.
165) Katritzky, A. R.; Fara, D. C.; Yang, H.; Tämm, K.; Tamm, T.; Karelson, M., Quantitative measures of solvent polarity. *Chemical reviews* 2004, *104*(1), 175-198.
166) Chiappe, C.; Malvaldi, M.; Pomelli, C. S., Ionic liquids: Solvation ability and polarity. *Pure and Applied Chemistry* **2009**, *81*(4), 767-776.
167) Xu, A.; Wang, J.; Wang, H., Effects of anionic structure and lithium salts addition on the dissolution of cellulose in 1-butyl-3-methylimidazolium-based ionic liquid solvent systems. *Green Chem.* **2010,** *12* (2), 268-275.
168) Lungwitz, R.; Strehmel, V.; Spange, S., The dipolarity/polarisability of 1-alkyl-3-methylimidazolium ionic liquids as function of anion structure and the alkyl chain length. *New Journal of Chemistry* **2010,** *34* (6), 1135-1140.

169) Lee, J.-M.; Prausnitz, J. M., Polarity and hydrogen-bond-donor strength for some ionic liquids: Effect of alkyl chain length on the pyrrolidinium cation. *Chemical Physics Letters* **2010,** *492* (1-3), 55-59.
170) Zhang, X.; Ma, J.; Ji, Z.; Yang, G. H.; Zhou, X.; Xu, F., Using confocal Raman microscopy to real-time monitor poplar cell wall swelling and dissolution during ionic liquid pretreatment. *Microscopy research and technique* **2014**, *77*(8), 609-618.
171) Charrier, A. M.; Lereu, A. L.; Farahi, R. H.; Davison, B. H.; Passian, A., Nanometrology of biomass for bioenergy: The role of atomic force microscopy and spectroscopy in plant cell characterization. *Frontiers in Energy Research* **2018**, *6*, 11.
172) Li, H. Y.; Chen, X.; Wang, C. Z.; Sun, S. N.; Sun, R. C., Evaluation of the two-step treatment with ionic liquids and alkali for enhancing enzymatic hydrolysis of Eucalyptus: chemical and anatomical changes. *Biotechnology for biofuels* **2016**, *9*(1), 166.
173) Payal, R. S.; Balasubramanian, S., Dissolution of cellulose in ionic liquids: an ab initio molecular dynamics simulation study. *Physical Chemistry Chemical Physics* 2014, *16*(33), 17458-17465.
174) Zubeltzu, J.; Formoso, E.; Rezabal, E., Lignin solvation by ionic liquids: The role of cation. *Journal of Molecular Liquids* **2020**, *303*, 112588.
175) Cláudio, A. F. M.; Swift, L.; Hallett, J. P.; Welton, T.; Coutinho, J. A.; Freire, M. G., Extended scale for the hydrogen-bond basicity of ionic liquids. *Physical Chemistry Chemical Physics* **2014**, *16*(14), 6593-6601.
176) Abraham, R. J.; Fisher, J.; Loftus, P., *Introduction to NMR spectroscopy* (Vol. 2). 1998 New York: Wiley.
177) Jacobsen, N. E. (2007). Fundamentals of NMR spectroscopy in liquids. *NMR Spectroscopy Explained: Simplified Theory, Applications and Examples for Organic Chemistry and Structural Biology*.
178) Headley, A. D. a. J., N. M., The effect of the anion on the chemical shifts of the aromatic hydrogen atoms of liquid 1-butyl-3-methylimidazolium salts. *Journal of Physical Organic Chemistry* **2002,** *15* (1), 52-55.
179) Zhang, J.; Zhang, H.; Wu, J.; Zhang, J.; He, J.; Xiang, J., NMR spectroscopic studies of cellobiose solvation in EmimAc aimed to understand the dissolution mechanism of cellulose in ionic liquids. *Physical Chemistry Chemical Physics* **2010,** *12* (8), 1941-1947.
180) Remsing, R. C.; Swatloski, R. P.; Rogers, R. D.; Moyna, G., Mechanism of cellulose dissolution in the ionic liquid 1-n-butyl-3-methylimidazolium chloride: a 13C and 35/37Cl NMR relaxation study on model systems. *Chemical Communications* **2006,** *12*, 1271-1273.
181) Ries, M. E.; Radhi, A.; Keating, A. S.; Parker, O.; Budtova, T., Diffusion of 1-ethyl-3-methyl-imidazolium acetate in glucose, cellobiose, and cellulose solutions. *Biomacromolecules* **2014**, *15*(2), 609-617.
182) Ausili, A.; Sánchez, M.; Gómez-Fernández, J. C., Attenuated total reflectance infrared spectroscopy: A powerful method for the simultaneous study of structure and spatial orientation of lipids and membrane proteins. *Biomedical Spectroscopy and Imaging* **2015**, *4*(2), 159-170.
183) Labbé, N.; Kline, L. M.; Moens, L.; Kim, K.; Kim, P. C.; Hayes, D. G., Activation of lignocellulosic biomass by ionic liquid for biorefinery fractionation. *Bioresource technology*, 2012, *104*, 701-707.

184) Keskar, S. S.; Edye, L. A.; Fellows, C. M.; Doherty, W. O., ATR-FTIR measurement of biomass components in phosphonium ionic liquids. *Journal of Wood Chemistry and Technology*, 2012, *32*(3), 175-186.
185) Moyer, P.; Kim, K.; Abdoulmoumine, N.; Chmely, S. C.; Long, B. K.; Carrier, D. J.; Labbé, N., Structural changes in lignocellulosic biomass during activation with ionic liquids comprising 3-methylimidazolium cations and carboxylate anions. *Biotechnology for biofuels* 2018, *11*(1), 1-13.
186) Muhammad, N.; Man, Z.; Mutalib, M.A.; Bustam, M.A.; Wilfred, C.D.; Khan, A.S.; Ullah, Z.; Gonfa, G.; Nasrullah, A., Dissolution and separation of wood biopolymers using ionic liquids. *ChemBioEng Reviews* 2015, *2*(4), pp.257-278.
187) Cheng, G.; Zhang, X.; Simmons, B.; Singh, S., Theory, practice and prospects of X-ray and neutron scattering for lignocellulosic biomass characterization: towards understanding biomass pretreatment. *Energy & Environmental Science* **2015,** *8* (2), 436-455.
188) Higgins, J. S.; Benoit, H. C., *Polymers and neutron scattering*. Clarendon Press: Oxford, 2009.
189) Melnichenko, Y. B. Basic Definitions and Essential Concepts of Small-Angle Scattering. In *Small-Angle Scattering from Confined and Interfacial Fluids* (1-18). Springer, Cham.2016.
190) Guinier, A.; Fournet, G.; Yudowitch, K. L., Small angle scattering of X-rays. **1955**.
191) Cullity, B. D.; Stock, S. R.; Pearson India Education, S., *Elements of X-ray diffraction*. Pearson India Education Services: [Miejsce nieznane], 2015.
192) Ilavsky, J.; Jemian, P.R., Irena: tool suite for modeling and analysis of small-angle scattering. *Journal of Applied Crystallography* **2009**, *42*, 347-353.
193) Breßler, I.; Kohlbrecher, J.; Thünemann, A. F., SASfit: a tool for small-angle scattering data analysis using a library of analytical expressions. *Journal of applied crystallography* **2015**, *48*(5), 1587-1598.
194) Beaucage, G., Approximations Leading to a Unified Exponential/Power-Law Approach to Small-Angle Scattering. *Journal of Applied Crystallography* **1995,** *28* (6), 717-728.
195) Janmey, P.A. and M. Schliwa, *Rheology.* Current biology: CB, 2008. 18(15): p. R639.
196) Barnes, H.A., J.F. Hutton, and K. Walters, *An introduction to rheology*. Vol. 3. 1989: Elsevier.
197) Barnes, H.A., *A handbook of elementary rheology.* 2000.
198) Batchelor, G.K., *An introduction to fluid dynamics*. 2000: Cambridge university press.
199) Barnes, H.A., *A Handbook of Elementary Rheology Institute of Non-Newtonian Fluid Mechanics.* University of Wales, 2000.
200) Gericke, M.; Schlufter, K.; Liebert, T.; Heinze, T.; Budtova, T., Rheological properties of cellulose/ionic liquid solutions: From dilute to concentrated states. *Biomacromolecules* **2009,** *10* (5), 1188-1194.
201) Lu, F.; Song, J.; Cheng, B. W.; Ji, X. J.; Wang, L. J., Viscoelasticity and rheology in the regimes from dilute to concentrated in cellulose 1-ethyl-3-methylimidazolium acetate solutions. *Cellulose* **2013**, *20*(3), 1343-1352.
202) Chen, X.; Zhang, Y.; Wang, H.; Wang, S. W.; Liang, S.; Colby, R. H., Solution rheology of cellulose in 1-butyl-3-methyl imidazolium chloride. *Journal of Rheology* **2011**,*55*(3), 485-494.

203) Lu, F.; Song, J.; Cheng, B. W.; Ji, X. J.; Wang, L. J., Viscoelasticity and rheology in the regimes from dilute to concentrated in cellulose 1-ethyl-3-methylimidazolium acetate solutions. *Cellulose* **2013**, *20*(3), 1343-1352.

Chapter 3. Multiple length scale investigation of interactions between cellulose and 1-alkyl-methyl imidazolium ionic liquids

A version of this chapter will be submitted as a peer-reviewed article.

Aparna Annamraju, Kalavathy Rajan, Xiobing Zuo, Brian K Long, David P. Harper, Sai Venkatesh Pingali and Nicole Labbé. (2020). Multi-length scale Investigation of Molecular interactions between cellulose and 1-alkyl-3-methylimidazolium ionic liquids

Aparna Annamraju performed the experiments, conducted data analysis, and wrote the first draft of the manuscript. Dr. Kalavathy Rajan edited the manuscript. Dr. Xiobing Zuo helped in SAXS data collection. Dr. Sai Venkatesh Pingali assisted in small angle X-ray scattering (SAXS) data interpretation. Drs. Brain Long and David Harper assisted in NMR and rheological data interpretation. Dr. Nicole Labbé oversaw the experimental design, assisted with data analysis, and edited the manuscript.

3.1. Abstract

Numerous ionic liquids (ILs) have an exceptional ability to solubilize biopolymers like cellulose, however, the specific nature of interactions between the polymer and IL ion pairs remain largely unknown. To investigate the interactions between cellulose and 1-alkyl-3-methylimidazolium ionic liquids, we selected two cations (1-ethyl-3-methylimidazolium [EMIM] and 1-allyl-3-methylimidazolium [AMIM]) and two anions (formate and acetate) in four combinations. Molecular interactions were probed by ^{13}C NMR spectroscopy, which indicates that both the IL anions and cations interact with cellulose. [EMIM]acetate exhibited the strongest shielding/deshielding effects while [AMIM]formate displayed the weakest. Mesoscale interactions measured using small-angle X-ray scattering showed that, although cellulose assumed a single stranded conformation in both [EMIM]acetate and [AMIM]formate, twice the number of acetate

ions were bound to individual cellulose strands than the formate ions. Furthermore, microscale interactions investigated by rheology revealed that, [AMIM]formate exhibited shear thinning behavior at higher rates than [EMIM]acetate. Thus, our comprehensive investigations spanning multiple length scales provided useful insights about factors affecting the dissolution of cellulose in 1-alkyl-3-methylimidazolium ILs.

Keywords: Cellulose; ionic liquid; interactions; NMR; SAXS; rheology.

3.2.Introduction

Cellulose is the most abundant polymer on earth with an annual production of 7.5 x 10^{10} tons.[1] Cellulose is used for a wide variety of applications due to its biodegradability and ability to undergo various chemical modifications.[2-5] Structurally, cellulose is a linear homopolymer that consists of repeating β-D-glucopyranose units connected by 1,4 glycosidic linkages. It has a strong propensity to form inter and intramolecular hydrogen (H) bonds, which are often cited as the reason for cellulose's complex structure[6] and lack of solubility in common solvents, such as water and ethanol.[7] Solvents such as N-methylmorpholine-N-oxide (NMMO) and ionic liquids (ILs) are known to disrupt the H-bonding network and dissolve cellulose,[8] with the advantages that ILs have lower toxicity and recyclability.[9]

ILs are low melting temperature salts with an organic cation and either an organic or inorganic anion. The physical properties of ILs, such as viscosity and density, can be tailored by varying the combination of cation and anion, hence, ILs are often referred to as "designer solvents".[10] ILs have several attractive features, such as low vapor pressure, high chemical stability, and high thermal stability, making them suitable for applications in numerous fields, e.g. electrochemistry, catalysis, and material engineering, to cite a few.[11-14] In the last decade, ILs have garnered great momentum in the field of cellulose processing.[15,16]

Since the initial report of cellulose dissolution,[8] the use of ILs has increased exponentially with several different types being identified as good solvents for cellulose.[17] However, the rationale for selecting an appropriate IL remains unclear due to the lack of clear understanding of the interactions between cellulose and a given IL. Investigating the interactions between ILs and cellulose will allow us to 1) establish a suitable set of dissolution parameters, 2) design and develop low cost ILs with superior cellulose solubility, and 3) evaluate IL-cellulose solutions for bio-product development.

Experimental techniques such as ^{1}H and ^{13}C nuclear magnetic resonance (NMR) spectroscopy elucidate the molecular-scale interactions between cellulose and ILs.[18-21] Using ^{13}C NMR spectroscopy, Remsing *et al*. studied the interactions between the oligomers of cellulose and three different ILs, i.e., 1-n-butyl-3-methylimidazolium chloride ([BMIM]chloride), 1-allyl-3-methylimidazolium chloride ([AMIM]chloride) and 1-ethyl-3-methylimidazolium acetate ([EMIM]acetate). They found that, while the relaxation time of the anion (^{13}C and $^{35/37}Cl$) was reduced in the presence of cellulose, the cation relaxation time remained unaltered.[18] This observation was interpreted as the ability of IL-anions to interact with cellulose via H-bonding. However, in a study by Zhang *et al*., where the chemical shift differences between cellobiose in [EMIM]acetate and neat IL were compared, both the IL-cation and anion were shown to interact with cellobiose.[20]

Apart from NMR spectroscopy, meso and microscale techniques have also been used to elucidate the role of ILs in dissolving cellulose. In the past decade, small-angle X-ray and neutron scattering techniques have been vital in obtaining mesoscale details, such as cellulose confirmation in ILs. For example, the work by Napso *et al*. indicated that cellulose was present in semi-flexible or rigid conformation in [EMIM]acetate.[22] On the other hand, cellulose was found to adopt a

flexible conformation in [BMIM]chloride.[23] This difference in confirmation was attributed to the chloride anion's ability to disrupt both intra- and inter-molecular H-bonds, in contrast to [EMIM]acetate which only disrupted the inter-molecular H-bonds. In a more recent study utilizing small-angle neutron scattering, [EMIM]acetate was reported to penetrate cellulose fibers and bind tightly to individual cellulose strands thereby bringing about cellulose dissolution.[24]

These studies suggest that, by investigating cellulose conformation at mesoscale, we can gather details about interactions between ILs and cellulose, which otherwise may not be captured by NMR spectroscopy. Therefore, unlike past work in which macroscopic solubility measurements were correlated with semi-empirical solvent scales or atomic correlations, herein we employ a comprehensive investigative methodology, ranging from molecular to bulk polymer scale, to understand the interactions between cellulose and 1-alkyl-3-methylimidazolium ionic liquids. Furthermore, because most previously reported studies of cellulose/IL systems utilized either acetate or chloride anions,[25] we chose to study formate-based ILs (e.g. [EMIM]formate and [AMIM]formate) that have been shown to dissolve higher weight percentage of cellulose.[26]

The primary objective of this study is to probe the interactions between cellulose and four different ILs using a combination of two cations ([EMIM], [AMIM]) and two carboxylate anions (acetate, formate). Interactions at molecular, meso and microscale were investigated using ^{13}C NMR spectroscopy, small-angle X-ray scattering (SAXS), and rheological techniques. The ^{13}C NMR spectroscopy shielding/deshielding effects provided evidence for interactions between both IL-cations and anions with cellulose. [EMIM]acetate and [AMIM]formate exhibited the most and least molecular-scale interactions with cellulose, respectively. SAXS data showed that the acetate ions bound in greater number to anhydroglucose units than the formate ions. Furthermore, rheological measurements demonstrated that the inter-molecular interactions were higher between

[EMIM]acetate and cellulose. These collective data imply that not only the molecular level interactions between cellulose, IL-cation and anion, but other bulk inter-molecular forces are responsible for the dissolution of cellulose in 1-alkyl-3-methylimidazolium ILs.

3.3. Experimental section

3.3.1. Materials

The four studied ILs, i.e., 1-ethyl-3-methylimidazolium formate ([EMIM]formate), 1-ethyl-3-methylimidazolium acetate ([EMIM]acetate), 1-allyl-3-methylimidazolium formate ([AMIM]formate), and 1-allyl-3-methylimidazolium acetate ([AMIM]acetate) were purchased from IoLiTec GmbH (Tuscaloosa, AL). The moisture content of [EMIM]formate, [EMIM]acetate, [AMIM]formate and [AMIM]acetate measured using Thermo gravimetric analysis (TGA) was 5.0, 6.9, 7.0 and 5.4 % (an average based on duplicate measurement). Avicel (microcrystalline cellulose, PH-101, DP = 230) was purchased from Alfa Aesar (Tewksbury, MA). The moisture content of Avicel was 3.2 % (an average based on a duplicate measurement). Dimethyl sulfoxide-d6 (DMSO-d6) (99.9 %) containing tetramethylsilane (TMS) (0.03 %, v/v) was purchased from Cambridge Isotope Laboratories, Inc., (Tewksbury, MA).

3.3.2. Preparation of cellulose-IL solutions

Cellulose-IL solutions were prepared by dissolving different amount of cellulose in each IL at 80 °C, following a previously published method.[27] Briefly, 2 g of IL were weighed out in a vial then heated at 100 °C for 10 min to remove any excess moisture. To confirm the moisture loss of ILs, TGA was conducted using thermogravimetric analyzer (Pyris 1 TGA, Perkin Elmer, Shelton, CT) with 5-10 mg of ionic liquid. ILs were heated in a platinum pan from 30 to 105 °C at a rate of 10 °C /min and held for 10 min at 105 °C under 10 mL/min of nitrogen. After 10 mins the mass loss of ILs was constant suggesting, 10 min heating at 100 °C prior to cellulose addition was

sufficient to remove water from ILs (Data in Appendix). The temperature was then reduced to 80 °C and cellulose was added in 20 mg increments to the neat IL. The dissolution of cellulose was confirmed by placing an aliquot of the solution under a bright-field optical microscope (20X magnification); absence of visible fiber bundles was assumed to indicate complete dissolution. Upon confirmation, the next increment of cellulose was added until the targeted concentrations of 2, 4, 6, 8 and 10 % (w/w) were achieved.

3.3.3. Preparation of ^{13}C NMR samples

To observe the changes in ^{13}C NMR chemical shifts as a function of cellulose concentration, samples were prepared by mixing 575 μL of the prepared cellulose-IL solution and 125 μL of DMSO-d6. Based on previously published work DMSO-d6 was chosen the solvent for NMR experimental setup.[28] Preliminary experiments were conducted to determine the minimum amount of DMSO-d6 needed to provide the lock frequency without significantly affecting cellulose-IL interactions. A control containing 575 μL of each neat IL and 125 μL of DMSO-d6 was also prepared. Samples with 0, 2, 4, 6, 8 and 10 % (w/w) cellulose concentration in the four ILs were prepared. The sample tubes were sealed with Teflon tape and stored under ambient conditions in between the NMR runs.

3.3.4. NMR instrumentation and ^{13} C NMR experiments

NMR spectra were recorded on a Bruker 400 MHz spectrometer at 353 K (80 °C). Both DMSO-d6 and tetramethylsilane (TMS) were used as an internal reference. The change in chemical shifts was calculated by subtracting the chemical shift of each carbon in the presence of different IL cellulose solutions and neat IL. The data were processed (base line correction and chemical shift assignment) using MNOVA software. A one-way ANOVA was performed to determine if there was any significant difference between the chemical shift value of neat IL and

those containing different concentrations of cellulose. Each experiment was repeated at least three times and a p-value of < 0.05 was considered significant. All statistical analyses were conducted using the IBM SPSS Statistics for Windows, Version 26.0 (IBM Corp, Armonk, NY).

3.3.5. SAXS and WAXS experiments

Small angle and wide-angle X-ray scattering (SAXS and WAXS) experiments were conducted at the 12-ID-B beamline of Advanced Photon Source (APS) (Argonne National Laboratory, Lemont, IL). All measurements were carried out at room temperature. Sample solutions were injected into a 2 mm diameter capillary and sealed with epoxy. Based on the NMR findings, we selected the 2 % (w/w) cellulose in [EMIM]acetate and [AMIM]formate for the SAXS study. The X-ray wavelength was 0.9322 Å. A PILATUS (Dectris) detector was used as the area detector. The irradiation time was 10 s (1 s irradiation X10). The observed X-ray scattering intensities were normalized to the absolute intensity using glassy carbon (a secondary standard sample for intensity calibration).[29] The solvent scaling factor for each IL was determined from the WAXS data, where no scattering signal from cellulose was observed. The scattering intensity of the cellulose molecules $I_{cellulose}(q)$ was obtained after subtracting the scattering intensity of the neat IL, $I_{neat\ IL}(q)$.

SAXS data were analyzed using a cylinder form factor with Gaussian distribution. The SAXS scattering intensity for a cylinder fit with radial polydispersity was implemented using the IRENA package[30] of Igor Pro (WaveMetrics, Inc., Portland, OR) software, which can be expressed as follows:

$$I(Q) = I_o \overline{P(Q)}\, S(Q) \quad (1)$$

I_0 is the intensity scalar which is given by the equation below:

$$I_o = \frac{\phi}{V_{poly}} (\Delta\rho)^2 \quad (2)$$

Where (*f*) accounts for the cylinder particle concentration with a polydisperse volume and □□ is the contrast (□cylinder − □solvent). $\rho_{cylinder}$ and $\rho_{solvent}$ are the scattering length densities (SLD) of the cylinder particles and the solvent, respectively. V_{poly}, the volume of polydisperse cylinders using second moment, is given as $V_{poly} = \pi r^2 L(1 + p^2)$, where *r* and *L* are the cylinder's radius and length, respectively. Polydispersity of cylinder, $p = \sigma / r_{avg}$, is the ratio of width of Gaussian distribution to its center. The form factor of a radially polydisperse cylinder, modeled as Gaussian distribution, is expressed as:

$$\overline{P(Q)} = \int_0^{\pi/2} G(r)\ F^2\ (q, \alpha)\ \sin\alpha\ d\alpha \quad (3)$$

where *F* is the form factor of a cylinder and *G*(*r*) is the radial Gaussian distribution function expressed as:

$$F(q, \alpha) = \ 2\ V_{cyl} J_0(qH\ cos\ \alpha)\ \frac{J_1(qr\ sin\ \alpha)}{(qr\ sin\ \alpha)} \quad (4)$$

$$G(r) = \frac{1}{\sigma\sqrt{2\pi}} \int_0^x exp\left[-\frac{1}{2\sigma^2}(r - r_{avg})^2\right]\ dr \quad (5)$$

In the equation 4, $J_0(x)$ = sin(x)/x is the zeroth order Bessel function, α is the angle between cylinder axis and the scattering vector, and *H* equals half the length of the cylinder. For our current analysis, a polydisperse function in cylinder fit was set to the limit of a monodisperse cylinder and no inter particle correlation was used, i.e., S(Q) = 1.

3.3.6. Rheological measurements of the cellulose-IL solutions

The steady shear viscosity of the different concentrations of cellulose in [EMIM]acetate and [AMIM]formate and the corresponding neat ILs was measured using a controlled stress rheometer, AR-G2 (TA Instruments, Newcastle, DE) equipped with a Peltier temperature-controlled plate. The measuring system had a cone and plate geometry with 2° angle, 40 mm diameter and 56 µm of sample thickness. For rheological measurements, the samples studied included 0, 2, and 10 %

(w/w) cellulose concentration in [EMIM]acetate and [AMIM]formate. For each solution, steady shear experiments were carried out in the shear range of 1 – 1000 s^{-1} at a constant temperature (80 °C). Silicon oil and metal plate covers were used to prevent the solutions from absorbing moisture during the measurement. Duplicate experiments were performed for each cellulose-IL solution.

3.4. Results and Discussion

To investigate the interactions between IL ion pairs and cellulose, two cations i.e., [EMIM] and [AMIM], and two anions i.e., formate and acetate, were chosen based on previous cellulose solubility reports.[26] The structure of the ILs along with the notation of atom numbers are shown in Figure 3.1.

3.4.1. Molecular scale interactions between cellulose, IL-cation and anion

The interaction parameter between cellulose and ILs is measured in terms of chemical resonance of the IL carbon atoms, in the presence and absence of cellulose. The calculated chemical shift changes of imidazolium ring carbon atoms (C2, C4 and C5) in [EMIM]acetate, [AMIM]acetate, [EMIM]formate and [AMIM]formate with increasing cellulose concentration, at 80 °C, are shown in Figure 3.2. Figures 3.2a and 3.2b compare the ring carbons of ILs having the same anion, acetate and formate, respectively. The comparison of chemical shift differences between ILs having the same cation and the raw NMR data are included in supplementary information.

In all four ILs, atoms C2, C4, and C5 underwent deshielding or increase in electron density (shown as negative chemical shift difference) with increase in cellulose concentration. Even at 2 % (w/w) of cellulose, the largest change was recorded for C2.

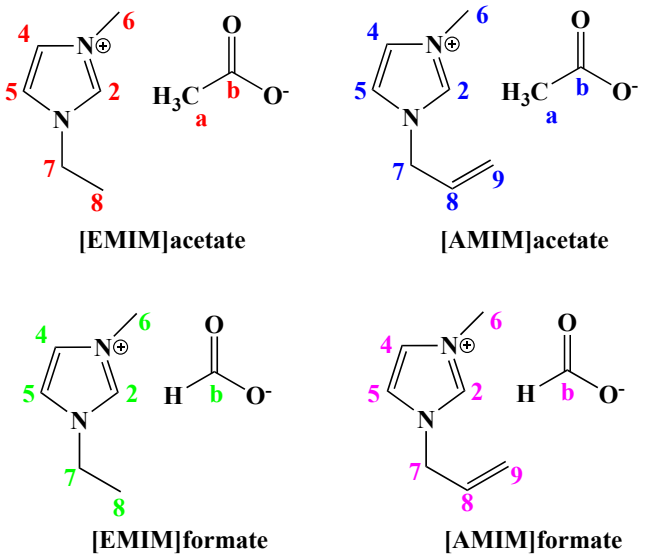

Figure 3. 1. Chemical structures and notation of carbon atom numbers of the four ionic liquids investigated.

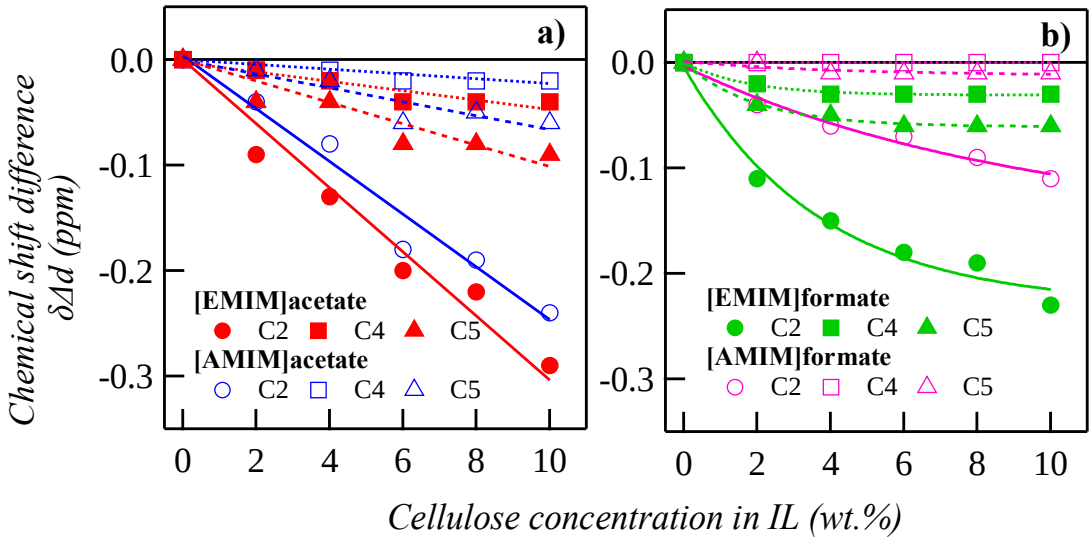

Figure 3. 2. Changes in ^{13}C NMR chemical shift value ($\delta_{(cellulose\ plus\ IL)} - \delta_{(IL)}$) of imidazolium ring carbons C2, C4 and C5 in **(a)** [EMIM]acetate (red) and [AMIM]acetate (blue); **(b)** [EMIM]formate (green) and [AMIM]formate (pink) as a function of cellulose concentration, at 80 °C.

When comparing C4 and C5, a greater change was observed for C5. The overall trend in deshielding for imidazolium carbons was C2 > C5> C4. Despite these common traits, there are two distinct differences between ILs containing acetate and formate anions. First, the magnitude of deshielding was not as pronounced for [AMIM]formate (at 10 % (w/w) C2, C4 and C5 $\Delta\delta$ are -0.11, 0.00 and -0.01) and secondly, the deshielding did not fit a linear trend for the formate IL, especially [EMIM]formate. The observation of non-linear trend for [EMIM]formate and C2 carbon of [AMIM]formate was unique among the tested ILs.

With increasing cellulose concentration, the side chain carbon atoms also experienced deshielding/shielding effects. The methyl group carbon (C6) in all the four ILs underwent shielding effect (positive chemical shift difference) with increase in cellulose concentration (Figure 3.3). The ethyl side chain carbon atoms, C7 and C8, in [EMIM]acetate (Figure 3.3a) and [EMIM]formate also exhibited shielding effect (Figure 3.3b). However, the changes are not statistically significant at low concentration of cellulose (2 and 4 % (w/w)) (data in supplementary information). In the [AMIM] set of ILs the side chain carbons, C7 and C9, underwent shielding, whereas the C8 carbon atom underwent deshielding. Once again, the magnitude of changes was the smallest for [AMIM]formate.

The anion carbon atoms also experienced deshielding/shielding effect due to a gradual increase in cellulose concentration. The chemical resonance changes observed for the anion carbons, Ca and Cb, in all four ILs are shown in Figure 3.4. With increasing cellulose concentration, the carbonyl carbon Cb underwent shielding. This shielding effect is in contrast to the deshielding of the alkyl group (Ca). The observed change is greater for the acetate (Figure 4a) set of ILs than the formate (Figure 4b).

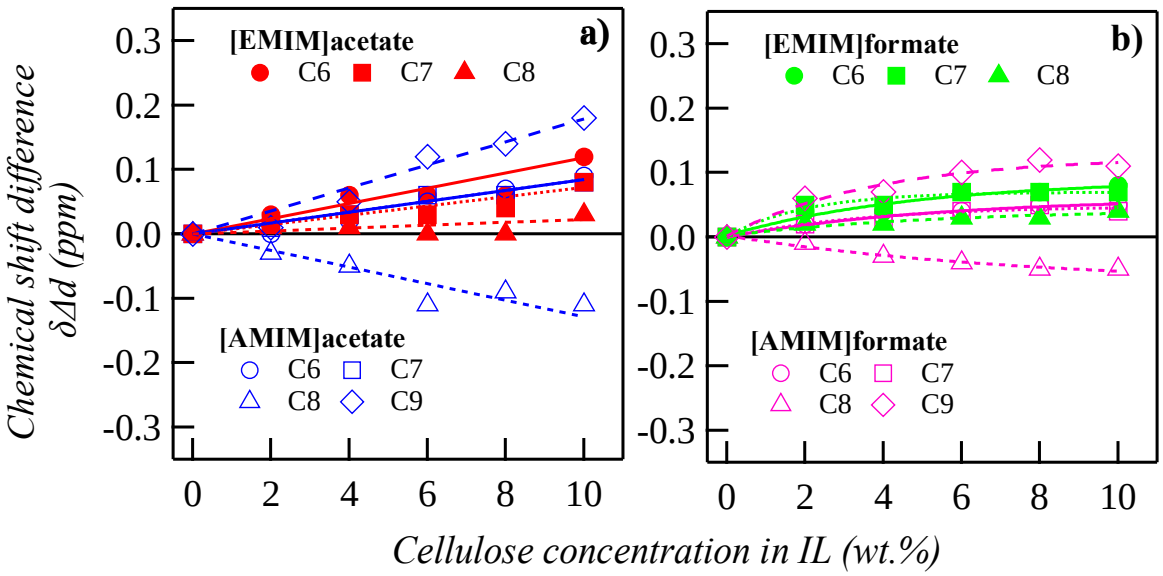

Figure 3. 3. Changes in ^{13}C NMR chemical shift value ($\delta_{(\text{cellulose plus IL})} - \delta_{(\text{IL})}$) of side chain carbons C6, C7, C8 and C9 in **(a)** [EMIM]acetate and [AMIM]acetate; **(b)** [EMIM]formate and [AMIM]formate as a function of cellulose concentration, at 80 °C.

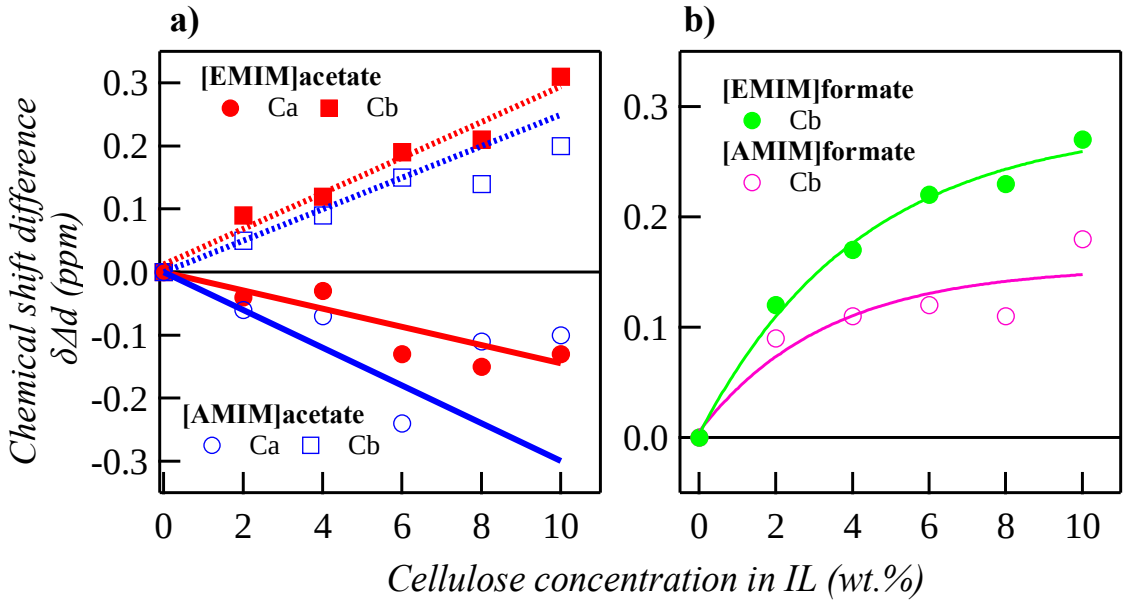

Figure 3. 4. Changes in ^{13}C NMR chemical shift values ($\delta_{(\text{cellulose plus IL})} - \delta_{(\text{IL})}$) of anion carbons, Ca and Cb, in **(a)** [EMIM]acetate and [AMIM]acetate; **(b)** [EMIM]formate and [AMIM]formate as a function of cellulose concentration, at 80 °C.

Similar to trend noted for imidazolium ring carbons a non-linear trend is obtained for carbonyl carbons of [EMIM]formate and [AMIM]formate.

It is well known that chemical shift values of imidazolium ring protons and carbons are altered by the IL anion, the NMR solvent and the presence of cellulose.[31, 28, 20] To understand the interactions between cellulose and ILs, studies using [EMIM]acetate have been performed in the past.[20, 21] In our study, the marked deshielding of the C2 carbon atom in both acetate and formate set of ILs is in agreement with the trend observed for [EMIM]acetate in previous studies. The possible reason for such a change is H-bond interaction between hydrogen at C2 position and oxygen of the hydroxyl or ether group of cellulose.[20, 21, 28] The lower magnitude in deshielding of C4 and C5 is due to lower acidity of the hydrogens as referenced to in other studies.[19, 21] Additionally, in all the four ILs, the greater deshielding of the C5 carbon could be due to the closer proximity of nitrogen (at position one) with the electron donating alkyl group.[31]

The observed shielding effect of the methyl side chain carbon (C6) could be due to the interaction of hydrogen atoms with the hydroxyl group of cellulose. Because of this interaction, electron density increases around the C6 carbon atom and results in the shielding effect. Conflicting reports exist in the literature about methyl group interaction, with a few studies reporting a shielding effect[32] while others reporting no changes.[33] However, similar to our study, Endo *et al*. recently reported shielding effect for methyl group carbon of [EMIM]acetate.[32] The observed upfield shift of ethyl side chain carbons, C7 and C8, of [EMIM]acetate and [EMIM]formate might be due to potential interactions between ethyl group hydrogens and cellulose hydroxyl group. Although the lower magnitude changes in [AMIM]-based ILs suggest a weaker mode of interaction, the higher shielding/deshielding effects of allyl side chain carbons

imply greater level of interaction with cellulose when compared to ethyl side chain carbons. This greater interaction of allyl group carbons is similar to the trend observed in [AMIM]chloride.[34] Due to the electron-withdrawing nature of allyl group (sp^2 carbons), the [AMIM] cation is rendered more electronegative and this increase in electron density of allyl carbons may be responsible for greater interaction with cellulose.

In case of IL-anions, the shielding effect of carbonyl carbon can be explained on the basis of H-bond formation between carbonyl oxygen and hydrogen atom of cellulose hydroxyl group. Because of this interaction the electron density around Cb decreases causing a shielding effect. As the acetate anion is a stronger conjugate base (pKa 4.75) than the formate anion (pKa 3.75), the carbonyl carbon of acetate anion can form stronger H-bond which is reflected as greater shielding effect of acetate ILs.[32] The deshielding of Ca is due to the increased electron density as a result of strong H-bond interactions between carbonyl group and hydroxyl group of cellulose.[20]

To understand the overall trend in our ^{13}C NMR results and highlight the magnitude of differences between the four ILs, the shielding and deshielding of all carbon atoms are consolidated in Figure 3.5. When the absolute values are compared, the interactions of all four ILs can be summarized as follows: [EMIM]acetate > [AMIM]acetate > [EMIM]formate > [AMIM]formate. In addition, we can conclude that the two carbons displaying the highest shielding and deshielding effects are the carbonyl group (Cb) of anions and the C2 carbon of cations. Between the [EMIM] and [AMIM] set of cations, the allyl side chain carbons exhibited greater change in chemical resonance than the ethyl side chain carbons.

Our ^{13}C NMR results thus far offer a perspective on the interactions between cellulose and ILs at molecular level.

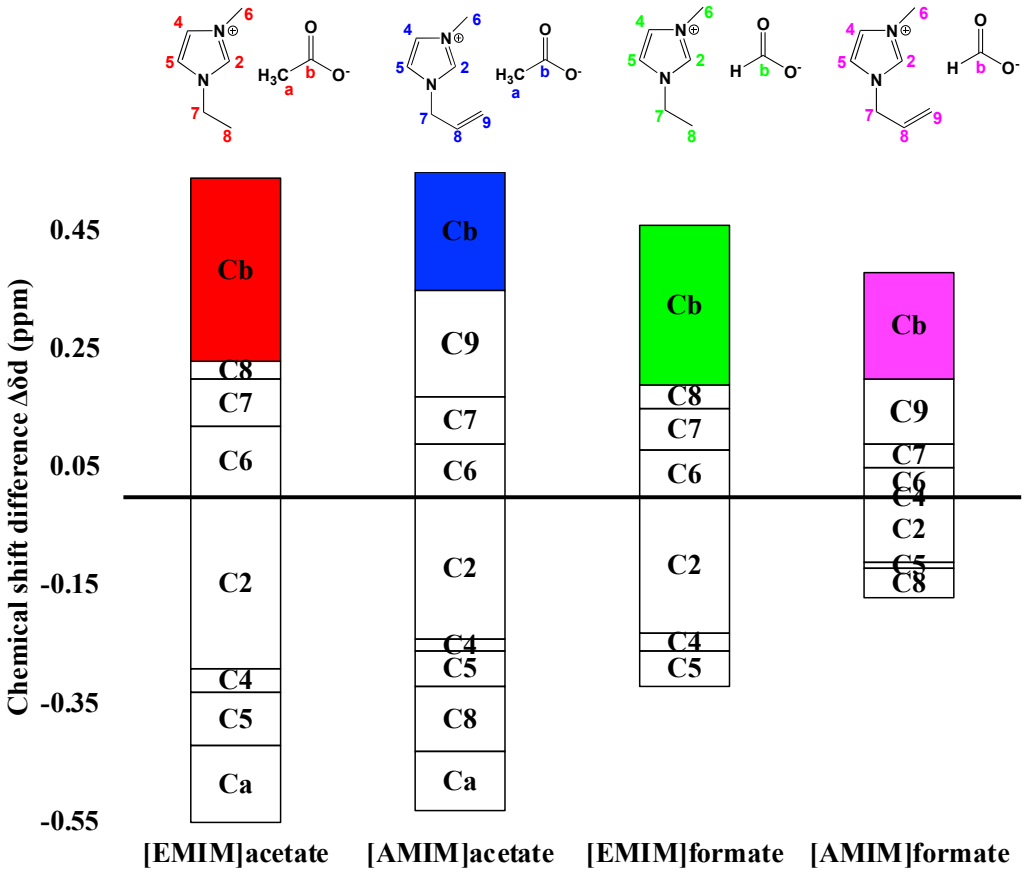

Figure 3. 5. Changes in chemical shift values ($\delta_{(\text{cellulose plus IL})} - \delta_{(\text{IL})}$) of all carbon atoms in [EMIM]acetate, [AMIM]acetate, [EMIM]formate and [AMIM]formate, each containing 10 % (w/w) of cellulose, determined using ^{13}C NMR analysis at 80 °C.

Previous studies have widely concluded that [AMIM]formate dissolved higher amount of cellulose (17 %), pectin (2.5 %), xylan (11 %)[26] and lignocellulosic biomass (7 %).[35]Interestingly, in our study, we observed the lowest carbon shielding/deshielding effects for [AMIM]formate indicating that the electronic environment around these IL carbon atoms is the least perturbed by the presence of cellulose. Since ILs are amphiphilic in nature and the cellulose molecule contains both hydrophilic and hydrophobic regions,[36, 37, 38, 39] it is plausible that inter-molecular interactions omitted by ^{13}C NMR are responsible for the superior performance of [AMIM]formate. To elucidate our proposed reasoning, the solution-state behavior of cellulose in [AMIM]formate and [EMIM]acetate (the two extreme ILs in term of changes (Figure 5)) was investigated using SAXS and rheological techniques.

3.4.2. Mesoscale state of cellulose in ILs

To investigate the structure of cellulose at mesoscale and to understand the differences noted between [EMIM]acetate and [AMIM]formate, SAXS studies were performed. The low cellulose concentration, i.e., 2 % (w/w), was selected to identify cellulose features by preventing any aggregate formation. The SAXS profiles of cellulose in the two ILs were similar except for a vertical scalar (Figure 3.6). The observed monotonic increase of scattering intensity proportional to Q^{-1} implied that cellulose adopted a rod-like particle shape in both ILs. Therefore, the SAXS data were fit to a cylinder shape. Further, the high flux of synchrotron X-rays was beneficial in observing a feature representative of the cross-sectional dimension of an individual cellulose strand in the high-Q region.

The evaluated parameters for 2 % (w/w) cellulose in [EMIM]acetate and [AMIM]acetate are listed in Table 1. The volume fraction (*f*) of cellulose was calculated from the weight percent of cellulose in the ILs and was fixed while performing the fit analysis.

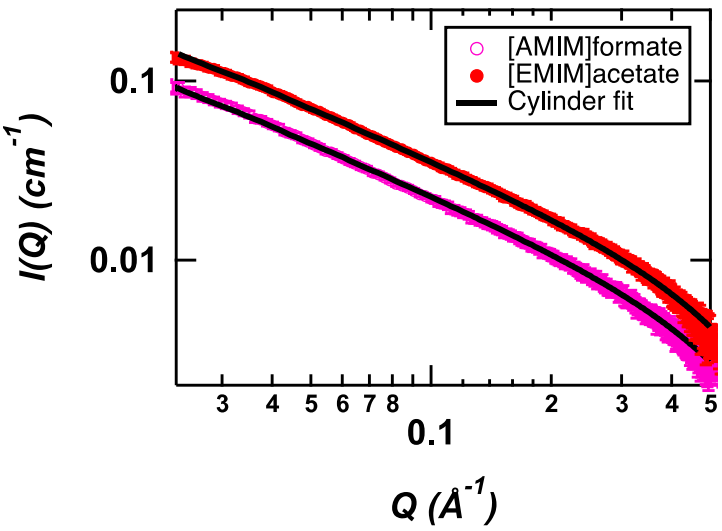

Figure 3. 6. SAXS profiles of 2 % (w/w) cellulose in [EMIM]acetate and [AMIM]formate with a cylinder shape fit indicated by the solid black lines.

On the other hand, the contrast parameter (Δρ) was altered to improve the overall fit intensity. The data presented in table 1 show that the cross-sectional radius of the cylindrical cellulose strand is identical in both ILs, at ~2.87 Å. The other result from the cylinder fit leads to the experimental contrast ($\Delta\rho_{exp}$), which is higher than the calculated theoretical contrast ($\Delta\rho_{theo}$) for the two ILs. Even though the difference between the experimental and theoretical contrasts is higher for both ILs, the difference is less pronounced for [AMIM]formate than [EMIM]acetate.

Raguwanshi *et al.*, first reported on the phenomenon of increased experimental contrast between IL and cellulose.[24] Using the ratio of the experimental and theoretical contrasts ($\Delta\rho_{exp}/\Delta\rho_{theo}$), they concluded that IL anions bound irreversibly to cellulose strands. As a similar increase in contrast was observed for both [EMIM]acetate and [AMIM]formate, we implemented the approach developed by Raguwanshi *et al*. (eqn. 3.6), to obtain a quantitative estimation of anhydroglucose units (*x*) bound to the IL anions.

$$x = \frac{\left(\frac{(\sum b_i)_{anion}}{(\sum b_i)_{cellulose}}\right)}{\left(1-\frac{\rho_{IL}}{\rho_{cellulose}}\right)\left(\frac{\Delta\rho_{exp}}{\Delta\rho_{theo}}-1\right)} \qquad (3.6)$$

Where b is the scattering length densities (SLDs) of cellulose and IL-anions; ρ_{IL} and $\rho_{cellulose}$ are the SLDs of ILs and cellulose, respectively; and $\Delta\rho_{exp}$ and $\Delta\rho_{theo}$ are experimental and theoretical contrasts, respectively.

Following eqn. 6, one formate anion was calculated to bind to 4.6 anhydroglucose units (AGUs), while one acetate anion would bind to 2.8 AGUs (Table 3.1). This result is consistent with the higher shielding change observed using NMR. The Kratky plot of 2% cellulose in the [EMIM]acetate and [AMIM]formate is shown in Figure 3.7. With increase in Q a smooth transition from power law1 to power 2 was observed for both [EMIM]acetate and [AMIM]formate.

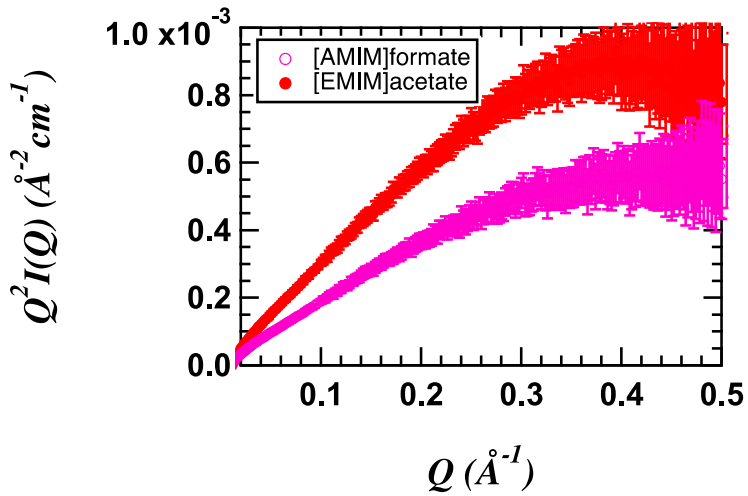

Figure 3. 7. Kratky plots of 2 wt.% cellulose in [EMIM]acetate (red) and [AMIM]formate (pink).

This observation means that at the 2 wt.% cellulose concentration SAXS data does not show any interferences due to structure factor. Therefore, our assumption of S(Q) = 1 is valid under the current experimental set up. These results are consistent with Raguwanshi *et al.* observation as well.

SAXS has been used to probe the structure of cellulose in various solvents such as water, acetone and ethanol.[40, 41] In these solvents, a characteristic shoulder was observed around Q ~ 0.1 $Å^{-1}$ which is consistent with cellulose microfibril cross-sectional dimension.[41] A similar feature was observed in [EMIM]acetate and [AMIM]formate but at a higher Q value, ~ 0.3 $Å^{-1}$, indicating that these ILs diffuse into the cellulose microfibril and resolve individual elementary fibrils. Furthermore, the obtained diameter of cellulose (5.75 ± 0.12 Å) in both ILs aligns well with the cross-sectional diameter (6.38 Å) of a cellulose strand obtained using cellulose crystal structure, thereby confirming that these rod-like molecules are in fact individual cellulose strands.[42]

Recently, several SAXS studies were conducted to determine the interactions between cellulose and various ILs.[22, 23, 43] Similar to our findings, cellulose was reported to exhibit a stiff rod-like conformation in [EMIM]acetate and [EMIM]methylphosphonate.[24,43] This non-flexible conformation implies that [EMIM]acetate and [AMIM]formate did not disrupt the intramolecular H-bonds, thereby keeping the individual cellulose strands intact. The main distinction between cellulose dissolved in [AMIM]formate and [EMIM]acetate is in the number of anions binding to cellulose. The acetate anions exhibit ~2 times higher propensity to bind to anhydroglucose units than formate anions. This higher binding affinity of acetate anion mirrors the higher shielding obtained by ^{13}C NMR. However, despite the lower number of formate anions binding to the anhydroglucose units the conformation of cellulose strands remained the same in both ILs.

Table 3. 1. Summary of cylinder fit parameters of SAXS data for 2% (w/w) cellulose in [EMIM]acetate and [AMIM]formate.

Fit parameters	**[EMIM]acetate**	**[AMIM]formate**
*Volume fraction (*f*)	0.0148	0.0151
Mean radius (Å)	2.89 ± 0.06	2.85 ± 0.06
Experimental contrast ($\Delta\rho_e$) $^{\#}$ ($\times 10^{-6}$ Å^{-2})	5.14	4.04
$^{\#}$Theoretical contrast ($\Delta\rho_t$) ($\times 10^{-6}$ Å^{-2})	3.42	3.25
$^{\wedge}$Number of AGU per anion	2.8	4.6

* Calculated from weight percent; # Calculated contrast values; ^ Obtained from Eqn. 6.

This observation leads to the conclusion that anion – cellulose interactions alone do not determine the dissolution of cellulose in ILs.

3.4.3. Microscale changes in cellulose-IL interactions

To study the structure of cellulose at microscopic scale, the viscosity of [AMIM]formate and [EMIM]acetate was measured as a function of cellulose concentration (Figure 3.7). Typical to classic solution state polymers, the viscosity of cellulose-IL solutions increased with cellulose concentration. While the viscosity of neat [EMIM]acetate was higher than [AMIM]formate, at 2 % (w/w) of cellulose, the two IL solutions had the same viscosity (0.064 Pa.s) with a broad Newtonian plateau over the measured shear range. This observation is in line with our SAXS results, i.e., in both [EMIM]acetate and [AMIM]formate cellulose assumed the same conformation. However, at 10 % (w/w) of cellulose, the viscosity of [AMIM]formate was 2.3 times higher than that of [EMIM]acetate. In addition to higher viscosity, the 10% [AMIM]formate solution exhibited a shear thinning behavior at higher shear rates when compared to the [EMIM]acetate solution.

The structure of polymers like cellulose is governed by various inter-molecular interactions such as excluded volume, van der Waals, electrostatic and hydrophobic forces. Examining the flow behavior of cellulose-IL solutions will shed light on such interactions. Previous studies on specific viscosity of cellulose dissolved in [EMIM]acetate and [AMIM]formate reported that the calculated R_g and Kuhn length were the same in both solvents suggestive of similar solvating properties.[44,45] This observation is consistent with the SAXS results which also showed identical conformation of cellulose polymer in both ILs.

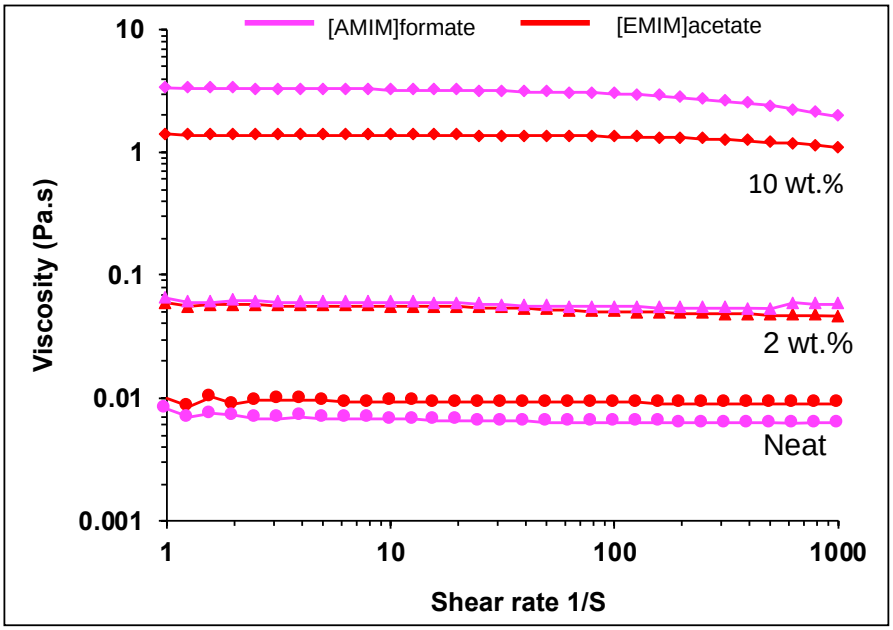

Figure 3. 8. Steady state shear of cellulose and ionic liquid mixtures, as a function of cellulose concentration, measured at 80 °C.

Gericke *et al.*, compared the viscosity of [BMIM]chloride and [EMIM]acetate-based cellulose solutions[46] and found that the viscosity of [BMIM]chloride solution was higher than [EMIM]acetate at similar (1 and 5 % w/w) concentrations. This observation was attributed to the high room-temperature viscosity of [BMIM]chloride, which in turn was due to the strong interactions between the [BMIM] cation and chloride anion. In contrast to [BMIM]chloride, [AMIM]formate has lower room-temperature viscosity. Further, our NMR and SAXS data have shown that there are fewer formate ions binding to cellulose. Therefore, the higher viscosity observed at the highest cellulose concentration (Figure 3.7) is likely due to higher inter-molecular interactions between cellulose strands rather than the interactions between cellulose and [AMIM]formate. As a result of this enhanced attraction between cellulose strands, we observed a shear thinning behavior for [AMIM]formate at high shear rates (Figure 7). Thus, the rheology and SAXS results prove our earlier hypothesis that complex interactions other than anion-dominant interactions must be responsible for the dissolution of cellulose in [AMIM]formate-like ILs.

3.5. Conclusion

By combining molecular, meso- and micro-scale interactions between ILs and cellulose, determined using ^{13}C NMR, SAXS and rheological measurements, respectively, we determined the complexity of factors leading to the dissolution of cellulose. It was found that the ^{13}C NMR chemical resonances of both IL-cation and anion altered as a function of cellulose concentration. This observation leads to the conclusion that both anions and cations interact with cellulose, leading to cellulose dissolution. Among the tested ILs, the ^{13}C NMR shielding/deshielding effects were highest in absolute magnitude for [EMIM]acetate and the lowest for [AMIM]formate. SAXS data showed that almost twice the number of acetate ions were bound to cellulose AGUs than the formate ions. Rheological studies determined a shear thinning behavior for [AMIM]formate at

higher shear rates, further illustrating fewer interactions between cellulose strands and this IL. These combined results suggest that acetate based ILs dissolve cellulose by virtue of strong interactions between acetate anions and cellulose fibrils. However, further research is necessary to elucidate the set of interactions leading to cellulose dissolution in [AMIM]formate-like ILs.

Associated content

The supporting information document contains ^{13}C NMR chemical shift values of imidazolium ring carbons (C2, C4, C5), side chain carbons (C6, C7, C8, C9) and anion carbons (Ca, Cb) of [AMIM]acetate, [AMIM]formate, [EMIM]formate and [EMIM]acetate, as a function of IL-cation. Annotated NMR spectra of [AMIM]acetate, [AMIM]formate, [EMIM]formate and [EMIM]acetate, with and without cellulose and one-way ANOVA results of ^{13}C NMR shielding and deshielding. It also includes molecular weight, density and scattering length density of [EMIM]acetate and [AMIM]formate.

Acknowledgments

This work was supported by the Research Council of Norway. (grant no. R113215138). This research was also partially supported by the DOE Office of Science, Office of Biological and Environmental Research under the Genomic Science Program (FWP ERKP752; Biofuels SFA). The authors thank Dr. Carlos Steren from the Department of Chemistry, The University of Tennessee Knoxville for assisting with the NMR experiments. The authors also thank Dr. Byeongdu Lee at Advanced Photo Source, Argonne National Laboratory for assisting in SAXS data analysis. The authors thank Loukas Petridis, Hugh M O'Neil and Mark D. Dadmun for reviewing the manuscript and providing critical feedback. Finally, the authors would like to thank

Dr. Yachin Cohen from the Department of Chemical Engineering, Technion Israel Institute of Technology, Haifa for email correspondence on cellulose ion binding calculations.

References

1) Lindström, T.; Aulin, C.; Naderi, A.; Ankerfors, M., Microfibrillated Cellulose. In *Encyclopedia of Polymer Science and Technology*, Herman. F.M., Ed, John Wiley and Sons; Hoboken, USA 2014, p 1-34
2) Tsioptsias, C.; Stefopoulos, A.; Kokkinomalis, I.; Papadopoulou, L.; Panayiotou, C., Development of micro- and nano-porous composite materials by processing cellulose with ionic liquids and supercritical CO_2. *Green Chemistry* **2008**, *10*, 965-971.
3) Fink, H.-P.; Weigel, P.; Purz, H. J.; Ganster, J., Structure formation of regenerated cellulose materials from NMMO-solutions. *Progress in Polymer Science* **2001**, *26*(9), 1473-1524.
4) McCormick, C.L.; Dawsey, T.R., Preparation of cellulose derivatives via ring opening reactions with cyclic reagents with lithium chloride/N,N-dimethylacetamide. *Macromolecules* **1990**, *23*, 3606-3610.
5) Dai, L.; Cheng, T.; Duan, C.; Zhao, W.; Zhang, W.; Zou, X.; Aspler, J.; Ni, Y., 3D printing using plant-derived cellulose and its derivatives: A review. *Carbohydrate Polymers* **2019,** *203*, 71-86.
6) Updegraff, D. M., Semimicro Determination of Cellulose in Biological Materials. *Analytical Biochemistry* **1969,** *32* (3), 420-424.
7) Hiroyuki, O.; Yukinobu, F., Task Specific Ionic Liquids for Cellulose Technology. *Chemistry Letters* **2009,** *38* (1), 2-7.
8) Swatloski, R. P.; Spear, S. K.; Holbrey, J. D.; Rogers, R. D., Dissolution of Cellose with Ionic Liquids. *Journal of the American Chemical Society* **2002,** *124* (18), 4974-4975.
9) Weerachanchai, P.; Lee, J.M., Recyclability of an ionic liquid for biomass pretreatment. *Bioresource technology* **2014**, *169*, 336-343.
10) Plechkova, N. V.; Seddon, K. R., Ionic Liquids: "Designer" Solvents for Green Chemistry. In *Methods and Reagents for Green Chemistry*, Tundo.P.; Perosa.A.; Zecchini.F., Ed(s). John Wiley and Sons; Hoboken, USA 2007, p 103-130.
11) Wang, H.; Gurau, G.; Rogers, R. D., Ionic liquid processing of cellulose. *Chemical Society Reviews* **2012,** *41* (4), 1519-1537.
12) Boroujeni, K. P.; Shirazi, E. R.; Doroodmand, M. M., Synthesis of α-aminophosphonates using carbon nanotube supported imidazolium salt-based ionic liquid as a novel and environmentally benign catalyst. *Phosphorus, Sulfur, and Silicon and the Related Elements* **2016,** *191* (5), 683-688.
13) Smiglak, M.; Pringle, J. M.; Lu, X.; Han, L.; Zhang, S.; Gao, H.; MacFarlane, D. R.; Rogers, R. D., Ionic liquids for energy, materials, and medicine. *Chemical Communications* **2014,** *50* (66), 9228-9250.
14) Wilkes, J. S.; Levisky, J. A.; Wilson, R. A.; Hussey, C. L., Dialkylimidazolium chloroaluminate melts: a new class of room-temperature ionic liquids for electrochemistry, spectroscopy and synthesis. *Inorganic Chemistry* **1982,** *21* (3), 1263-1264.
15) Cao, Y.; Zhang, R.; Cheng, T.; Guo, J.; Xian, M.; Liu, H., Imidazolium-based ionic liquids for cellulose pretreatment: recent progresses and future perspectives. *Applied Microbiology and Biotechnology* **2017,** *101* (2), 521-532.
16) Fort, D. A.; Remsing, R. C.; Swatloski, R. P.; Moyna, P.; Moyna, G.; Rogers, R. D., Can ionic liquids dissolve wood? Processing and analysis of lignocellulosic materials with 1-n-butyl-3-methylimidazolium chloride. *Green Chemistry* **2007,** *9* (1), 63-69.

17) Isik, M.; Sardon, H.; Mecerreyes, D., Ionic liquids and cellulose: dissolution, chemical modification and preparation of new cellulosic materials. *International Journal of Molecular Sciences* **2014,** *15* (7), 11922-11940.
18) Remsing, R. C.; Swatloski, R. P.; Rogers, R. D.; Moyna, G., Mechanism of cellulose dissolution in the ionic liquid 1-n-butyl-3-methylimidazolium chloride: a 13C and 35/37Cl NMR relaxation study on model systems. *Chemical Communications* **2006,** *12*, 1271-1273.
19) Palomar, J.; Ferro, V. R.; Gilarranz, M. A.; Rodriguez, J. J., Computational Approach to Nuclear Magnetic Resonance in 1-Alkyl-3-methylimidazolium Ionic Liquids. *The Journal of Physical Chemistry B* **2007,** *111* (1), 168-180.
20) Zhang, J.; Zhang, H.; Wu, J.; Zhang, J.; He, J.; Xiang, J., NMR spectroscopic studies of cellobiose solvation in EmimAc aimed to understand the dissolution mechanism of cellulose in ionic liquids. *Physical Chemistry Chemical Physics* **2010,** *12* (8), 1941-1947.
21) Zhang, J.; Xu, L.; Yu, J.; Wu, J.; Zhang, X.; He, J.; Zhang, J., Understanding cellulose dissolution: effect of the cation and anion structure of ionic liquids on the solubility of cellulose. *Science China Chemistry* **2016,** *59* (11), 1421-1429.
22) Napso, S.; Rein, D. M.; Khalfin, R.; Cohen, Y., Semidilute solution structure of cellulose in an ionic liquid and its mixture with a polar organic co-solvent studied by small-angle X-ray scattering. *Journal of Polymer Science Part B: Polymer Physics* **2017,** *55* (11), 888-894.
23) Jiang, X.; Kitamura, S.; Sato, T.; Terao, K., Chain dimensions and stiffness of cellulosic and amylosic Chains in an ionic liquid: cellulose, amylose, and an amylose carbamate in BmimCl. *Macromolecules* **2017,** *50* (10), 3979-3984.
24) Raghuwanshi, V. S.; Cohen, Y.; Garnier, G.; Garvey, C. J.; Russell, R. A.; Darwish, T.; Garnier, G., Cellulose dissolution in ionic liquid: ion binding revealed by neutron scattering. *Macromolecules* **2018,** *51* (19), 7649-7655.
25) Bharadwaj, V. S.; Schutt, T. C.; Ashurst, T. C.; Maupin, C. M., Elucidating the conformational energetics of glucose and cellobiose in ionic liquids. *Physical Chemistry Chemical Physics* **2015,** *17* (16), 10668-10678.
26) Fukaya, Y.; Sugimoto, A.; Ohno, H., Superior solubility of polysaccharides in low viscosity, polar, and halogen-free 1,3-dialkylimidazolium formates. *Biomacromolecules* **2006,** *7* (12), 3295-3297.
27) Kilpelainen, I.; Xie, H.; King, A.; Granstrom, M.; Heikkinen, S.; Argyropoulos, D.S., Dissolution of wood in ionic liquids. *Journal of Agricultural and Food Chemistry* **2007**, *55*, 9142-9148.
28) Hesse-Ertelt, S.; Heinze, T.; Kosan, B.; Schwikal, K.; Meister, F., Solvent effects on the NMR chemical shifts of imidazolium-based ionic liquids and cellulose therein. *Macromolecular Symposia* **2010,** *294* (2), 75-89.
29) Zhang, F.; Ilavsky, J.; Long, G.G.; Quintana, J.P.G.; Allen, A.J.; Jemian, P.R., Glassy carbon as an absolute intensity standard for small-angle scattering. *Metallurgical and Materials Transactions A* **2010**, *41*, 1151-1158.
30) Ilavsky, J.; Jemian, P.R., Irena: tool suite for modeling and analysis of small-angle scattering. *Journal of Applied Crystallography* **2009**, *42*, 347-353.
31) Headley, A. D. a. J., N. M., The effect of the anion on the chemical shifts of the aromatic hydrogen atoms of liquid 1-butyl-3-methylimidazolium salts. *Journal of Physical Organic Chemistry* **2002,** *15* (1), 52-55.

32) Endo, T.; Hosomi, S.; Fujii, S.; Ninomiya, K.; Takahashi, K., Anion bridging-induced structural transformation of cellulose dissolved in ionic liquid. *Journal of Physical Chemistry Letters* **2016,** *7* (24), 5156-5161.
33) Lu, B.; Xu, A.; Wang, J., Cation does matter: how cationic structure affects the dissolution of cellulose in ionic liquids. *Green Chemistry* **2014,** *16* (3), 1326-1335.
34) Zhang, Y.; Xu, A.; Lu, B.; Li, Z.; Wang, J., Dissolution of cellulose in 1-allyl-3-methylimizodalium carboxylates at room temperature: A structure–property relationship study. *Carbohydrate Polymers* **2015,** *117*, 666-672.
35) Moyer, P.; Smith, M. D.; Abdoulmoumine, N.; Chmely, S. C.; Smith, J. C.; Petridis, L.; Labbé, N., Relationship between lignocellulosic biomass dissolution and physicochemical properties of ionic liquids composed of 3-methylimidazolium cations and carboxylate anions. *Physical Chemistry Chemical Physics* **2018,** *20* (4), 2508-2516.
36) Medronho, B.; Lindman, B., Competing forces during cellulose dissolution: From solvents to mechanisms. *Current Opinion in Colloid & Interface Science* **2014,** *19* (1), 32-40.
37) Medronho, B., Romano, A., Miguel, M. G., Stigsson, L., & Lindman, B., Rationalizing cellulose (in)solubility: reviewing basic physicochemical aspects and role of hydrophobic interactions. *Cellulose*, **2012,** *19* (3), 581-587.
38) Yamane, C.; Aoyagi, T.; Ago, M.; Sato, K.; Okajima, K.; Takahashi, T., Two different surface properties of regenerated cellulose due to structural anisotropy. *Polymer Journal* **2006,** *38* (8), 819-826.
39) Pingali, S.V.; Smith, M.D.; Liu, S-H.; Rawal, T.B.; Pu, Y.; Shah, R. S.; Evans, B. R.; Urban, V.S.; Davison, B.H.; Cai, C.M.; Ragauskas, A.J.; O'Neill, M.H.; Smith, J.C.; Petridis, L., Deconstruction of biomass enabled by local demixing of cosolvents at cellulose and lignin surfaces. *Proceedings of the National Academy of Sciences* **2020**,
40) Leppänen, K.; Pirkkalainen, K.; Penttilä, P.; Sievänen, J.; Kotelnikova, N.; Serimaa, R., Small-angle x-ray scattering study on the structure of microcrystalline and nanofibrillated cellulose. *Journal of Physics: Conference Series* **2010,** *247*, 012030.
41) Pingali, S. V.; Urban, V. S.; Heller, W. T.; McGaughey, J.; O'Neill, H. M.; Foston, M.; Myles, D. A.; Ragauskas, A. J.; Evans, B. R., SANS study of cellulose extracted from switchgrass. *Acta Crystallographica Section D* **2010,** *66* (11), 1189-1193.
42) Nishiyama, Y.; Langan, P.; Chanzy, H. Crystal structure and hydrogen-bonding system in cellulose I beta from synchrotron X-ray and neutron fiber diffraction. *Journal of American Chemical Society* **2002,** *124* (31), 9074-9082
43) Hirosawa, K.; Fujii, K.; Hashimoto, K.; Shibayama, M., Solvated structure of cellulose in a phosphonate-based ionic liquid. *Macromolecules* **2017,** *50* (17), 6509-6517.
44) Haward, S. J.; Sharma, V.; Butts, C. P.; McKinley, G. H.; Rahatekar, S. S., Shear and extensional rheology of cellulose/ionic liquid solutions. *Biomacromolecules* **2012,** *13* (5), 1688-1699.
45) Lu, F.; Wang, L.; Ji, X.; Cheng, B.; Song, J.; Gou, X., Flow behavior and linear viscoelasticity of cellulose 1-allyl-3-methylimidazolium formate solutions. *Carbohydrate Polymers* **2014,** *99*, 132-139.
46) Gericke, M.; Schlufter, K.; Liebert, T.; Heinze, T.; Budtova, T., Rheological properties of cellulose/ionic liquid solutions: From dilute to concentrated states. *Biomacromolecules* **2009,** *10* (5), 1188-1194.

3.6. Appendix

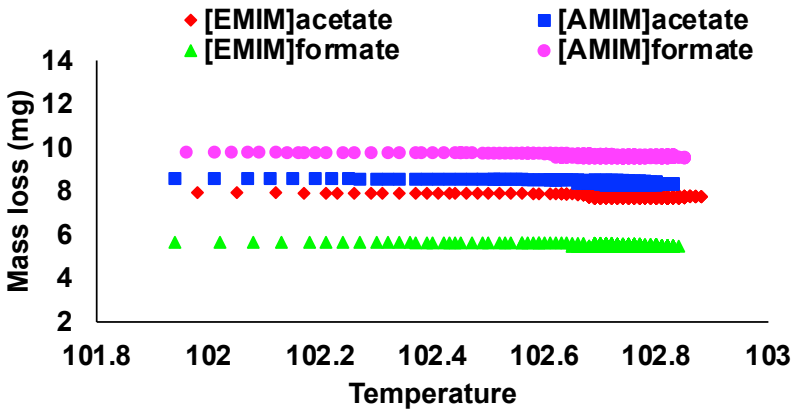

Figure 3. 9. Mass loss versus temperature data of [EMIM]acetate (red), [AMIM]acetate (blue), [EMIM]formate (green) and [AMIM]formate (pink) at 102 ˚C.

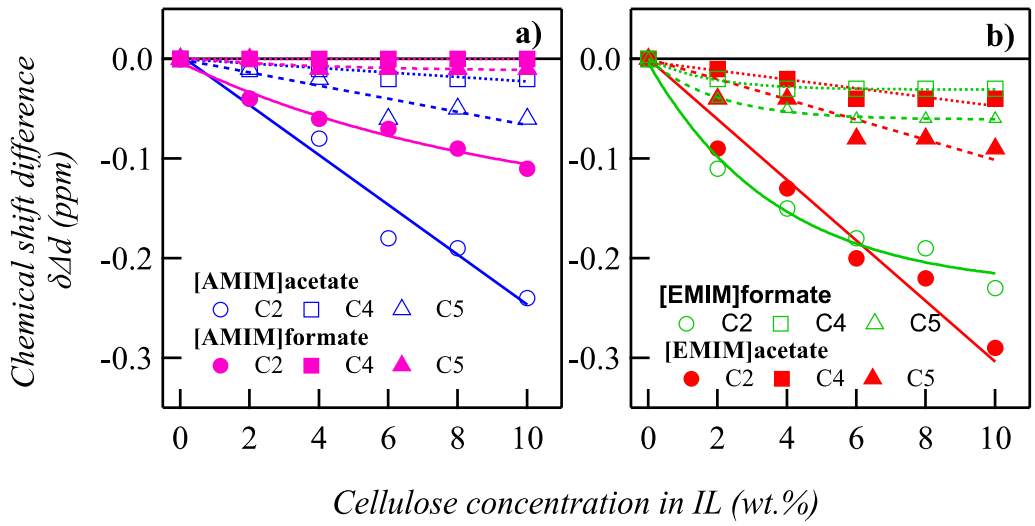

Figure 3. 10. Changes in ^{13}C NMR chemical shift value ($\delta_{(\text{cellulose plus IL})} - \delta_{(\text{IL})}$) of imidazolium ring carbon C2, C4 and C5 in **(a)** [AMIM]acetate (blue) and [AMIM]formate (pink) and **(b)** in [EMIM]formate (green) and [EMIM]acetate (red) as a function of cellulose concentration at 80 °C.

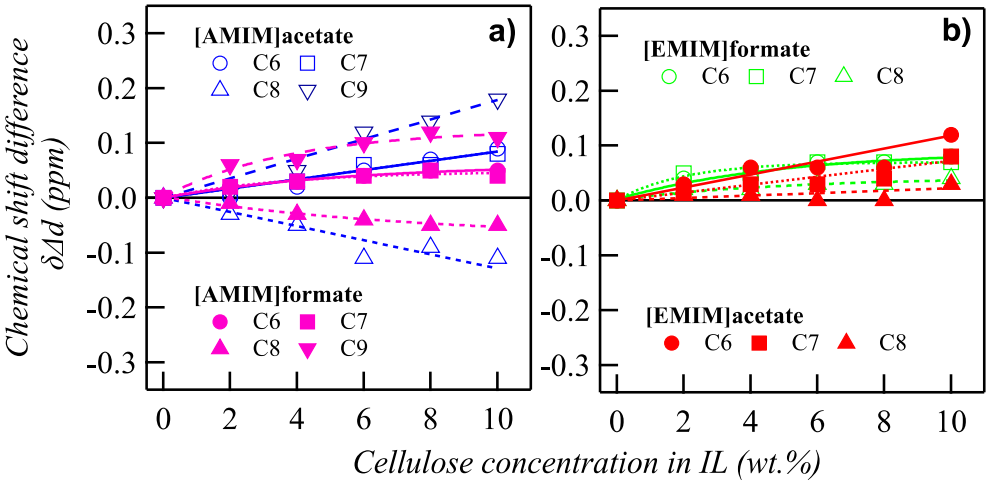

Figure 3. 11. Changes in ^{13}C NMR carbon chemical shift values ($\delta_{(\text{cellulose plus IL})} - \delta_{(\text{IL})}$) of side chain carbon C6, C7, C8 and C9 in **(a)** [AMIM]acetate and [AMIM]formate, and **(b)** in [EMIM]formate and [EMIM]acetate, as a function of cellulose concentration at 80 °C

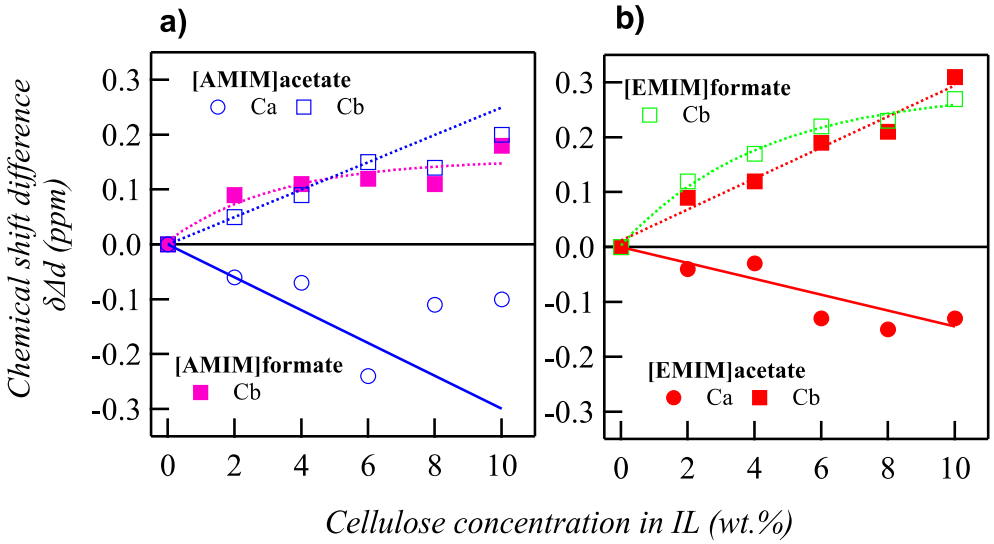

Figure 3. 12. Changes in ^{13}C NMR carbon chemical shift values ($\delta_{(\text{cellulose plus IL})} - \delta_{(\text{IL})}$) of anion carbons, Ca and Cb in **(a)** [AMIM]acetate and [AMIM]formate and **(b)** in [EMIM]formate and [AMIM]formate, as a function of cellulose concentration at 80 °C.

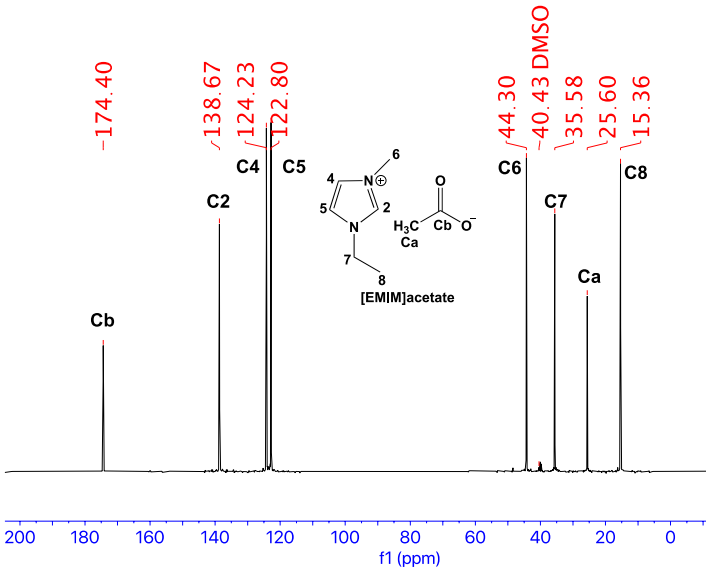

Figure 3. 13. ^{13}C NMR {^{1}H} (400 MHz DMSO-d6) spectrum of 1-ethyl-3methylimidazolium acetate at 80 °C.

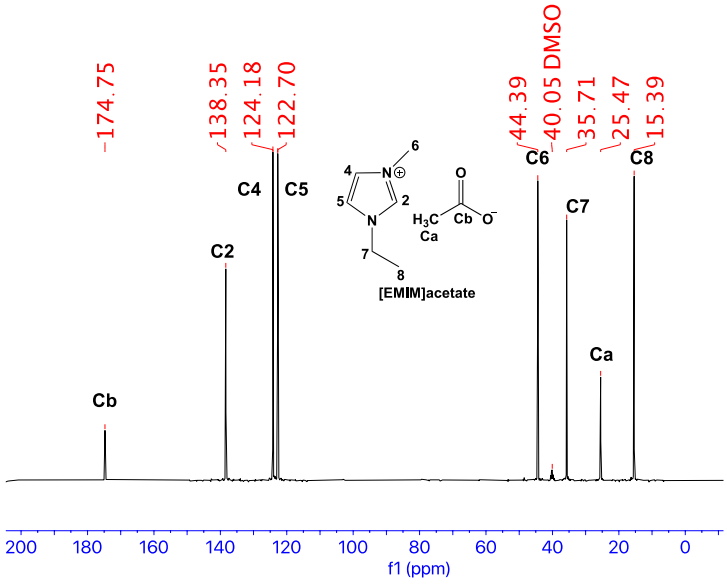

Figure 3. 14. ^{13}C NMR {^{1}H} (400 MHz DMSO-d6) of 10 wt.% cellulose in [EMIM]acetate at 80°C.

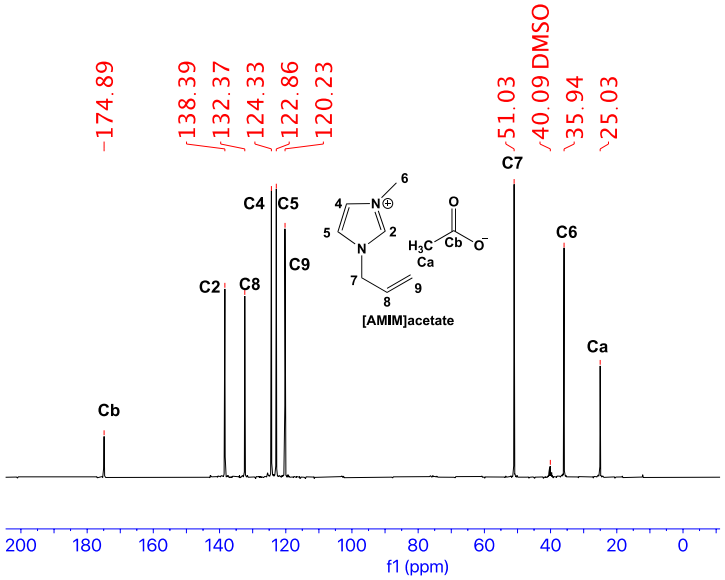

Figure 3. 15. ^{13}C NMR {^{1}H} (400 MHz DMSO-d6) of [AMIM]acetate at 80°C.

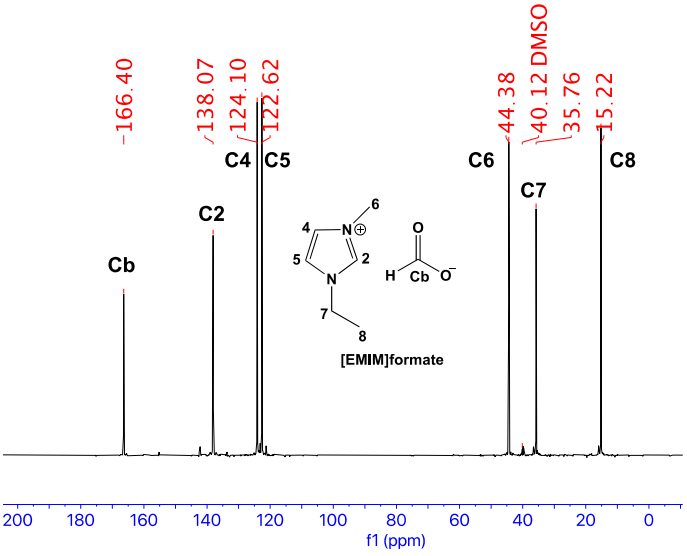

Figure 3. 16. ^{13}C NMR {^{1}H} (400 MHz DMSO-d6) of 10 wt.% cellulose in [AMIM]acetate at 80°C.

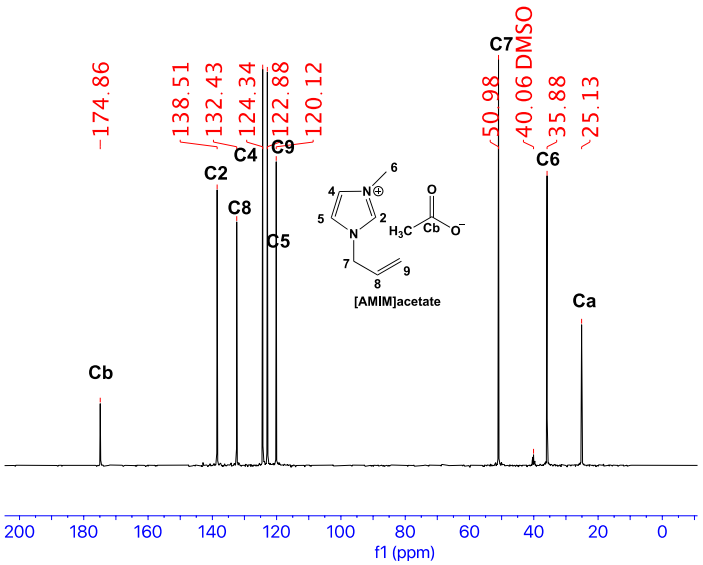

Figure 3. 17. ^{13}C NMR {^{1}H} (400 MHz DMSO-d6) of [EMIM]formate at 80°C.

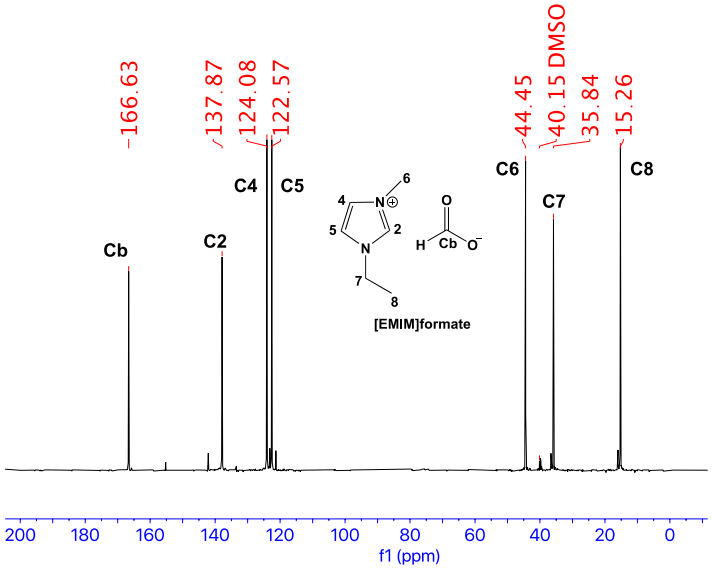

Figure 3. 18. ^{13}C NMR {^{1}H} (400 MHz DMSO-d6) of 10 wt.% cellulose in [EMIM]formate at 80°C.

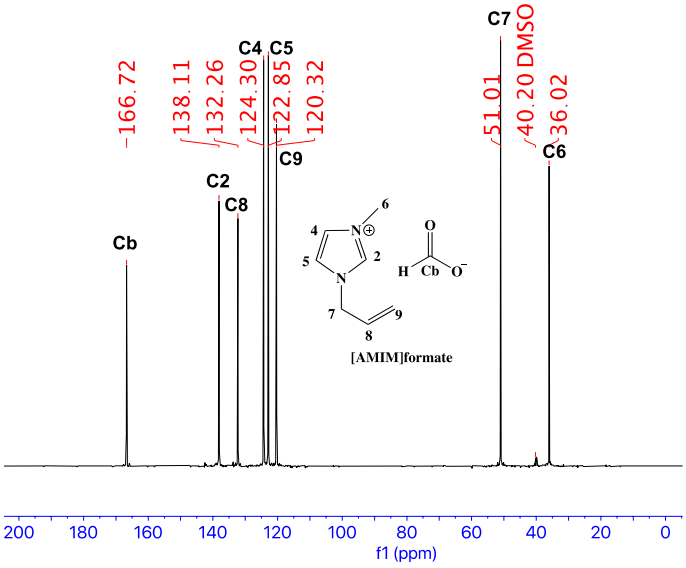

Figure 3. 19. ^{13}C NMR {^{1}H} (400 MHz DMSO-d6) of [AMIM]formate at 80°C.

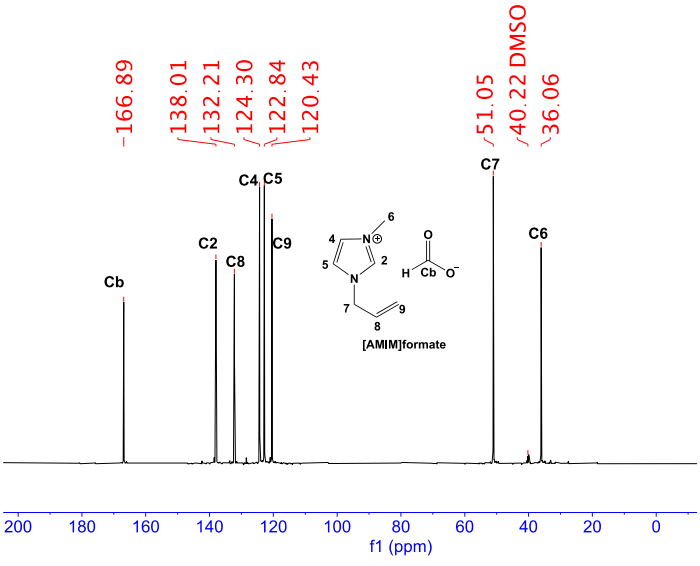

Figure 3. 20. ^{13}C NMR {^{1}H} (400 MHz DMSO-d6) of 10 wt.% cellulose in [AMIM]formate at 80°C.

Table 3. 2. Calculated carbon chemical shift difference as a function of cellulose concentration for [EMIM]acetate

Carbon number	Cellulose concentration (wt.%)					
	0	2	4	6	8	10
C2	0	-0.09[a]	-0.13[b]	-0.2[c]	-0.22[c]	-0.29[d]
C4	0	-0.01[a]	-0.02[a]	-0.04[b]	-0.04[b]	-0.04[b]
C5	0	-0.04[a]	-0.04[a]	-0.08[b]	-0.08[b]	-0.09[c]
C6	0	0.03[a]	0.06[b]	0.06[b]	0.06[b]	0.12[c]
C7	0	0.02[a]	0.03[b]	0.03[b]	0.04[b]	0.08[c]
C8	0	0.01	0.02[a]	0[b]	0[b]	0.03[c]
Ca	0	-0.04[a]	-0.03[a]	-0.13[b]	-0.15[b]	-0.13[b]
Cb	0	0.09[a]	0.12[a]	0.19[b]	0.21[b]	0.31[b]

Means followed by the same letter are not statistically significant at an alpha value of 0.05

Table 3. 3. Calculated carbon chemical shift difference as a function of cellulose concentration for [AMIM]acetate

Carbon number	Cellulose concentration (wt.%)					
	0	2	4	6	8	10
C2	0	-0.04[a]	-0.08[b]	-0.18[c]	-0.19[c]	-0.24[d]
C4	0	-0.01	-0.01	-0.02[a]	-0.02[a]	-0.02[a]
C5	0	-0.01	-0.02[a]	-0.06[b]	-0.05[b]	-0.06[b]
C6	0	0	0.02	0.05[a]	0.07[b]	0.09[c]
C7	0	0.01[a]	0.03[b]	0.06[c]	0.06[c]	0.08[d]
C8	0	-0.03[a]	-0.05[b]	-0.11[c]	-0.09[d]	-0.11[e]
C9	0	0.01	0.05[a]	0.12[b]	0.14[b]	0.18[c]
Ca	0	-0.06[a]	-0.07[a]	-0.24[b]	-0.11[c]	-0.10[c]
Cb	0	0.05[a]	0.09[b]	0.15[c]	0.14[c]	0.20[c]

Means followed by the same letter are not statistically significant at an alpha value of 0.05

Table 3. 4. Calculated carbon chemical shift difference as a function of cellulose concentration for [EMIM]formate

Carbon number	Cellulose concentration (wt.%)					
	0	2	4	6	8	10
C2	0	-0.11[a]	-0.15[b]	-0.18[c]	-0.19[c]	-0.23[c]
C4	0	-0.02[a]	-0.03[a]	-0.03[a]	-0.03[a]	-0.03[a]
C5	0	-0.04[a]	-0.05[a]	-0.06[a]	-0.06[a]	-0.06[a]
C6	0	0.04[a]	0.04[a]	0.07[b]	0.07[b]	0.08[b]
C7	0	0.05[a]	0.05[a]	0.07[b]	0.07[b]	0.07[b]
C8	0	0.02[a]	0.02[a]	0.03[b]	0.03[b]	0.04[b]
Cb	0	0.12[a]	0.17[b]	0.22[c]	0.23[c]	0.27[c]

Means followed by the same letter are not statistically significant at an alpha value of 0.05

Table 3. 5. Calculated carbon chemical shift difference as a function of cellulose concentration for [AMIM]formate

Carbon number	Cellulose concentration (wt.%)					
	0	2	4	6	8	10
C2	0	-0.04[a]	-0.06[b]	-0.07[b]	-0.09[c]	-0.11[d]
C4	0	0.00	0.00	0.00	0.00	0.00
C5	0	0.00	-0.01	-0.01	-0.01	-0.01
C6	0	0.02[a]	0.03[a]	0.04[a]	0.05[a]	0.05[a]
C7	0	0.02[a]	0.03[a]	0.04[b]	0.05[b]	0.04[b]
C8	0	-0.01[a]	-0.03[b]	-0.04[b]	-0.05[b]	-0.05[b]
C9	0	0.06[a]	0.07[a]	0.10[a]	0.12[b]	0.11[b]
Cb	0	0.09[a]	0.11[b]	0.12[b]	0.11[b]	0.18[c]

Means followed by the same letter are not statistically significant at an alpha value of 0.05

Table 3. 6. Molecular weight, density and scattering length density of cellulose, [AMIM]formate, [EMIM]acetate, formate ion (formic acid) and acetate ion (acetic acid).

Sample	Molecular weight, M_w (g/mol)	Density (g/cm^3)[1]	SLD ($x10^{-6}$ $Å^{-2}$)
Cellulose (MCC)	162.1	1.50	13.561 ($C_6H_{10}O_5$)
[AMIM] formate	168.2	1.13[1]	10.298 ($C_8H_{12}N_2O_2$)
[EMIM] acetate	170.2	1.10	9.481 ($C_8H_{14}N_2O_2$)

Chapter 4. Investigating xylan and lignin interactions with 1,3 dialkyl imidazolium ionic liquids by NMR and SAXS

A version of this chapter will be submitted as a peer-reviewed article.

Aparna Annamraju, Kalavathy Rajan, Xiobing Zuo, Sai Venkatesh Pingali and Nicole Labbé. (2020). Investigating xylan and lignin interactions with 1,3 dialkyl imidazolium ionic liquids by NMR and SAXS.

Aparna Annamraju performed the experiments, conducted data analysis, and wrote the first draft of the manuscript. Dr. Kalavathy Rajan helped with editing the manuscript. Dr. Xiobing Zuo helped in SAXS data collection. Dr. Sai Venkatesh Pingali assisted in small angle X-ray scattering (SAXS) data interpretation. Dr. Nicole Labbé oversaw the experimental design, assisted with data analysis, and edited the manuscript.

4.1.Abstract

Understanding interactions between hemicellulose/lignin and ionic liquids is essential to identify the most efficient ionic liquid (IL) either for fractionating or extracting individual biomass biopolymers from lignocellulosic biomass. The current study proposes to utilize two sets of imidazolium cations (1-ethyl-3-methylimidazolium and 1-allyl-3-methylimidazolium) and two sets of anions (acetate and formate) to investigate the electronic and structural interactions between birchwood xylan and an organosolv hybrid poplar lignin and these ILs. The NMR results showed that both, the cation and anion of these ILs, are involved in the electronic interactions with xylan and lignin. Based on the significant changes in the ^{13}C NMR shifts, we found that the IL-xylan interactions are greater by an average of 50% than the IL-lignin interactions. Conformational and quantitative estimation of the structural interactions by SAXS revealed that the xylan conformation remains the same in the studied ILs. Furthermore, the number of acetate and formate anions bound

to a single anhydroxylose unit was determined to be same. On the other hand, aggregates of lignin were formed in the studied ILs. In the acetate ILs, lignin was dispersed in a monomeric state while in the formate ILs it assumed a dimeric state within the aggregates. Macroscopic solubility aside, this systematic study demonstrates that ILs containing acetate and formate anion have similar interactions towards xylan but differ towards lignin. This knowledge could be utilized for selective extraction of hemicellulose or lignin from biomass for potential product applications.

Key words: xylan; ionic liquids; lignin; interactions; SAXS; NMR

4.2.Introduction

Lignocellulosic biomass is an available underutilized renewable source[1] which is composed of three main polymers, i.e., cellulose, hemicellulose and lignin. The percent composition of these polymers varies based on the plant species, age and growth environment.[2] Although, attempts to use this abundant source for fuel and value-added products production have been prevalent from the past three decades, the primary challenge for the efficient utilization of lignocellulosic biomass is the network of covalent interactions between the polymers making it resistant to deconstruction and fractionation using common solvents.[3, 4] Traditional acid and alkali pretreatments are effective, but have been mainly optimized for cellulose isolation and conversion.[5, 6]

Like cellulose, hemicellulose and lignin are also potential low-cost feedstocks with amendable functional groups for the production of chemicals and materials.[7, 8] The main polymers that make up hemicellulose are xylan, mannan, galactan and arabinan, with xylan making up the major portion of hemicellulose in hardwood and herbaceous species.[9] Xylan backbone is made up of β-1,4-linked xylose units with side branches of O-acetyl groups and other sugars. Lignin is composed of multifunctional phenolic rings. Several chemical, enzymatic and mechanical methods have been

developed to isolate lignin.[10,11] Recently, targeted valorization efforts have ensured the better utilization of xylan and lignin as raw material in resins, films and other composite material applications.[12,13,14]

One of the key steps in utilization of hemicellulose and lignin is the identification of suitable solvent for efficient separation with minimal degradation to their native structure. Organic solvent systems such as γ-valero lactone (GVL) and tetrahydrofuran (THF) are efficient but suffer from drawbacks such as toxicity and thermal instability.[15] Ionic liquids (ILs) on the other hand are for the most part environmentally benign.[16] Compositionally, ILs are molten salts made of anion and cations. Over the last two decades, several different ILs with a suite of cation and anion combinations have demonstrated their ability to dissolve cellulose, lignin and whole biomass.[17,18] Its solvation ability along with a low vapor pressure and high thermal stability make ILs an attractive choice for green processing technologies.[19] The most popular cations are 1-alkyl-3-methylimidazolium (alkyl = ethyl/butyl/allyl) and pyrrolidium, while acetate, phosphonate and chloride are the most commonly used anions.[20,21,22]

To ensure the economic viability of biorefineries, utilization of all three biomass polymers at par is essential. Unlike aqueous based solvent systems, ILs with their ability to solvate all three polymers are an attractive option. But, to make a rational choice among the different ILs available, a thorough understanding of the interactions of the different ILs with not just cellulose, but all the three biomass polymers will aid in the 1) selective fractionation of carbohydrate polymers (cellulose and hemicellulose) from lignin, 2) identification of IL suited for whole biomass dissolution and 3) optimization of the processing conditions to achieve increased solubilities in ILs to improve the efficiency of the process.

Experimental and theoretical studies have been useful in providing important details about the interactions between xylan and ILs in comparison to cellulose. For example, using density functional theory (DFT) calculations Payal *et al*. reported that binding energy (BE) between xylan and IL ion pairs is greater by 20 kcal mol^{-1} when compared to cellulose. This higher BE was interpreted as stronger interactions between xylan and ILs.[23] On the other hand, when performing dissolution experiment of extracted hemicellulose from bamboo, Bylin *et al.* noted that the dissolution of xylan was slower than cellulose, owing to the chemical diversity of hemicellulose.[24] Apart from these cellulose/xylan comparison studies, other research works have mostly focused on ascertaining the role of anion and cation in xylan dissolution.[25, 26] NMR studies performed to understand the interactions based on chemical shift differences offered evidence for a defined role of anion however the role of IL cation remains uncertain.[26]

Similar to xylan studies, several reports on characterizing interactions between lignin and ILs ion pairs exist in literature. One of the earliest studies was performed by Pu *et al*. using softwood kraft lignin, wherein it was shown that the nature of anion was key to lignin dissolution.[27] Besides experimental studies, theoretical studies have also aided in understanding the interactions between lignin and ILs. For example, using DFT calculations with lignin model compounds in imidazolium ILs, it was shown that, while IL anions interact via intermolecular H-bonding, IL cations interact with lignin via H-bond and pi stacking interactions.[28] However, using the same lignin model compounds and simulation data Wang *et al*. concluded that the cation's role was non-deterministic.[29]

The objective of this study is two part: 1) to compare the interactions of xylan and lignin with a set of ILs, and 2) to understand the interactions between IL ion pairs with lignin and xylan. To achieve these goals, we extend on our work with cellulose by using the same set of four ILs, with

1-ethyl-3-methyl([EMIM]) and 1-allyl-3-methyl ([AMIM]) imidazolium as the cations and acetate and formate as the anions. Electronic interactions measured in terms of carbon chemical shift change by NMR revealed that both cation and anion interact with xylan and lignin. Structural interactions measured using SAXS indicated that xylan assumed the same conformation in the four ILs and the number of anions bound to anhydroxylose units were similar as well. On the other hand, lignin existed as aggregate particles with lower oligomeric state in acetate based ILs ([EMIM]acetate and [AMIM]acetate) when compared to [AMIM]formate. These results suggest that among the studied ILs, xylan interactions are similar but lignin interactions are different.

4.3.Experimental section

4.3.1. Materials

The four ILs, i.e., 1-ethyl-3-methylimidazolium formate ([EMIM]formate), 1-ethyl-3-methylimidazolium acetate ([EMIM]acetate), 1-allyl-3-methylimidazolium formate ([AMIM]formate), and 1-allyl-3-methylimidazolium acetate ([AMIM]acetate) utilized in this study were purchased from IoLiTec GmbH (Tuscaloosa, AL). The moisture content of [EMIM]formate, [EMIM]acetate, [AMIM]formate and [AMIM]acetate measured using Thermo gravimetric analysis (TGA) was 5.0, 6.9, 7.0 and 5.4 % (an average based on duplicate measurement). Birchwood xylan was purchased from Sigma Aldrich. Lignin was produced though an organosolv process from hybrid poplar at Center for Renewable Carbon, University of Tennessee following an established method.[30] The moisture content of xylan and lignin was 10 and 3.5 % (an average based on a duplicate measurement). Dimethyl sulfoxide-d6 (DMSO-d6) (99.9%) containing tetramethylsilane (TMS) (0.03%, v/v) was purchased from Cambridge Isotope Laboratories, Inc., USA. In brief, poplar chips were loaded into a flow through reactor at 140 ˚C with 16/34/50 wt % solution of MIBK, ethanol, and water, respectively with sufficient sulfuric

acid to make a 0.05 M solution. Biomass and solvent were pumped through reactor for 120 min until the solvent to biomass ratio of 1:10 was achieved. Lignin was isolated from liquor generated from the reactor upon solid sodium chlorite addition to induce phase separation into organic and aqueous phase. Lignin collected in the organic phase was subsequently washed with deionized water. The organic solvent was removed from lignin in final step, which was then dried in vacuum oven overnight at 80 ˚C. Lignin purity, determined using standard procedures (NREL/TP-510-42618 and NREL/TP-510-42622) was 84 %.

The weight average molecular weight (M_w), number average molecular weight (M_n), and polydispersity index (M_w/M_n, PDI) of the lignins were determined by gel permeation chromatography (GPC).[31] Approximately 50 mg of a lignin sample were acetylated with 1 mL of pyridine/acetic anhydride (1 : 1, v/v) and stirred for 24 h at room temperature, after which 25 mL was ethanol was added to reaction mixture. The addition of ethanol and rotary evaporation were repeated several times to ensure complete pyridine and acetic anhydride removal. Lignin was then dissolved in chloroform and diethyl ether and subsequently washed with X3 25 mL diethyl ether. The recovered lignin was then vacuum dried at 80 ˚C for 24 h. The acetylated lignin was dissolved in tetrahydrofuran (THF), filtered through a 0.45 μm filter, and immediately analyzed using a size exclusion chromatography system (Tosoh ECO SEC) equipped with a UV detector (265 nm). The analysis was carried out with THF as the eluent (0.35 mL min^{-1}) on a Tosoh TSK gel Super Multipore HZ-M column (4.6 × 150 mm, 4 μm packing) preceded by a TSK gel Super Multipore HZ-M guard column and calibrated against polystyrene. The PDI of the lignin used in the study was 1.2. The molecular weight, glass transition temperature and PDI of lignin are listed in Table 4.1.

Table 4. 1. Polydispersity index, number average molecular weight, weight average molecular weight, glass transition temperature and purity of organosolv lignin used in the study.

Poly dispersity index (PDI)	1.2
Number average molecular weight (Mn g/mol)	3501
Weight average molecular weight (Mw g/mol)	2995
Glass transition temperature (Tg ˚C)	121
Purity of lignin	84 %

4.3.2. Preparation of polymer-IL solutions

All the xylan-IL and lignin-IL solutions were prepared at 80 °C following the previously published methods.[32] In brief, 2 g of IL were weighed out in a vial and heated at 100 °C for 10 minutes to remove excess moisture. To confirm the moisture loss of ILs, TGA was conducted using thermogravimetric analyzer (Pyris 1 TGA, Perkin Elmer, Shelton, CT) with 5-10 mg of ionic liquid. ILs were heated in a platinum pan from 30 to 105 °C at a rate of 10 °C /min and held for 10 min at 105 °C under 10 mL/min of nitrogen. After 10 mins the mass loss of ILs was constant suggesting, 10 min heating at 100 °C prior to cellulose addition was sufficient to remove water from ILs (Data in Appendix). After reducing the temperature to 80 °C, xylan or lignin was added in 20 mg increments. The dissolution of the polymer was confirmed by placing an aliquot of the solution under microscope (X 20). Upon the complete dissolution the next increment of 20 mg of polymer was added into IL until the target weight of 10 wt.% was achieved.

4.3.3. Preparation of ^{13}C NMR samples

The NMR samples were prepared following the protocols established in our earlier study with cellulose. Briefly, to the prepared polymer IL solutions, 125 μL of DMSO-d6 were added to reduce viscosity of the system. To account for the DMSO interaction parameter, a triplicate of neat IL with 125 μL of DMSO-d6 was used as reference when calculating the chemical shift differences. The sample tubes were sealed with Teflon tape and stored under ambient conditions in between the NMR runs.

4.3.4. NMR instrumentation and ^{13}C experiments

NMR spectra were recorded on a Bruker 400 MHz spectrometer at 353K (80 °C). Both DMSO-d6 and TMS were used as an internal reference. All the spectra were collected within 48 h of sample preparation to avoid for any additional moisture content variations. The change in chemical

shifts was calculated by subtracting the chemical shift of each carbon in the presence of xylan or lignin in IL and the corresponding neat IL. The data were processed (base line correction and chemical shift assignment) using MNOVA software. A one-way ANOVA was performed to determine if there was a significant difference between chemical shift value of neat IL and IL with xylan/ lignin for each carbon. Each experiment was repeated at least three times and a p-value of <0.05 was considered significant. All analyses were conducted using the IBM SPSS Statistics for Windows, Version 26.0 (IBM Corp, Armonk, NY)**.**

4.3.5. SAXS of xylan- and lignin-IL solutions

Small and wide-angle X-ray scattering (SAXS and WAXS) experiments were conducted at the 12-ID-B beamline of Advanced Photon Source (APS) (Argonne National Laboratory, Lemont, IL). All measurements were carried out at room temperature. Xylan/ligin-IL solutions were injected into a 2 mm diameter capillary and sealed with epoxy. The X-ray wavelength was 0.9322 Å. A PILATUS (Dectris) detector was used as the area detector. The irradiation time was 10 s (1 s irradiation X10). Data were acquired on all four ILs, however the quality of data was low for the [EMIM]formate system to obtain any discernable differences. The observed X-ray scattering intensities were normalized to the absolute intensity using glassy carbon (a secondary standard sample for intensity calibration).[33] The solvent scaling factor for each IL was determined from the WAXS data, where no scattering signal from xylan/lignin was observed. The scattering intensity of the xylan/lignin molecules $I_{xylan/lignin}(q)$ was obtained after subtracting the scattering intensity of the neat IL, $I_{neat\ IL}(q)$.

SAXS data of xylan over a specific q range were analyzed using a power law analysis. The SAXS scattering intensity for a power law fit was implemented using the IRENA package[34] of Igor Pro (WaveMetrics, Inc., Portland, OR) software, which can be expressed as follows:

$$I(Q) = (AQ)^{-P} + Bkg \quad (1)$$

where A is length scale factor, Bkg is background intensity of neat IL and *P = power law feature*.

The full q range of lignin data in ILs was analyzed using the two-level unified exponential/power law model,[35] which is a combination of Guinier and power law models given by the equation as shown below

$$I(Q) = \sum_{i-1}^{N} G_i \, exp\left[-\frac{q^2 \, {R_g}^2}{3}\right] + \frac{B_i\left[erf(qR_{g,i}/\sqrt{6})\right]^{3P_i}}{q^{pi}} + Bkg \quad (2)$$

In this equation, i = 2, for two level fit. G is the Guinier pre-factor, B is the pre-factor of power law scattering, P_i is the power law exponent, R_g is the radius of gyration and Bkg is the background scattering of neat IL. R_g of the particles obtained from the Guinier law at the value of the scattering q = 0 is independent of the shape of the particles. The value of P_i provides information about the shape of the scattering objects and its fractal structure.

4.4.Results

In this work, two cations and two anions in four different combinations were chosen to investigate the interactions between ILs and xylan or lignin. The chemical structure of the four ILs along with carbon atom numbering are shown Figure 4.1.

4.4.1. NMR interaction of xylan and lignin with ILs

The electronic interaction parameter between xylan and lignin with ILs was obtained by comparing ^{13}C NMR of ILs with and without xylan/lignin at 80 °C. The ^{13}C NMR spectra of the neat ILs and their corresponding mixtures with 10 wt.% xylan or lignin are included in the supplementary information file. Figure 4.2 shows the ^{13}C chemical resonance difference of IL carbon atoms obtained by subtracting chemical shift values of IL sample with xylan and neat IL.

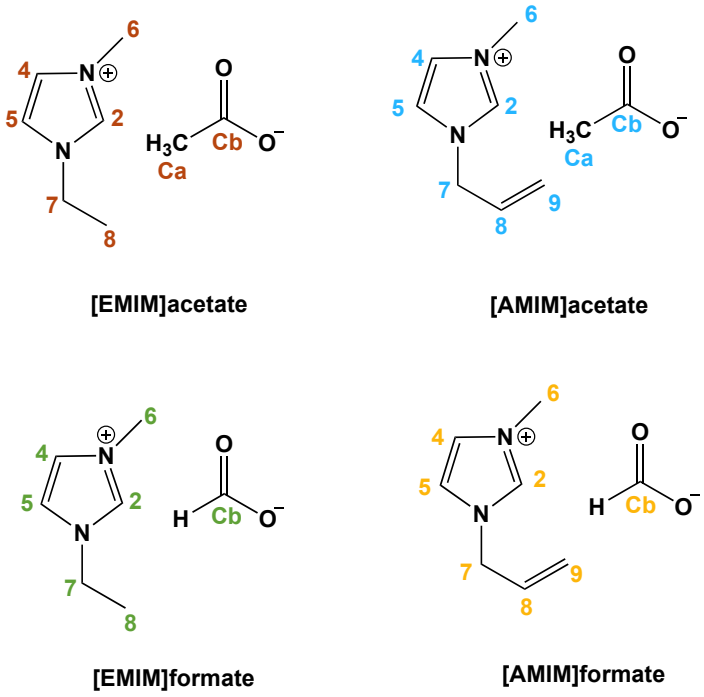

Figure 4. 1. Chemical structures and notation of carbon atom numbers of four ILs used in the study.

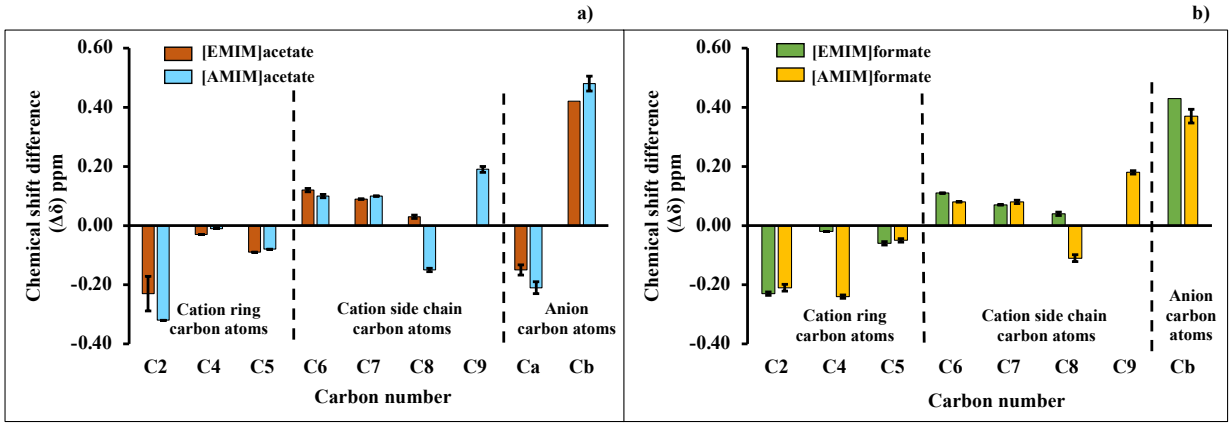

Figure 4. 2. Changes in ^{13}C NMR chemical shift values ($\delta_{(xylan\ plus\ IL)} - \delta_{(IL)}$) of carbon atoms in a) [EMIM]acetate (brown) and [AMIM]acetate (blue); b) [EMIM]formate (green) and [AMIM]formate (yellow) with 10 wt.% xylan at 80 °C.

Apart from the two anions, all the four ILs have side chains of imidazolium cation at position 1 and 6 (Figure 4.1) and they also experienced a change in chemical environment in the presence of xylan. In order to clearly understand the observed differences, results are showcased on the basis of carbon atom classification into two categories: cation carbon atoms and anion carbon atoms. The cation set of carbon atoms are further divided into imidazolium ring carbon atoms and side chain carbon atoms.

Cation carbon atoms: Imidazolium ring carbon atoms C2, C4 and C5

In presence of xylan the carbon at position 2 (C2) underwent deshielding i.e., signal moved upfield due to the increase in electron density which is shown as negative chemical shift difference (Figures 4.2a and b). Carbons C4 and C5 also underwent deshielding in presence of xylan. However, among the three carbon atoms the deshielding of C2 carbon was most pronounced (with the largest negative chemical shift difference of -0.25 ppm), followed by C5 (-0.07 ppm) and C4 (-0.02* ppm) carbon atoms. Between C4 and C5 carbon atoms, C5 carbon underwent greater deshielding than C4 carbon. And, at an p value of 0.05, the chemical shift difference noted for C4 carbon was not statistically different for xylan. One exception to this observation was C4 carbon (0.24±0.01 ppm) in [AMIM]formate (Figure 4.2). This observation was recorded in all the three samples measured.

Cation carbon atoms: Side chain carbon atoms C6, C7, C8 and C9

In all the four ILs, the methyl group at C6 showed as positive chemical shift difference of 0.10 which indicate a shielding effect, i.e., a decrease in electron density in presence of xylan (Figures 2). Further, in the [EMIM] set of ILs, the ethyl side chain carbons, i.e., C7 (0.08) and C8(0.04) underwent shielding in presence of xylan. On the other hand, in the [AMIM] ILs, carbons C7

(0.09) and C9 (0.19) underwent shielding while C8 (-0.13) experienced a deshielding effect. In summary, the shielding effect of the ethyl side chain carbon atoms was smaller in magnitude than allyl side chain carbon atoms.

Anion carbon atoms Ca and Cb

Between the four ILs, there are two anion carbon atoms: the methyl group of the acetate anion and the carbonyl carbon. The carbonyl carbon, Cb (0.43) of all the four ILs underwent shielding, in another word the NMR signal moved downfield in presence of xylan (Figure 2). This downfield movement of the signal implied that electron density around the carbon increased in presence of xylan. On the other hand, the signal of methyl group of the acetate ILs, Ca moved upfield in reference to solvent peak in presence of xylan (-0.18), characteristic of deshielding, i.e., a decrease in electron density.

The chemical shift differences observed for the four ILs in presence of lignin are shown in Figure 4.3. Overall, the trends noted in presence of xylan hold up well in presence of lignin. The imidazolium ring carbons, C2, C4 and C5 underwent deshielding. In [EMIM] ILs, both the side chain carbons, C7 and C8 underwent shielding, while in the [AMIM] ILs the side chain carbons experienced both shielding (C7 and C9) and deshielding (C8). In presence of lignin the carbonyl carbon (Cb) of all the four carbons underwent shielding while methyl group (Ca) in acetate anion ILs underwent deshielding.

While the chemical shift difference of IL cation and anion followed a similar pattern in presence of xylan and lignin, there exists certain differences due to IL structures and the type of biomass polymer. For instance, in presence of xylan, the chemical shift changes experienced by [EMIM]acetate, [EMIM]formate and [AMIM]formate were identical, with [AMIM] acetate values slightly higher.

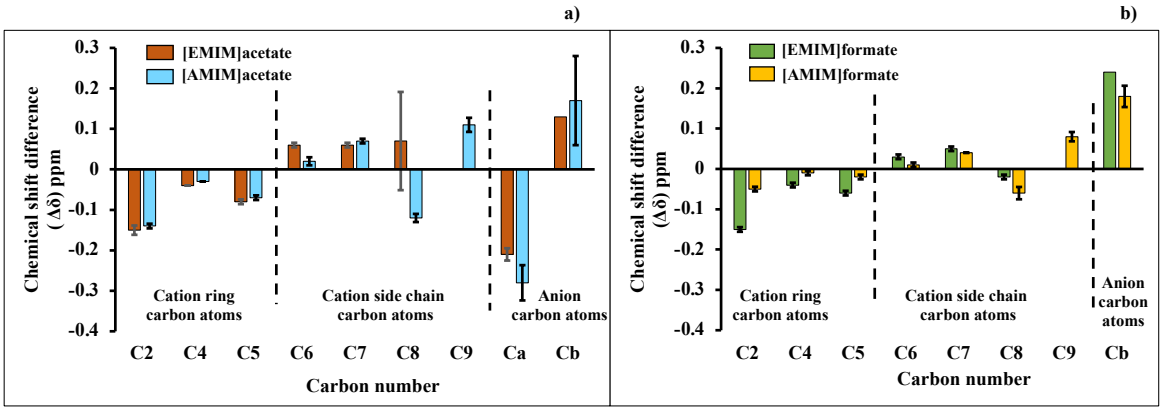

Figure 4. 3. Changes in ^{13}C NMR chemical shift values ($\delta_{(\text{lignin plus IL})} - \delta_{(\text{IL})}$) of carbon atoms in a) [EMIM]acetate (brown) and [AMIM]acetate (blue) b) [EMIM]formate (green) and [AMIM]formate (yellow) with 10 wt.% lignin at 80 °C.

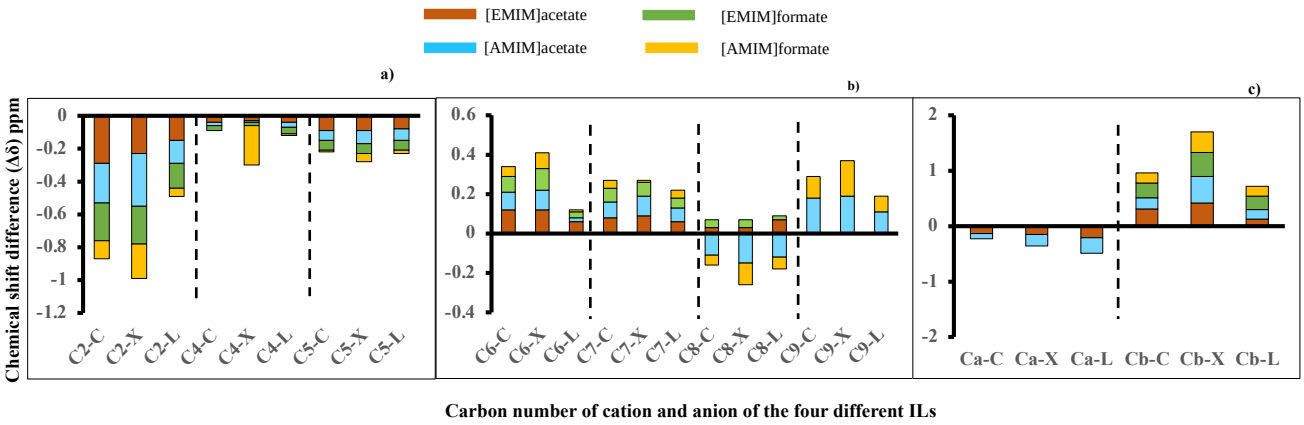

Figure 4. 4. Comparison of relative ^{13}C NMR chemical shift values ($\Delta\boldsymbol{\delta}$) of a) imidazolium ring carbon atoms C2, C4 and C5 b) side chain carbon atoms: C6, C7, C8 and C9 and c) anion carbon atoms: Ca and Cb of [EMIM]acetate (brown), [AMIM]acetate (blue), [EMIM]formate (green) and [AMIM]formate (yellow) with 10 wt.% xylan (X) or lignin (L) at 80 °C.

In contrast, in presence of lignin, [EMIM]acetate, [AMIM]acetate and [EMIM]formate changes were similar while [AMIM]formate system recorded the smallest change (Figure 4.4).

In addition to differences between the four ILs, the NMR measurement was also useful to understand the difference in magnitude of chemical shift for the two polymers as well (Figure 4.4). The systematic variation of IL ion pairs was useful to conclude that the anion and C2 of the cation participate in the interaction process with the two polymers. In case of xylan the chemical shift difference noted for the carbonyl carbon was twice than for the C2 of the cation. The C2 in presence of lignin and the carbonyl carbon chemical shift differences were almost identical. Further, the allyl side chain demonstrated stronger participation than the ethyl side chain (Figure 4.4).

4.4.2. SAXS of xylan and lignin in ILs

SAXS studies were performed to understand how the local electronic changes measured by NMR translate into conformational details of xylan and lignin in ILs. The low concentration solutions (2 % (w/w)) utilized for this experiment were beneficial to ensure scattering pattern consistent with single strand feature of xylan and lignin. As SAXS data collected from [EMIM]formate were of poor quality, the profiles of only three ILs are shown here. From Figure 4.5, we can infer that the SAXS profiles of xylan look similar in the three studied ILs. The steady increase of scattering intensity from high to low Q region implied that xylan assumed a rod-shaped particle conformation. A power law fit analysis across specific Q range was performed on the data. The parameters obtained from this fit analysis are listed in Table 4.1 and include intensity scalar, volume fraction, experimental and theoretical contrasts. The volume fraction parameter of ILs was calculated from the concentration of prepared xylan solutions in ILs and it was not altered during the fit analysis. The intensity scalar, ~ 0.0025 was similar for all three ILs (before the offset).

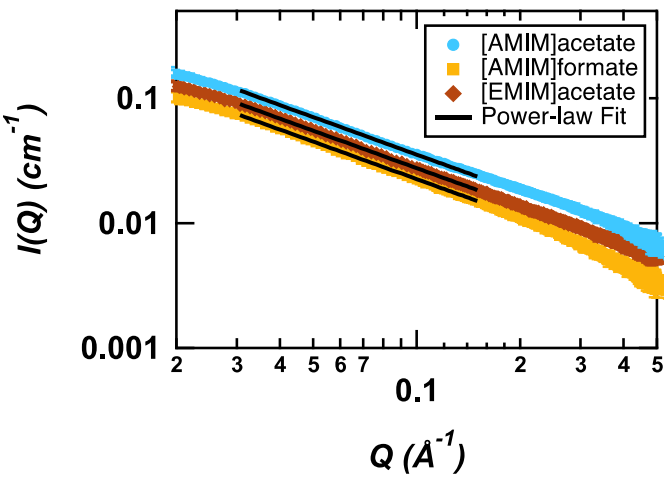

Figure 4. 5. SAXS curves of xylan 2 % (w/w) in [EMIM]acetate (brown), [AMIM]acetate (blue) and [AMIM]formate (yellow). The [AMIM]acetate curve is scaled by a factor of 0.8 for the purpose of clarity. The solid black lines are the power law fit lines.

The experimental contrast was calculated from the intensity scalar and the volume fraction. For all three ILs, the experimental contrast, 4.28, 4.34 and 3.9 ×10-6 $Å^{-2}$ was higher than theoretical 3.42, 3.38 and 3.52 ×10-6 $Å^{-2}$ contrasts. This difference in contrasts is similar to the observation made in our prior study using cellulose as well as in the study by Raguwanshi *et.al.*[36] This contrast difference was used to calculate the number of anions bound to single anhydroxylose unit using equation 3. Based on the obtained numbers it can be concluded that same number of anions ~ 6 were bound to one anhydroxylose unit (AXU).

$$x = \frac{\left(\frac{(\sum b_i)_{anion}}{(\sum b_i)_{xylan}}\right)}{\left(1-\frac{\rho_{IL}}{\rho_{xylan}}\right)\left(\frac{\Delta\rho_{exp}}{\Delta\rho_{theo}}-1\right)} \quad (3)$$

Where b is the scattering length densities (SLDs) of xylan and IL-anions; ρ_{IL} and ρ_{xylan} are the SLDs of ILs and xylan, respectively; and $\Delta\rho_{exp}$ and $\Delta\rho_{theo}$ are experimental and theoretical contrasts, respectively.

SAXS profiles of lignin in ILs are shown in Figure 4.6a. We observed a flattening of the profile in the low Q region. This implied that lignin assumed a globular conformation. For all three ILs, the profiles are similar, i.e., lignin polymer conformation is that of globular particles. But the specific lignin polymer arrangement within this globular feature is different in these three ILs. To showcase those differences in polymer arrangements a Kratky plot is often used.[37] Figure 4.6b shows the Kratky representations of lignin in ILs where $I(q)q^2$ is plotted as a function of Q. The figure shows that for [AMIM]acetate and [EMIM]acetate, $I(q)q^2$ increased exponentially with q in the high Q, which implied an expanded conformation of lignin in these ILs. On the other hand, for [AMIM]formate, $I(q)q^2$ remains constant with increasing Q at high Q region, implying a random Gaussian chain conformation of lignin.[38]

Table 4. 2. Summary of Q-1 power-law fit parameters of SAXS data for 2% (w/w) xylan in [EMIM]acetate, [AMIM]acetate and [AMIM]formate.

Fit parameters	**[EMIM]acetate**	**[AMIM]acetate**	**[AMIM]formate**
Intensity Scalar (cm-1 $Å^{-1}$)	0.0027	0.0028	0.0023
*Volume fraction (ϕ)	0.0146	0.0149	0.015
Experimental contrast (Δρe) (×10-6 $Å^{-2}$)	4.28	4.34	3.9
+Theoretical contrast (Δρt) (×10-6 $Å^{-2}$)	3.42	3.38	3.52
^Number of AXU per anion	6	5	6

* Calculated from weight percent; + Calculated contrast values; ^ Obtained from Eqn. 3.

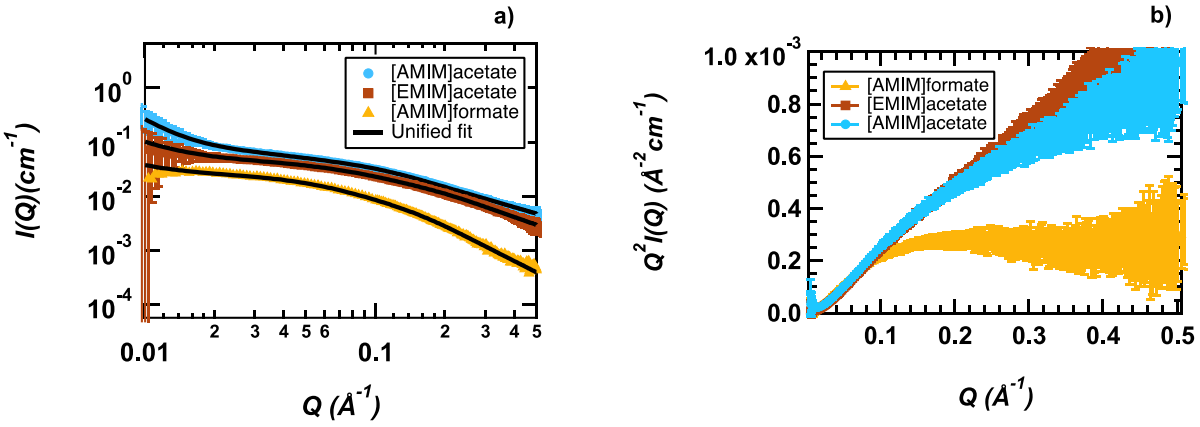

Figure 4. 6. a) SAXS curves of lignin 2 % (w/w) in [EMIM]acetate (brown), [AMIM]acetate (blue) and [AMIM]formate (yellow). [AMIM]formate and [EMIM]acetate profiles were scaled by 0.4 and 0.8 clarity. The solid black lines are the unified fit curves. b) Kratky plots of [EMIM]acetate, [AMIM]acetate and [AMIM]formate.

The size of the globular feature was obtained by performing a two-level Unified fit analysis. Due to a slight up-turn in the low-Q region (0.01-0.025 $Å^{-1}$), a two-level Unified fit was employed to extract the Guinier region reliably. The fit parameters for the three ILs are listed in Table 4.2. The Rg and scalar G were obtained from the Guinier feature while scalar B and power law P were obtained from the Porod feature. The Rg value of lignin, 20.0+2.5/-1.5, 20.0±1.2, 23.0+3.6/-2.5 in the three ILs is very similar. The Guinier scalar (G) values is similar for acetate ILs (~0.05) while it is higher for [AMIM]formate (0.064). The other difference between the acetate set of ILs and [AMIM]formate is the power-law exponent of the Porod feature which is between 1 and 1.5 for acetate ILs and for [AMIM]formate it is 2.16±0.04. Utilizing the Kratky representations along with Rg values, the molecular weight of lignin dissolved in ILs was calculated.[39] In [EMIM]acetate and [AMIM]acetate the SAXS determined molecular weight is 3.5k g/mol, which is almost the same as the GPC determined molecular weight of lignin (3.5k g/mol average of two runs). On the other hand, a SAXS determined molecular weight of 6.9k g/mol was obtained for [AMIM]formate.

4.5.Discussion

The aim of our study was to determine the roles of IL cation and anion in xylan and lignin dissolution and compare the IL-xylan and IL-lignin interactions. Previous IL structural studies have shown that the chemical shift values of the IL carbon atoms are sensitive to variation of the anion, alkyl side chain at position 1 and concentration of IL relative to solvent used for NMR measurement.[40, 41, 42] This variation of chemical resonance value was also observed upon cellulose addition and was used to investigate interactions between cellulose and ILs.[43] To implement the same methodology towards hemicellulose and lignin, extracted forms of hemicellulose and lignin were utilized in the past studies.[25, 26]

Table 4. 3. Summary of Unified fit parameters of SAXS data for 2% (w/w) lignin in [EMIM]acetate, [AMIM]acetate and [AMIM]formate.

Fit parameters	**[EMIM]acetate**	**[AMIM]acetate**	**[AMIM]formate**
Rg	20.0+2.5/-1.5	20.0±1.2	23.0+3.6/-2.5
Scalar (G)	0.046	0.051	0.064
Scalar (B)	0.0021	0.0013	0.00021
Power law (P)	1.12±0.04	1.40±0.05	2.16±0.04

However, none of the studies so far offer a systemic alteration of cations and anion along with a comparative picture of xylan and lignin interactions as the current study.

Our NMR and SAXS analyses highlighted the difference between xylan and lignin interactions in the four different imidazolium ILs. The magnitude and directionality of the chemical shift change were used to understand the interactions between individual IL carbon atoms and xylan/lignin. The imidazolium ring carbons experienced negative chemical shift differences in presence of both polymers. This downfield shift relative to the solvent peak can be related to H-bond formation with electron rich atoms such as oxygen in xylan/lignin. This is consistent with the increased electron density of carbon atoms experienced by imidazolium ring carbons as reported in previous studies conducted using extracted hemicellulose such as arabinoxylan as well as lignin.[25, 26] This downfield shift of the imidazolium ring carbons is better understood in terms of the hydrogens of imidazolium ring. All the three hydrogens of imidazolium ring are acidic due to the aromatic nature of imidazolium ring. However, the hydrogen at position 2 is rendered most acidic as it is sandwiched between two electronegative nitrogens. Due to the polarity induced charge difference of carbon hydrogen bond, the electron rich C2 interacts with the hydrogen of the hydroxyl group of xylan or lignin. As the hydrogens at position 4 and 5 are not acidic enough, a lower chemical resonance change is observed for these carbons.[44]

In addition to the imidazolium ring carbon atoms, the side chain carbons, i.e., methyl group at C6 and ethyl/allyl side chain at position 1, also experienced a change in electronic environment in presence of xylan/lignin. However, the magnitude of change is much smaller when compared to the C2 carbon. The primary reason for the differential variation of electronic density observed in the side chain carbon atoms can be understood in terms of the hybridization of ethyl and allyl carbons. The two ethyl carbons are SP^3 hybridized while in allyl group two carbons are SP^2

hybridized and one is SP^3 hybridized. The SP^3 hybridized carbons are less electronegative when compared with SP^2 hybridized carbons. The chemical shift difference experienced by ethyl and allyl chain carbons are in agreement with these electronegative differences based on hybridization (Figures 4.2 and 4.3). SP^3 hybridized carbons of ethyl (0.08 ppm) and allyl groups (0.09 ppm) experienced almost identical chemical shift difference in presence of xylan/lignin. The SP^2 carbons of allyl group exhibited higher chemical shift difference (-0.11 ppm, 0.19 ppm) confirming the electronegative nature of allyl group.

Since the initial report of cellulose dissolution in IL, the role of anion has been clear and straight forward.[45] In both acetate and formate anions, due to the electronegativity difference between carbon (2.55) and oxygen (3.44), the carbonyl bond is polarized with negative charge on oxygen and positive charge on the carbonyl carbon. The negatively charged oxygen forms H-bond with the hydrogen of the hydroxyl groups in xylan/lignin. This H-bond formation results in the reduction of electronic density around the carbonyl carbon (Cb) of all four ILs, which is recorded as downfield shift. However, in presence of xylan the downfield shift magnitude experienced by Cb carbon is almost double (Figure 4.2) when compared to the carbon shift in presence of lignin. The upfield shift of the methyl group observed for the acetate anion ILs is often equated to the redistribution of electronic cloud density. Although, in presence of lignin the upfield shift noted for the methyl group (an average value of (-0.25 ppm)) was far higher than the carbonyl carbon [an average value of (0.15 ppm)]. This observation suggests that there could be a potential direct interaction between the IL methyl group and lignin instead of reorganization of electron density. Overall, even though the directionality of the chemical shift difference is similar in presence of lignin and xylan the magnitude of change was consistently higher for xylan than lignin (Figure 4.4).

SAXS analysis showed that xylan was dispersed at molecular level and the conformation, a non-flexible stiff rod, is the same in all the ILs, which implied similar magnitude of interactions between the ILs and xylan. This observation is consistent with previous studies where intermolecular H-bond network of xylan was disrupted in ILs.[46, 47] A closer examination of the NMR data also confirmed this observation (Figure 4.4) for all ILs, but [AMIM]formate. In order to further understand xylan-IL interactions, we employed the same ion binding calculation methodology used in our cellulose study. These binding calculations were possible due to the observed difference between theoretical and experimental contrasts (Table 4.1).[36] The other parameter needed to perform the calculations were SLD's of xylan and IL ions and in case of xylan-IL system the density of xylan was assumed to be similar to cellulose [48] (Appendix table 4.4). Approximately, the same number of acetate and formate anions were bound to a single anhydroxylose unit (AXU). Lignin, on the other hand, assumed two different conformations in the ILs, a relaxed conformation in the acetate set of ILs and a rigid conformation in [AMIM]formate. Beside the conformation, the low radius of gyration (Rg) value of lignin implied that favorable interactions between lignin and ILs outweigh the IL-IL or lignin-lignin interactions, an observation also noted in studies with THF and DMSO solvents. [39, 49, 50, 51, 52] As the scalar quantity is similar for the acetate set of ILs and [AMIM]formate, the volume of the lignin aggregates is similar as well. Therefore, the implication that lignin is in monomeric form in [EMIM]acetate and dimeric form in [AMIM]formate suggests that lignin-[EMIM]acetate interactions are higher in magnitude compared to lignin-[AMIM]formate interactions. Molecular weight calculations performed using scattering intensity scalar and Kratky plot variables showed that lignin existed as monomer in the acetate set of ILs and as an oligomer in [AMIM]formate. The rigid conformation along with

oligomeric (dimer) nature of lignin in [AMIM]formate are in line with the low magnitude of shielding and deshielding in the NMR results section (Figure 4.3).

In addition to differences between the ILs, SAXS profiles of lignin were different than the xylan profiles. While xylan assumed a linear single strand conformation, a globular feature was observed for lignin. This difference of SAXS profiles was also captured as lower magnitude NMR chemical shift differences of lignin-IL system in comparison to xylan-IL system. These combined NMR and SAXS results showed that formate and acetate ILs exhibited similar binding capacity towards xylan. In case of lignin, ILs formed similar sized aggregates. However, the polymer arrangement within these aggregates was different for the acetate set of ILs ([EMIM]acetate and [AMIM]acetate) and [AMIM]formate.

4.6.Conclusion

The current study utilized four different ILs with two sets of cations and anions to investigate the role of cation/anion and to compare interactions between xylan and lignin. The local electronic interactions measured using ^{13}C NMR showed that both cation and anion interact with xylan and lignin. Conformational studies conducted using SAXS revealed that xylan attained a rod-like conformation in the ILs. Additionally, SAXS studies indicated that the number of acetate and formate anions bound to a single anhydroxylose unit (AXU) was the same. Lignin, on the other hand, achieved different conformations in the acetate and formate ILs, respectively; with an expanded conformation with monomeric form in the acetate ILs, whereas a Gaussian chain conformation with oligomeric form was observed in the formate ILs. These reported results along with our earlier cellulose study in chapter 3 will be applicable in the field of IL biomass processing, not only for the selective isolation of individual biomass polymers but also for whole biomass dissolution for direct product production.

Associated content

The supporting information document contains annotated NMR spectra of [AMIM]acetate, [AMIM]formate, [EMIM]formate and [EMIM]acetate, with and without xylan and lignin. It also includes one-way ANOVA results of ^{13}C NMR shielding and deshielding. Additionally, it also includes high weight percent xylan and lignin SAXS curves, molecular weight calculation details of lignin in ILs.

Acknowledgments

This work was supported by the Research Council of Norway. (grant no. R113215138). This research was also partially supported by the DOE Office of Science, Office of Biological and Environmental Research under the Genomic Science Program (FWP ERKP752; Biofuels SFA). The authors thank Dr. Carlos Steren from the Department of Chemistry, The University of Tennessee Knoxville for assisting with the NMR experiments. The authors also thank Dr. Byeongdu Lee at Advanced Photo Source, Argonne National Laboratory for assisting in SAXS data analysis.

References

1) Tadesse, H and Luque, R., Advances on biomass pretreatment using ionic liquids: An overview. *Energy and Environmental Science* **2011**, 4 (10), 3913-3929.
2) Brandt, A.; John, G.; Jason, P. H.; Welton, T., Deconstruction of biomass with ionic liquids. *Green Chemistry* **2013**, 15 (3), 550-583.
3) Himmel, E.M.; Ding, S.; Johnson, K.D.; Adney, S.W.; Nimlos, R.M.; Brady, W.J.; Foust, D.T., Biomass recalcitrance: engineering plants and enzymes for biofuels production. *Science* **2007**, 315 (5813), 804-807.
4) Petridis, L and Smith, J.C., Molecular-level driving forces in lignocellulosic biomass deconstruction for bioenergy. *Nature Reviews Chemistry* **2018**, 2 (11), 382-389.
5) Putro, J. N.; Soetaredjo, F. E.; Lin, Shi-Yow.; Ju, Yi-Hsu.; Ismadji, S., Pretreatment and conversion of lignocellulose biomass into valuable chemicals. *RSC Advances* **2016**, 6 (52), 46834-46852.
6) Rabemanolontsoa, H.; Saka, S., Various pretreatments of lignocellulosics. *Bioresource Technology* **2016**, 199, 83-91.
7) Ragauskas, A. J.; Beckham, G. T.; Biddy, Mary J.; Chandra, R.; Chen, Fang.; Davis, M. F.; Davison, B. H.; Dixon, R. A.; Gilna, P.; Keller, M.; Langan, Paul.; Naskar, A. K.; Saddler, J. N.; Tschaplinski, T.J.; Tuskan, G. A.; Wyman, C.E., Lignin Valorization: Improving Lignin Processing in the Biorefinery. *Science* **2014**, 344 (6185) 709-720.
8) Huang, C.; Lai, C.; Wu, X.; Huang, Y.; He, J.; Huang, C.; Li, X.; Y, Q., An integrated process to produce bioethanol and xylooligosaccharides rich in xylobiose and xylotriose from high ash content waste wheat straw. *Bioresource Technology* **2017**, 241, 228-235.
9) Motta, F. L.; Andrade, C. C. P.; Santana, M. H. A., A review of xylanase production by the fermentation of xylan: Classification, characterization and applications. In Characterization and applications, sustainable degradation of lignocellulosic biomass - techniques, applications and aommercialization, Anuj K. Chandel and Silvio Silvério da Silva, IntechOpen.
10) Duval, A.; Vilaplana, F.; Crestini, C.; Lawoko, M., Solvent screening for the fractionation of industrial kraft lignin. *Holzforschung*, *70* (1), 11-20.
11) Sannigrahi, P.; Ragauskas, A.J. Fundamentals of biomass pretreatment by fractionation. In Aqueous pretreatment of plant biomass for biological and chemical conversion to fuels and chemicals; John Wiley & Sons, Ltd.: Chichester, UK, 2013; p. 201.
12) Farhat, W.; Venditti, R.; Quick, A.; Taha, M.; Mignard, N.; Becquart, F.; Ayoub, A., Hemicellulose extraction and characterization for applications in paper coatings adhesives. *Industrial Crops and Products* **2017** 107, 370-377.
13) Fernandes, E. M.; Pires, R. A.; Mano, J. F.; Reis, R. L., Bionanocomposites from lignocellulosic resources: Properties, applications and future trends for their use in the biomedical field. *Progress in Polymer Science* **2013** *38*(10-11), 1415-1441.
14) Xing, Q.; Ruch, D.; Dubois, P.; Wu, L.; Wang, W.-J., Biodegradable and high-performance poly (butylene adipate-*co*-terephthalate)–lignin UV-blocking films. *ACS Sustainable Chemistry and Engineering* **2017** 5, 10342–10351.

15) Sayyed, A. J.; Deshmukh, N. A.; Pinjari, D. V., A critical review of manufacturing processes used in regenerated cellulosic fibres: viscose, cellulose acetate, cuprammonium, LiCl/DMAc, ionic liquids, and NMMO based lyocell. *Cellulose* **2019** 26(5), 2913-2940.
16) Costa, S. P.; Azevedo, A. M.; Pinto, P. C.; Saraiva, M. L. M., Environmental impact of ionic liquids: recent advances in (eco) toxicology and (bio) degradability. *ChemSusChem*, **2017** 10(11), 2321-2347.
17) Singh. S. K., Solubility of lignin and chitin in ionic liquids and their biomedical applications. *International Journal of Biological Macromolecules* **2019** *132*, 265-277.
18) Fort, D. A.; Remsing, R. C.; Swatloski, R. P.; Moyna, P.; Moyna, G.; Rogers, R. D., Can ionic liquids dissolve wood? Processing and analysis of lignocellulosic materials with 1-n-butyl-3-methylimidazolium chloride. *Green Chemistry* **2007** *9*(1), 63-69.
19) Adeleye, A.T.; Louis, H.; Temitope, H.A.; Philip, M.; Amos, P.I.; Magu, T.O.; Ozioma, A.U.; Amusan, O.O., Ionic liquids (ILs): advances in biorefinery for the efficient conversion of lignocellulosic biomass. *Asian Journal of Green Chemistry* **2019** 3, 391-417
20) Zhang, H.; Wu, J.; Zhang, J.; He, J., 1-Allyl-3-methylimidazolium chloride room temperature ionic liquid: A new and powerful nonderivatizing solvent for cellulose. *Macromolecules* **2005** 38(20), 8272-8277.
21) Sun, N.; Rahman, M.; Qin, Y.; Maxim, M. L.; Rodríguez, H.; Rogers, R. D., Complete dissolution and partial delignification of wood in the ionic liquid 1-ethyl-3-methylimidazolium acetate. *Green Chemistry* **2009** 11(5), 646-655.
22) Fukaya, Y.; Hayashi, K.; Wada, M.; Ohno, H., Cellulose dissolution with polar ionic liquids under mild conditions: required factors for anions. *Green Chemistry* **2008** 10(1) 44-46.
23) Payal, R. S.; Bharath, R.; Periyasamy, G.; Balasubramanian, S., Density functional theory investigations on the structure and dissolution mechanisms for cellobiose and xylan in an ionic liquid: gas phase and cluster calculations. *The Journal of Physical Chemistry B* **2012** 116(2) 833-840.
24) Bylin, S.; Olsson, C.; Westman, G.; Theliander, H., Solvation Behavior of Cellulose and Xylan in the MIM/EMIMAc Ionic Liquid Solvent System: Parameters for Small-Scale Solvation. *Bio Resources* **2014** 9(1) 1038-1054.
25) Yuan, L., Peng, H., Hu, L., Yu, R., Peng, W., Ruan, R., Xia, Q., Zhang, Y., and Liu, A. Dissolution of bamboo hemicellulose in 1-butyl-3-methylimidazolium halide-based ionic liquids 2019 *Bio Resources* **2019** 14(1), 2097-2112.
26) Hu, L.; Peng, H.; Zhang, Y.; Xia, Q.; He, H.; Ruan, R.; Liu, Y.; Liu, A., Insight into the interaction between arabinoxylan and imidazolium acetate-based ionic liquids. *Carbohydrate Polymers* **2020** 231 115699
27) Pu, Y.; Jiang, N.; Ragauskas, A. J., Ionic liquid as a green solvent for lignin. *Journal of Wood Chemistry and Technology* 2007 *27*(1), 23-33.
28) Janesko, B. G., Modeling interactions between lignocellulose and ionic liquids using DFT-D. **2011** *Physical Chemistry Chemical Physics*, *13*(23), 11393-11401.
29) Ji, W.; Ding, Z.; Liu, J.; Song, Q.; Xia, X.; Gao, H.; Gu, W., Mechanism of lignin dissolution and regeneration in ionic liquid. **2012** *Energy & fuels*, *26*(10), 6393-6403.
30) Bozell, J. J.; Black, S. K.; Myers, M.; Cahill, D.; Miller, W. P.; Park, S., Solvent fractionation of renewable woody feedstocks: Organosolv generation of biorefinery

process streams for the production of biobased chemicals. *Biomass and bioenergy* **2011**, *35*(10), 4197-4208.

31) Tao, J.; Hosseinaei, O.; Delbeck, L.; Kim, P.; Harper, D.P.; Bozell, J.J.; Rials, T.G.; Labbe, N., Effects of organosolv fractionation time on thermal and chemical properties of lignins. *RSC advances* **2016**, *6*(82), pp.79228-79235.

32) Kilpelainen, I.; Xie, H.; King, A.; Granstrom, M.; Heikkinen, S.; Argyropoulos, D.S., Dissolution of wood in ionic liquids. *Journal of Agricultural and Food Chemistry* **2007** *55*, 9142-9148.

33) Zhang, F.; Ilavsky, J.; Long, G.G.; Quintana, J.P.G.; Allen, A.J.; Jemian, P.R., Glassy carbon as an absolute intensity standard for small-angle scattering. *Metallurgical and Materials Transactions A* **2010** *41*, 1151-1158.

34) Ilavsky, J.; Jemian, P.R., Irena: tool suite for modeling and analysis of small-angle scattering. *Journal of Applied Crystallography* **2009** *42*, 347-353.

35) Beaucage, G., Small angle scattering from polymeric mass fractals of arbitrary mass fractal dimension. *Journal of Applied Crystallography* **1996** 29, 134-146.

36) Raghuwanshi, V. S.; Cohen, Y.; Garnier, G.; Garvey, C. J.; Russell, R. A.; Darwish, T.; Garnier, G., Cellulose dissolution in ionic liquid: ion binding revealed by neutron scattering. *Macromolecules* **2018,** *51* (19), 7649-7655.

37) Kikhney, A. G.; Svergun, D. I., A practical guide to small angle X-ray scattering (SAXS) of flexible and intrinsically disordered proteins. *FEBS letters* 2015, *589*(19), 2570-2577.

38) Receveur-Bréchot, V.; Durand, D., How random are intrinsically disordered proteins? A small angle scattering perspective. *Current Protein and Peptide Science* 2012, *13*(1), 55-75.

39) Pingali, S.V.; Smith, M.D.; Liu, S-H.; Rawal, T.B.; Pu, Y.; Shah, R. S.; Evans, B. R.; Urban, V.S.; Davison, B.H.; Cai, C.M.; Ragauskas, A.J.; O'Neill, M.H.; Smith, J.C.; Petridis, L., Deconstruction of biomass enabled by local demixing of cosolvents at cellulose and lignin surfaces. *Proceedings of the National Academy of Sciences* **2020**, *117* (29), 16776-16781.

40) Bonhote, P.; Dias, A. P.; Papageorgiou, N.; Kalyanasundaram, K.; Grätzel, M., Hydrophobic, highly conductive ambient-temperature molten salts. *Inorganic chemistry* **1996** *35*(5), 1168-1178.

41) Headley, A. D. a. J., N. M., The effect of the anion on the chemical shifts of the aromatic hydrogen atoms of liquid 1-butyl-3-methylimidazolium salts. *Journal of Physical Organic Chemistry* **2002** *15* (1), 52-55.

42) Hesse-Ertelt, S.; Heinze, T.; Kosan, B.; Schwikal, K.; Meister, F., Solvent effects on the NMR chemical shifts of imidazolium-based ionic liquids and cellulose therein. *Macromolecular Symposia* **2010,** *294* (2), 75-89.

43) Zhang, J.; Xu, L.; Yu, J.; Wu, J.; Zhang, X.; He, J.; Zhang, J., Understanding cellulose dissolution: effect of the cation and anion structure of ionic liquids on the solubility of cellulose. *Science China Chemistry* **2016** *59* (11), 1421-1429.

44) Chen, Y.; Li, S. H.; Xue, Z. M.; Hao, M. Y.; Mu, T. C., Quantifying the hydrogen-bonding interaction between cation and anion of pure [EMIM][AC] and evidencing the ion pairs existence in its extremely diluted water solution: Via ^{13}C, ^{1}H, ^{15}N and 2D NMR. *Journal of Molecular Structure* **2015** *1079*, 120–129

45) Swatloski, R. P.; Spear, S. K.; Holbrey, J. D.; Rogers, R. D., Dissolution of cellose with ionic liquids. 2002 *Journal of the American chemical society 124*(18), 4974-4975.
46) Mason, P. E.; Neilson, G. W.; Enderby, J. E.; Saboungi, M. L.; Brady, J. W., Neutron diffraction and computer simulation studies of D-xylose. 2005 *Journal of the American Chemical Society 127*(31), 10991-10998.
47) Peng, X. W.; Ren, J. L.; Sun, R. C., Homogeneous esterification of xylan-rich hemicelluloses with maleic anhydride in ionic liquid 2010 *Biomacromolecules 11*(12), 3519-3524
48) Nishiyama, Y.; Langan, P.; Chanzy, H. Crystal structure and hydrogen-bonding system in cellulose I beta from synchrotron X-ray and neutron fiber diffraction. *Journal of American Chemical Society* **2002,** *124* (31), 9074-9082.
49) Hirosawa, K.; Fujii, K.; Hashimoto, K.; Shibayama, M., Solvated structure of cellulose in a phosphonate-based ionic liquid. *Macromolecules* **2017,** *50* (17), 6509-6517.
50) Petridis, L.; Schulz, R.; Smith, J. C., Simulation analysis of the temperature dependence of lignin structure and dynamics. 2011 *Journal of the American Chemical Society, 133*(50), 20277-20287.
51) Zhao, W.; Xiao, L. P.; Song, G.; Sun, R. C.; He, L.; Singh, S.; Simmons, B.A.; Cheng, G., From lignin subunits to aggregates: insights into lignin solubilization. 2017 *Green Chemistry, 19*(14), 3272-3281.
52) Petridis, L.; Pingali, S. V.; Urban, V.; Heller, W. T.; O'Neill, H. M.; Foston, M.; Smith, J. C., Self-similar multiscale structure of lignin revealed by neutron scattering and molecular dynamics simulation. 2011 *Physical Review E, 83*(6), 061911.
53) Xu, A.; Zhang, Y.; Li, Z.; Wang, J., Densities and conductivities of seven 1-allyl-3-methylimidazolium carboxylate ionic liquids. *Journal of Molecular Liquids* **2016**, *214*, 192-195.

4.7.Appendix

Thermal analysis of ionic liquids

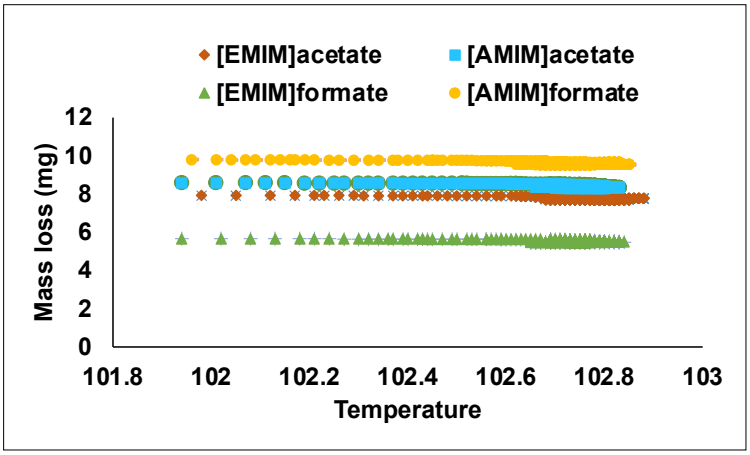

Figure 4. 7. Mass loss versus temperature data of [EMIM]acetate (red), [AMIM]acetate (blue), [EMIM]formate (green) and [AMIM]formate (pink) at 102 ˚C.

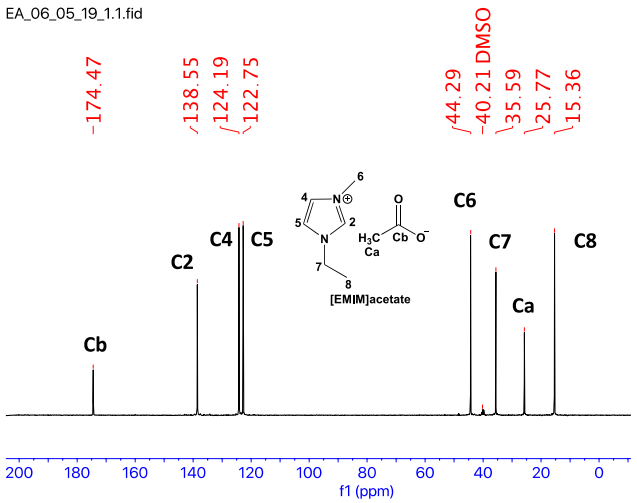

Figure 4. 8. ^{13}C NMR (400 MHz, DMSO-d6) of neat [EMIM]acetate at 80 °C.

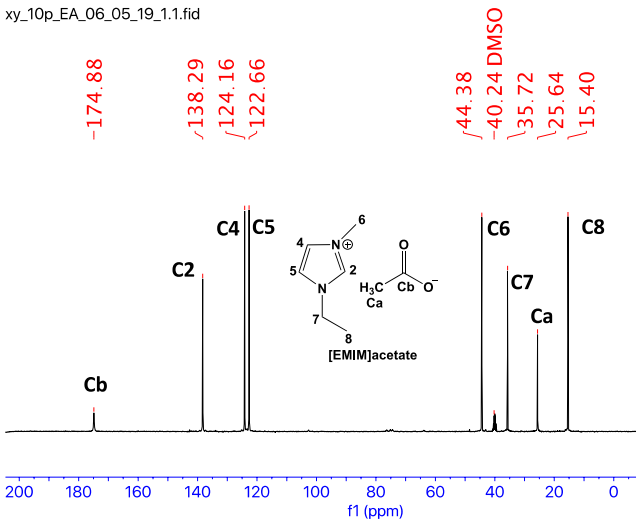

Figure 4. 9. ^{13}C NMR (400 MHz, DMSO-d6) of [EMIM]acetate with 10 wt.% xylan at 80 °C.

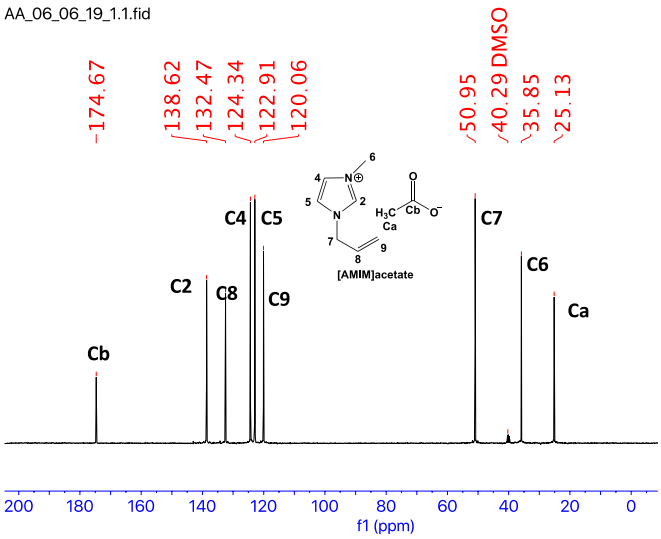

Figure 4. 10. ^{13}C NMR (400 MHz, DMSO-d6) of neat [AMIM]acetate at 80 °C.

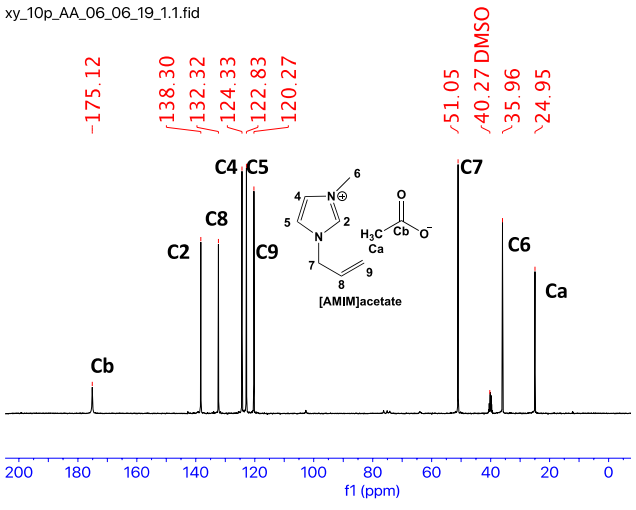

Figure 4. 11. ^{13}C NMR (400 MHz DMSO-d6) of [AMIM]acetate with 10 wt.% xylan at 80 °C.

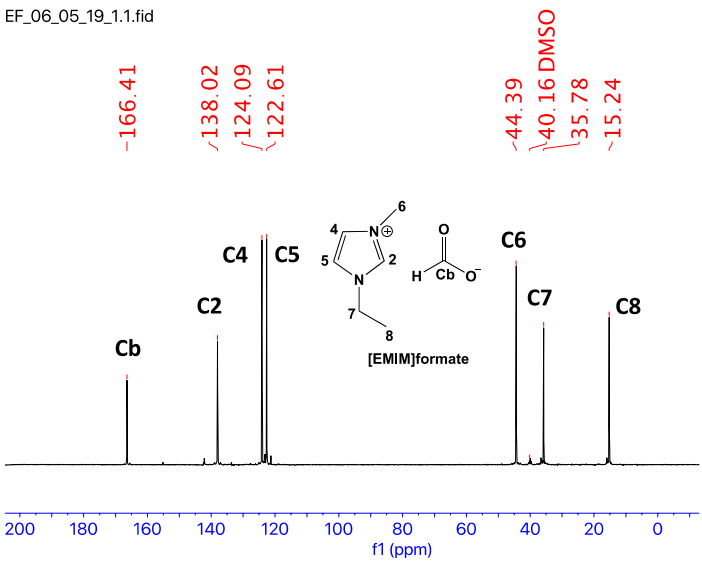

Figure 4. 12. ^{13}C NMR (400 MHz, DMSO-d6) of neat [EMIM]formate at 80 °C.

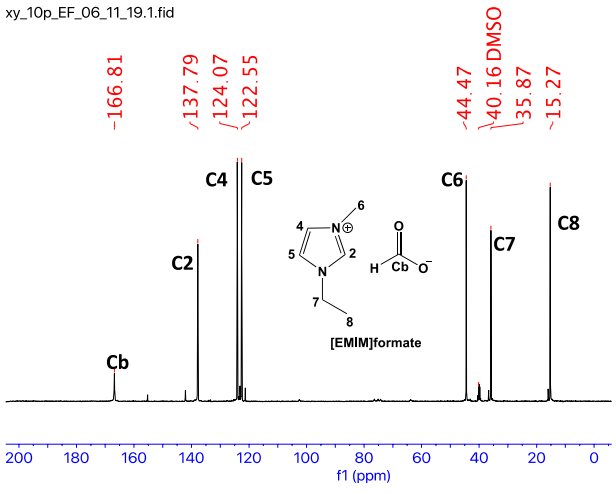

Figure 4. 13. ^{13}C NMR (400 MHz, DMSO-d6) of [EMIM]formate with 10 wt.% xylan at 80 °C.

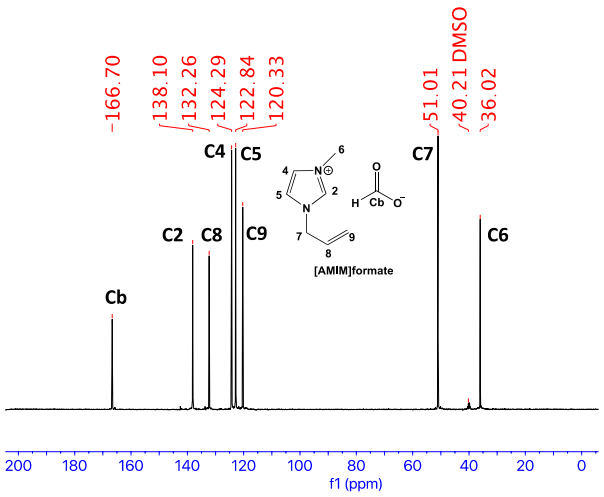

Figure 4. 14. ^{13}C NMR (400 MHz, DMSO-d6) of neat [AMIM]formate at 80 °C.

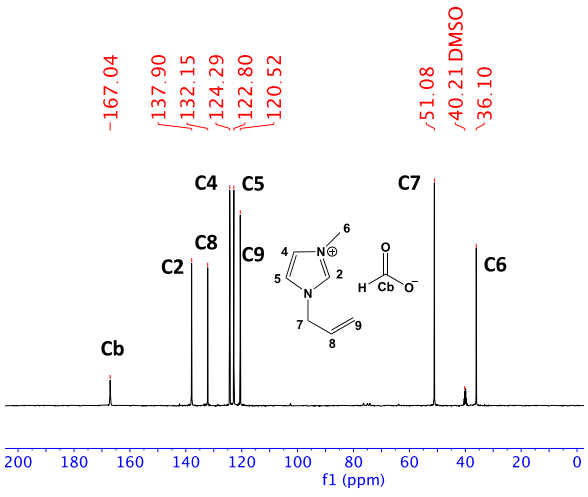

Figure 4. 15. ^{13}C NMR (400 MHz, DMSO-d6) of [EMIM]formate with 10 wt.% xylan at 80 °C.

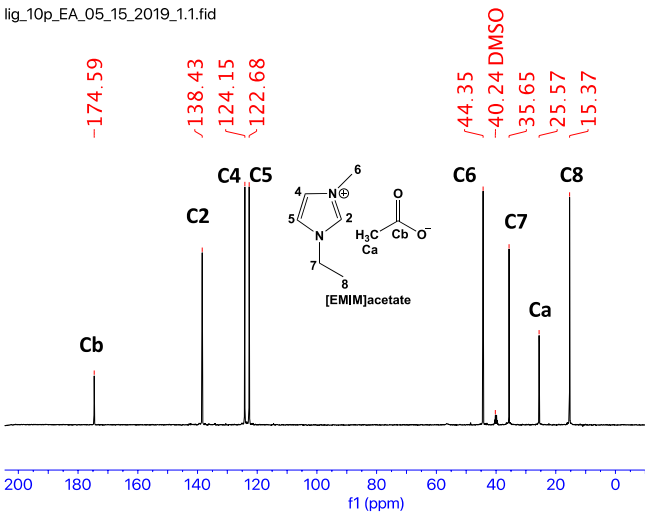

Figure 4. 16. ^{13}C NMR (400 MHz, DMSO-d6) of [EMIM]acetate with 10 wt.% lignin at 80 °C.

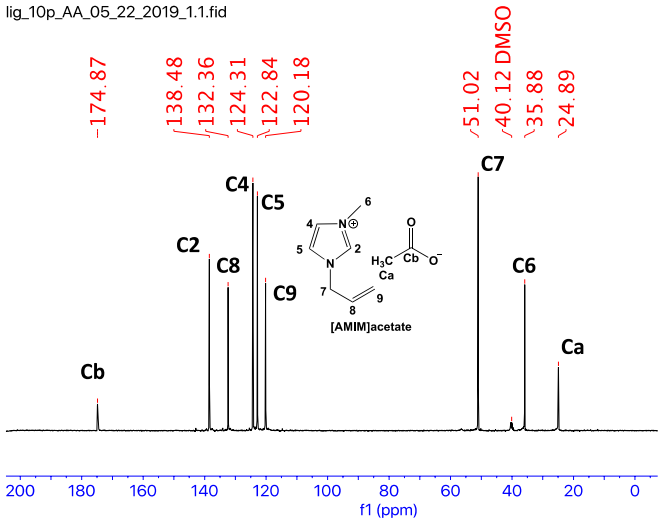

Figure 4. 17. ^{13}C NMR (400 MHz, DMSO-d6) of [AMIM]acetate with 10 wt.% lignin at 80 °C.

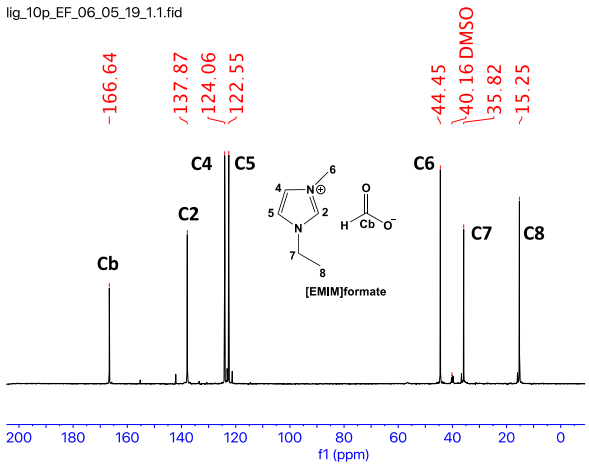

Figure 4. 18. ^{13}C NMR (400 MHz, DMSO-d6) of [EMIM]formate with 10 wt.% lignin at 80 °C.

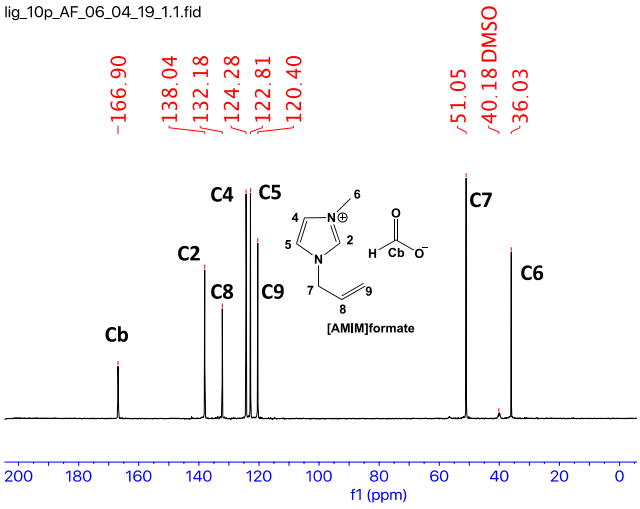

Figure 4. 19. ^{13}C NMR (400 MHz, DMSO-d6) of [AMIM]formate with 10 wt.% lignin at 80 °C.

Table 4.4 4. Chemical shift values of [EMIM]acetate and [EMIM]acetate with 10 wt.% xylan

Carbon number	Chemical shift of neat IL (an average of three runs)	Chemical shift of IL with 10 wt.% xylan	Chemical shift difference (Δδ)
C2	138.55	138.31	-0.23±0.06
C4	124.19	124.16	-0.03±0*
C5	122.75	122.66	-0.09±0
C6	35.59	35.72	0.12±0.01
C7	44.29	44.38	0.09±0
C8	15.36	15.40	0.03±0.01*
Ca	25.77	25.62	-0.15±0.02
Cb	174.47	174.89	0.42±0.02

Means followed by the same letter are not statistically significant at an alpha value of 0.05

Table 4. 5. Chemical shift values of [AMIM]acetate and [AMIM]acetate with 10 wt.% xylan

Carbon number	Chemical shift of neat IL (an average of three runs)	Chemical shift of IL with 10 wt.% xylan	Chemical shift difference (Δδ)
C2	138.62	138.30	-0.32±0
C4	124.34	124.33	-0.01±0*
C5	122.91	122.83	-0.08±0
C6	35.85	35.96	0.10±0.01
C7	50.95	51.05	0.10±0
C8	132.47	132.32	-0.15±0.01
C9	120.07	120.26	0.19±0.01
Ca	25.14	24.93	-0.21±0.02
Cb	174.66	175.15	0.48±0.03

Means followed by the same letter are not statistically significant at an alpha value of 0.05

Table 4. 6. Chemical shift values of [EMIM]formate and [EMIM]formate with 10 wt.% xylan

Carbon number	Chemical shift of neat IL (an average of three runs)	Chemical shift of IL with 10 wt.% xylan	Chemical shift difference (Δδ)
C2	138.01	137.78	-0.23±0.01
C4	124.10	124.07	-0.02±0*
C5	122.61	122.54	-0.06±0.01
C6	35.76	35.87	0.11±0
C7	44.40	44.47	0.07±0
C8	15.23	15.27	0.04±0.01
Cb	166.39	166.82	0.43±0.01

Means followed by the same letter are not statistically significant at an alpha value of 0.05

Table 4. 7. Chemical shift values of [AMIM]formate and [AMIM]formate with 10 wt.% xylan

Carbon number	Chemical shift of neat IL (an average of three runs)	Chemical shift of IL with 10 wt.% xylan	Chemical shift difference (Δδ)
C2	138.10	137.89	-0.21±0.01
C4	124.53	124.28	-0.24±0.01
C5	122.84	122.79	-0.05±0.01
C6	36.02	36.1	0.08±0
C7	51.01	51.09	0.08±0.01
C8	132.25	132.14	-0.11±0.01
C9	120.34	120.53	0.18±0.02
Cb	166.70	167.07	0.37±0.02

Means followed by the same letter are not statistically significant at an alpha value of 0.05

Table 4. 8. Chemical shift values of [EMIM]acetate and [EMIM]acetate with 10 wt.% lignin

Carbon number	Chemical shift of neat IL (an average of three runs)	Chemical shift of IL with 10 wt.% xylan	Chemical shift difference (Δδ)
C2	138.56	137.42	-0.15±0.01
C4	124.19	124.15	-0.04±0.0*
C5	122.75	122.67	-0.08±0.01
C6	35.59	35.65	0.06±0.01
C7	44.29	44.35	0.06±0.01
C8	15.37	15.44	0.07±0.12
C9	25.78	25.57	-0.21±0.02
Cb	174.46	174.59	0.13±0.02

Means followed by the same letter are not statistically significant at an alpha value of 0.05

Table 4. 9. Chemical shift values of [AMIM]acetate and [AMIM]acetate with 10 wt.% lignin

Carbon number	Chemical shift of neat IL (an average of three runs)	Chemical shift of IL with 10 wt.% xylan	Chemical shift difference (Δδ)
C2	138.62	138.48	-0.14±0.01
C4	124.34	124.31	-0.03±0.01*
C5	122.91	122.84	-0.07±0.01
C6	35.85	35.87	0.02±0*
C7	50.95	51.02	0.07±0.01
C8	132.47	132.35	-0.12±0.01
C9	120.05	120.16	0.11±0.02
Ca	25.12	24.84	-0.28±0.04
Cb	174.71	167.07	0.17±0.11

Means followed by the same letter are not statistically significant at an alpha value of 0.05

Table 4. 10. Chemical shift values of [EMIM]formate and [EMIM]formate with 10 wt.% lignin

Carbon number	Chemical shift of neat IL (an average of three runs)	Chemical shift of IL with 10 wt.% xylan	Chemical shift difference (Δδ)
C2	138.02	137.87	-0.15±0.01
C4	124.1	124.06	-0.04±0.01
C5	122.61	122.55	-0.06±0.01
C6	35.80	35.82	0.03±0.01*
C7	44.39	44.45	0.05±0.01
C8	15.28	15.26	-0.02±0.01*
Cb	166.39	166.64	0.24±0.02

Means followed by the same letter are not statistically significant at an alpha value of 0.05

Table 4. 11. Chemical shift values of [AMIM]formate and [AMIM]formate with 10 wt.% lignin

Carbon number	Chemical shift of neat IL (an average of three runs)	Chemical shift of IL with 10 wt.% xylan	Chemical shift difference (Δδ)
C2	138.09	138.48	-0.05±0.01
C4	124.29	124.31	-0.01±0.0
C5	122.84	122.84	-0.02±0.0
C6	36.02	35.87	0.01±0*
C7	51.01	51.02	0.04±0.0
C8	132.26	132.35	-0.06±0.01
C9	120.33	120.16	0.08±0.02
Cb	166.69	167.07	0.18±0.11

Means followed by the same letter are not statistically significant at an alpha value of 0.05

Table 4. 12. Molecular weight, density and scattering length density of xylan, [AMIM]formate, [EMIM]acetate and [AMIM]acetate

Sample	Molecular weight, M_w (g/mol)	Density (g/cm^3)[53]	SLD ($x10^{-6}$ $Å^{-2}$)
Xylan (Birchwood)	150.12	1.5	13.561 ($C_5H_{10}O_5$)
[AMIM] formate	168.2	1.13[1]	10.23 ($C_8H_{12}N_2O_2$)
[EMIM] acetate	170.2	1.10	9.481 ($C_8H_{14}N_2O_2$)
[AMIM]acetate	182.2	1.11	10.11($C_9H_{11}N_2O_2$)

Chapter 5. *In-situ* biomass dissolution in two different 1,3 dialkyl imidazolium ionic liquids

5.1. Introduction

Lignocellulosic biomass is an abundant renewable source which has the potential to be used for the sustainable production of fuels, chemicals, and products.[1] Biomass is mainly composed of three major polymers: cellulose, hemicellulose, and lignin. These polymers are hierarchically organized to form a composite cell wall structure, with cellulose encased in lignin-hemicellulose matrix. It is this encasement architecture of plant cell wall that poses a major challenge for the complete utilization of lignocellulosic biomass for products and fuel production. Several chemical, physical, and biological methods have been utilized to fractionate biomass into its constituent polymers for this purpose.[2] Among the various solvent systems, ionic liquids (ILs) offer several advantages such as, high thermal stability and low volatility along with the ability to selectively dissolve biomass constituents and whole biomass. These properties position ILs favorably for developing "green" biomass processing technologies.[3]

ILs are low melting temperature salts with an organic cation and either an organic/inorganic anion. The physical properties of IL such as viscosity and density can be amended by varying the combination of cation and anion of an IL; hence, ILs are often referred to as "designer solvents".[4] By altering processing conditions (such as temperature and time), ILs can be utilized for biomass processing in three different ways: 1) biomass fractionation to isolate high purity cellulose, hemicellulose and lignin streams[5] 2) biomass activation to reduce recalcitrance and augment saccharification rate[6] and 3) whole biomass dissolution for direct bio-product development.[7]

Imidazolium (1,3 dialkyl) ILs are the most commonly used ILs to pretreat or dissolve biomass due to their ease of synthesis and high purity standard that can be achieved. Currently, there are several different imidazolium ILs reported as promising biomass solvents for processing.[8]

Nevertheless, the factors responsible for efficacy of one IL over another remain unclear. Obtaining a discerning picture is necessary to identify an ideal IL for commercialization which will in turn bring down the overall cost of IL biomass processing technologies.

Biomass dissolution occurs over multiple length scales, ranging from angstrom (cellulose microfibril) to micron (pore size of biomass) levels. Based on the key findings of past research works, the three main steps of biomass dissolution process are: 1) permeation of IL through biomass layers, 2) swelling of biomass polymers, and 3) disruption of biomass encasement architecture. [9, 10, 11, 12] Imaging, microscopy, scattering, diffraction, chemical composition analysis and saccharification measurements have offered some insights into the above-mentioned changes. For example, using bright-field optical microscopy it was shown that at temperatures higher than 100 ˚C, complete biomass dissolution happened in about 90 minutes.[9] Cross polarizing filters that identify cellulose crystallite changes were used in several studies and based on the bright field patterns it was concluded that cellulose dissolution occurred rapidly due to loss of its crystallite integrity.[13]

While microscopy techniques provided crucial information on micron level, imaging techniques such as scanning electron microscopy (SEM) and atomic force microscopy (AFM) were useful in generating a wholesome global picture of biomass changes by extrapolating micrometer (μm) level changes. One of the most prominent changes noted using SEM is the increased porosity of biomass/ cellulose.[14] This morphological observation was interpreted as the result of disruption of encasement architecture, hemicellulose/lignin relocation and reduction of cellulose crystallinity. AFM was useful to measure the surface roughness alterations of biomass, which were in turn interpreted as a result of cellulose fibril reorganization and hemicellulose dissolution.[15]

Small angle scattering techniques using neutrons (SANS) or X-rays (SAXS) are another set of techniques useful in obtaining architectural changes of biomass based on the differences in electron contrast (SAXS) or neutron contrast (SANS).[16] While X-ray scattering is influenced by electron density of the studied sample, neutrons are sensitive to the nuclear composition and consequently isotope dependent. The difference in the electron contrast between individual biomass polymers (e.g. micro crystalline cellulose (MCC) or extracted lignin) and ILs allowed SAXS studies to provide structural details such as polymer conformation, size and shape.[17, 18, 19, 20] SANS techniques, on the other hand, have provided whole biomass structural details pertaining to cellulose microfibril reorganization, lignin agglomeration, lignin-hemicellulose network and biomass surface characteristics.[21, 22, 23, 24] Despite these reported studies, the nano to sub-micron details of biomass polymers *during* IL dissolution process remain largely obscure.

Therefore, the main goal of this study is to investigate the evolution of structural and morphological changes of biomass *during* its exposure to IL. This was achieved by using *in-situ* reaction SANS approach. Further, infrared analysis was used as a complementary technique to understand the chemical changes in the samples recovered after the reaction SANS measurements. The choice of the ILs was based on our findings in chapters 3 and 4. ILs 1-allyl-3-methylimidazolium formate ([AMIM]formate) and 1-ethyl-3-metylimidazolium acetate ([EMIM]acetate) were shown to exhibit similar set of interactions towards xylan but distinct interactions towards cellulose and lignin. But the substrates for the earlier chapter studies were individual biomass polymers. Therefore, for the current study, hybrid poplar, a dedicated bioenergy crop was used. [25] Cellulose microfibril changes measured using SANS showed that [EMIM]acetate started permeating through the fibril arrangement within 30 min of exposure. With progression of time, the average size of cellulose microfibrils was reduced from ~ 8.6 Å to 7.4 Å

in [EMIM]acetate. On the other hand, when biomass was exposed to [AMIM]formate its cellulose microfibril architecture did not alter during the entire run time (44h) of reaction. FT-IR analysis showed that biomass treated with [EMIM]acetate underwent deacetylation consistent with mass loss. On the other hand, biomass recovered from [AMIM]formate did not have any mass loss. IR analysis showed that biomass treated in [AMIM]formate was different from the control/ untreated biomass However, the analysis was inconclusive in identifying the specific biomass polymer changes in the [AMIM]formate biomass system. The results of the current study of whole biomass combined with our earlier chapter conclusions demonstrated that [AMIM]formate and [EMIM]acetate differ in their action towards cellulose. Future analysis will focus on understanding the structural details of hemicellulose and lignin in these two ILs.

5.2.Experimental section

5.2.1. Materials

The biomass used in this study, hybrid poplar (*Populus spp*.) was obtained from the Center for Renewable Carbon, The University of Tennessee. Biomass discs (16 mm diameter, 0.35 mm thick) were obtained by slicing through the cross section. Each sample had three growth rings, with central growth ring of 1 cm width. Deuterated [EMIM]acetate and [AMIM]formate used in our SANS experiments were synthesized following previously published protocols.[24] The ^{1}H spectra of the ILs are shown in the appendix portion of this chapter. The hybrid poplar biomass discs were soaked in the ILs (~1mL) for (~40 min) at room temperature prior to loading into the sample cell for our *in-situ* SANS measurement study. The treatment temperature for the SANS measurement was 80 ˚C.

5.2.2. Small angle neutron scattering (SANS)

The SANS measurements were performed using the Bio-SANS instrument located at the High Flux Isotope Reactor (HFIR) facility at Oak Ridge National Laboratory.[26] A large dynamic Q range, spanning $0.003 < Q$ ($Å^{-1}$) < 0.8 was accessed in a single configurational setting using 6 Å neutrons and a relative wavelength spread ($\Delta\lambda/\lambda$) of 15%. The main and wing detector arrays were positioned at 15.5 m and 1.13 m from the sample position, and the wing detector array was positioned at an angle of 1.4 °. The sample cell setup used for the SANS experiment is shown in Figure 5.1A. The 2D images displayed anisotropic patterns with scattering data in two wedges. Wedge 0 contained aligned and isotropic features of the system (horizontal wedge) and wedge 1 contained only the isotropic underlying features (vertical wedge) (Figure 5.1B and 5.1C). Two scattering intensity profiles, $I(Q)$ versus Q, were obtained for each sample; one from the horizontal wedges and the other from the vertical. These profiles were obtained by azimuthally averaging within each group of wedges (horizontal to vertical) of the processed anisotropic 2D image. The reduction process normalized to incident beam monitor counts, corrected for detector dark current, pixel sensitivity and scattering from backgrounds such as solvent and titanium cell.

5.2.3. SANS data reduction and analysis

The 2D patterns of the prepared samples exhibited distinct intensity flares in the horizontal direction (wedge 0) that arises from the aligned component in biomass (Figure 5.1B and 5.1C). The 1D scattering profile for the anisotropic cellulose features, wedge 1 was obtained by subtracting the profile with all features IL, cellulose, hemicellulose and lignin wedge 0. The resultant profile was used for the analysis presented in this chapter.

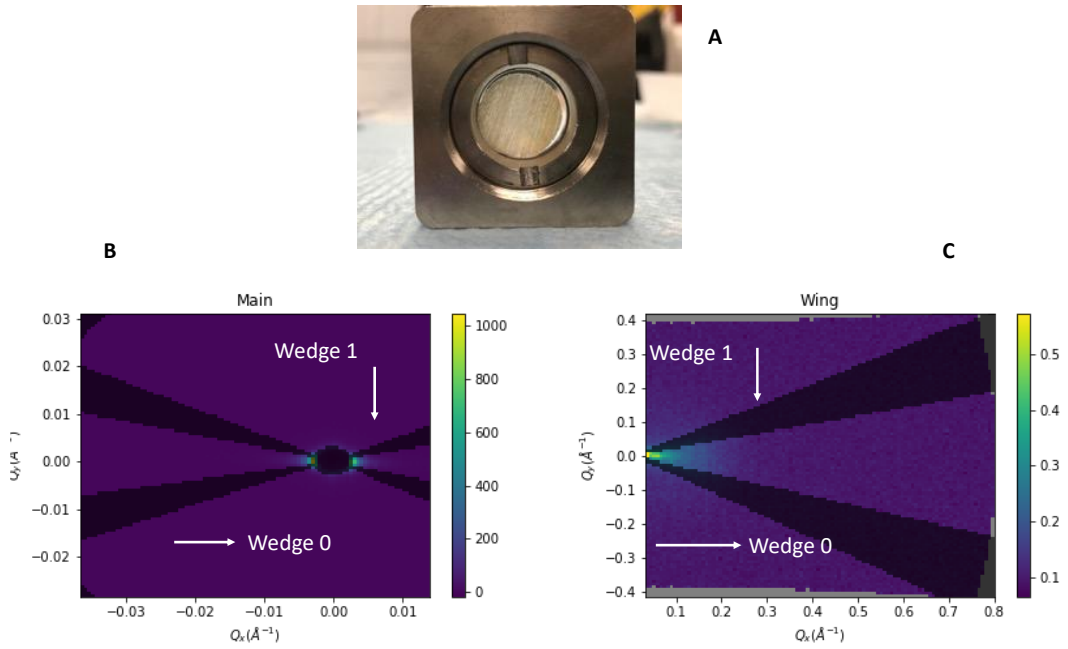

Figure 5. 1. A. Biomass disc in titanium cell for SANS study. B. 2-D image of scattering signal obtained from main detector C. 2D image obtained from wing detector of Bio-SANS instrument.

SANS data analysis was performed on the subtracted curves using the 'Modeling-II' tool in IRENA package of Igor Pro (WaveMetrics, Inc., Portland, OR) software.[28] The low Q region of the SANS curve was modeled to the power law function in the Unified Fit. The function implemented in IRENA package of Igor Pro (WaveMetrics, Inc., Portland, OR) software is expressed as:

$$I(Q) = AQ^{-P} + I_{bkg} \quad (1)$$

where A is the intensity scale factor, *P* the power-law exponent and I_{bkg} the background intensity of neat IL.

The high Q region was fit to a log-normal radial distribution of polydisperse cylinder function, as implemented in the IRENA package of Igor Pro (WaveMetrics, Inc., Portland, OR) software:

$$I(Q) = I_0 \overline{P(Q)}\, S(Q) \quad (1)$$

I_0 is the intensity scalar which is given by the equation below:

$$I_0 = \frac{\phi}{V_{poly}} (\Delta\rho)^2 \quad (2)$$

where (ϕ) accounts for the cylinder particle volume fraction and $\Delta\rho$ is the particle contrast ($\rho_{\text{cylinder}} - \rho_{\text{solvent}}$). $\rho_{cylinder}$ and $\rho_{solvent}$ are the scattering length densities (SLD) of the cylinder particles and the solvent, respectively. V_{poly}, the volume of polydisperse cylinders using second moment, is given as $V_{poly} = \pi r^2 L(1 + p^2)$, where *r* and *L* are the cylinder's radius and length, respectively. Polydispersity of cylinder radius, $p = \sigma / r_{avg}$, is the ratio of the width of log- normal distribution to its peak value. The form factor, $\overline{P(Q)}$ of a radially polydisperse log-normal distribution of cylinders is expressed as:

$$\overline{P(Q)} = \int_0^{\pi/2} G(r)\ F^2\ (q, \alpha)\ \sin\alpha\ d\alpha \quad (3)$$

where F is the form factor of a cylinder and $G(r)$ is the radial log-normal distribution function expressed as:

$$F(q,\alpha) = 2\,V_{cyl}J_0(qH\cos\alpha)\,\frac{J_1(qr\sin\alpha)}{(qr\sin\alpha)} \quad (4)$$

$$G(r) = \frac{1}{\sigma R\sqrt{2\pi}}\,exp\left[-\frac{1}{2\sigma^2}(ln(R)-\mu)^2\right] \quad (5)$$

Where $\mu = \ln(R_{med})$, R_{med} is the mean radius and polydispersity is given by $\boldsymbol{\sigma}$. In equation 4, $J_0(x) = \sin(x)/x$ is the zeroth order Bessel function, α is the angle between cylinder axis and the scattering vector, and H equals half the length of the cylinder. For our current analysis, all samples exhibited monodisperse cylinder characteristics except for 44 h reaction time stamp of biomass in [EMIM]acetate. Further, no inter particle correlation was used, i.e., S(Q) = 1 for biomass reaction samples in [EMIM]acetate. While a weak interference between fibrils was modeled for biomass samples in [AMIM]formate. The structure factor chosen for this purpose was the spherical correlation (interference) as $S(Q) = \frac{1}{1+k\frac{3(Sin(Q\xi)-q\xi(cos(Q\xi)))}{(Q\xi)^3}}$ Where, k = packing correlation and $\boldsymbol{\xi}$ = Bragg like spacing between domains.

5.2.4. Recovery of samples after SANS experiment

Due to the low energy of neutrons used for our SANS experiment, the biomass samples do not undergo radiation damage and therefore can be recovered. In brief, after the 2-days treatment time, the remaining solid biomass discs were washed in DI water (15 ml X 3) and the complete removal of ILs from the biomass was confirmed by the absence of the infrared band at 1565 cm^{-1} which corresponds to C-N stretch, after which the biomass disc was air dried for 3 days or until constant weight was achieved.

5.2.5. Fourier transform infrared (FT-IR) spectroscopy

The chemical signature of the HP biomass discs before and after IL exposure was obtained using a Perkin–Elmer Spectrum One FT-IR spectrometer (Waltham, MA). Biomass disc was placed on the ATR accessory of the spectrometer and a pressure gauge was used to ensure proper contact between the sample and the accessory. FT-IR spectra were collected over a range of 4000-600 cm^{-1} in the absorbance mode, with a 4 cm^{-1} resolution and 16 scans per sample. Five spectra were collected for each sample. The spectra were pre-treated with an ATR correction, normalized and corrected by Multiplicative Scatter Correction (MSC) in The *Unscrambler*® X software version 9 (CAMO software).

5.2.6. Statistical analysis: Principal component analysis of FT-IR spectra

Principal component analysis (PCA), a type of multivariate analysis, was used to analyze the FT-IR spectral data. PCA allows for the visualization of composite data by identifying the main sources of variation by removing noise variability and redundancy from the data. The spectral data are compressed and transformed into a data set that shows its most relevant factors, known as principal components or PC. The first principal component has the largest possible variance and accounts for most of the variability in the spectral data. Scatter plots of principal component scores show the pattern of the data and is called a scores plot. The relationship between wavenumber of the FT-IR spectrum and the PCs is shown on another plot called a loadings plot. The pattern on the loadings plot then shows how much each variable contribute to each PC.

5.3.Results and discussion

5.3.1. Small angle neutron scattering analysis

The time resolved SANS profiles of cellulose in biomass in [EMIM]acetate at two different time points, 0.5h and 44h are shown in panels A and B of Figure 5.2. Panels C and D of Figure 5.2 show the profiles for cellulose in [AMIM]formate. The two profiles in panel A look mostly similar except for two differences. As the experiment progressed, the scattering intensity in the low Q region (0.003 – 0.01 $Å^{-1}$) decreases and the shoulder feature in the high Q region becomes shallower (Blue dots, panel B). The data in the low Q region which provide surface morphology information of large-scale features were fit to a power-law function while the high Q region which provides information on the cellulose microfibril architecture was fit to a lognormal polydisperse cylinder form factor. The fit parameters extracted from the data presented in Figure 5.2 are listed in Table 5.1.

In biomass treated with [EMIM]acetate the radius of the cellulose microfibrils (cylinder feature) decreased from 11.6 to 7.5 Å (Table 5.1) while the distribution width (FWHM) increased from 0.20 to 8.13. Figure 5.3A elaborates this change by showing the transition from a narrow radial distribution of cellulose microfibrils to a broad radial distribution during the 2 days of IL reaction in [EMIM]acetate. At 30 min of IL treatment, the cellulose microfibrils were of uniform size, which suggests minimal penetration of [EMIM]acetate into cellulose microfibrils. However, after ~2 days of reaction, the transition to a polydisperse radial distribution of cellulose microfibrils resulted in the appearance of both, smaller and larger dimensions of microfibrils. The observation of larger and more importantly smaller sizes of the microfibrils can help us understand on how [EMIM]acetate interacts with cellulose.

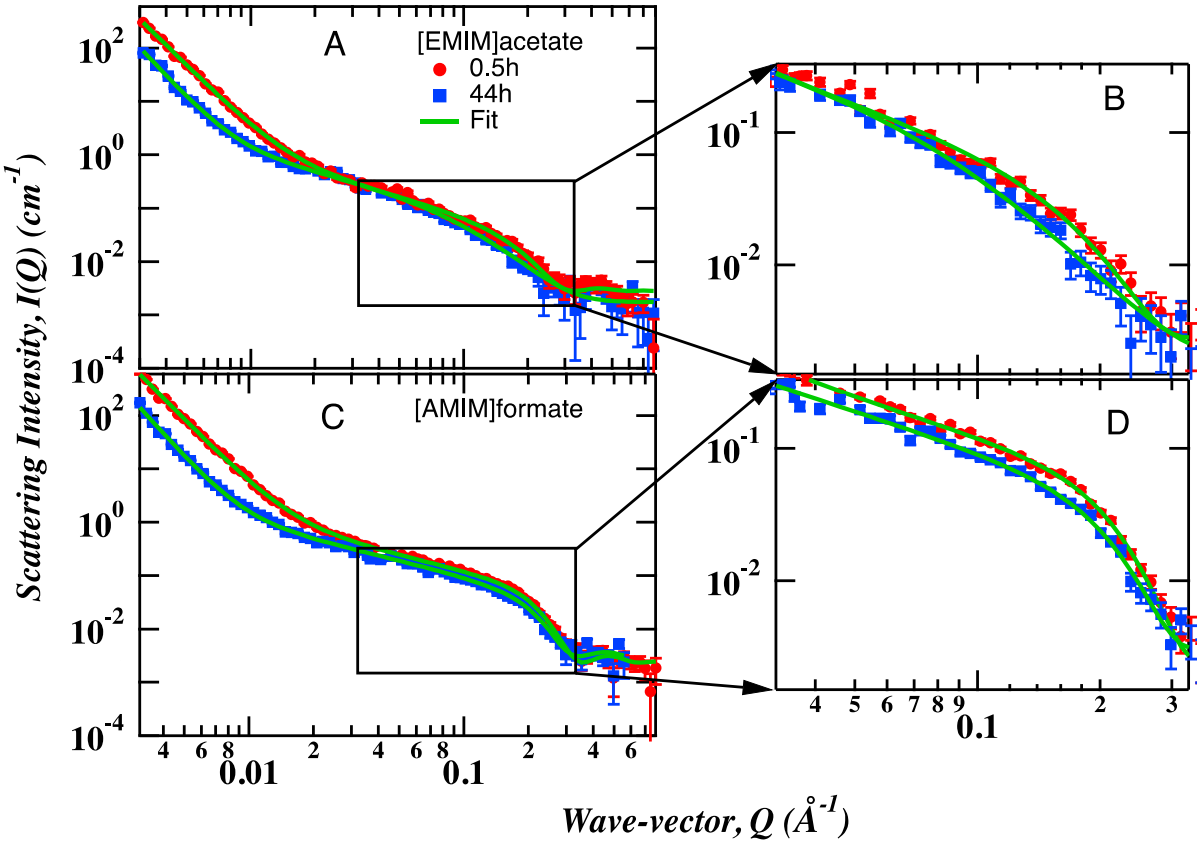

Figure 5. 2. Time resolved SANS profiles of cellulose in biomass for [EMIM]acetate (A) and [AMIM]formate (C) at 80 ˚C. The panels B and D show the enlarged insets in A and C, respectively.

[EMIM]acetate preferentially swells the microfibril to form larger radial microfibrils and as the swelling continues further, the peripheral strands slowly dissociate from the regular fibrillar arrangement contributing to the appearance of smaller microfibrils. This process of how [EMIM]acetate deconstructs the microfibril morphology during reaction is uniquely observable only by reaction SANS measurements. Meanwhile, the power-law exponent in the low Q region increased from 4.0±0.1 to 4.4±0.2. This increase implied a transition in the surface morphology of the large structures (possibly macrofibrils or cell wall lumens) from a smooth surface to a diffuse interface.[29] A diffuse interface is consistent with a gradient of IL molecules on the surface of the large structures as the IL molecules gradually penetrate along with the leaching of the surface polymers from these large structures.

Unlike [EMIM]acetate, the cellulose cross-sectional feature (Q ~ 0.1 $Å^{-1}$) in [AMIM]formate is more defined and showed no measurable change after 2 days of reaction (Figure 5.2 panels C and D). The prominence of the shoulder feature suggests that the regular order of cellulose microfibril is preserved in [AMIM]formate. The next neighbor distance, i.e., center to center distance between cellulose microfibrils, obtained at t = 30 min in [AMIM]formate is 27±8 Å (Table 5.1). This lack of change can be interpreted as minimal penetration of [AMIM]formate into the individual cellulose microfibrils from the initial 30 min time instant to the end of 2-day reaction. Accordingly, the radial distribution plot of [AMIM]formate shows the lack of any specific changes in cellulose microfibrils in [AMIM]formate (Figure 5.3 B). An important aspect to note is the scale (Y-axis intensity) of the volume distributions. A reduction in the intensity of volume distribution peak can be attributed to one of three parameters- contrast, volume and number of particles.

Table 5. 1. Composite model fit of log Normal radial distribution of interacting cylinders combined with a power-law fit of biomass in [EMIM]acetate and [AMIM]formate ILs at the starting and ending time points of 2 days of reaction.

	[EMIM]acetate		[AMIM]formate	
	0.5h_EA	44h_EA	0.5h_AF	44h_AF
log Normal radial distribution of cylinders with interference [$]				
Mean (Å)	11.6	11.9	10.7	11.2
Mode (Å)	11.6	7.5	10.7	11.2
Median (Å)	11.6	10.2	10.7	11.2
Full width half maximum (FWHM)	0.20	8.1	0.2	0.2
Next neighbor distance (Å)	N/A	N/A	27±8	23±8
Power law				
Scale	3.0E-09	7.4E-11	2.7E-09	4.8E-11
Exponent	4.0±0.1	4.4±0.2	4.1±0.1	4.5±0.2

[$]polydisperse cylinder length was fixed at 1000 Å for all samples.

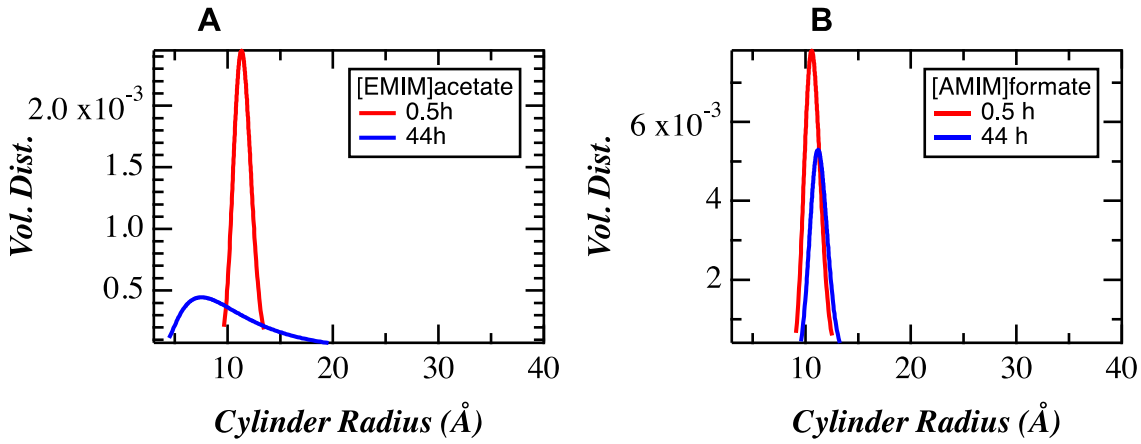

Figure 5. 3. A. Polydisperse cylinder radius distribution of cellulose in biomass for [EMIM]acetate at t = 0.5h and t = 44h. B. Polydisperse cylinder radius distribution of cellulose in biomass for [AMIM]formate at t = 0.5h and t = 44h.

Since, both volume and number of particles remain unchanged during the reaction, the reduction in intensity could possibly be due to change in the contrast. However, contrast was assumed constant during data analysis (reaction). Therefore, the reduction in volume distribution scale/intensity for [AMIM]formate does not correspond to size reduction of microfibrils. Unlike the lack of changes to the cellulose microfibril sizes in the high-Q region, the power law exponent in the low Q region increased from 4.1±0.1 to 4.5±0.2. This low-Q region alteration is similar to the trend noted for [EMIM]acetate, where a smooth surface gave way to a more diffuse interface.

Along with the time resolved changes within individual IL, SANS measurement was useful to identify the differences between the two ILs as well (Figure 5.4). At 30 min reaction time, cellulose microfibril feature at Q ~ 0.2 $Å^{-1}$ in [AMIM]formate is clearly discernable by its sharper profile. To highlight the difference in cellulose arrangement between the two samples, a Porod plot (Q^4 I(Q)) is shown in panel B. In case of [AMIM]formate, the cellulose correlation peak (green fit curve) indicates a weakly ordered organization (27±8 Å) of cellulose microfibrils. For [EMIM]acetate no correlation function was necessary to fit the high Q data of 30 min sample. This evidence further affirms [EMIM]acetate's propensity to fill inter-fibrillar spaces and therefore disrupt the regular order of cellulose fibrils.

The overall aim of this research work is to investigate the structural changes in biomass during exposure to [EMIM]acetate and [AMIM]formate. Previous studies on biomass dissolution in ILs have provided insights into the modifications of biomass pores and quantified the changes by measuring the post-treated biomass saccharification rates.[11,12,13,14,15,30] In our study, *in-situ* SANS showed that cross sectional diameter of cellulose microfibril and surface morphology were impacted by [EMIM]acetate. This change can be inferred as the penetration of [EMIM]acetate into interstitial spaces of individual cellulose macrofibrils, followed by cellulose microfibrils.

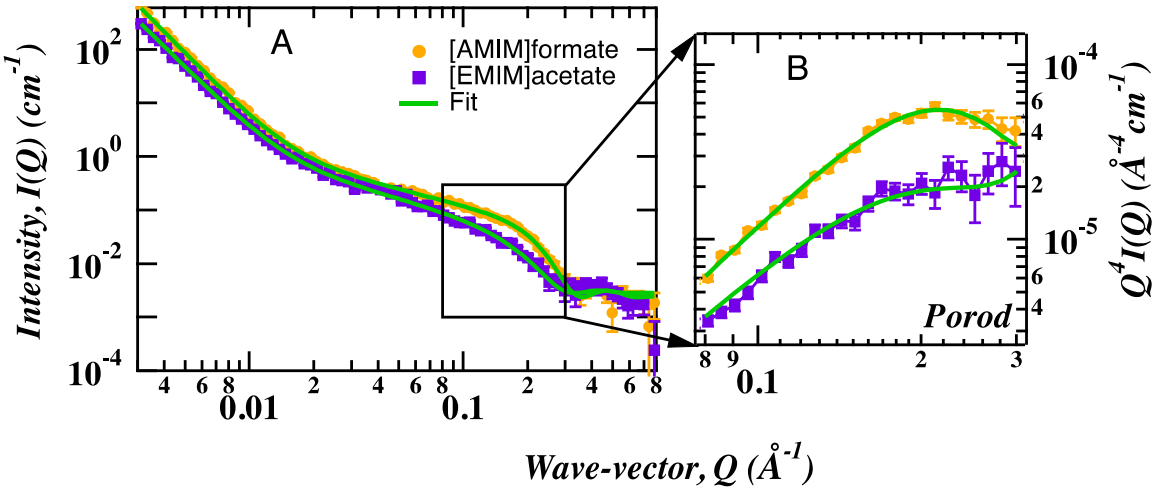

Figure 5. 4. (A) SANS profiles of cellulose in biomass for [AMIM]formate (yellow) and [EMIM]acetate (purple) at t = 0.5h. The green lines are the fits obtained from analysis. (B) The inset region in (A) is plotted as porod plots for [EMIM]acetate and [AMIM]formate.

The shoulder feature in the high Q in [EMIM]acetate was not as sharp as in solvents such as water which provides evidence for the better soaking/ penetration capacity of [EMIM]acetate. On the other hand, the prominence of diffraction peak observed in biomass treated with [AMIM]formate meant that [AMIM]formate did not permeate through the biomass layers.

In the field of biomass processing, [EMIM]acetate has long been considered as an efficient solvent for pretreatment, fractionation and dissolution purposes due its ability to form covalent linkages with woody biomass through cellulose reducing end via conjugation and transacetylation.[35,36,37] This IL is also known to have highly reactive carbene intermediates at room temperature.[38,39] However, high room temperature viscosity is often cited as a major drawback, therefore low viscosity ILs with formate anions have been considered as potential better option.[26] A recent study demonstrated that [AMIM]formate was able to dissolve 40% more biomass when compared to [EMIM]acetate.[40] Therefore, the lower architectural changes noticed in [AMIM]formate biomass system imply that low viscosity may not be a defining factor for biomass dissolution in ILs. Chloride anion ILs such as 1-allyl-3-methylimidazolium chloride ([AMIM]chloride)[41] and 1-butyl-3-methylimidazolium chloride ([BMIM]chloride)[42] are another example where high viscosity (room temperature viscosity of [AMIM]chloride is 244.5 mPa.s [BMIM]chloride 531.32 mPa.s) doesn't interfere with their ability to disrupt the cellulose architecture.[43] The increased alteration of cellulose feature in [EMIM]acetate is in agreement with our chapter 3 binding calculations, where twice the number of acetate anions were bound to a single anhydroglucose unit compared to [AMIM]formate. The current results imply that interactions between cellulose and [EMIM]acetate remain invariant to the nature of cellulose whether in biomass or as an individual component.

5.3.2. Mass loss and infrared analysis of IL- recovered biomass

Table 5. 2. Biomass weight in [EMIM]acetate and [AMIM]formate before and after SANS experiment

Ionic liquid (IL) name	Biomass disc wt. (mg)		Difference in biomass recovery (mg)	Mass loss (% oven dry wt. basis)
	0 h	44 h		
[EMIM]acetate	27.50	26.30	1.20	4.36
[AMIM]formate	28.11	27.98	0.11	0.40

Based on Table 5.2, higher biomass recovery was recorded for biomass treated with [AMIM]formate when compared to [EMIM]acetate. To understand this mass loss, the chemical signature of the IL-treated biomass samples was collected by FTIR and compared to untreated/control biomass by principal component analysis (PCA). Figures 5.5 and 5.6 are the scatter plots of principal component scores, i.e., scores plots showing the pattern in the FTIR data, and a loadings plot displaying the relationship between the wavenumbers of the FTIR spectrum and the PCs. PCA scores and loadings plots highlight the differences due to IL treatment on the biomass with [EMIM]acetate (Fig. 5.5A, B, corresponding to scores and loadings plot, respectively) and [AMIM]formate (Fig. 5.6A, B, corresponding to scores and loadings plot, respectively) when compared to the control that consisted of untreated biomass. The scores plot (Fig. 5.5A) show that [EMIM]acetate sample recovered after 44h treatment and untreated biomass (control) are separated by PC1 which accounts for 83 % of the data variation. The PC1 loadings plot (Fig. 5.4B) shows that spectral changes occurred at 1739 and 1243 cm^{-1}which correspond to acetyl groups, C=O and C-O stretch respectively. Since these bands are negative in intensity and the biomass recovered from IL treatment is located in the positive quadrant of PC1 (Fig. 5.4A), we can infer that there are fewer acetyl groups in the [EMIM]acetate treated biomass than in the untreated/control biomass. Similarly, the [AMIM]formate recovered biomass sample and the untreated biomass (control) separated along PC-1 (75% variation, Fig. 5.5A). However, unlike [EMIM]acetate, the corresponding loadings plot (Fig. 5.5B) did not display any bands associated with the loss of acetyl groups. Nevertheless, loading plot show bands at 1075, 1043 and 1015 cm^{-1} corresponding to C-O and C-C stretching.

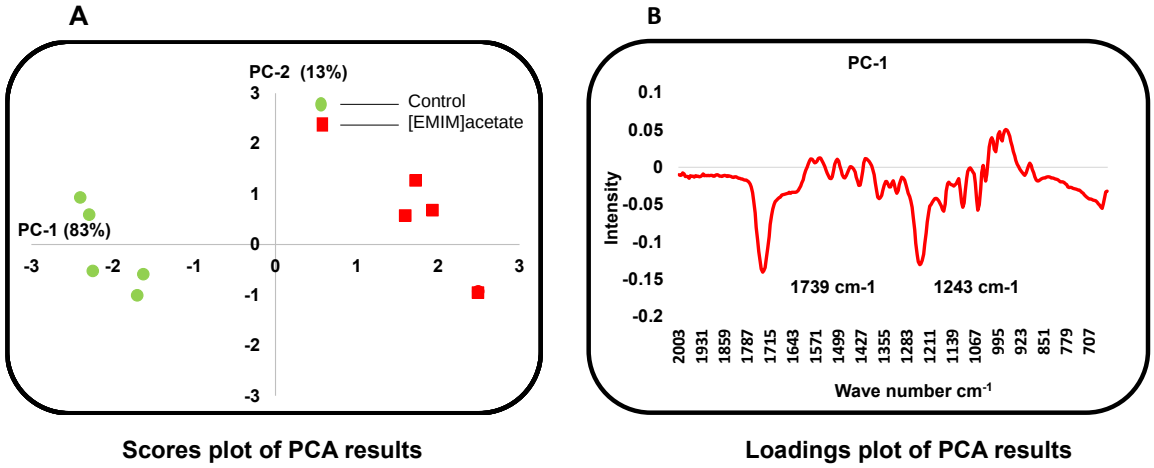

Figure 5. 5. Principal component analysis (PCA) on [EMIM]acetate-recovered biomass disc (after 44-h reaction time) compared to untreated hybrid poplar. The scores plot is shown on the left (A) and the loadings plot for PC1 on the right (B).

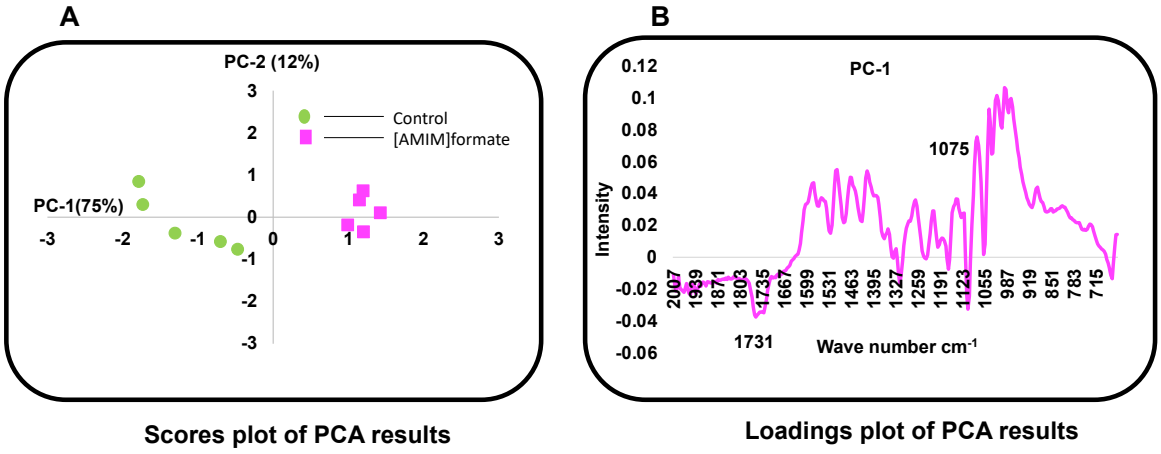

Figure 5. 6. Principal component analysis (PCA) on [AMIM]formate-recovered biomass disc after 44-h reaction time compared to untreated hybrid poplar. The scores plot is shown on the left (A) and the loadings plot for PC1 on the right (B).

The intensity of these bands is lower when compared to acetyl group stretching observed for [EMIM]acetate treated sample. This observation along with the minimal mass loss indicate that the biomass sample in [AMIM]formate did not undergo higher amount amount of deacetylation.

Figure 5.7 shows the PCA of the FTIR spectra collected from both ILs. According to the loadings plot (Fig. 5.7B), the most significant spectral changes occurred at 1739 and 1243 cm^{-1} corresponding to C=O and C-O stretching of acetyl group. Similar to Fig. 5.5, the acetyl group bands in Fig. 5.7B have negative intensity while biomass recovered from [EMIM]acetate is located on the positive quadrant of PC1. Overall, variations in the FTIR spectra confirm that [EMIM]acetate altered the chemical features of biomass the most (PC1 accounts for 70%), when compared to [AMIM]formate. The close proximation of [AMIM]formate-treated biomass to the control in Figure 5.7A shows that they have similar chemical structure. This is consistent with past research where [EMIM]acetate was used for activation of lignocellulose biomass a similar loss of acetyl groups was observed.[33,34]

5.1.Conclusion and future work

In-situ SANS study of intact hybrid biomass was performed in the presence of two 1,3-dialkylimidazolium ILs. In [EMIM]acetate, the cellulose microfibril feature in biomass underwent size reduction with time. On the other hand, no such change was observed with [AMIM]formate. The greater change induced by [EMIM]acetate is consistent with our results in Chapter 3 where [EMIM]acetate was shown to exhibit higher number of interactions with micro crystalline cellulose. Further, FT-IR analysis showed that [EMIM]acetate also caused significant deacetylation in hybrid poplar when compared to [AMIM]formate which may have partly enhanced the accessibility to cellulose and promoted cellulose dissolution.

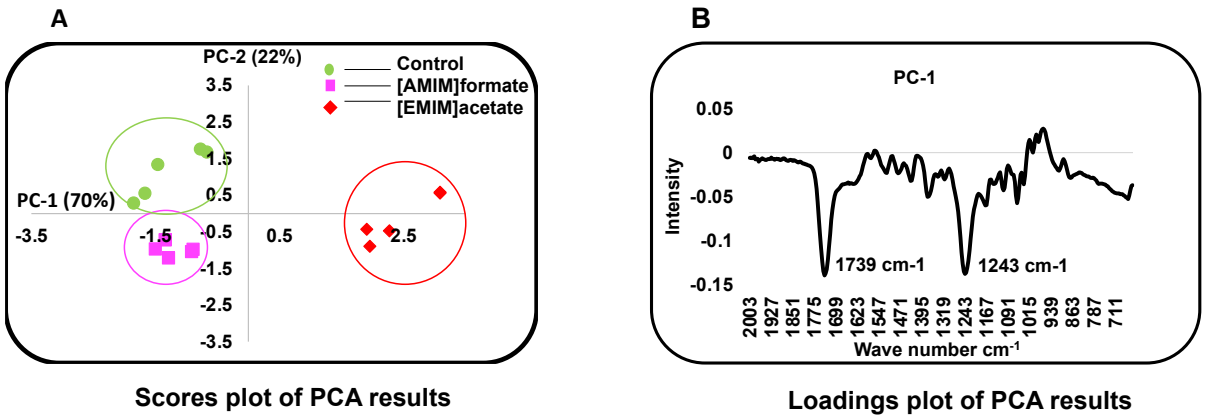

Figure 5. 7. Principal component analysis (PCA) on biomass recovered from [EMIM]Acetate and [AMIM]formate after 44h and untreated biomass. PCA scores plot is shown on the left (A), and the loadings plot for PC 1 on the right (B).

On the other hand, IR analysis showed that biomass recovered from [AMIM]formate did not undergo deacetylation. However, the chemical signature of biomass sample recovered from [AMIM]fromate treatment was different from untreated biomass. For the first time, we show that delamination of cellulose microfibrils during IL-treatments is essential for enhanced dissolution and reduction in biomass recalcitrance.

5.1.1. Future SANS analysis

The samples for the study included whole biomass, holocellulose and $\boldsymbol{\alpha}$-cellulose. In this chapter only the anisotropic scattering signal of cellulose microfibril was presented. Our preliminary IR analysis showed that biomass sample in [AMIM]formate underwent alterations. Therefore, to understand the behavior of biomass in [AMIM]formate isotropic scattering data of hemicellulose and lignin will be analyzed in future. In addition to those data, scattering data of $\boldsymbol{\alpha}$-cellulose isolated from biomass will also be analyzed.

References

1) Isikgor, F. H.; Becer, C. R., Lignocellulosic biomass: a sustainable platform for the production of bio-based chemicals and polymers. *Polymer Chemistry* **2015**, *6*(25), 4497-4559
2) Kumar, P.; Barrett, D. M.; Delwiche, M. J.; Stroeve, P., Methods for pretreatment of lignocellulosic biomass for efficient hydrolysis and biofuel production. *Industrial & engineering chemistry research* **2009**, *48*(8), 3713-3729
3) Wang, H.; Gurau, G.; Rogers, R. D., Ionic liquid processing of cellulose. *Chemical Society Reviews* **2012**, *41*(4), 1519-1537.
4) Plechkova, N. V.; Seddon, K. R., Ionic liquids:"designer" solvents for green chemistry. *Methods and Reagents for Green Chemistry* **2007**,105-130.
5) da Costa Lopes, A. M.; João, K. G.; Rubik, D. F.; Bogel-Łukasik, E.; Duarte, L. C.; Andreaus, J.; Bogel-Łukasik, R., Pre-treatment of lignocellulosic biomass using ionic liquids: wheat straw fractionation. *Bioresource technology* **2013**, *142*, 198-208.
6) Labbé, N.; Kline, L. M.; Moens, L.; Kim, K.; Kim, P. C.; Hayes, D. G., Activation of lignocellulosic biomass by ionic liquid for biorefinery fractionation. *Bioresource technology* **2012**, *104*, 701-707.
7) Nguyen, N.A.; Kim, K.; Bowland, C.C.; Keum, J.K.; Kearney, L.T.; André, N.; Labbé, N.; Naskar, A.K., A fundamental understanding of whole biomass dissolution in ionic liquid for regeneration of fiber by solution-spinning. *Green Chemistry* **2019**, *21*(16), 4354-4367.
8) Yoo, C. G.; Pu, Y.; Ragauskas, A. J., Ionic liquids: Promising green solvents for lignocellulosic biomass utilization. *Current Opinion in Green and Sustainable Chemistry* **2017**, *5*, 5-11.
9) Singh, S.; Simmons, B. A.; & Vogel, K. P., Visualization of biomass solubilization and cellulose regeneration during ionic liquid pretreatment of switchgrass. *Biotechnology and Bioengineering* **2009**, *104*(1), 68-75.
10) Zhang, X.; Ma, J.; Ji, Z.; Yang, G. H.; Zhou, X.; Xu, F., Using confocal Raman microscopy to real-time monitor poplar cell wall swelling and dissolution during ionic liquid pretreatment. *Microscopy research and technique* **2014**, *77*(8), 609-618.
11) Li, H. Y.; Chen, X.; Wang, C. Z.; Sun, S. N.; Sun, R. C., Evaluation of the two-step treatment with ionic liquids and alkali for enhancing enzymatic hydrolysis of Eucalyptus: chemical and anatomical changes. *Biotechnology for biofuels* **2016**, *9*(1), 166.
12) Miyafuji, H.; Suzuki, N., Observation by light microscope of sugi (Cryptomeria japonica) treated with the ionic liquid 1-ethyl-3-methylimidazolium chloride. *Journal of wood science* **2011**, *57*(5), 459-461.
13) Kanbayashi, T.; Miyafuji, H., Effect of ionic liquid treatment on the ultrastructural and topochemical features of compression wood in Japanese cedar (Cryptomeria japonica). *Scientific reports* **2016**, *6*, 30147.
14) Moyer, P.; Kim, K.; Abdoulmoumine, N.; Chmely, S. C.; Long, B. K.; Carrier, D. J.; Labbé, N., Structural changes in lignocellulosic biomass during activation with ionic liquids comprising 3-methylimidazolium cations and carboxylate anions. *Biotechnology for biofuels* **2018**, *11*(1), 1-13.

15) Charrier, A. M.; Lereu, A. L.; Farahi, R. H.; Davison, B. H.; Passian, A., Nanometrology of biomass for bioenergy: The role of atomic force microscopy and spectroscopy in plant cell characterization. *Frontiers in Energy Research* **2018**, *6*, 11.
16) Cheng, G.; Zhang, X.; Simmons, B.; Singh, S., Theory, practice and prospects of X-ray and neutron scattering for lignocellulosic biomass characterization: towards understanding biomass pretreatment. *Energy & Environmental Science* **2015**, *8*(2), 436-455.
17) Raghuwanshi, V. S.; Cohen, Y.; Garnier, G.; Garvey, C. J.; Russell, R. A.; Darwish, T.; Garnier, G., Cellulose dissolution in ionic liquid: ion binding revealed by neutron scattering. *Macromolecules* **2018,** *51*(19), 7649-7655.
18) Yuan, X.; Duan, Y.; He, L.; Singh, S.; Simmons, B.; Cheng, G., Characterization of white poplar and eucalyptus after ionic liquid pretreatment as a function of biomass loading using X-ray diffraction and small angle neutron scattering. *Bioresource technology* **2017**, *232*, 113-118.
19) Hirosawa, K.; Fujii, K.; Hashimoto, K.; Shibayama, M., Solvated structure of cellulose in a phosphonate-based ionic liquid. *Macromolecules* **2017**, *50*(17), 6509-6517.
20) Jiang, X.; Kitamura, S.; Sato, T.; Terao, K., Chain dimensions and stiffness of cellulosic and amylosic chains in an ionic liquid: cellulose, amylose, and an amylose carbamate in BmimCl. *Macromolecules* **2017**, *50*(10), 3979-3984.
21) Pingali, S. V.; O'Neill, H. M.; Nishiyama, Y.; He, L.; Melnichenko, Y. B.; Urban, V.S.; Petridis, L.; Davison, B. H.; Langan, P., Morphological changes in the cellulose and lignin components of biomass occur at different stages during steam pretreatment. *Cellulose* **2014,** *21*(2), 873-878.
22) Langan, P.; Petridis, L.; O'Neill, H.M.; Pingali, S.V.; Foston, M.; Nishiyama, Y.; Schulz, R.; Lindner, B.; Hanson, B.L.; Harton, S.; Heller, W.T.; Urban, V.S.; Evans, B. R.; Gnanakaran.; Ragauskas, A. J.; Smith, J. C.; Davison, B. H., 2014. Common processes drive the thermochemical pretreatment of lignocellulosic biomass. *Green Chemistry* **2014,** *16*(1), 63-68.
23) Wang, H.; Gurau, G.; Pingali, S. V.; O'Neill, H. M.; Evans, B. R.; Urban, V. S.; Heller, W.T.; Rogers, R. D., Physical insight into switchgrass dissolution in ionic liquid 1-ethyl-3-methylimidazolium acetate. *ACS Sustainable Chemistry & Engineering* **2014,** *2*(5), 1264-1269.
24) Cheng, G.; Varanasi, P.; Arora, R.; Stavila, V.; Simmons, B. A.; Kent, M. S.; Singh, S., Impact of ionic liquid pretreatment conditions on cellulose crystalline structure using 1-ethyl-3-methylimidazolium acetate. *The Journal of Physical Chemistry B* **2012**, *116*(33), 10049-10054.
25) Sannigrahi, P.; Ragauskas, A. J.; Tuskan, G. A., Poplar as a feedstock for biofuels: a review of compositional characteristics. *Biofuels, Bioproducts and Biorefining* **2010,** *4*(2), 209-226.
26) Fukaya, Y.; Sugimoto, A.; Ohno, H., Superior solubility of polysaccharides in low viscosity, polar, and halogen-free 1,3-dialkylimidazolium formates. *Biomacromolecules* **2006**, *7* (12), 3295-3297.
27) Heller, W. T.; Urban, V. S.; Lynn, G. W.; Weiss, K. L.; O'Neill, H. M.; Pingali, S. V.; Qian, S.; Littrell, K. C.; Melnichenko, Y. B.; Buchanan, M. V.; Selby, D. L.; Wignall, G. D.; Butler, P. D.; Myles, D. A., (2014). *Journal of Applied Crystallography* **2014**, *47*, 1238-1246.

28) Ilavsky, J.; Jemian, P.R., Irena: tool suite for modeling and analysis of small-angle scattering. *Journal of Applied Crystallography* **2009**, *42*, 347-353.
29) Paul, W. S.; David, A.; David, L.; Axel, H.; Mathias, S.; Armin, R., Small-angle x-ray scattering from the surfaces of reversed-phase silicas: Power-law scattering exponents of magnitudes greater than four. *The Journal of Chemical Physics* **1991,** 94, (2), 1474-1479.
30) Cheng, G.; Varanasi, P.; Arora, R.; Stavila, V.; Simmons, B. A.; Kent, M. S.; Singh, S., Impact of ionic liquid pretreatment conditions on cellulose crystalline structure using 1-ethyl-3-methylimidazolium acetate. *The Journal of Physical Chemistry B* **2012,** *116*(33), 10049-10054.
31) Nishiyama, Y.; Langan, P.; O'Neill, H.; Pingali, S. V.; Harton, S., Structural coarsening of aspen wood by hydrothermal pretreatment monitored by small-and wide-angle scattering of X-rays and neutrons on oriented specimens. *Cellulose* **2014,** *21*(2), 1015-1024.
32) Plaza, N. Z.; Pingali, S. V.; Qian, S.; Heller, W. T.; Jakes, J. E., Informing the improvement of forest products durability using small angle neutron scattering. *Cellulose* **2016,** *23*(3), 1593-1607.
33) Parthasarathi, R.; Sun, J.; Dutta, T.; Sun, N.; Pattathil, S.; Konda, N.M.; Peralta, A.G.; Simmons, B.A.; Singh, S., Activation of lignocellulosic biomass for higher sugar yields using aqueous ionic liquid at low severity process conditions. *Biotechnology for biofuels* **2016,** *9*(1), 160.
34) Labbé, N.; Kline, L. M.; Moens, L.; Kim, K.; Kim, P. C.; Hayes, D. G., Activation of lignocellulosic biomass by ionic liquid for biorefinery fractionation. *Bioresource technology* **2012,** *104*, 701-707.
35) Kyllönen, L.; Parviainen, A.; Deb, S.; Lawoko, M.; Gorlov, M.; Kilpeläinen, I.; King, A., W. On the solubility of wood in non-derivatising ionic liquids. *Green chemistry* **2013**, *15*(9), 2374-2378.
36) Liebert, T.; Heinze, T., Interaction of ionic liquids with polysaccharides. 5. Solvents and reaction media for the modification of cellulose. *BioResources* **2008,** *3*(2), 576-601.
37) Ebner, G.; Schiehser, S.; Potthast, A.; Rosenau, T., Side reaction of cellulose with common 1-alkyl-3-methylimidazolium-based ionic liquids. *Tetrahedron Letters* **2008,** *49*(51), 7322-7324.
38) Rodríguez, H.; Gurau, G.; Holbrey, J. D.; Rogers, R. D., Reaction of elemental chalcogens with imidazolium acetates to yield imidazole-2-chalcogenones: direct evidence for ionic liquids as proto-carbenes. *Chemical Communications* **2011,** *47*(11), 3222-3224.
39) Kelley, S. P.; Narita, A.; Holbrey, J. D.; Green, K. D.; Reichert, W. M.; Rogers, R. D., Understanding the effects of ionicity in salts, solvates, co-crystals, ionic co-crystals, and ionic liquids, rather than nomenclature, is critical to understanding their behavior. *Crystal growth & design* **2013,** *13*(3), 965-975.
40) Moyer, P.; Smith, M. D.; Abdoulmoumine, N.; Chmely, S. C.; Smith, J. C.; Petridis, L.; Labbé, N., Relationship between lignocellulosic biomass dissolution and physicochemical properties of ionic liquids composed of 3-methylimidazolium cations and carboxylate anions. *Physical Chemistry Chemical Physics* **2018,** *20*(4), 2508-2516.

41) de Pablo, L.; Segovia, J. J.; Martín, A.; Martín, M. C.; Bermejo, M. D., Determination of density, viscosity and vapor pressures of mixtures of dimethyl sulfoxide+ 1-allyl-3-methylimidazolium chloride at atmospheric pressure. *The Journal of Chemical Thermodynamics* **2018**, *123*, 185-194.
42) Li, J.; Zhu, H.; Peng, C.; Liu, H., Densities and viscosities for ionic liquids [BMIM][BF4] and [BMIM][Cl] and their binary mixtures at various temperatures and atmospheric pressure. *Chinese Journal of Chemical Engineering*, **2019**, *27*(12), 2994-2999.
43) Luo, N.; Lv, Y.; Wang, D.; Zhang, J.; Wu, J.; He, J.; Zhang, J., Direct visualization of solution morphology of cellulose in ionic liquids by conventional TEM at room temperature. *Chemical Communications* **2012,** *48*(50), 6283-6285.

5.2.Appendix

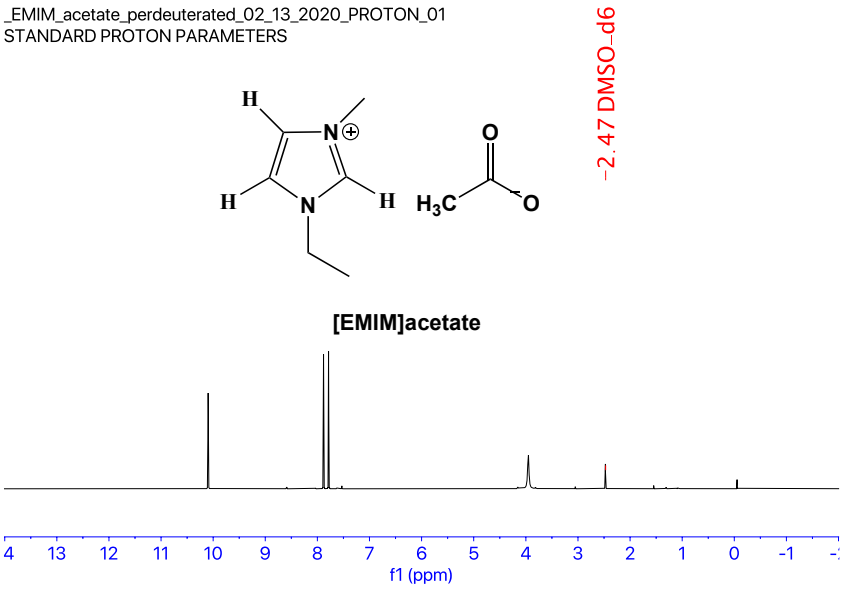

Figure 5. 8. ^{1}H (400 MHz DMSO-d6) of deuterated [EMIM]acetate at RT.

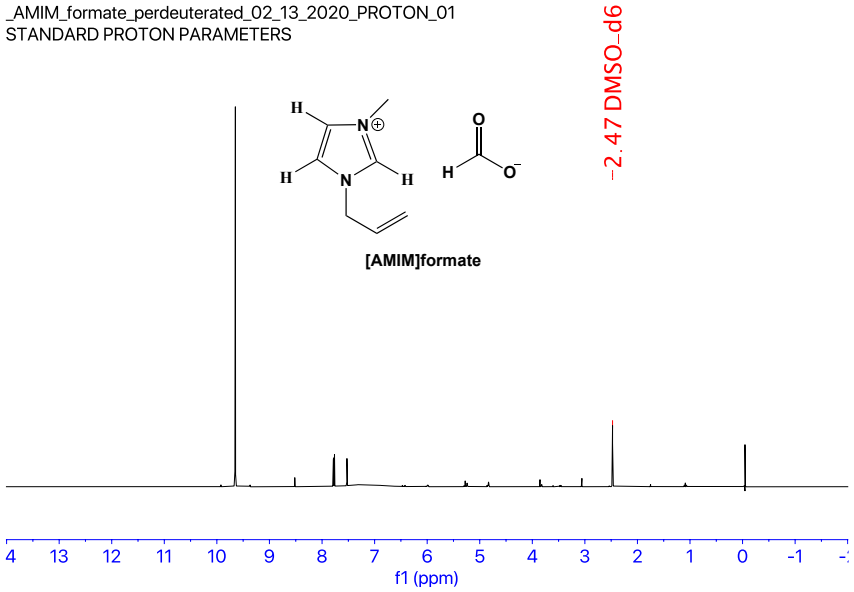

Figure 5. 9. ^{1}H NMR (400 MHz DMSO-d6) of deuterated [AMIM]formate at RT.

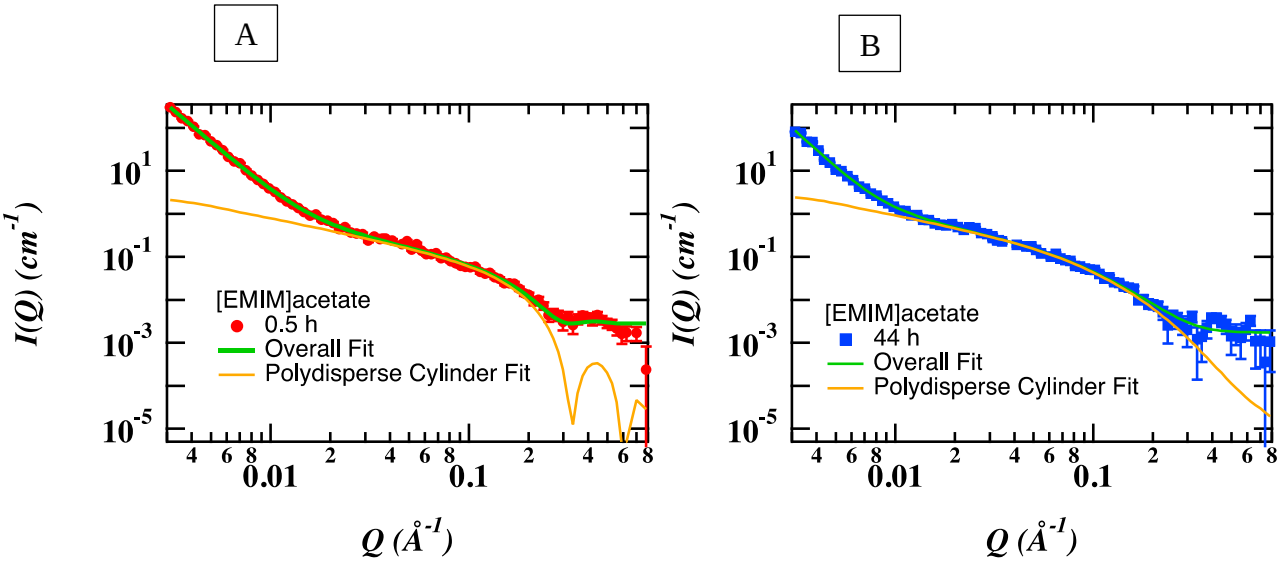

Figure 5. 10. SANS profiles of biomass in [EMIM]acetate with polydisperse cylinder fit and overall fit at t = 0.5h (A) and t = 44h (B).

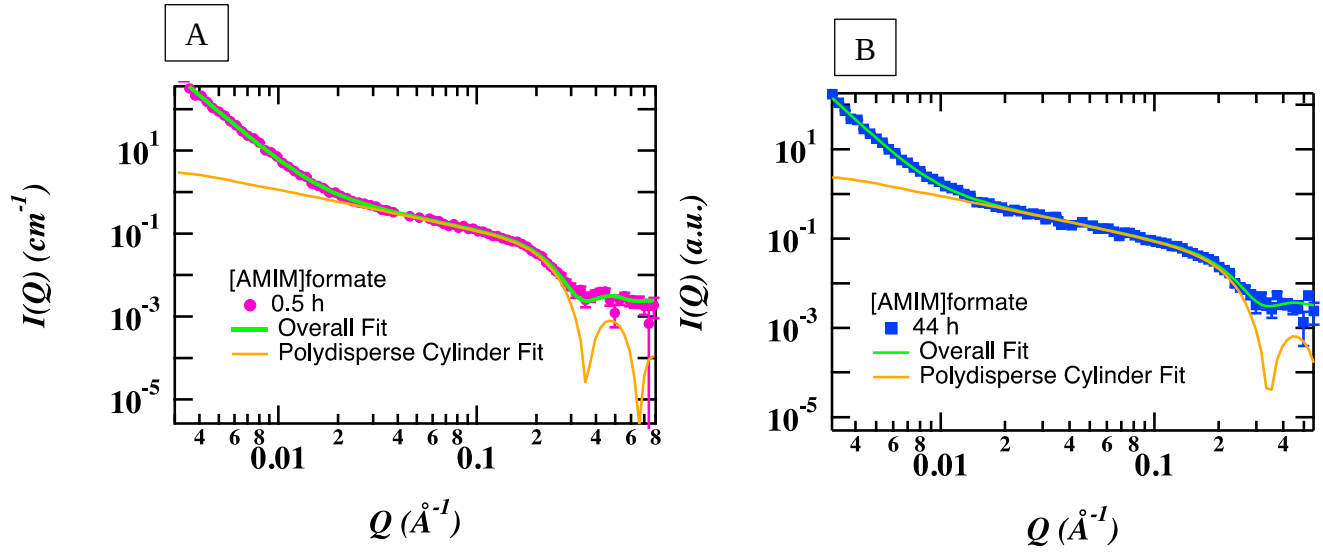

Figure 5. 11. SANS profiles of biomass in [AMIM]acetate with polydisperse cylinder fit and overall fit at t = 0.5h (A) and t = 44h (B).

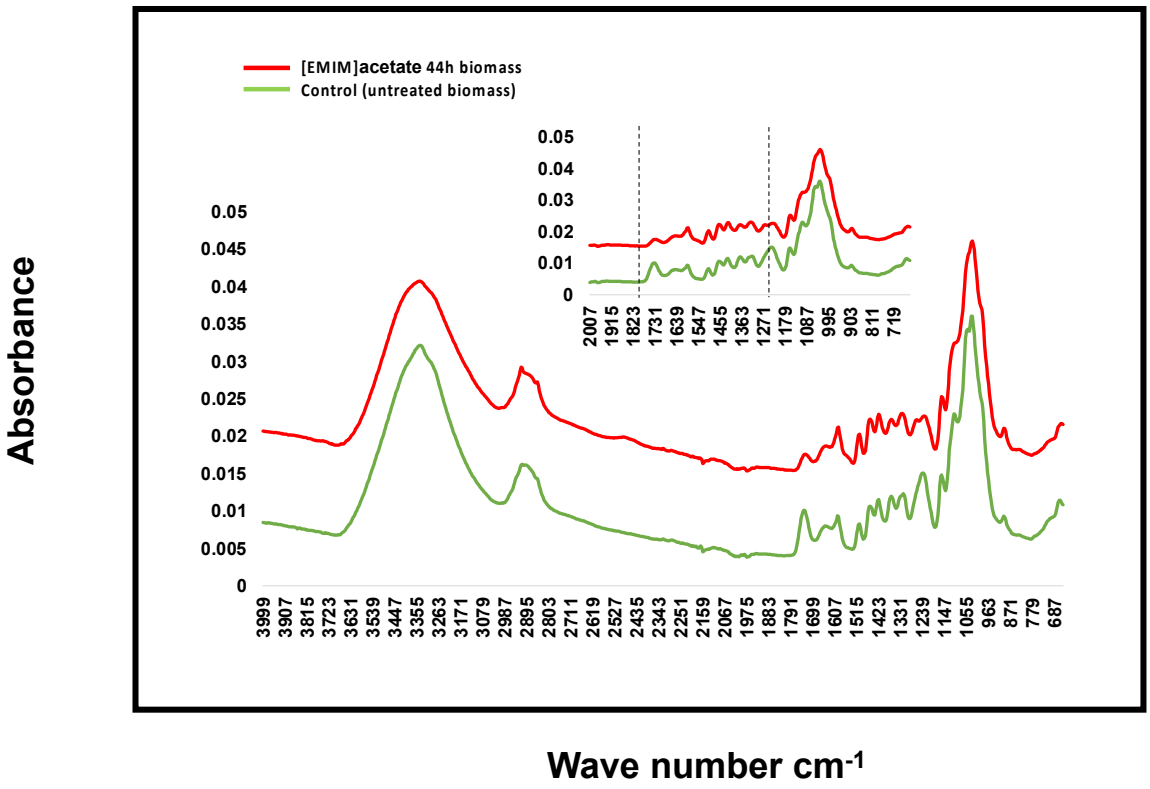

Figure 5. 12. ATR corrected FT-IR spectra of untreated (green) and [EMIM]acetate treated (red) hybrid poplar disc for 44 h. Inset: Finger-print region of FT-IR absorption spectra of hybrid poplar.

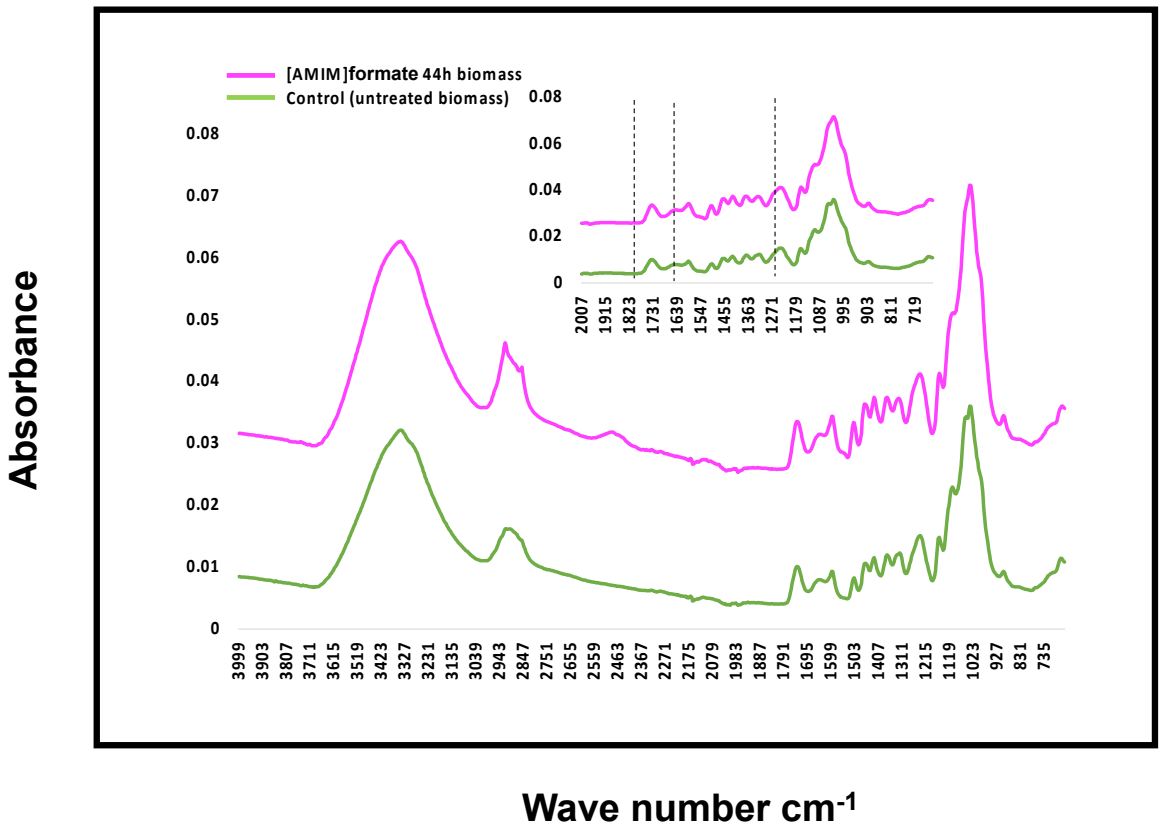

Figure 5. 13. ATR corrected FT-IR spectra of untreated (green) and [AMIM]formate treated (magenta) hybrid poplar disc for 44 h. Inset: Finger-print region of FT-IR absorption spectra of hybrid poplar.

Chapter 6. Conclusion and future outlook

6.1.Overall conclusions

Biomass has complex structure essentially entrapping high carbon content polymers in a network architecture that is resistant to breakdown. Progress towards understanding plant cell wall structure has provided detailed information about cell wall component chemistry and potential causes of biomass recalcitrance. This information can now be used to shift the focus from a sugar-centric separation to efficient isolation procedures, which will enable the utilization of all the polymers within the biomass.

ILs are capable of dissolving biomass and biomass constituent polymers at milder processing conditions compared to traditional pretreatment approaches. Research of the past decade have shown that ILs bring about changes such as reduced cellulose crystallinity, increased cellulose access, lignin relocation, and higher saccharification rates. Despite the advantages of ILs, the laboratory to industrial scale adaptation has been slow due to high costs and the lack of understanding of molecular-level mechanisms of biomass dissolution in ILs. Therefore, in this research, using the four different ILs in combination of two cations (1-ethyl-3-methylimidazolium [EMIM] and 1-allyl-3-methylimidazolium [AMIM]) and anions (formate and acetate), we evaluated the micro, meso and molecular interactions that bring about the ultrastructural changes in biomass during IL dissolution. We have used a multiple length scale approach to provide comprehensive insights about the interactions between IL ion pairs and biomass polymers.

We first applied a bottom to top approach where individual biomass polymers were tested with ILs. In the first study the interactions between the four ILs and cellulose was investigated using NMR, SAXS and rheology. NMR analysis showed that local environment of IL carbons altered as a function of cellulose concentration. NMR also helped to identify [EMIM]acetate system with

most interactions and [AMIM]formate-cellulose system with least interactions. To identify the molecular-level differences leading to these NMR changes, cellulose dissolved in [EMIM]acetate and [AMIM]formate was studied by SAXS. The results showed that both ILs dissolved cellulose molecularly to the point where individual cellulose strands were observed. Quantitative analysis of SAXS results showed that almost twice the number of [EMIM]acetate ions were bound to a cellulose strand than [AMIM]formate. Rheological behavior of cellulose-[EMIM]acetate and cellulose-[AMIM]formate also confirmed higher number of interactions between [EMIM]acetate and cellulose. Therefore, we conclude that the high magnitude of local interactions with [EMIM]acetate is due to the higher binding affinity of formate anion to cellulose and the higher number of dispersive interactions.

We used the same analytical approach to assess the interactions between xylan and lignin with the four selected ILs. The NMR data demonstrated that the presence of xylan induced similar level of local interactions in the four ILs. However, in case of lignin, [EMIM]acetate showed higher magnitude changes compared to [AMIM]formate. Mesoscale interactions measured by SAXS showed that the same number of [EMIM]acetate and [AMIM]formate ions were bound to xylan. However, unlike the carbohydrate (cellulose and xylan) molecules, we did not observe a single stranded feature for lignin dissolved in ILs. Only a globular feature of similar size was observed in both [EMIM]acetate and [AMIM]formate. Interestingly, molecular weight analysis showed that lignin was present in a monomeric form in [EMIM]acetate while assuming an oligomeric form in [AMIM]formate. These results, combined with our cellulose study, demonstrate that [EMIM]acetate and [AMIM]formate have same magnitude of interactions with xylan, but varied in interactions with cellulose and lignin.

Our third objective was to investigate the behavior of native/whole biomass in [EMIM]acetate and [AMIM]formate. By performing a time resolved *in-situ* study using SANS, we specifically monitored real time changes in cellulose architecture embedded in the biomass matrix. In the [EMIM]acetate treated biomass, cellulose microfibril feature lost integrity within the first 30 min of measurement. Further, as the treatment progressed, we observed larger size cellulose microfibrils indicating that [EMIM]acetate permeated between and within the cellulose microfibril bundles. On the other hand, for biomass treated with [AMIM]formate, cellulose microfibril featured weak interference factor, implying close arrangement. Additionally, the diffraction feature did not undergo change as a function of time with [AMIM]formate, further supporting its weak interaction with cellulose. Complementary FT-IR analysis of regenerated samples showed that, the [EMIM]acetate treatment resulted in significant reduction of acetyl content and therefore, combined with the higher mass loss, indicated significant hemicellulose removal when compared to [AMIM]formate. The combined results implied that [EMIM]acetate brought about enhanced access to cellulose via hemicellulose removal. Furthermore, by virtue of higher number of interactions, [EMIM]acetate produced delamination of cellulose microfibril bundles, and hence, the superior performance in lignocellulosic biomass dissolution. Taken together, these studies provide compelling evidence that [EMIM]acetate is better suited for biomass processing technologies.

6.2. Future outlook

The research work put forth in thesis can be utilized to carry forward our understanding of IL-biomass interactions in different ways, few of which are listed below:

- ***Expanding the understanding of interactions by including chloride anion based ILs***

In addition to [EMIM]acetate, chloride anion ILs such as [AMIM]chloride and [BMIM]chloride are also considered as powerful non-derivatizing ILs for cellulose and biomass.[1] Preliminary SAXS studies demonstrated that chloride ILs disrupt, inter and intra molecular H-bonds of cellulose to achieve faster solubility when compared to [EMIM]acetate.[2] A comparative multilength scale study of chloride IL versus acetate IL will help further our understanding of IL biomass interactions.

- ***Interactions of different types of hemicellulose with ILs***

Hemicellulose polymer is made of diverse sets of sugars such as mannan, glucuronoxylan and arabinoxylan. Since the current study utilized only xylan for the sake of simplicity, future studies can focus on other types of hemicellulose polysaccharides in order to develop a comprehensive picture of biomass disintegration.

- ***Diffusion rate measurement of [AMIM]formate in comparison to [EMIM]acetate***

In the present study the interaction parameter measured by NMR is the chemical shift difference between IL with polymer and neat IL. Although reliable, this method suffers from the deficiency of low magnitude. Using Diffusion Ordered Spectroscopy (DOSY) method, the diffusion rate of IL ion pairs in relation to temperature and concentration can be measured.[3] A comparative study on the diffusion rates of [AMIM]formate and [EMIM]acetate will help better understand the observed chemical shift differences noted in the current study.

- ***SANS study with different time treated biomass samples***

For the objective 3, time resolved SANS study was performed on biomass samples for 2 days at 80 ˚C. In the current configuration, the titanium cell does not allow for solvent motion (in

comparison to lab setup) once the SANS measurement begins. Therefore, the magnitude of difference between the start and end time point was significantly smaller. To overcome the issue, a future SANS measurement with biomass samples pre-treated in lab to different time points is recommended.

- ***[AMIM]acetate IL for biomass processing***

In the current research work, four different ILs were utilized to understand interactions between biomass polymers and ILs in objectives 1 and 2. As ILs [AMIM]formate and [EMIM]acetate differed in their binding affinity towards cellulose and lignin, these two ILs were carried forward to conduct time resolved study of biomass dissolution. However, [AMIM]acetate and [EMIM]acetate have similar physicochemical properties and cellulose/ biomass solubilities.[4] And based on the current study, the interaction magnitude with individual biomass polymers is similar as well. So, a study comparing these two ILs with whole biomass will help us understand the molecular differences between these two ILas.

References

1) Zhang, H.; Wu, J.; Zhang, J.; He, J., 1-Allyl-3-methylimidazolium chloride room temperature ionic liquid: a new and powerful nonderivatizing solvent for cellulose. *Macromolecules* **2005**, *38*(20), 8272-8277.
2) Jiang, X.; Kitamura, S.; Sato, T.; Terao, K., Chain dimensions and stiffness of cellulosic and amylosic chains in an ionic liquid: cellulose, amylose, and an amylose carbamate in BmimCl. *Macromolecules* **2017**, *50*(10), 3979-3984.
3) Ries, M. E.; Radhi, A.; Keating, A. S.; Parker, O.; Budtova, T., Diffusion of 1-ethyl-3-methyl-imidazolium acetate in glucose, cellobiose, and cellulose solutions. *Biomacromolecules* **2014**, *15*(2), 609-617.
4) Xu, A.; Zhang, Y.; Li, Z.; Wang, J., Densities and conductivities of seven 1-allyl-3-methylimidazolium carboxylate ionic liquids. *Journal of Molecular Liquids* **2016**, *214*, 192-195.

VITA

Aparna Annamraju was born and raised in Hyderabad, India. She attended Savithri Bhai Phule University (formerly University of Pune) and graduated with master's degree in Organic chemistry. In 2003, she moved to US in pursuit of advanced studies and graduated with a master's degree in Inorganic chemistry in 2005. After a break from science, she joined Oak Ridge National Laboratory (ORNL) as post-master's research associate. During the course of the project, she was introduced to the basics of biomass processing technologies. To learn further on the subject matter, she enrolled into the PhD program at University of Tennessee in 2017. After graduating with PhD degree in December 2020, she intends to continue on career path of understanding and designing new biomass processing technologies. She lives in Knoxville, TN with her husband and two kids.